3-24-2016

Evaluation of Unmanned Aircraft Flying Qualities Using JSBSim

Joshua P. Kim

Evaluation of Unmanned Aircraft Flying Qualities Using JSBSim

THESIS

Joshua P. Kim, Second Lieutenant, USAF

AFIT-ENY-MS-16-M-221

DEPARTMENT OF THE AIR FORCE
AIR UNIVERSITY

AIR FORCE INSTITUTE OF TECHNOLOGY

Wright-Patterson Air Force Base, Ohio

AFIT-ENY-MS-16-M-221

EVALUATION OF UNMANNED AIRCRAFT FLYING QUALITIES USING JSBSIM

THESIS

Presented to the Faculty

Department of Aeronautical Engineering

Graduate School of Engineering and Management

Air Force Institute of Technology

Air University

Air Education and Training Command

in Partial Fulfillment of the Requirements for the

Degree of Master of Science in Aeronautical Engineering

Joshua P. Kim, B.S.A.E.

Second Lieutenant, USAF

March 7, 2016

AFIT-ENY-MS-16-M-221

EVALUATION OF UNMANNED AIRCRAFT FLYING QUALITIES USING JSBSIM

THESIS

Joshua P. Kim, B.S.A.E.
Second Lieutenant, USAF

Committee Membership:

Dr. D. L. Kunz, PhD
Chair

Dr. R. G. Cobb, PhD
Member

Dr. M. F. Reeder, PhD
Member

Abstract

Flying qualities data can be used to predict the future performance of aircraft during the early design stages of the system when the changes can be made easily and inexpensively; however, no flying qualities requirements exist for Unmanned Aerial Vehicles (UAVs). The intent of UAV flying qualities requirements is to guarantee the safety and operational effectiveness of the aircraft as do the flying qualities of piloted aircraft. Flying qualities requirements have been extensively researched and specified for fixed-wing and rotary-wing manned aircraft based on a substantial database of assessments. The critical issue today in flying qualities is how to extend them to pilotless aircraft. It is the goal of this thesis to provide data on the flying qualities assessments of UAVs in order to propel the development of a UAV flying qualities standard. A simulation study using an open-source flight dynamics model (JSBSim) was conducted to perform various performance maneuvers and evaluate how well the aircraft followed the desired maneuver. Criteria from MIL-STD-1797 were used to evaluate the flying quality characteristics and compared to the simulation results. It was found that the application of manned criteria to autonomous UAVs did not provide an accurate depiction of its flying qualities. Instead the requirements should be focused on the closed-loop task evaluation and the limitations of the flight control system. By synthesizing proven fixed-wing and rotary-wing standards with updated unmanned criteria applicable to modern autonomous unmanned aircraft design, the maximum performance of these systems can be achieved. The need for further research and accumulation of UAV flying qualities assessments will be necessary to bring about a successful flying qualities standard for unmanned aircraft.

Acknowledgements

This research has been the culmination of the past eighteen months at AFIT which has been a tremendous journey for me and the pinnacle of my academic career. I could not have done it without the love and support of my parents, whose drive has pushed me beyond my own expectations. I thank my mother who taught me that "I can do all things through Christ who gives me strength."

First and foremost, I want to thank Dr. Kunz for not only being my thesis advisor but giving me continued guidance and support. His patience and advice were instrumental in helping me lay down the foundation for this undertaking. His passion in this field has inspired me to never stop learning and that there is always room for improvement. As I continue throughout my career, I look forward to our continued interaction in advancing such an exciting field.

I would like to thank Lt. Col Greene for her assistance and for answering the multitude of questions I had. Her dissertation work made my transition to working on my thesis much less stressful and I am grateful for her advice and help. I would like to also thank Dr. Bradley Liebst (AFIT) and Mr. David Leggett (AFRL) for providing their insight and expertise on flying qualities. Major Mark Vahle, for his assistance in the start of using JSBSim in our research together as fellow JSBSimers. I would like to give a special thanks to Captain George Ip for being a supportive roommate and always giving helpful life advice. It has been an honor to share this time with all of you.

Joshua P. Kim

Table of Contents

Page

Page

List of Figures

List of Tables

List of Symbols

v_t true velocity

α angle of attack

h altitude

$\dot{h}$ rate of climb

θ pitch angle

ϕ roll angle

ψ yaw angle

β sideslip angle

p roll rate

q pitch rate

r yaw rate

x state vector

$\dot{x}$ derivative state vector

τ pilot delay

ζ_{sp} short period damping ratio

ω_{sp} short period natural frequency

ζ_p phugoid damping ratio

ω_p phugoid natural frequency

ζ_d Dutch damping ratio

ω_d Dutch natural frequency

T_R roll mode time constant

T_S minimum doubling time for spiral mode

ω_{BW} bandwidth

C_l roll moment coefficient

C_m pitch moment coefficient

C_n yaw moment coefficient

C_{m_α} static pitch stability

C_{m_q} pitch damping

C_{l_p} roll damping

$C_{m_{\delta_e}}$ pitch control derivative

$C_{l_{\delta_a}}$ roll control derivative

δ_a aileron deflection

δ_e elevator deflection

δ_r rudder deflection

δ_t throttle position

List of Acronyms

BADA Base of Aircraft Data

BIUG Background Information and User Guide

CAP Control Anticipation Parameter

CAS Control Augmentation System

DoF Degrees-of-Freedom

FAA Federal Aviation Administration

FAR Federal Aviation Regulation

FDM Flight Dynamics Model

GUI Graphical User Interface

HITL Hardware-In-The-Loop

ISR Intelligence Surveillance Reconnaissance

HOS High-Order System

JSBSim Jon S. Berndt Simulation

LOES Low-Order Equivalent System

MATLAB Matrix Laboratory

MIL-STD Military Standard

MTE Mission Task Element

NACA National Advisory Committee on Aeronautics

NASA National Aeronautics and Space Administration

PIO Pilot Induced Oscillation

PID Proportional Integral Derivative

RPM Revolution Per Minute

RPV Remotely Piloted Vehicle

SAS Stability Augmentation System

SIO System Induced Oscillation

SQP Sequential Quadratic Programming

TIC Theil's Inequality Coefficient

UAS Unmanned Aerial System

UAV Unmanned Aerial Vehicle

UCAV Unmanned Combat Aerial Vehicle

US United States

USAF United States Air Force

USM United States Military

XML eXtensible Markup Language

EVALUATION OF UNMANNED AIRCRAFT FLYING QUALITIES USING JSBSIM

I Introduction

The importance and need of good flying and handling qualities have been evident since the origin of flight beginning with the Wright Flyer. Throughout the development of the airplane, success has been achieved by combining two distinct parameters: maximum performance and adequate flying qualities. Flying qualities are defined as the "stability and control characteristics that have an important bearing on the safety of flight and on the pilots' impressions of the ease of flying an airplane in steady flight and in maneuvers" [39]. Flying qualities help ensure not only performance but also safety in flight. Flying qualities requirements have been extensively researched and specified for fixed-wing and rotary-wing manned aircraft based on a substantial database of assessments. A key issue today in flying qualities is how to extend them to pilotless aircraft. A focus of this research is to provide data in building that substantial database of Unmanned Aerial Vehicle (UAV) characteristics.

1.1 Background

There has been an increased emphasis on the use and importance of UAVs for both military and civilian missions, due to the distinct advantages of having the pilot out of the loop. Duties that were considered "dirty, dull, or dangerous," where exposure of human life was too costly or unsafe, have been increasingly delegated to UAVs [24]. Unmanned aerial systems have significantly fewer limitations, carrying with them the ability to operate in hazardous conditions, darkness, extreme heat,

and other conditions that pose a threat to pilots. Another advantage of UAVs is weight reduction, which is a significant concern in the aviation industry. Weight corresponds to amount of fuel needed during the mission, which links to operational cost. Life support systems and equipment associated with the pilot can be discarded with UAVs—enabling a smaller airframe.

The capabilities of Unmanned Aircraft Systems (UAS) started with tactical reconnaissance and expanded to include most missions within the Intelligence, Surveillance, and Reconnaissance (ISR) fields, eventually branching out to strike missions and force protection. Some UAVs, such as the Predator, are able to detect, acquire, and strike targets significantly shortening the kill chain. Unmanned systems designated for combat missions are known as Unmanned Combat Aerial Vehicles (UCAV). UCAVs are different from previous unmanned systems, because those systems were initially designed to carry out ISR duties. Armaments were later attached to that aircraft frame to carry out air strikes. The UCAV is the evolution of the UAV, representing a more advanced and deadlier offshoot of the UAV aircraft group. Unmanned systems provide diverse capabilities to battlefield commanders across a wide range of military operations. As the capabilities of unmanned systems increase, there is a continued trend of increasing use and dependence on these systems.

Flight data have shown that flight hours dramatically increased between 1996 and 2011, as the potential of UAVs was being realized. With the military operational tempo increased with Operation Enduring Freedom and Operation Iraqi Freedom, the majority of the flight hours represented in Figure 1 are missions flown in support of those operations [55]. As the capabilities of these systems continue to increase, the UAV will continue to see increased use in both the military and civilian sectors.

The reliability of an aircraft is crucial to its acceptance into airspace, whether it is domestic, foreign, or international. With unmanned aerial systems, no human is

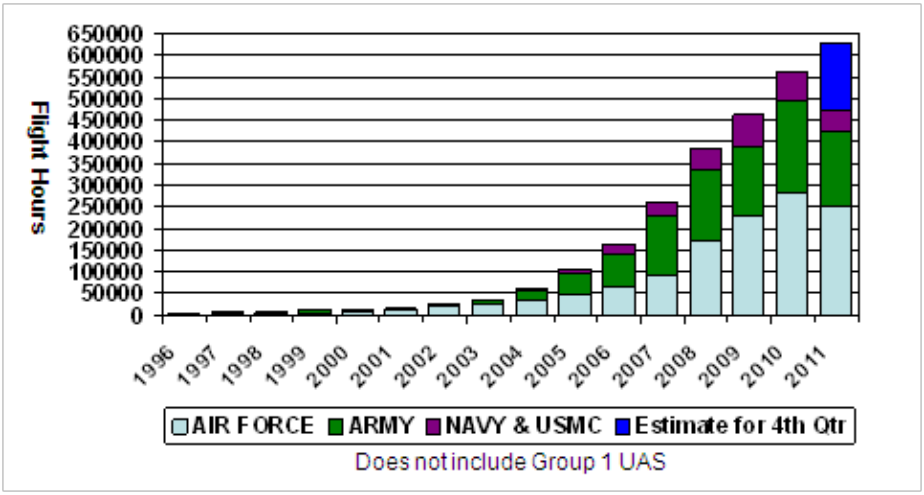

Figure 1. Flight Hours for Unmanned Systems between 1996 and 2011 [55]

onboard the aircraft. As a result, the safety of the pilot is not considered in the same manner as its manned counterparts. Vulnerability reduction techniques, such as component redundancy, active damage suppression, and component shielding, were not heavily incorporated into the initial designs, resulting in high mishap rates. "Historically, UAS have suffered mishaps at one to two orders of magnitude greater than the rate (per 100,000 hours) incurred by manned military aircraft" [8]. Figure 2 shows that as the cumulative flight hours increased along with improved technology, the mishap rates decreased and approached the reliability rates of their military manned counterparts. Unmanned aerial systems were on a "build-fly-fix-fly" philosophy to expedite the development process into the operational field, resulting in high mishap rates early in the process [24]. The cost of fixing such deficiencies could be very high after the aircraft has flown; therefore, it would beneficial to consider operational maneuvers as early as possible in the design phase.

Furthering the reliability of these systems can be viewed under the scope of the overall airworthiness of a system which stems from having rigorous standards in place. Standards and methods of compliance establish a baseline-level of design and performance requirements to safely operate an aircraft. These standards are dependent

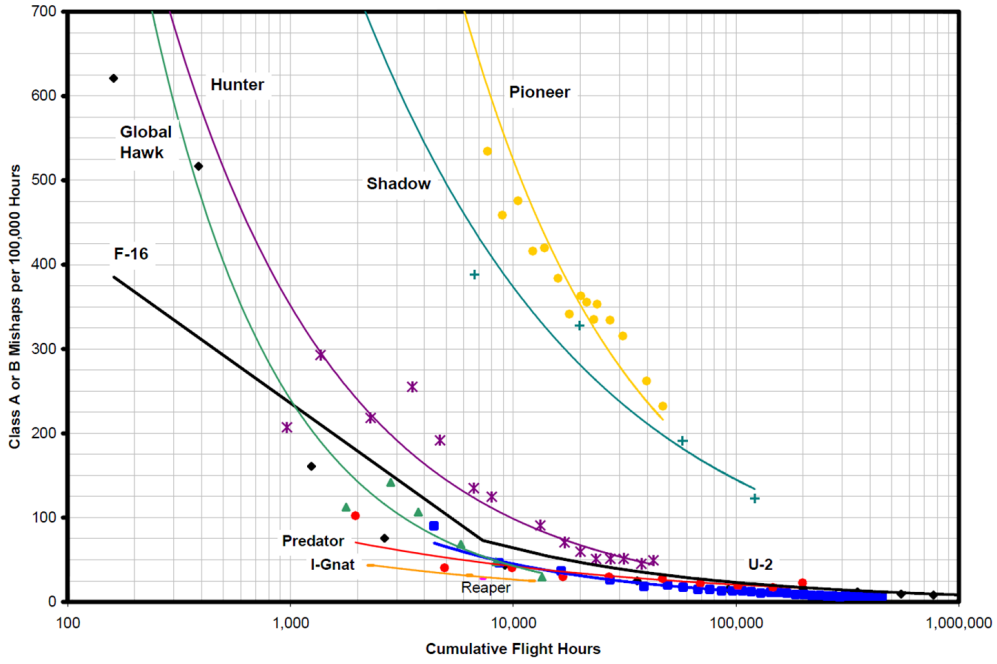

Figure 2. U.S. Military Manned and Unmanned Aircraft Mishap Rates [8]

on an extensive database of flying quality assessments. The ultimate objective of the aircraft/pilot system is to complete a mission or task. The effectiveness of the aircraft in performing the mission is highly valued, which correlates to aircraft flying qualities. While the rapid pace of technology has advanced the UAV, one area that has been lagging is assessing the flying qualities of UAVs.

1.2 Research Problem Motivation and Description

As UAVs become more prevalent, there must be a method to allow the quantification, collection, and standardization of UAV flying qualities data. In doing so, it will allow the designer to incorporate ideal flying qualities during the early stages of a design, rather than redesigning the aircraft due to repeated design errors. The flying qualities are properties of the aircraft, which link directly to mission performance. Superior flying qualities equate to superior mission performance. Before identifying the problem statement, it is necessary to define and differentiate between "flying

qualities" and "handling qualities."

Most military and civilian specifications refer to "flying qualities," not handling qualities. As stated before, flying qualities are defined as the "stability and control characteristics that have an important bearing on the safety of flight and on the pilots' impressions of the ease of flying an airplane in steady flight and in maneuvers" [39]. The intent of UAV flying qualities is to guarantee the safety and operational effectiveness of the aircraft as in the piloted flying qualities. Handling qualities, which differ from flying qualities, are more than just stability and control characteristics. Handling qualities deal with the response characteristics necessary for a human to control the aircraft. According to Cooper and Harper, handling qualities are, "those qualities or characteristics of an aircraft that govern the ease and precision with which a pilot is able to perform the tasks required in support of an aircraft role" [11]. Other factors that influence handling qualities are the cockpit interface, environment, and pilot stress level. Assessing handling qualities is difficult because it is subject to one or more pilot's opinion using a standard Cooper-Harper Handling Qualities Rating Scale.

The flying qualities requirements for fixed-wing manned aircraft is based heavily on the MIL-STD-1797 for guidance on detailed specifications; however, there has been no guide in the application of flying qualities to unmanned systems [1]. There is no requirement for UAVs to abide by the MIL-STD-1797. A database of flight test data and experience is essential in supporting the flying qualities standard, which is lacking for unmanned systems. Furthermore, it is difficult to correlate the manned aircraft flying qualities to UAVs due to the method of how aircraft are classified.

Manned aircraft are divided into four classes in the MIL-STD-1797 based on size, maneuverability, and missions; however, this isn't applicable to UAVs [1]. Typically, manned aircraft performing a certain type of mission are usually similar in terms of

size and maneuverability. For example, larger and less maneuverable manned aircraft typically perform bombing or logistical roles in military aviation. One fundamental problem pertaining to UAVs is that all classes of unmanned systems perform many of the same types of missions—making it difficult to apply the MIL-STD-1797 criteria to unmanned systems. Certain criteria such as stick force gradients do not apply to UAVs, due to the inherent design and operation of UAVs. An ISR type of mission can be completed by either an unmanned aircraft flying over 18000 ft with a weight of over 1320 lbs, or an unmanned aircraft flying below 1200 ft with a weight below 20 lbs. This type of disparity reveals that the current flying qualities standard does not serve as an effective basis for UAVs and necessitates new criteria applicable directly to unmanned systems. Flying qualities are related to mission performance. Without updated requirements and guidelines for UAVs, the lack of a flying qualities standard could jeopardize the effectiveness of future UAVs.

The overall question of the airworthiness of an aircraft is based on its flying and handling qualities, which are objective and subjective in nature respectively. The flying qualities standard was supported by an extensive database of assessments. Without a database to support the criteria, any attempt to establish a flying qualities standard will fail. Therefore, it is the goal of this thesis to provide data on the flying qualities assessments of UAVs in order to propel the development of a UAV flying qualities standard. The data on the flying qualities assessments will include the flying qualities ratings of the aircraft's longitudinal and lateral-directional dynamic modes according to the manned requirements. The manned flying qualities ratings will then be compared to the quantified simulation results to investigate the applicability of manned requirements to unmanned systems.

1.3 Research Objectives

In the absence of flying qualities requirements for UAVs, this research sought to expand this field of research by using an unmanned aircraft model to perform various desired maneuvers and post-processing the results from the simulations. JSBSim is the flight dynamics model (FDM) used to model the aircraft and simulate the flight maneuvers. Unfortunately, there are no UAV JSBSim models available due to the lack of publicly available data. Autopilots used in conjunction with the selected aircraft model will model the autonomous nature of UAVs. For the purpose of the current research, the T-41 Mescalero aircraft, which is a military variant of the Cessna 172 designated for student pilots, will be used. It should be noted that the model in JSBSim is based on the Cessna 172 Skyhawk, but it will be assumed that the variation between the T-41 and Cessna 172 is small enough to be ignored. Due to the fact that more Cessna 172s have been built than any other mass-produced light aircraft in history with its first flight flown in 1955, the Cessna 172 will have a large database to pull information from and validate the simulations [9]. This research builds upon the 2014 work of Lt. Col Greene *Toward a Flying Qualities Standard for Unmanned Aircraft* [24], with the following objectives:

1. Evaluate the flying qualities of unmanned aircraft using JSBSim's capability to simulate maneuvers.
2. Determine how best to analyze the flying qualities for the various maneuvers. Current flying qualities standards (MIL-STD-1797A and ADS-33E) will be a major source for the methods for this analysis.
3. Validate the data and post-processed results by comparing it to known databases for the T-41.

1.4 Thesis Overview

The present chapter provided the background information on the motivation for more research into the area of UAV flying qualities and defined the research objectives. The following chapter will discuss the literature review of the overall context of flying qualities. Following the literature review, the research methodology is described to include detailed explanation of modifications to the JSBSim models and files for the setup of the simulation. It will also include methods to post-process the data and quantify results from the simulation. Once the methodology is explained, the results from the simulation will be presented and evaluated. Current flying qualities standards will be the major source for the methods in the analysis. Finally, the overall conclusions of the research and recommendations for future research will be presented.

II Literature Review

This chapter first reviews the early history of flying qualities with an emphasis on need of a substantial database, in order to form a flying qualities standard. Next, the flying qualities standards for fixed-wing, rotary-wing, and unmanned aircraft will be discussed. Following this, the JSBSim program will be presented and its relationship to the research in flying qualities. Finally, this chapter will provide an overview of the work leading up to this field of research and makes an argument for more research in UAV flying qualities.

2.1 Early History of Flying Qualities

In order to gain a better understanding of the current state of UAV flying qualities, the historical dimension of flying qualities must be examined. The very first US military flying qualities requirement came not long after the birth of aviation. In 1908, the U.S. Army Signal Corps issued Specification 496 for the acquisition of a heavier-than-air machine [3]. In this one page document, there was only one sentence pertaining to flying qualities. It stated that the aircraft, "must be steered in all flight directions without difficulty and at all times under perfect control and equilibrium" [3]. The subjective nature of this sentence left its interpretation to qualitative terms with no design guidance. The terms "without difficulty" and "perfect" are left completely dependent on the pilot's evaluation. What may be perceived as "difficult" may not be necessarily difficult for another pilot. There did not exist a scientific quantitative evaluation of the aircraft's flying qualities at this time.

In the 1930s, the needed art and science of flying qualities did not see extensive progression. *The Army Air Corps Designers Handbook* encompassed flying qualities requirement into one sentence stating that "the stability and control characteristics

must be satisfactory" [53]. There were still no objective requirements specified for flying qualities. Capt. Hatcher captured the situation best in his words:

> At present we simply specify that the airplane shall be perfect in all respects and leave it up to the contractor to guess what we really want in terms of degree of stability, controllability, maneuverability, control forces, etc. He does the best he can and then starts building new tails, ailerons, etc. until we say we are satisfied [25].
>
> – Capt Robert S. Hatcher

During this time, there was a limited understanding of aerodynamics, stability, and control. To further the problem, there were no air data measuring and recording systems. There was no database of flying quality assessments to support the criteria needed for a standard. In addition, a method of correlating pilot opinion with engineering theory did not exist. The culmination of these problems made it difficult to quantify flying qualities requirements.

In the late 1930s, the National Advisory Committee on Aeronautics (NACA) spearheaded a research effort in flying qualities to provide quantitative design criteria. Flying qualities requirements were tested using more than 60 airplanes and simulated cockpits for the flight data [28]. The combination of aircraft design analysis, flying qualities data, and pilot comments formed the initial foundation to start their efforts. Now that this flying quality assessment database was formed, the beginnings of a flying qualities standard could now commence. The culmination of all the work up to this time produced NACA Report 755, *Requirements for Satisfactory Flying Qualities of Airplanes*, published in 1943 [21]. With sections on longitudinal stability and control, lateral stability and control, and stall characteristics, NACA Report 755 was one of the first efforts to set actual specifications for flying qualities [21]. It may be argued that the first real flying qualities standard was this document written by Gilruth, paving the way for objective flying qualities criteria.

Following a set of quantitative design criteria culminates in an aircraft that pilots can characterize as having adequate handling qualities. The NACA provided flying qualities data were instrumental in providing the initial foundation for a flying qualities standard. By studying the correlation of various design parameters and pilot ratings from a large database of past aircraft, aircraft flying qualities ratings can be predicted before the aircraft is actually built. With a flying qualities assessment to support the criteria, the area of flying qualities was able to move forward toward a flying qualities standard.

During a flying qualities investigation, two types of data are analyzed. The first and foremost is the subjective pilot opinion of the aircraft's handling characteristics. Pilot opinion is gathered through the use of the Cooper-Harper Handling Qualities Rating Scale to standardize the data. The second is the quantitative data on static stability, natural modes of motion, and other physical characteristics of the aircraft. Together, the subjective and quantitative data determine the flying and handling qualities, determining the overall airworthiness of an aircraft.

2.2 Manned Fixed-Wing Standards

MIL-STD-1797 was a product of its predecessor, MIL-F-8785; thus, it is important to understand how MIL-STD-1797 came about. The MIL-F-8785 Series was the first tri-service flying qualities specification published in August 1969 as MIL-F-8785B(ASG) [32]. Aircraft dynamics modes were quantified for the short period, phugoid, dutch roll, and spiral modes in terms of natural frequencies and damping ratios. The defining characteristics for certain types of aircraft were defined from years of operating the aircraft. The Background Information and User Guide (BIUG) for MIL-F-8785B(ASG) was published the same year in 1969—explaining the rationale for the specifications and what it was based on [32]. The MIL-F-8785B was revised

and republished in 1980 as MIL-F-8785C [32]. The BIUG was updated and republished as the Background Information and User Guide for MIL-F-8785C in 1982 to complement the latest version of the 8785 series [32].

In 1987, MIL-STD-1797 was published, significantly advancing the field of flying qualities [32]. The MIL-STD-1797 series incorporated the BIUG into the flying qualities specification and included discussion about bandwidth requirements. The MIL-STD-1797 now included the Cooper-Harper Rating Scale, which was widely used throughout the world but not officially adopted [1]. The adoption of the Cooper-Harper Rating Scale was instrumental in standardizing pilot opinion data.

The MIL-STD-1797 was further revised and republished in 1990, bringing about MIL-STD-1797A [32]. At the same time, there was a shift in flying qualities. There was consideration of eliminating flying qualities standards and instead following the Federal Aviation Administration (FAA) requirements [31]. The FAA requirements, however, are primarily concerned about safety and not about superior flying qualities. This lack of concern for superior flying qualities equated to suboptimal mission performance. As a result, the MIL-STD-1797 was readopted as the flying qualities standard and further updated. The latest version was published in 2006 as MIL-STD-1797B [31].

2.2.1 Cooper-Harper Rating Scale

The Cooper-Harper scale was a pilot rating scale standardizing the way to test the handling characteristics of an aircraft, leading to the correlation of pilot opinion with engineering theory. One of the main reasons for the Cooper-Harper scale's universal adoption in the flying qualities region was its use of a decision tree, and the answers to a series of questions led to a pilot rating. The pilot determines if the aircraft was: 1) controllable, 2) if adequate performance is attainable with a tolerable

pilot workload, 3) if the aircraft is satisfactory without improvement. The relative ease of use and simplicity made the Cooper-Harper scale very attractive. A rating of 1 considers the aircraft to be excellent, while a rating of 10 considers the aircraft to be uncontrollable. The Cooper-Harper scale provides a consistent standard among pilots across a broad range of aircraft, which is essential when analyzing the test results. The Cooper-Harper Rating Scale, as seen in Figure 3, has been adopted into the current flying qualities standard, MIL-STD-1797 [1].

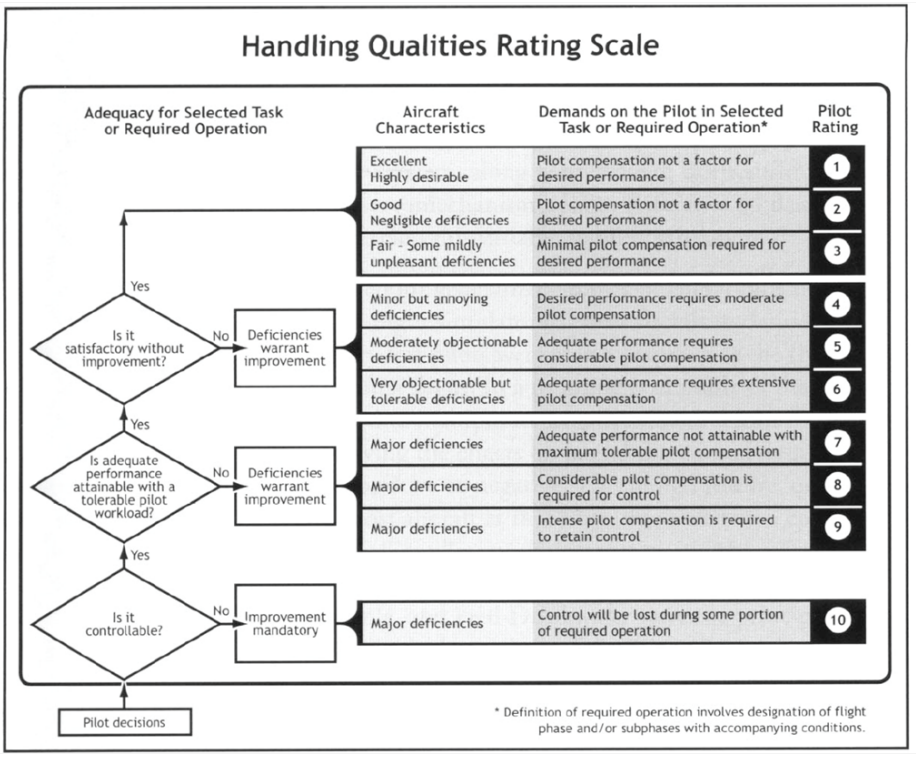

Figure 3. Cooper Harper Pilot Rating Scale [1]

The Cooper-Harper ratings can be roughly related to handling characteristics levels. Level 1 is satisfactory, Level 2 is acceptable, and Level 3 is controllable [1]. A Level 1 aircraft has flying qualities clearly adequate for the mission flight phase. Desired performance is achievable with no more than minimal pilot compensation. A Level 2 aircraft has flying qualities adequate to accomplish the mission flight phase,

but some increase in pilot workload or degradation in mission effectiveness, or both, exists. A Level 3 aircraft has flying qualities, such that the aircraft can be controlled in the context of the mission flight phase, even though pilot workload is excessive or mission effectiveness is inadequate, or both. Levels apply to aircraft performing a mission task, while Cooper-Harper ratings are given by a pilot performing the task with the aircraft in a given environment. As a result, the Cooper-Harper rating can vary depending on environmental conditions. Having stated these caveats, given a well-defined task in a "calm-to-light" environment, the levels closely correspond to 1 to 3, 4 to 6, and 7 to 9 Cooper-Harper ratings.

2.2.2 Aircraft Classification and Flight Phase Category

Aircraft classification in the MIL-STD-1797 is based upon maximum design gross weight and flight limit load factor [1]. For example, high-performance aircraft, such as fighters and attack aircraft, are classified under high-limit load factor typically weighing in-between 5,000 and 100,000 lbs. The flying qualities are expected to be a function of the aircraft type: fighter, bomber, or transport. MIL-STD-1797 has four basic aircraft classifications [1]. Class I aircraft are small, light aircraft with low maneuverability. Class II aircraft are medium-weight aircraft with low-to-medium maneuverability. Class III aircraft are heavy-weight aircraft with low-to-medium maneuverability. Class IV aircraft are high-maneuverable aircraft. Table 1 lists the various characteristics of each aircraft class.

The aircraft classification scheme can also be depicted graphically. Figure 4 is a graphical depiction of the aircraft classification, based on load factor and maximum gross weight. Figure 4 shows that aircraft can fall into multiple classes. If that is the case, flying qualities requirements from those corresponding classes may be combined.

Flying qualities not only depend on the aircraft type, but also on the phase of

Class I – Small light aircraft such as:	Light utility Primary trainer Light observation
Class II – Medium weight, low-to-medium maneuverability aircraft such as:	Heavy utility/search and rescue Light or medium transport/cargo/tanker Early warning/electronic countermeasures/airborne command,control, or communications relay Antisubmarine Assault transport Reconnaissance Tactical bomber Heavy attack Trainer for Class II
Class III – Large, heavy, low-to-medium maneuverability aircraft such as:	Heavy transport/cargo/tanker Heavy bomber Patrol/early warning/electronic countermeasures/airborne command, control, or communications relay Trainer for Class III
Class IV – High-maneuverability aircraft such as:	Fighter-interceptor Attack Tactical reconnaissance Observation Trainer for Class IV

Table 1. Aircraft Classification in MIL-STD-1797 [1]

the mission. MIL-STD-1797 has three basic flight phases [1]. Category A Flight Phase involves high-precision and high-workload tasks, such as air-to-air combat, aerial refueling, and terrain following. Category B Flight Phase are the nonterminal non-precision tasks, such as climb, cruise, and descent. Category C Flight Phase is the terminal task of takeoff and landing.

2.2.3 Lower Order Equivalent System

Modern aircraft employ automatic flight control systems that modify the dynamic response according to the control laws, sensors, filters, and actuators. The complexity associated with these control systems is the result of desired performance and control characteristics. One method of simplifying a complex high-order system (HOS) such as an aircraft in evaluating the complex aircraft control system is using a low-order equivalent system (LOES). The LOES takes a high-order dynamic model and extracts the reduced-order realization. The LOES methodology yields a set of guidelines for pilot input to aircraft response in the form of transfer functions that are simplified

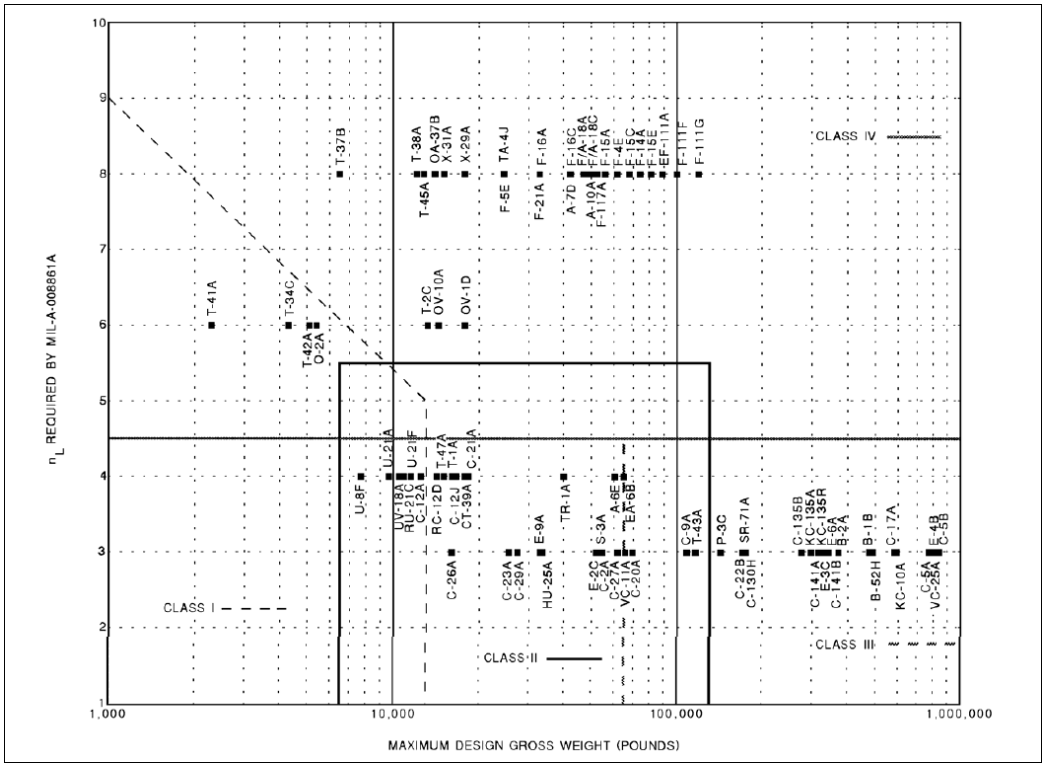

Figure 4. Aircraft Classification in MIL-STD-1797 [1]

models of the total aircraft response. The question now arises if LOES can be applied to UAVs or if the dynamic responses lost are critical to its flying qualities. MIL-STD-1797 presents a process to analyze the mismatch between HOS and LOES by evaluating the error in gain and phase [1]. Figure 5 shows the maximum envelope allowed with the difference between the HOS and LOES falling between the black limit lines. By minimizing the following cost functional for discrete frequencies:

$$J = \frac{20}{n} \sum_{\omega_1}^{\omega_n} [(G_{HOS} - G_{LOES})^2 + .02(\phi_{HOS} - \phi_{LOES})^2] \tag{1}$$

where J is the cost, n is the number of discrete frequencies, G is the gain in decibels, and ϕ is the phase in degrees, the parameters for the LOES can be extracted. Once the parameters for the LOES are set, the gain and phase difference between the HOS and LOES are plotted in-between the envelopes. The envelopes are used only after

the matching process has been performed. The envelopes represented by the black lines in Figure 5 represent the LOES boundaries for matching high-order to low-order transfer functions. The blue line in Figure 5 is the difference between the HOS and LOES, which falls in between the envelope lines; hence, the mismatch between the HOS and LOES is not significant. If the mismatch were to lie outside the envelope, it could be suspected that the equivalent parameters may not accurately predict pilot opinion. If this application were to extend to UAVs, the error envelope reflects how well the lower-order model matches the actual model.

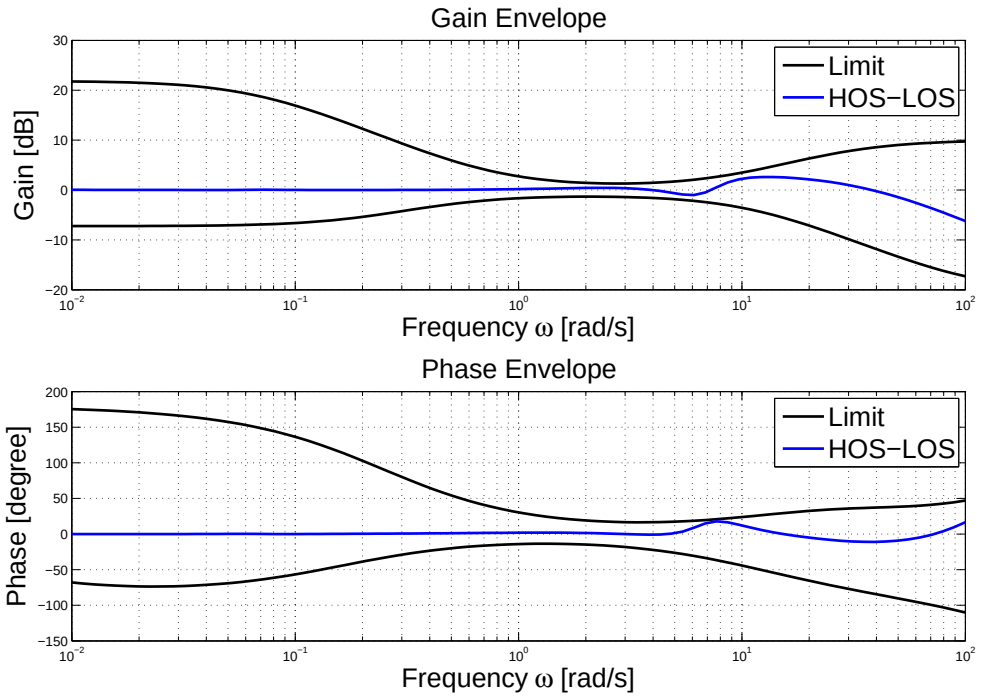

Figure 5. Envelopes of Maximum Unnoticeable Added Dynamics Example

2.2.4 Literal Factors to Predict Flying Qualities

Literal factors have proved effective in determining the handling qualities of the aircraft. Literal factors are those parameters which correlate strongly between aircraft stability and control characteristics and pilot opinion. Bihrle introduced the concept

of the control anticipation parameter (CAP) [27]. CAP is defined as the ratio of the instantaneous acceleration in pitch, $\dot{q_0}$, to the steady-state change in load factor, Δn_{ss}.

$$CAP = \frac{\dot{q_0}}{\Delta n_{ss}} \tag{2}$$

It is considered one of the earliest and most-used piloted flying qualities criteria—especially in unaugmented aircraft. The importance of this parameter is based on the ability to make precise adjustments in the flight path. If the CAP is too small, the pilot will not sense the change in acceleration, $\dot{q_0}$, and the pilot will continue to apply more control resulting in a large change in the steady-state load factor. As a result, the desired response is exceeded, and the response is described as sluggish. On the other hand, if the CAP is too large, the pilot will sense a large acceleration, $\dot{q_0}$, when the controls are moved. Consequently, the pilot will tend to undershoot the desired path, and the response is described as too sensitive. The equation for CAP can be further reduced as shown in Equation 3, where ω_{sp} is the short period frequency, and n/α is the load factor response to angle of attack [27].

$$CAP = \frac{\omega_{sp}^2}{n/\alpha} \tag{3}$$

Utilizing CAP and the short-period damping factor, ζ_{sp}, Figure 6 guides to a Level I, II, or III aircraft depending on the Flight Phase Category [1]. A noticeable feature of Figure 6 is the large area corresponding to Level 1 flying qualities for Flight Phase Category B. Flight Phase Category B includes non-terminal maneuvers such as climb, cruise, and descent. For such non-precision tasks, aircraft tend to have good flying qualities. As the maneuvers become more difficult and complex, it becomes more difficult to achieve Level 1 flying qualities. For Category A and C Flight Phases, the

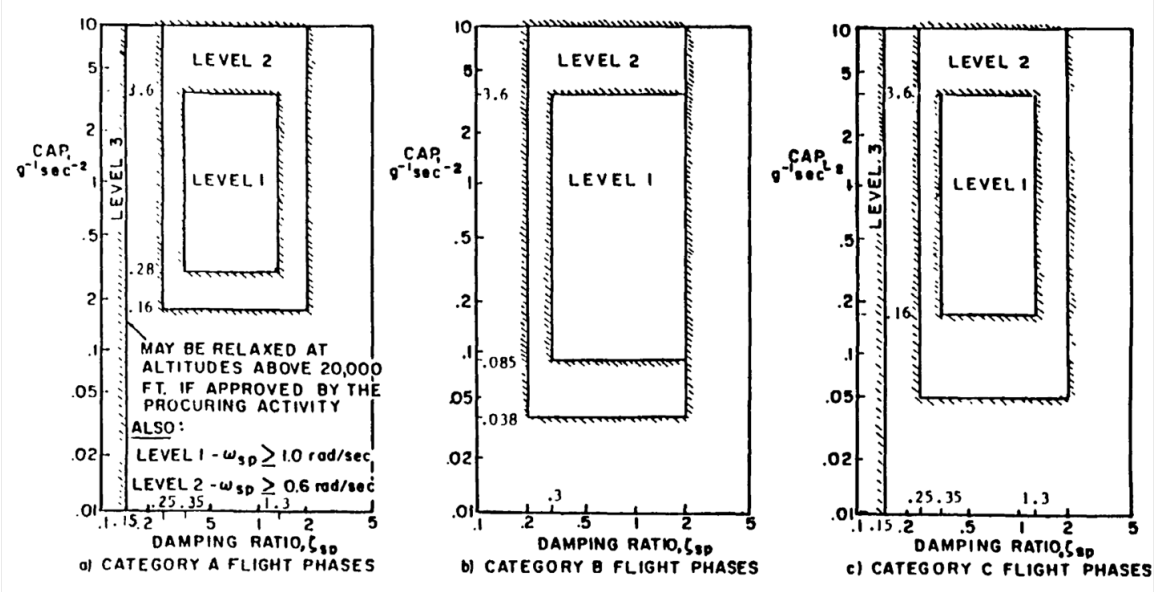

Figure 6. Short-period Dynamic Requirements [1]

target for Level 1 flying qualities has shrunk, and there is a limit on even Level 3 flying qualities. Concurrent with this criteria is the requirement on the equivalent pitch time delay, τ_θ. Level 1 flying qualities requires τ_θ to be less than 0.10 seconds; Level 2 flying qualities requires τ_θ to be less than 0.20 seconds; and Level 3 flying qualities requires τ_θ to be less than 0.25 seconds [1].

Another method of using literal factors to predict flying qualities uses $\omega_{sp}T_{\theta 2}$ instead of CAP [1]. CAP is proportional to $\omega_{sp}^2 T_{\theta 2}$; therefore, $\omega_{sp}T_{\theta 2}$ is a similar literal factor to CAP. As seen in Figure 7, the same trends can be seen as in the previous criteria as expected.

The transient response literal factors can provide insight into pilot ratings. By examining the transient response of the aircraft pitch response to a step input of pitch controller force, various time response characteristics such as transient peak ratio, effective rise time, and effective time delay can be correlated to pilot opinion [1]. Figure 8 is a graphical depiction of the transient peak ratio, effective time delay, and effective rise time.

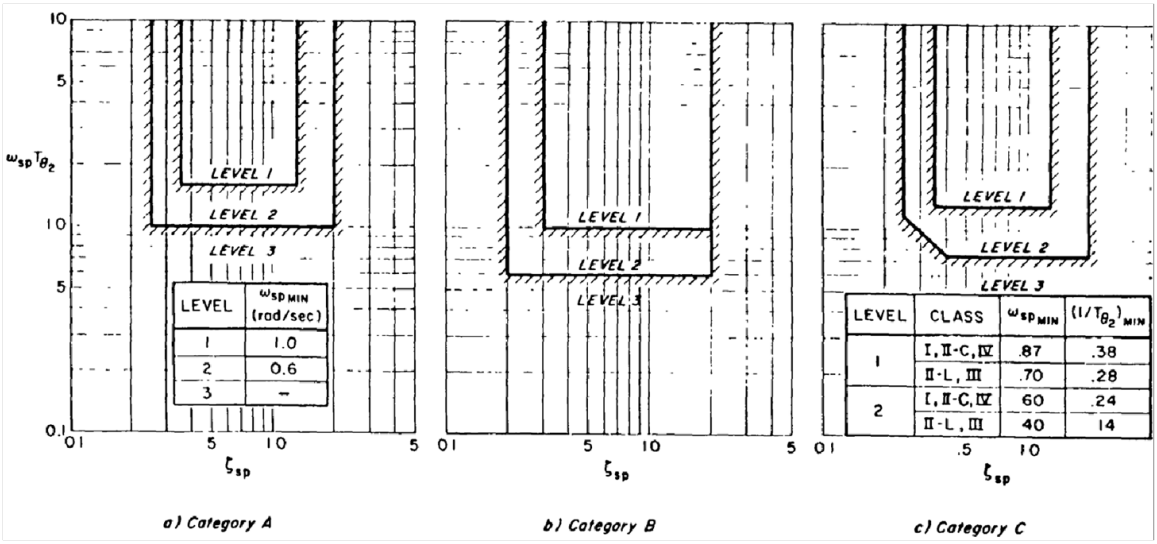

Figure 7. Short-period Pitch Response to Pitch Controller [1]

MIL-STD-1797 specifies requirements on the transient response literal factors for Levels 1, 2, and 3 flying qualities [1]. Table 2 contains the requirements for the equivalent time delay, t_1, and transient peak ratio $\frac{\Delta q_2}{\Delta q_1}$. Table 3 contains the specifications for effective rise time, which is the analog of CAP, where V_t is the true airspeed in feet per second.

Table 2. Equivalent Time Delay and Transient Peak Ratio Requirements[1]

Level	**Equivalent Time Delay t_1**	**Transient Peak Ratio $\frac{\Delta q_2}{\Delta q_1}$**
1	$t_1 \leq .12$ sec	$\frac{\Delta q_2}{\Delta q_1} \leq .30$
2	$t_1 \leq .17$ sec	$\frac{\Delta q_2}{\Delta q_1} \leq .60$
3	$t_1 \leq .21$ sec	$\frac{\Delta q_2}{\Delta q_1} \leq .85$

Table 3. Rise Time Values[1]

	Nonterminal Flight Phases		**Terminal Flight Phases**	
Level	Min Δt	Max Δt	Min Δt	Max Δt
1	$9/V_t$	$500/V_t$	$9/V_t$	$200/V_t$
2	$3.2/V_t$	$1600/V_t$	$3.2/V_t$	$645/V_t$

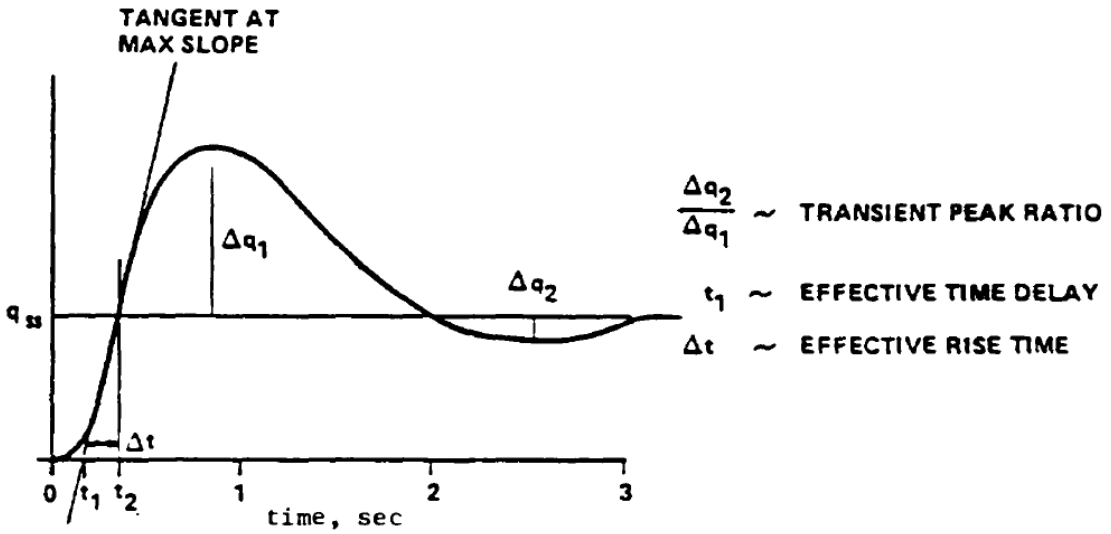

Figure 8. Transient Response Parameters [1]

2.2.5 Bandwidth and Time Delay Criteria

The bandwidth and time delay criteria examine the stability margins of the pilot closed loop system. The gain and phase margins provide a picture of the robustness of the overall system. A benefit of using this criterion is that a LOES does not need to be determined. For very complex and highly-augmented aircraft, the bandwidth criterion proves to be very beneficial. The bandwidth, as defined for this criterion, is the highest frequency at which the phase margin is at least 45 degrees and the gain margin is at least 6 dB [1]. Both criteria must be met. With the gain and phase margin parameters, the system is quite robust allowing the pilot to increase the gain and time delay without causing aircraft instability. The time delay, τ_p, is defined as:

$$\tau_p = \frac{-\phi_1 - 180^\circ}{57.3\omega_1} \tag{4}$$

where ω_1 is some frequency greater than the frequency for neutral stability and ϕ_1 is the associated phase. From ω_1 and ϕ_1, the flying qualities can be predicted using Figure 9.

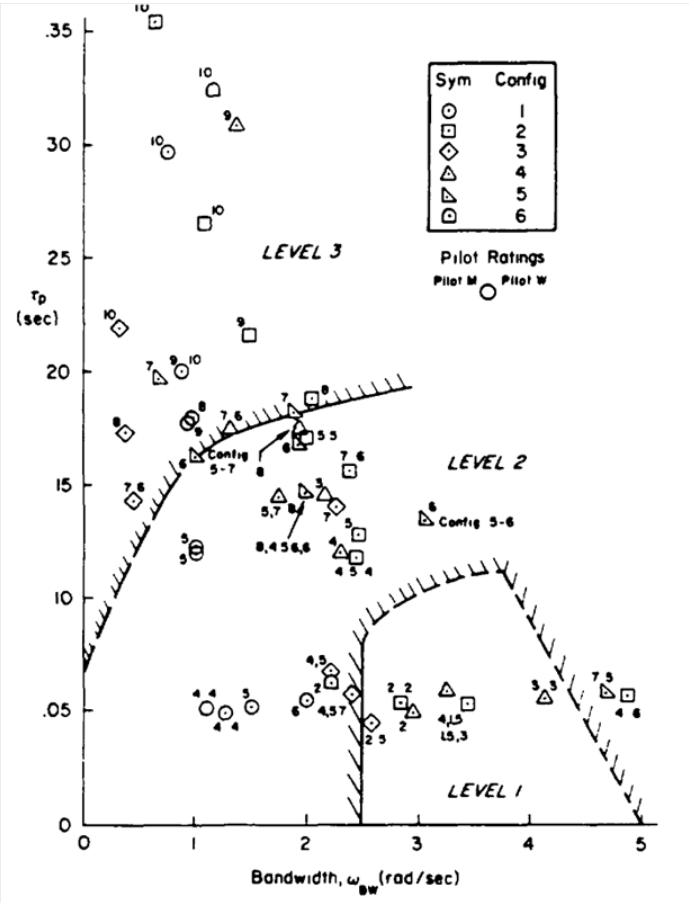

Figure 9. Bandwidth Requirements [1]

2.2.6 Neal-Smith Criteria

The Neal-Smith criteria are based on a database of piloted data to assist in the development of flying qualities. The Neal-Smith criteria assume a simplified pilot model in the evaluation of the closed-loop system. The modified Neal-Smith criterion states that bandwidth is defined as the frequency at which the closed-loop phase is -90 degrees [1]. The bandwidth requirement varies according to the flight phase, as seen in Table 4. Unlike the bandwidth criterion, the minimum closed-loop pitch attitude tracking bandwidth is specified for each flight phase. The closed-loop droop should be no more than -3 dB for Level 1 and 2 aircraft [1]. The closed-loop resonance should be no more than 3 dB for Level 1 and 9 dB for Level 2 flying qualities. It

should be noted that this criterion is geared towards piloted aircraft and may not be applicable to unmanned systems. The closed-loop and open-loop transfer functions can be directly related by a Nichols chart, as seen in Figure 10. As with the bandwidth and time delay criteria, an advantage of the Neal-Smith criteria is that a LOES does not need to be extracted.

Table 4. Neal-Smith Criteria for Bandwidth [1]

Flight Phase	Bandwidth
Category A	3.5 rad/s
Category B	1.5 rad/s
Landing	2.5 rad/s
Other Category C	1.5 rad/s

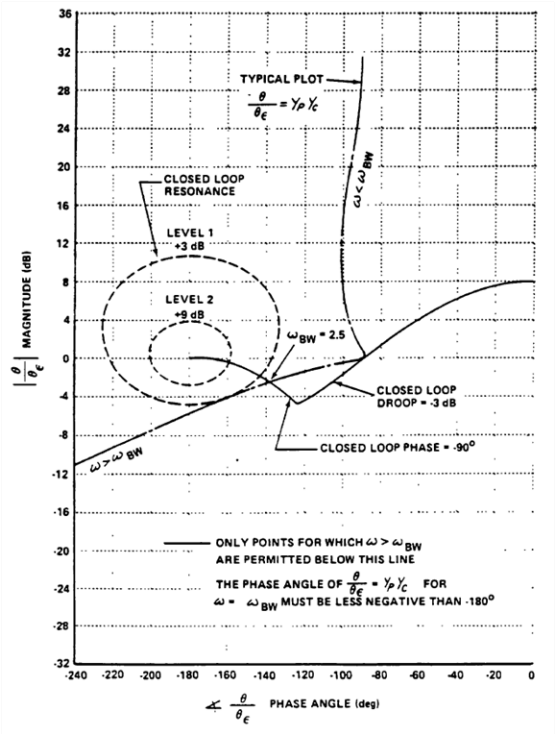

Figure 10. Design Criteria for Pitch Dynamics with the Pilot in the Loop [1]

2.3 Manned Rotary-Wing Standards

Just like MIL-STD-1797's predecessor is MIL-F-8785, the predecessor to ADS-33-PRF is MIL-H-8501 [32]. By first examining MIL-H-8501, a deeper understanding of the current regulation on rotary-wing aircraft will be obtained. The first rotorcraft flying qualities specification was MIL-H-8501, published in 1952, and later superseded by MIL-H-8501A in 1961 [31]. The main components consisted of "simple time-domain parameters such as control stick force and position gradients with speed; frequency and damping of oscillatory modes; normal acceleration response to a step input; and angular displacements in response to control steps that are a function of the helicopter weight" [32]. There was no background information or user guide to explain the rationale for the various criteria. In addition, MIL-H-8501 did not address the cross coupling characteristics exhibited by helicopters. In the fixed-wing community, pitch can be separated from yaw and roll. The rotorcraft community realized that the standards of fixed-wing aircraft were not suitable to the application of rotorcraft for their distinctive roles and missions.

In the late 1960s and early 1970s, the next generation rotorcraft were in design or entering operation and were significantly more complex than their predecessors. The MIL-H-8501 became obsolete; a much-needed revision came in the 1980s with the U.S. Army-led development of Aeronautical Design Standard 33 (ADS-33), based upon a large assembled database [37]. The required database was essential in the establishment and validation of a new flying qualities criteria. The absence of a database of flying qualities assessments was a major factor in the failure of MIL-H-8501 as a flying qualities standard [24].

ADS-33 was continually revised until its current state as ADS-33E-PRF, released in 2000 [32]. ADS-33 reflected criteria needed to operate in the extreme conditions for modern helicopters. It contained frequency-domain requirements and the interactions

of visual cuing and displays. A departure from the manned fixed-wing flying qualities standard, ADS-33-PRF included the first specific mission tasks to define adequate handling qualities. Examples of Mission Task Elements (MTEs) are hover, landing, and turn to target. The MTEs categorize the tasks according to aggressiveness and precision.

Mission-oriented flying qualities made the link between the internal attributes of the aircraft and external factors of the environment [20]. Internal attributes of the aircraft included the airframe, flight control system, and cockpit ergonomics. The external environment consisted of the mission task element and external influences like atmospheric disturbances. ADS-33E-PRF directly connects mission task elements to the required agility. "The required agility and required response types together define which boundaries of the handling qualities design criteria apply and which performance standards must be met" [32]. This systems engineering type of approach was accomplished by first defining the mission tasks that are then used to establish performance requirements for those mission tasks. Flight tests validated the performance of those mission tasks.

2.4 Unmanned Aerial Vehicle Standards

AFFDL-TR-76-125, Remotely Piloted Vehicle (RPV) Flying Qualities Design Criteria, is the only type of flying qualities standard for unmanned systems; however, it was published as a technical report in 1976 to propose certain criteria [24]. As a result, it is not a true flying qualities standard that has to be abided by. AFFDL-TR-76-125 was Phase II of a program plan to develop an RPV Flying Qualities Specification [24]. The primary purpose of Phase II was to form a framework for RPV flying qualities criteria that could be later validated through simulation and analysis. While the issue of stability augmentation was addressed, the command and control augmenta-

tion and automation levels were not mentioned; however, it did state that the entire system must be considered. This foresight came with the understanding that interaction between all subsystems of the UAV was yet to be fully comprehended. That entire system is now referred to as an unmanned aerial system (UAS) consisting of the bare airframe, augmentation systems, automatic and manual control, command and control, communication links, pilot console, displays, and controls [24].

AFFDL-TR-76-125 does not deal with autonomous aircraft control in enough detail to be applicable to modern autonomous UAVs. RPVs differ from UAVs by the fact that they are not autonomous systems, but the pilot is not physically in the airframe for RPVs. AFFDL-TR-76-125 defines an RPV as an "unmanned air vehicle which has the capability of being controlled by a remote operator during some flight phase of an operational mission" [41]. A central theme found in the manned flying qualities documents is the optimization of the pilot-aircraft interface. With the direct pilot-aircraft interface being replaced by augmented systems, the desired mission performance should no longer be directly linked to a pilot's ability to perform the task. Instead, UAV flying qualities should focus on the ability to achieve the mission objectives without the constraint of human intervention [7].

Initial efforts focused on adapting piloted specifications for UAVs, but this has proven difficult. One of those challenges is the classification of UAVs. Traditionally, UAVs have been designed and developed for specific missions and tasks. One such example is the use of UAVs to conduct airborne mining exploration [54]. Fixed-wing and rotary-wing manned aircraft are prone to high risk if utilized due to the low operational altitude and speed. This UAV is designed to operate at altitudes below 400 feet where turbulence, ground obstacle clearance, and radio frequency communications are major challenges. The airframe design and equipment to operate in such a harsh environment are tailored to meet those demands unique to a mining

exploration mission. The flying qualities specified in piloted requirements may be applicable to UAVs if the focus is shifted from the pilot to the sensor.

AFFDL-TR-76-125 classifies RPVs into four classes principally by maneuvering capability and aircraft size: Class I are small, light miniature RPVs; Class II are low-maneuverability RPVs; Class III are medium-maneuverability RPVs; Class IV are highly maneuverable RPVs [41]. The aircraft classification system for RPVs has a striking similarity to the manned fixed-wing aircraft classification at that time, MIL-F-8785B, which also had four classes.

The smaller size of UAVs poses weight advantages but also presents some challenges not frequently encountered by piloted aircraft. Aerodynamic effects that are frequently small for large aircraft can become quite significant for small UAVs. "Fundamentally these smaller aircraft respond to disturbances differently than their larger counterparts due to the low Reynolds Number effects that amplify turbulent flow effects and that would be considered insignificant in high Reynolds Number airflow" [12]. Williams recognized the challenges in the flying qualities evaluation due to the absence of control stick force feedback, absence of vibration and buffet response, and higher sensitivities in the longitudinal, directional, and lateral direction arising from the small size of the UAV [54]. Together, these areas are another aspect of UAVs that must be taken into consideration.

One of the principal differences between AFFDL-TR-76-125 and MIL-STD-8785B is the use of four flight-phase categories, as compared to the three categories in the manned flying qualities standard [41]. The four flight phases are based on maneuvering, tracking, and flight path control requirements. Category A Flight Phase requires rapid maneuvering, precision tracking, and/or precise flight path control. Category B Flight Phase involves gradual maneuvers without precision tracking such as climb, cruise, or descent. Category C Flight Phase is the launch and recovery portion requir-

ing high precision. Category D Flight Phase is also a launch and recovery flight phase but does not require high precision tracking such as a catapult takeoff or parachute descent.

The National Research Council conducted a study of National Aeronautics and Space Administration's (NASA's) aeronautics technology programs in 2004 highlighting the pursuit of research in flight controls and handling qualities for UAVs [14]. In identifying key technology areas that should be pursued, the report states:

> NASA's past work in flight controls and handling qualities provided the reference standard for today's system designs. However, as we move toward unmanned systems, the existing standards which are for manned systems, may be too restrictive. Further evolution of the base work done by NASA to include unmanned systems is essential to creating a competitive advantage for U.S. products as this market becomes more price-driven [14].

NASA's research has been a vital asset to military and commercial application. Due to NASA's competencies during the 1960s, 1970s, and 1980s, the U.S. aerospace industry took the dominant position worldwide. The need to further refine the current flying qualities and adapt them to unmanned systems will benefit both military and civilian interests.

2.5 JSBSIM Background

JSBSim is an open source, "lightweight, data-driven, non-linear, six-degree-of-freedom (6DoF), batch simulation application aimed at modeling flight dynamics and control for aircraft" [5]. A flight dynamics model is the mathematical representation of the steady-state performance and dynamic response. "The fundamental goal of flight dynamics modeling is to represent the flight motion numerically, as close to the flight motion in the real world as the applications need" [36]. This realistic environment allows the testing of components, such as autopilot controllers, in extreme conditions

before their implementation. Other applications of flight dynamics modeling is the prediction of stability and flying qualities of unmanned systems. The response of the vehicle for specific control commands can be obtained, which is necessary for flight characteristics data.

JSBSim had its origins back in 1996 beginning as a batch simulation application to model flight dynamics and control systems for aircraft. It is written in the C++ programming language with the equations of motion and flight dynamics derived in Stevens and Lewis [50] and Zipfel [57]. JSBSim can perform simulations of various aircraft relying on a model specification written in extensible markup language (XML) format. Although JSBSim is written in C++, JSBSim is driven by external XML-scripts. "XML is a text-based language from the World Wide Web Consortium (W3C) that supports the use of tags to describe structured data" [19]. Due to JSBSim's open source nature, users have access to the internal of the models, making JSBSim an attractive software tool. Users can modify the model if the available model is not the exact variation needed. JSBSim has been accepted as a tool in academia in aircraft design and control courses and intended to be useful to advanced aerospace engineering students.

JSBSim has also been incorporated into a larger flight simulation architecture being integrated with the FlightGear project in 1999 [5]. FlightGear is a "sophisticated, full-featured, desktop flight simulator framework for use in research or academic environments, for the development and pursuit of interesting flight simulation ideas, and as an end-user application" [4]. JSBSim remains the current default flight model for FlightGear. JSBSim and FlightGear together drive a motion base simulator at the University of Naples to analyze risk levels of near-ground flight operations. Outerra and OpenEaagles are other simulation environments that have also integrated JSBSim as their flight dynamics model [44].

JSBSim has been used in hardware-in-the-loop (HITL) simulations. Hardware-in-the-loop simulations use the actual aircraft avionics and most importantly the flight control system [26]. "The primary uses of HITL simulations are for pilot training, flight control system software validation, and failure modes effects testing (FMET)" [26]. JSBSim has been used in the HITL testing of the Aerocross Echo Hawk UAV with the core simulation code being unaltered JSBSim code [5]. In addition, JSBSim was also used in the HITL simulation and pilot/operator training at duPont Aerospace Company to test a vertical takeoff fan jet transport plane concept.

In terms of research purposes, JSBSim provides an accurate depiction of the flight dynamics and controls. One research effort focused on the integration of unmanned and manned aircraft in the same airspace [22]. JSBSim in conjunction with FlightGear modeled an unmanned aerial system and evaluated the flight performance for Base of Aircraft Data (BADA). BADA is the current standard for data used in air traffic control analysis. By creating models in JSBSim with sufficiently high fidelity, it allowed researchers to assess the impact of unmanned systems on the airspace management infrastructure. The estimated flight performance was compared to experimental wind tunnel testing to check the accuracy. One test case initialized the aircraft in free fall to determine if stability augmentation systems were needed to assist with manual flight. Another test scenario validated that the control surfaces were functioning correctly.

In a study by Risse et al., JSBSim modeled the aircraft's flight dynamics to determine its flying qualities for preliminary aircraft design [44]. The flying qualities analysis requires a thorough knowledge of aircraft stability and control derivatives in addition to an accurate flight dynamics model. JSBSim simulated the desired flight maneuvers and the time responses were recorded. The flying qualities were calculated from the corresponding aircraft reactions. The analysis determined if the

flying qualities were indeed adequate with respect to certification requirements. The United States military standard [1] laid out the quantified criteria for flying qualities evaluation. "The modular buildup scripts of the integrated JSBSim software allow for easy design and integration of feedback control structures and to analyze the influence of flying qualities characteristics" [44]. JSBSim was found to be the most convenient approach for this study. Automatic control systems were easily incorporated into the model and the influence it had on flying qualities were analyzed; thus, a general impression was formed by examining if it produced the intended results. The details about the JSBSim model specific for this research and its implementation will be explained in Chapter III.

2.6 Previous UAV Flying Qualities Research

Much of the work to date has been on remotely-piloted vehicles (RPVs). The guidance on unmanned systems, AFFDL-TR-76-125, is focused on RPVs based on MIL-F-8785B, which was the manned fixed-wing flying qualities standard of the time. The U.S. Naval Air Warfare Center evaluated the application of flying qualities of manned aircraft to RPVs [7]. This study concluded that mission relatable tasks need to be well defined for RPVs along with flight phases. An example of a mission-relatable task is landing the aircraft where the measured tolerance is the distance from the runway centerline. The performance of the landing can be easily quantified and can be compared to the desired and acceptable ratings.

In an effort to propose the development of new flying qualities specific to UAV platforms, one study suggested that the final UAV specification be a combination of adapted pilot specifications and new performance-based requirements [28]. Adapting the piloted requirements for UAVs has the advantage of using 100 years of knowledge in piloted-flying qualities. Some specifications such as stick force gradients do not

apply to unmanned systems. This vast experience and flight test data should assist with the development of UAV flying qualities. Holmberg's study noted that current UAV specifications do not take into account sensor and payload mission requirements; these considerations should be factored into the flying qualities' requirements.

"One of the biggest challenges for defining UAV flying qualities is the lack of a substantial database of UAV mission data, test data, lessons learned, and experience as was available for the first flying qualities specifications in the 1940s" [28]. As stated previously, the manned flying qualities criteria are based on over a century worth of data. As a result, the study proposed that a MTE approach may be an alternative to build a new basis for UAV flying qualities in the absence of a substantial database. An important note to take away from this study is the need of data and research in order to move toward a flying qualities standard for UAVs.

Another study investigated and proposed a modified version of the Cooper-Harper Piloted Rating Scale [13] for unmanned systems, depicted in Figure 11. The decision tree is similar to the piloted rating scale defined by: loss of stability, adequate mission performance, and satisfactory mission performance. Cotting defined UAV flying qualities as "those qualities or characteristics of *an aircraft and sensor system* that govern the ease and precision with which an *operator* is able to perform the tasks required in support of its *mission* role" [13]. The emphasis is placed on the evaluation of the UAV and the sensor system, which come together as an integrated system.

The current Cooper-Harper scale is no longer applicable to UAVs as the level of automation increases. Cotting does acknowledge that operator comments are necessary to justify the UAV rating for a specific task, but there should less rating variability because the human is primarily an observer or sensor operator. Cotting stated, "A historical case has been made that UAVs are at a similar point in their development to piloted aircraft when flying qualities were introduced" [13]. The rating scale stems

from the need to evaluate an integrated UAV and sensor system. Cotting approaches the flying qualities criteria from a set of Mission Task Elements, which can be further categorized into task categories based on aggressiveness and precision. Figure 12 illustrates a mission task approach example with a flying qualities criterion.

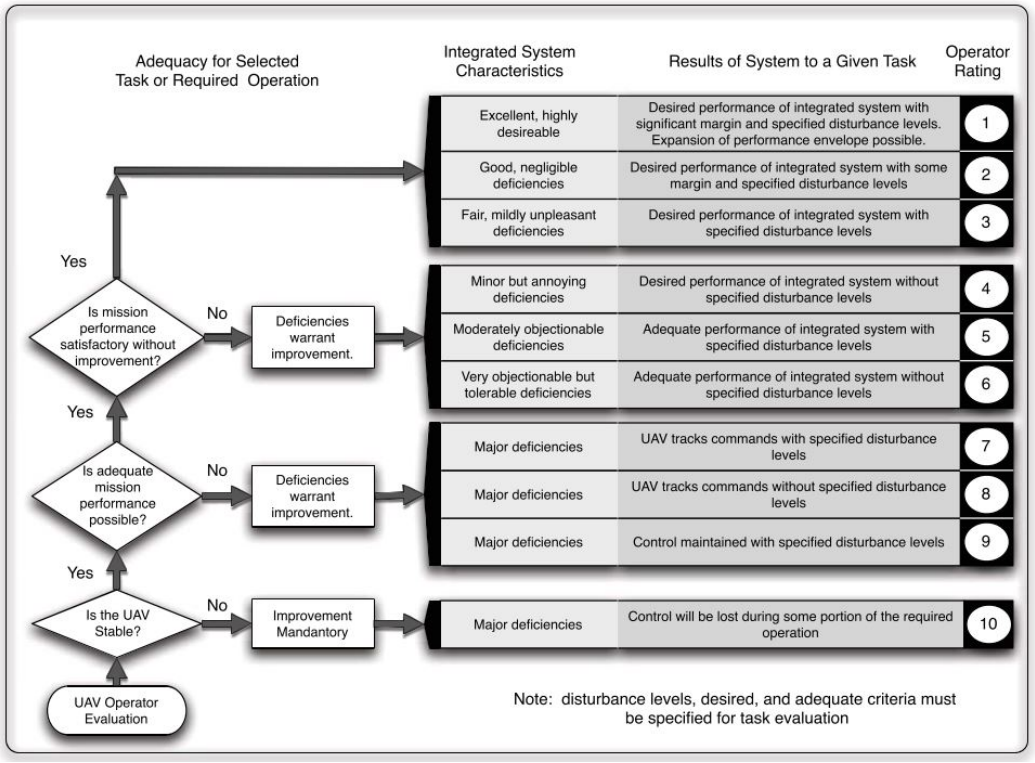

Figure 11. Modified Cooper-Harper Rating Scale for UAVs [13]

Cotting's research recommended the bandwidth criterion as the basis for the UAV flying qualities criterion [12]. There are some key advantages associated with using the bandwidth criterion:

> The bandwidth criterion does incorporate several of the flying qualities found in MIL-HDBK-1797, and has the added benefit of predicting PIO, or in the case of an UAV a limit cycle oscillation driven by a control system. Another advantage of the bandwidth criterion is its independence from vehicle response type, whether it be conventional, rate command attitude hold, or attitude command attitude hold [12].

This criterion can be applied to various aircraft dynamic modes outside of just the

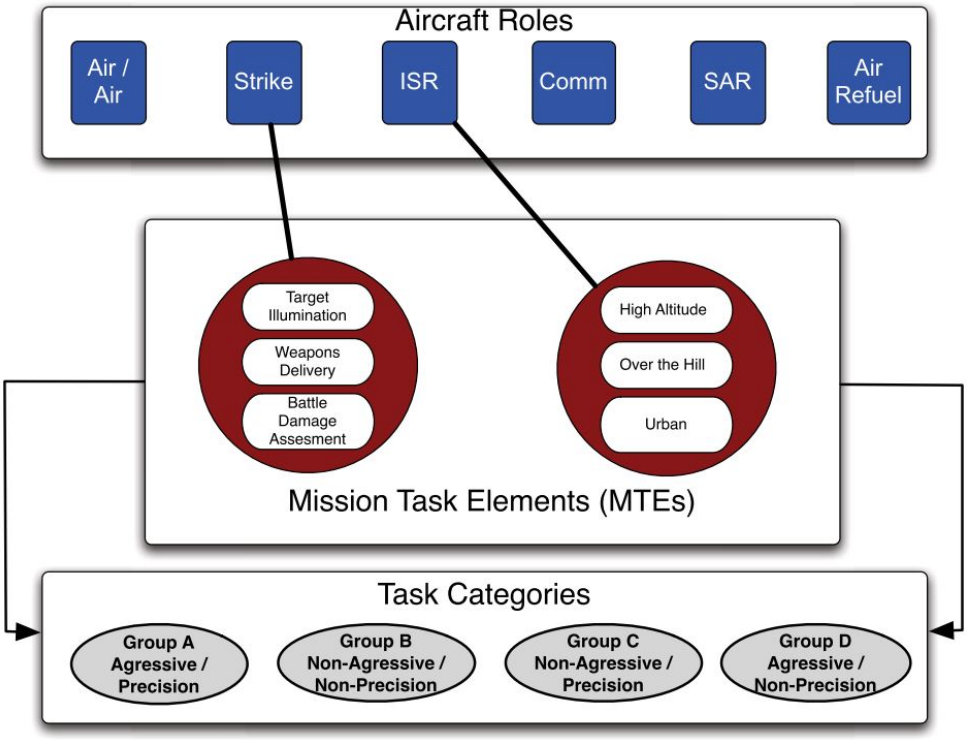

Figure 12. Notional Relation between UAV Roles, Mission Task Elements, and Task Categories [13]

short period mode. While this criterion can be applied, the pilot model must be adjusted to a sensor model to be applicable to UAVs similar to the one shown in Figure 13. The sensor model is modeled as a gain and time delay similar to the pilot model used in MIL-STD-1797. The integrated system of the UAV airframe and sensor system become key evaluation factors in the ability of the system to perform its mission task. In order to meet the bandwidth criterion, the system's bandwidth must exceed specified bandwidth for a certain mission task. By meeting the bandwidth requirements, the UAV could be pointed at the desired target or location. Cotting's suggestion of using the bandwidth criterion as a starting point while making modifications applicable to UAVs is duly noted.

As mentioned previously, this thesis builds upon Greene's research. Greene recognized the need for a flying qualities standard for unmanned aircraft in her conference

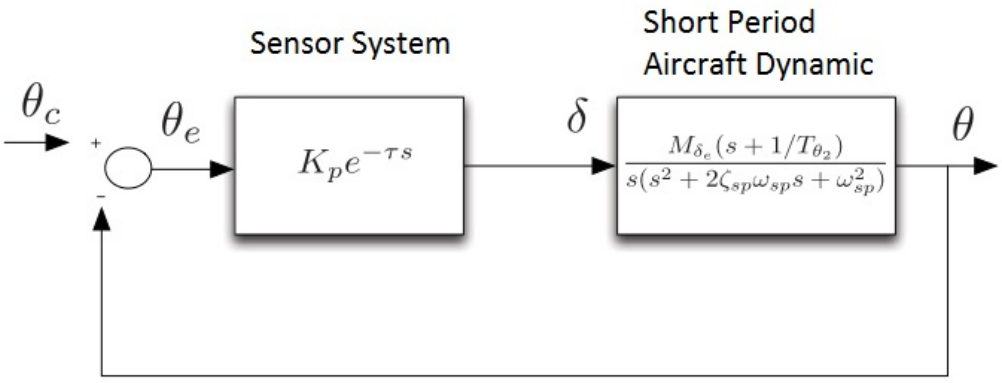

Figure 13. Bandwidth Longitudinal Diagram for UAVs [13]

article *Toward a Flying Qualities Standard for Unmanned Aircraft* [24]. The primary goal of Greene's research was to push toward a flying qualities standard for unmanned aircraft by determining the parameters applicable to UAV flying qualities and how to best analyze the flying qualities for an array of aircraft, maneuvers, and automation levels. The principal difference between the manned fixed-wing and manned rotary-wing standard is the method to define the flying quality requirements for the aircraft. Greene identified that the classification for manned fixed-wing aircraft was not easily transitioned to unmanned systems. "The correlation between class and mission tends to break down for unmanned aircraft, because unmanned aircraft of very different sizes often perform the same missions" [24]. In the FY 2013-2038 Unmanned Systems Integrated Roadmap, one motion to classify unmanned aircraft was to separate aircraft by operational altitude, weight, and airspeed illustrated in Figure 14 [56]. Cotting proposed another type of classification by Reynolds number and gross takeoff weight as shown in Figure 15 [12].

It was concluded, however, that physical characteristics of an aircraft do not form an effective foundation for the classification of unmanned systems. In Greene's study, she noted the lack of connectedness between unmanned aircraft size and mission task. A new basis for the unmanned aircraft standard had to be identified. By looking at

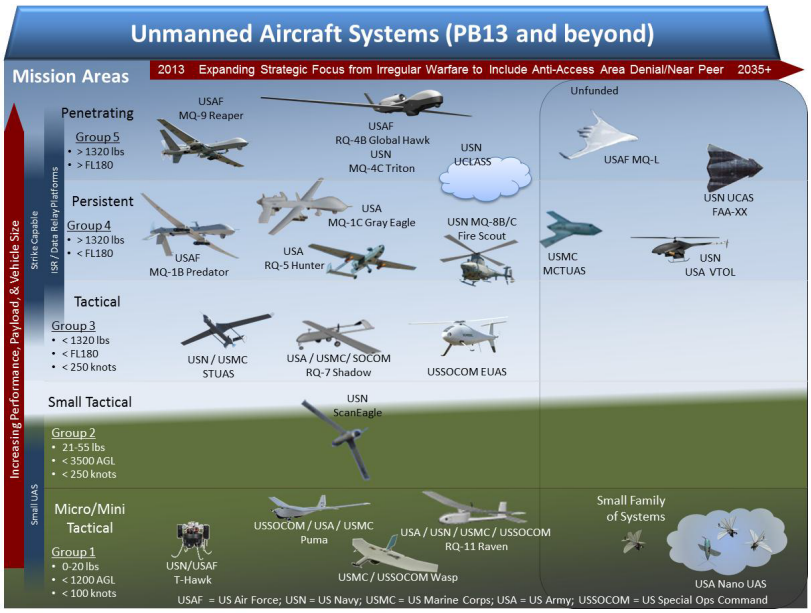

Figure 14. UAV Grouping by Operational Altitude, Weight, and Airspeed [56]

the manned rotary-wing flying qualities standard, ADS-33E-PRF, a mission-based standard could be effective.

In a report by Mitchell et al., a mission-oriented flying qualities was proposed in its incorporation into MIL-STD-1797A [33]. Mitchell et al. stated the following reasons for the deficiency in the current flight phase categories in MIL-STD-1797A:

> "Category A is too broad, ranging from air-to-air combat to reconnaissance."
> "Category B is too lenient and should apply only to flight in Visual Meteorological Conditions (VMC)."
> "Category C is not sufficiently stringent for the precision landing typically performed in flight research, and Category A is too stringent for that MTE" [33].

This study suggested dividing the flight phase categories into four sections according to the level of precision and aggressiveness, as illustrated in Table 5. In Table 5, a corresponding list of maneuvers is shown associated with each flight phase category. For example, reconnaissance, climb, and takeoff are listed under non-precision non-aggressive tasks, because these maneuvers do not require detailed attention or rapid

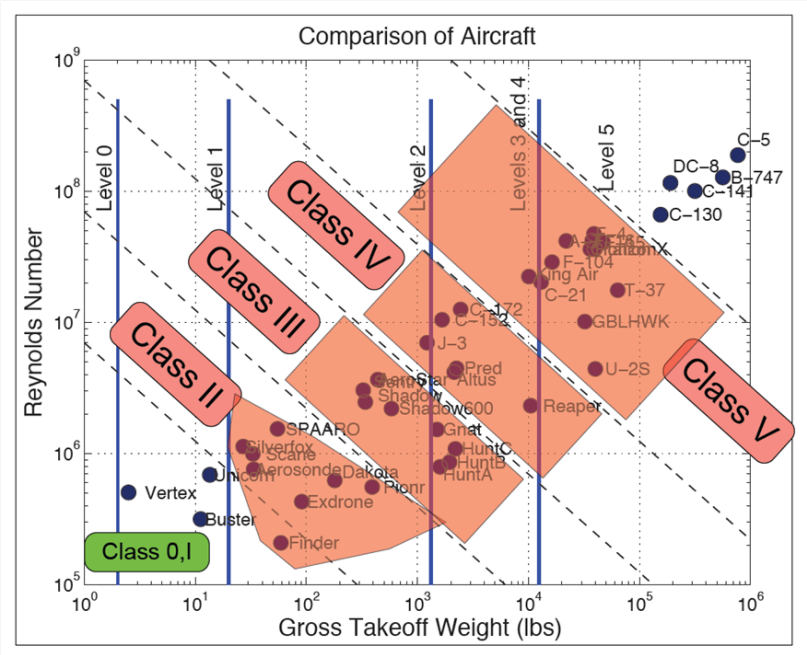

Figure 15. UAV Grouping by Reynolds Number and Aircraft Weight [12]

control activity. As a result of these groupings, a single criterion could be applied resulting in more distinction for mission tasks. Figure 16 is an illustration of the modified flight phase categories using the time delay, τ_p, and bandwidth criterion, ω_{BW}. It is advised that a mission task approach to flying qualities be implemented.

Table 5. Categorization of Mission-Task-Elements [33]

Non-Precision Tasks		Precision Tasks	
Non-Aggressive Category B	Aggressive Category D	Non-Aggressive Category C	Aggressive Category A
Reconnaissance	Gross Acquisition	Aerial recovery	Tracking
Climb	Anti-submarine	Close Formation	Ground attack
Takeoff	Max g Turn	Approach	Terrain Following
Non-precision Landing	"Herbst" Turn	Precision Landing	Precision Aerobatics

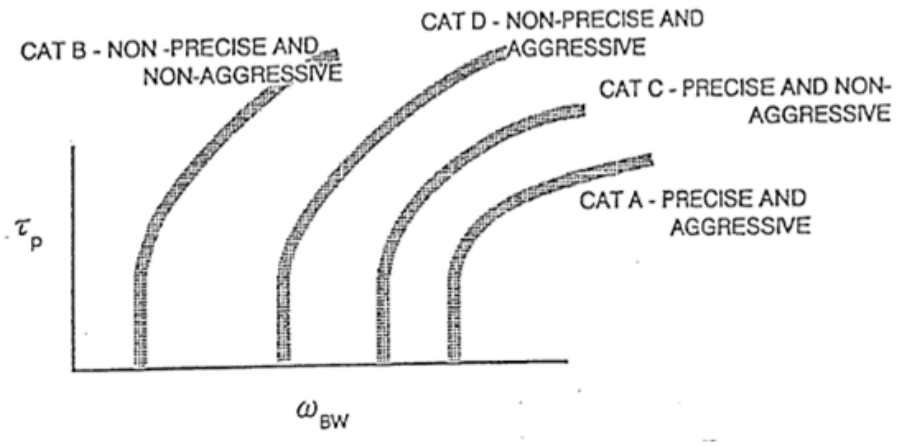

Figure 16. Flight Phase Categorization according to Time Delay and Bandwidth [33]

2.7 Summary

Leveraging the past research and the most recent work by Greene, the focus of this research is to build a database of UAV characteristics for a pre-defined mission task. The mission task will be defined by the level of precision and aggressiveness as advocated by Greene and Mitchell. The history of flying qualities has proven that a significant database of data, flight experience, and experience are essential to the success of a flying qualities standard.

III Research Methodology

The primary goal of this research was to contribute to a database of UAV characteristics in order to facilitate the development of flying qualities requirements for UAVs. Ultimately, the accumulated data may be used to identify certain trends that can correspond to various levels of flying qualities. JSBSim is the flight dynamics model used to model the aircraft and the various maneuvers based on the level of aggressiveness and precision.

3.1 JSBSim Model of T-41 Aircraft

JSBSim is a six degree-of-freedom simulation application aimed at modeling flight dynamics and control for aircraft as mentioned in Chapter II. It has the capability to model a variety of aircraft models, engines, and autopilots. JSBSim can run in standalone mode without the use of visuals, which is particularly useful for testing; however, JSBSim can be integrated within a simulator such as FlightGear [4]. The model used in this research is the baseline configuration of the T-41, which is a military variant of the Cessna 172 modeled in JSBSim. Appendix A contains additional specifications and properties of the T-41 aircraft used to model the aircraft in JSBSim.

3.1.1 Organizational Structure

In order to use JSBSim as a comprehensive analysis tool, it is important to understand its fundamental organization. JSBSim follows a hierarchical structure with models being successively broken down into subsystems. For the T-41 model used in this research, the three main folders utilized are the aircraft, engine, and scripts folder. A diagram representing the directory structure is shown in Figure 17.

Several files are involved in running JSBSim: aircraft file, engine file, thruster file,

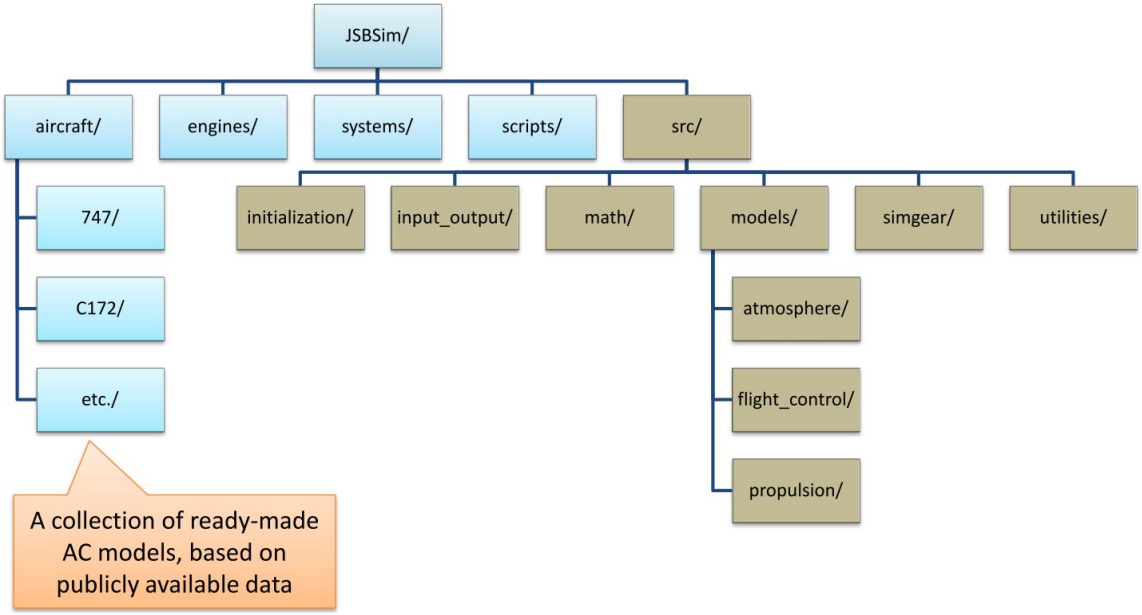

Figure 17. JSBSim Directory Structure [23]

initialization file, and script file. The aircraft file specifies the properties of the aircraft such as physical measurements, aerodynamic properties, and mass properties. The engine specification file specifies the model engine used for that aircraft. The thruster specification file includes items such as propellers or nozzles. The initialization file specifies the starting conditions of the aircraft such as takeoff runway conditions or midair steady level flight. The script file designates the maneuvers for the aircraft.

Within the aircraft folder, there is a collection of pre-made aircraft models based on publicly available data. The models are validated to "fly right" and possibly comply to published performance data, thus the model must be further validated to a certain extent to accurately represent the flight characteristics of the desired aircraft. The aircraft configuration file defines the aircraft properties. The primary sections of the model are divided into aircraft structure, control system, and aerodynamics model. The aircraft configuration file which is in XML format contains the necessary information to model the aircraft such as the mass and balance properties, aerodynamic characteristics, and flight control system. In the structural section, physical

characteristics of the aircraft are specified such as the wingspan, chord length, and tail area. The location of each structure component is also specified such as the placement of the landing gear and fuel tanks. The structural frame of the aircraft can be validated by referencing the flight handbook of the T-41.

Within the engine folder, various propulsion systems are modeled and the type of engine defined. The four engine types modeled in JSBSim are: piston, turbine, rocket and electric [4]. Each engine is paired to a thruster type of either a propeller or nozzle. The engine name is specified in the aircraft configuration XML file. The engine name references to an engine XML file containing all aspects of the propulsion system. The T-41 aircraft uses the piston type EI320 engine for its propulsion.

Within the scripts folder are files that support automatic, scripted flights allowing the aircraft to fly in a stable manner to a designated target, altitude, or heading. This is especially useful for performance testing and flight control system development. A script file "directs the aircraft to turn on its engine, advance the throttle, and fly to a target heading, altitude, and/or velocity" [5]. Scripting will be discussed in more detail in Section 3.1.4.

3.1.2 Aerodynamic Properties

The aerodynamic properties are looked up in a series of tables contained in the XML file. "JSBSim uses a coefficient build-up method for modeling the aerodynamic characteristics of aircraft" [4]. The aircraft configuration file also references to the autopilot file which will play a key role in commanding the aircraft to perform a certain maneuver. The T-41 model was created using publicly available data through technical reports and textbooks containing no proprietary or restricted data [38]. The T-41 model has been validated only to the extent that it complies with publicly known performance data.

The aerodynamic properties are key characteristics in the modeling of a UAV. The lift and drag forces do not always act on the aircraft's center of gravity, thus imparting moment forces. The control surfaces also act to impart forces and moments and are incorporated in the aircraft's stability derivatives. The forces in the six-degrees-of-freedom use aerodynamic coefficients to describe the forces and moments [50]. The coefficients in the six-degrees-of-freedom (6dof) are lift, drag, side, pitching moment, rolling moment, and yawing moment coefficient as shown in Equation 5 to Equation 10. The contribution from each aerodynamic coefficient is different; hence, main coefficients should be identified.

$$Lift\,Force:\ L = \frac{1}{2}\rho V^2 S C_L \tag{5}$$

$$Drag\,Force:\ D = \frac{1}{2}\rho V^2 S C_D \tag{6}$$

$$Side\,Force:\ Y = \frac{1}{2}\rho V^2 S C_Y \tag{7}$$

$$Roll\,Moment:\ l = \frac{1}{2}\rho V^2 S b C_l \tag{8}$$

$$Pitch\,Moment:\ m = \frac{1}{2}\rho V^2 S b C_m \tag{9}$$

$$Yaw\,Moment:\ n = \frac{1}{2}\rho V^2 S b C_n \tag{10}$$

The coefficients denoted C are the total aerodynamic coefficients for their respective moment or force with each coefficient built up by various aerodynamic and stability control derivatives. The pitch, roll, and yaw moment coefficients are shown below from

Equation 11 to Equation 13. Coefficients in the pitch moment include the change in pitch moment due to pitch rate C_{m_q}, change in pitch moment due to change in angle of attack C_{m_α}, change in pitch moment due to and the change in pitch moment due to to elevator deflection $C_{m_{\delta_e}}$ as shown in Equation 11. C_{m_α} is the pitching moment due to change in angle of attack, which must be negative for a statically stable aircraft. This stability derivative determines the static stability of the aircraft and must be negative in order to be stable. A negative value of C_{m_α} means that as the angle of attack increases, the pitching moment becomes more negative, bringing the aircraft back to its equilibrium position indicating that the aircraft is statically stable. This derivative is of primary importance to the longitudinal stability of vehicles especially in atmospheric disturbances. Since this moment acts in a direction opposite to the pitch rate, C_{m_q} is called the pitch damping derivative. As such, it contributes to the damping in pitch. Typically, the more negative this value is, the more damping that occurs. The stability derivative $C_{m_{\delta_e}}$ is often called the elevator control power. The larger the value of $C_{m_{\delta_e}}$, the more effective the elevator is in creating the pitching moment resulting in greater control effectiveness. This parameter can be related to the aerodynamic and geometric configuration of the horizontal tail. The elevator effectiveness is tied to the size of the flap used as the elevator.

$$C_m = C_{m_0} + C_m(\alpha, M, h, \delta_F, T_c) + \Delta C_{m_{\delta_e}}(\alpha, M, h, \delta_e) + \frac{\bar{c}}{2V_T}[C_{m_q}Q + C_{m_{\dot{\alpha}}}\dot{\alpha}] \quad (11)$$

Coefficients in the roll moment include the change in roll moment due to change in roll moment from the aileron deflection $C_{l_{\delta_a}}$, change in roll moment due to rudder deflection $C_{l_{\delta_r}}$, change in roll moment due to roll rate C_{l_p}, and change in roll moment due to yaw rate C_{l_r} as shown in Equation 12. The roll damping derivative, C_{lp}, plays a major part in the rolling motion of the aircraft. "It thus provides a moment that

damps rolling motion, plays the major role in the response of the aircraft to aileron inputs, and determines the associated handling qualities" [50]. C_{l_β} is the dihedral derivative determining the roll static stability and $C_{l_{\delta_a}}$ and $C_{l_{\delta_r}}$ are the roll control derivatives similar to the longitudinal control derivative $C_{m_{\delta_e}}$.

$$\begin{aligned} C_l = C_l(\alpha, M) + \Delta C_{l\delta_a}(\alpha, \beta, M, \delta_a) + \Delta C_{l\delta_r}(\alpha, \beta, M, \delta_r) \\ + \frac{b}{2V_T}[C_{lp}(\alpha, M)P + C_{lr}(\alpha, M)R] \end{aligned} \tag{12}$$

Coefficients in the yaw moment include the change in yaw moment due to rudder deflection $C_{n_{\delta_r}}$, change in yaw moment due to aileron deflection $C_{n_{\delta_a}}$, change in yaw moment due to roll rate C_{n_p}, and change in yaw moment due to yaw rate C_{n_r} all shown in Equation 13. C_{n_r} is the yaw damping derivative similar to the damping derivatives in the pitch and roll damping derivatives. C_{n_β} is the yaw stiffness derivative determining the directional stability, and $C_{n_{\delta_a}}$ and $C_{n_{\delta_r}}$ are the yaw control derivatives.

$$\begin{aligned} C_n = C_n(\alpha, \beta, M, T_c) + \Delta C_{n\delta_r}(\alpha, \beta, M, \delta_r) + \Delta C_{n\delta_a}(\alpha, \beta, M, \delta_a) \\ + \frac{b}{2V_T}[C_{np}(\alpha, M)P + C_{nr}(\alpha, M)R] \end{aligned} \tag{13}$$

The stability and control derivatives provide valuable information about the natural stability of the aircraft, the effectiveness of the control surfaces, and aircraft maneuverability. The derivatives determine the force and moments effects as the aircraft's position and motion changes providing the link to the airframe. As a result, the derivatives associate the physical shape and dimensions of the aircraft with the dynamic response, thus affecting the rating that a pilot assigns to that aircraft.

3.1.3 Flight Controls

The flight control system uses various components to model the control laws of the aircraft. Examples of flight control components are filters, integrators, summers, switches, gains, actuators, and PID (proportional-integral-derivative) controllers. The flight control system can interface to the autopilot definition file in JSBSim if it is separated. Figures 18, 19, and 20 are illustrations of the control systems on the T-41 used to control the roll, pitch and yaw.

The T-41 has ailerons on both wings, rudder on the trailing edge of the vertical stabilizer, elevators on the trailing edge of the horizontal stabilizer, and a motor for thrust. The flight control system ultimately deflects the control surfaces to maneuver the aircraft. Some aircraft have no separate elevator but use the entire horizontal tail to provide variable tail incidence, providing outstanding elevator effectiveness for increased control authority. The T-41 does not use an all-moving tail. The deflection limits for the control surfaces of the T-41 aircraft are shown in Table 6. These limitations should be taken into consideration in the simulation of the performance maneuver described in Section 3.4.

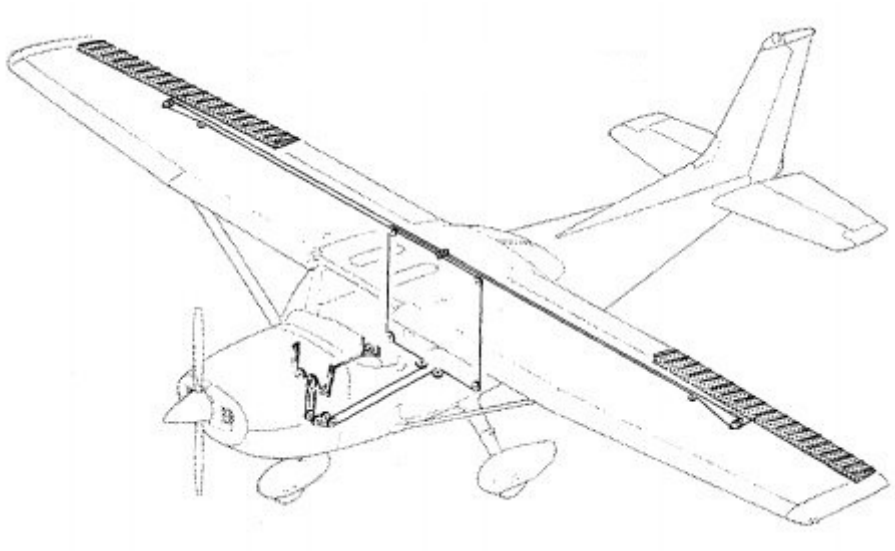

Figure 18. T-41 Aileron Control System [48]

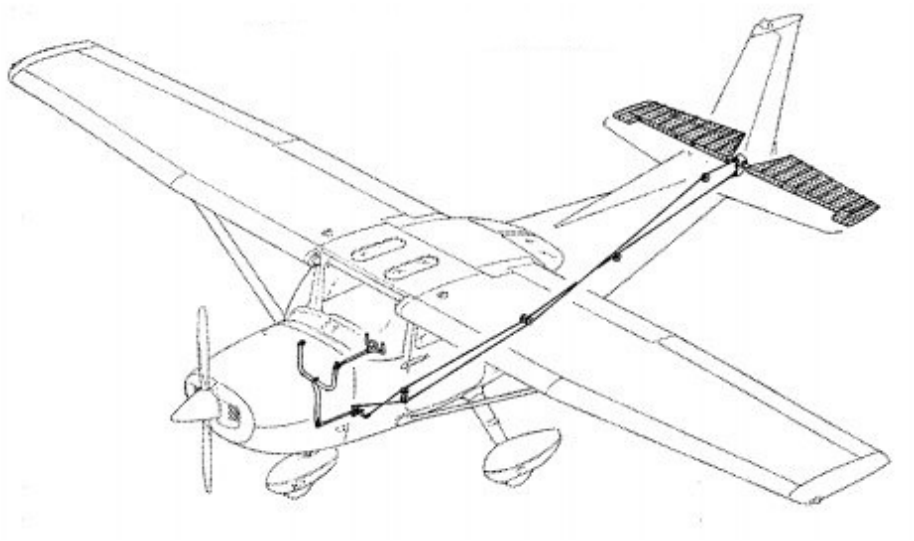

Figure 19. T-41 Elevator Control System [48]

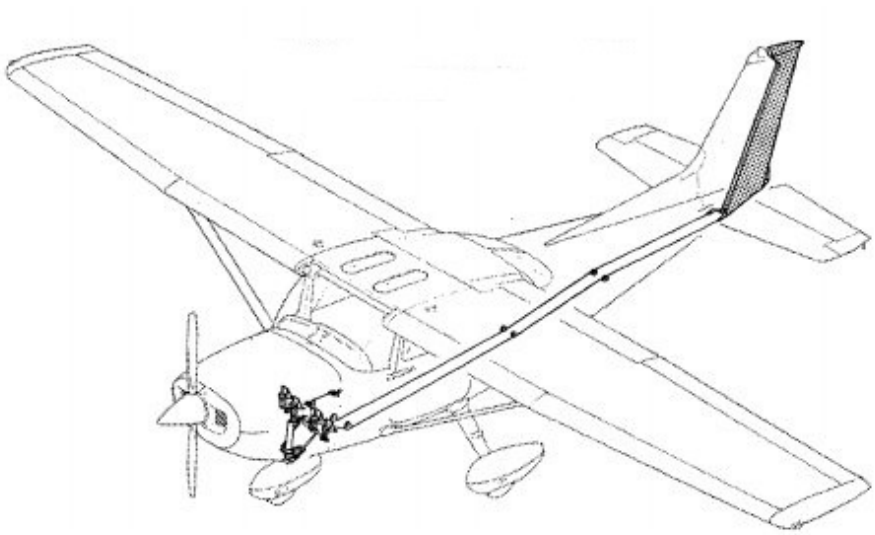

Figure 20. T-41 Rudder Control System [48]

Table 6. T-41 Control Surface Deflection Limits [2]

Elevator Deflection	min	-28°
	max	23°
Aileron Deflection	min	-20°
	max	15°
Rudder Deflection	min	-16°
	max	16°

3.1.4 JSBSim Interface

JSBSim can be built using a variety of environments but the one considered for this research is within Linux. This approach allows the model to be built directly within a XML file and run the simulation from the command terminal. JSBSim allows for two methods to interface with the user. The preferred approach is performing simulations through the software's Graphical User Interface (GUI), which guides the user to input the necessary data to run the simulation. The multiplatform GUI interfaces to the trimming and linearization code. As a result, the GUI makes finding a trim condition and creating a linear model simple, and helps the user with more intuitive feedback. For example, the trim conditions for a specified velocity and altitude can be used to find a nearby trim condition.

While the GUI may be appropriate for novice users, it has limited application for more advanced simulations. The GUI is only able to trim the aircraft and output a linear model. The GUI is unable to perform scripted flights and maneuvers. Consequently, the alternative approach is to build a script file.

Scripting allows the user to perform repeated testing for a certain set of conditions. The scripts are written within a JSBSim file in XML format [4]. A series of conditional statements are performed and when the conditional statement is evaluated to be true, events take place. When an event is evaluated to true for a given condition, parameters may take on a new numerical value. The change to the new numerical value may take on a step, ramp, or exponential approach specified by the user. The

events cause the aircraft to change a state such as the aircraft's heading, velocity, or altitude.

The script also includes references to a specific aircraft configuration file, initialization conditions, start and stop time, and an integration step size. For this research, the aircraft configuration file will be the T-41 model. The initialization conditions may be set on a runway or the aircraft may already start in steady-level flight in midair. This flexibility through scripting allows multiple maneuvers to be performed with relative ease.

The autopilot definition file supports automatic scripted flights using the same components used in defining the flight control system. The autopilot's function is to maintain a state such as wings level, altitude hold, or heading hold; therefore, allowing the aircraft to fly autonomously. In order to accomplish this task, the autopilot incorporates feedback control to detect the current state such as the aircraft's velocity and altitude and adjusts the control surfaces to maneuver the aircraft to the desired state.

3.2 Flight Envelope

The flight envelope represents the region on an altitude-airspeed plot in which the aircraft is capable of operating. Within this region, the aircraft is bounded by stall at low speeds and available thrust at high speeds. The flight envelope is a graphical depiction of the aircraft's operating limitations and is also known as the "operating envelope." Figure 21 is a generic altitude-airspeed flight envelope containing some of the defining factors along portions of the envelope.

The high speed boundary is determined from power-available, power-required curves that show the excess power available. Excess power provides the ability for the aircraft to accelerate or climb. As the aircraft approaches its thrust limit, the

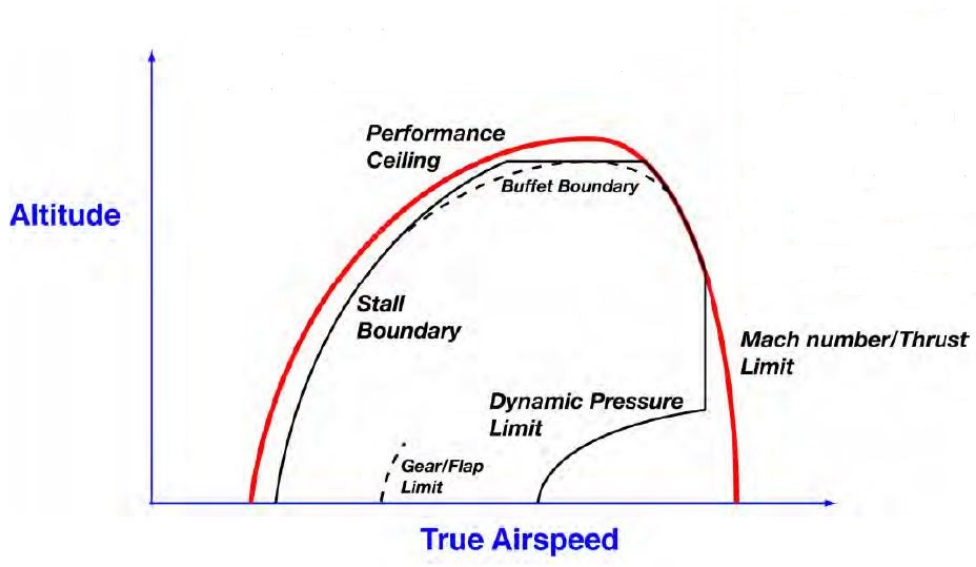

Figure 21. Aircraft Altitude-Velocity Flight Envelope [49]

aircraft can no longer climb in altitude.

The absolute ceiling is determined by the highest altitude at which specific excess power equals zero [43]. There is still some small rate-of-climb capability at the service ceiling however. The Federal Aviation Regulations (FARs) require a rate of climb of 100 fpm for propeller aircraft and 500 fpm for jets at the service ceiling. Military specifications require 100 fpm at the service ceiling. The altitude limit imposed on the flight envelope is a combination of the airframe and engine characteristics in which the aircraft can no longer pass a certain threshold for its rate of climb, known as the service ceiling.

For some aircraft, the limitation on usable ceiling is the pilot such as the need cockpit pressurization or oxygen masks above a specified altitude. Other factors to consider are structural limits of the aircraft, maximum allowable aerodynamic heating, and flow-separation buffet [49]. An additional consideration is the operation viability of the aircraft. Flight regulations may govern the altitudes deemed safe for the pilot and crew, thus limiting the service ceiling of the aircraft. For example,

Federal Air Regulations require the flight crew to be equipped with oxygen masks above certain altitudes. The additional equipment and procedures associated with the regulations may hinder some aircraft from flying above those altitudes. Safety concern for the pilot and the crew must be taken into consideration. By knowing the flight envelope, the flying and handling qualities can be analyzed as the aircraft pushes its envelope towards more difficult conditions.

Because the boundaries vary with aircraft weight, some assumption about aircraft weight must be made. Typically, the flight envelope is calculated at takeoff weight, cruise weight, or combat weight. The flight envelope will be determined at a fixed weight with the aircraft in steady level flight. The aircraft will be trimmed at various velocities and altitudes to determine if those conditions are feasible, giving an overall picture of the aircraft's capabilities and limitations.

3.3 Dynamics Trimming

Determining the aircraft's trim states are of primary importance because the trim conditions establish initial conditions in simulations by determining the combination of flight control settings and other states to make steady-level flight achievable. The simulations will be set up to calculate the trim conditions for level un-accelerated flight at the beginning of each simulation. The trimmed state refers to the aircraft's steady-state level flight condition where the control inputs remain constant. The trim conditions also provide a method to compare aircraft models. The aircraft trim problem falls underneath the context of simulation-based-optimization. In order to do so, one has to choose a cost function minimization technique.

JSBSim utilizes thirteen states to describe its state vector, x, and four states to describe its input or control vector, u. The state vector and control vector are shown in Equation 14 respectively. The first four states (v_t, α, θ, q) correspond to

parameters associated with the aircraft's longitudinal mode of motion. The next four states (β, ϕ, p, r) correspond to parameters associated with the aircraft's lateral mode of motion. The following four states $(lat, long, \psi, h)$ correspond to navigational states. The last state (RPM) is the revolutions per minute motor rate associated with propeller-driven aircraft. The input or control vector is constrained to four dimensions corresponding to the throttle, ailerons, elevator, and rudder.

$$x = \begin{bmatrix} v_t \\ \alpha \\ \theta \\ q \\ \beta \\ \phi \\ p \\ r \\ lat \\ long \\ \psi \\ h \\ RPM \end{bmatrix} \qquad u = \begin{bmatrix} \delta_t \\ \delta_a \\ \delta_e \\ \delta_r \end{bmatrix} \tag{14}$$

The numerical trimming algorithm used in the JSBSIM flight dynamics library is the Nelder-Mead Simplex method proposed by J.A. Nelder and R. Mead in 1965 [34]. The Nelder-Mead Simplex method does not require the computation of derivatives making it more easily applicable to complex systems; however, it is important to note that the algorithm can become stuck at a local minimum. As a result, the Nelder-

Mead simplex method is capable of only determining local minima, not a global minimum. A randomization factor is incorporated into the algorithm to help escape a local minimum in order to complete a more thorough search in the design space. A good initial guess is instrumental in assuring that the algorithm does not get stuck at a local minimum. De Marco et al. examine the general solution to the aircraft trim problem and illustrate how the Nelder-Mead Simplex algorithm is used in an open source flight dynamics model like JSBSim [15].

In Figure 22, a T-41 is trimmed for steady-level flight with specified trim conditions in the JSBSim GUI. Once the cost function has passed a certain threshold, the algorithm has converged on a solution to the trimming problem. For most of the simulations in this research, the T-41 was trimmed at a feasible flight condition in the flight envelope of 100 knots (168.78 ft/s) at 4,000 ft altitude. The aircraft will be kept trimmed for a specified time interval in order to ensure that the aircraft is kept at level un-accelerated flight.

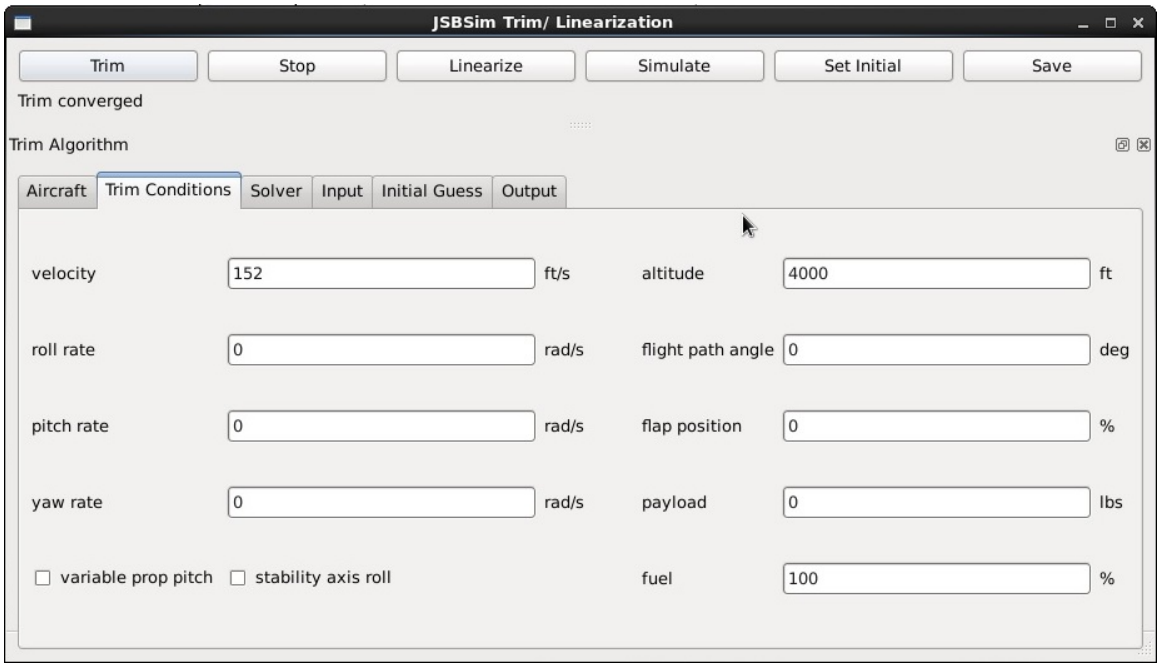

Figure 22. Specified T-41 Trim Conditions in JSBSim GUI

The output of the JSBSim GUI trimming program is shown below. The T-41 did in fact trim at the specified velocity of 152 ft/s and an altitude of 4000 ft.

T41trim.txt

```
aircraft state
        vt, ft/s     :        152
        alpha, deg   :        0.98212
        theta, deg   :        0.98212
        q, rad/s     :        0
        thrust, lbf  :        198.114
        beta, deg    :        -0.21373
        phi, deg     :        -4.41455e-32
        p, rad/s     :        0
        r, rad/s     :        0
        mass, lbm    :        1893.99

actuator state
        throttle, %  :        70.1761
        elevator, %  :        14.6556
        aileron, %   :        0.0687038
        rudder, %    :        -4.58293

nav state
        altitude, ft :        4000
        psi, deg     :        360
        lat, deg     :        0
        lon, deg     :        0

aircraft d/dt state
        d/dt alpha, deg/s   :        6.068627e-02
        d/dt theta, deg/s   :        0.000000e+00
```

```
        d/dt q, rad/s^2     :        2.091645e-02
        d/dt beta, deg/s    :        1.455256e-03
        d/dt phi, deg/s     :        0.000000e+00
        d/dt p, rad/s^2     :        5.556549e-03
        d/dt r, rad/s^2     :        1.718376e-02

d/dt nav state
        d/dt altitude, ft/s :        1.465494e-14
        d/dt psi, deg/s     :        0.000000e+00
```

The linearized state-space model is output from the JSBSim GUI in matrices A, B, C, D developing the first-order state differential equation $\dot{x} = Ax + Bu$ and the output equation $y = Cx + Du$. The matrix A is the 13x13 plant matrix; the matrix B is the 13x4 input matrix; matrix C is the 4x13 output matrix; and matrix D is the 4x4 feed forward matrix. With the linearized matrices, an analysis on the longitudinal and lateral flying qualities can be performed using well documented methods from MIL-STD-1797. The linearized matrices are for a known flight trimmed condition in order to gain insight about the aircraft's modes of motion.

3.4 Simulation

3.4.1 Mission Tasks

For the purposes of this research, the focus will be on a non-precision, non-aggressive maneuver, specifically a climbing spiral maneuver. As discussed earlier in Chapter II, the maneuvers are associated with the level of precision and aggressiveness. In the report WL-TR-97-3100 by Wright Laboratory, it lists a variety of maneuvers based on precision and aggressiveness as shown in Table 7 [30]. The maneuvers that were chosen are supposed to mirror the task of unmanned systems such

as ISR duties focused on the ground. "The task definition should reflect the mission for which the aircraft and sensor integrated system is to be evaluated. The adequate desired criteria should also be clearly defined and be related to mission success requirements" [13]. For the non-precision, non-aggressive demonstration maneuver, the altitude and heading change will be incorporated. This is a relatively simple maneuver performed by all aircraft that should be successfully executed without any significant hindrances. It is expected that the flight control system will have a sufficient amount of control authority since this maneuver does not require rapid movements or large amplitudes associated with more difficult tasks.

No.	Mission Task Element (MTE)	Related Flight Phase (Ref. 1)	MTE Status at Program Completion		
			Evaluated (Flight)	Evaluated (Simulator)	Needs Refinement
Non-Precision, Non-Aggressive Demonstration Maneuvers					
1	Takeoff and Departure Climb	TO	✓	✓	
2	Heading Change	CR, LO	✓	✓	
3	Supersonic Heading Change	CR, LO		✓	
4	Altitude Change	CL, D	✓	✓	
5	Supersonic Altitude Change	CL, D		✓	
6	Waveoff/Go-Around	WO		✓	
7	Landing	L	✓	✓	
Non-Precision, Aggressive Demonstration Maneuvers					
8	Air-to-Air Longitudinal Gross Acquisition	CO			
9	Post-Stall Air-to-Air Longitudinal Gross Acquisition	CO	✓		
10	Air-to-Air Lateral Gross Acquisition	CO			
11	Post-Stall Air-to-Air Lateral Gross Acquisition	CO	✓		
12	Air-to-Ground Gross Acquisition	GA			
13	Loaded Roll Reversal	CO			✓
14	Post-Stall Roll Reversal	CO	✓		
Precision, Non-Aggressive Demonstration Maneuvers					
15	Catapult Takeoff	CT			✓
16	Flightpath Capture and Hold	AR		✓	
17	Altitude Rate Capture and Hold	*	✓	✓	
18	Supersonic Altitude Rate Capture and Hold	*		✓	
19	Pitch Attitude Capture and Hold	*	✓	✓	
20	Supersonic Pitch Attitude Capture and Hold	*		✓	
21	Post-Stall Pitch Attitude Capture and Hold	*	✓		
22	Bank Angle Capture and Hold	*	✓	✓	
23	Supersonic Bank Angle Capture and Hold	*		✓	
24	Close Formation	FF			✓
25	Probe-and-Drogue Refueling	RR	✓		
26	Tanker Boom Tracking	RR			
27	Simulated Aerial Refueling	RR	✓		
28	Precision Low-Altitude Flight	LAPES			✓
29	Precision ILS Capture and Track	PA	✓	✓	
30	Precision Offset Landing	L	✓	✓	
31	STOL Precision Offset Landing	L			✓
Precision, Aggressive Demonstration Maneuvers					
32	Air-To-Air Fine Tracking	CO			
33	Post-Stall Air-To-Air Fine Tracking	CO	✓		
34	Air-To-Ground Tracking	GA			
35	Pitch and Roll Discrete Tracking	CO	✓		
36	Pitch and Roll Sum of Sines Tracking	CO	✓		

Table 7. Mission Task Elements [30]

3.4.2 Flight Control System

Before the specifics of the autopilot system are defined, the aircraft's flight control system must be explored in order to understand how the autopilot interacts with the aircraft's control surfaces. The T-41 has three basic flight control channels: pitch, roll, and yaw. Figure 23 is the schematic illustration of the pitch channel flight control system.

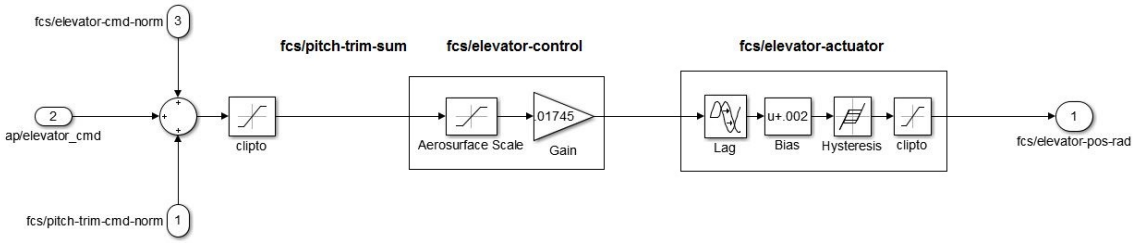

Figure 23. T-41 Pitch Channel Flight Control System

Three commands are fed into the pitch channel and summed: elevator command, normalized elevator command, and the normalized pitch trim command. The 'clipto' element permits limiting of the output of a component between -1 and +1 called 'pitch-trim-sum.' The next major component in the flight control system is the elevator control composed of two elements. The first element is the 'aerosurface' scale whose purpose is to take control inputs from a known domain and map them to a specified domain. The control input is in the range from -1 to +1. The 'aerosurface' scale converts the control input from -1 to +1 and maps it to -28 to 23, corresponding to the elevator deflection limit in units of degrees. The gain block of .01745 ($\pi/180$) converts the elevator control from degrees to radians. The elevator control is fed into the elevator actuator block composed of four elements: lag, bias, hysteresis, and limited output (clipto). The actuator simulates the mechanical characteristics between the elevator control command and the actual elevator position. The final output is the elevator position in units of radians. The elevator position is then used to de-

termine the aerodynamic coefficients such as the lift, drag, and pitch moment due to elevator deflection.

Similar to the pitch channel, the roll channel follows a similar structure as shown in Figure 24. It consists of similar components with the biggest difference accounting for the opposite signs of the left and right ailerons. This ensures that the left and right ailerons are deflected in opposite directions to generate a roll moment. The roll command from the autopilot, normalized aileron command, and the normalized roll trim command are summed up with the output limited between -1 and +1. This output is defined as the 'roll-trim-sum' which is fed into two separate channels for the left and right aileron. The 'aerosurface' block maps the control input from -1 to +1 and maps them to -20 to +15, corresponding to the aileron deflection limit in units of degrees. The gain block of .01745 ($\pi/180$) converts the aileron control from degrees to radians. The aileron control is fed into the aileron actuator block composed of three elements: rate limit, hysteresis, and limited output (clipto). The left and right aileron channels are essentially copies of each other except that the right aileron includes a gain of -1 to account for the opposite surface deflection. Like the pitch channel, the aileron position is used to determine the aerodynamic coefficients such as the side force, roll moment, and yaw moment due to aileron deflection.

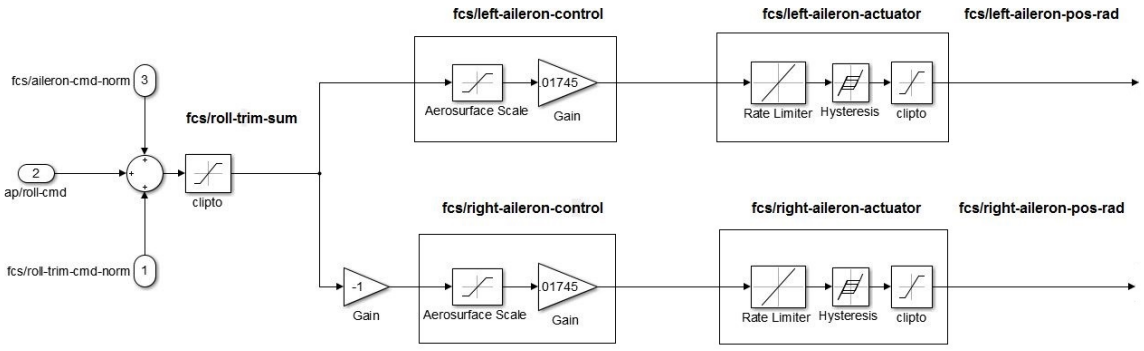

Figure 24. T-41 Roll Channel Flight Control System

To account for all three axes, the final channel is the yaw flight control system as shown in Figure 25. Unlike the previous two channels, there are only two inputs. The normalized rudder command and normalized yaw trim command are fed into this channel with the output limited between -1 and +1. The output, 'yaw-trim-sum', is fed into the rudder control mapping the control input to -16 and +16, corresponding to the rudder deflection limit in units of degrees. It is then converted into units of radians through the gain block resulting in the rudder position. Just like the previous two channels, the rudder position is used to determine the aerodynamic characteristics by determining the side force, roll moment, and yaw moment due to rudder deflection.

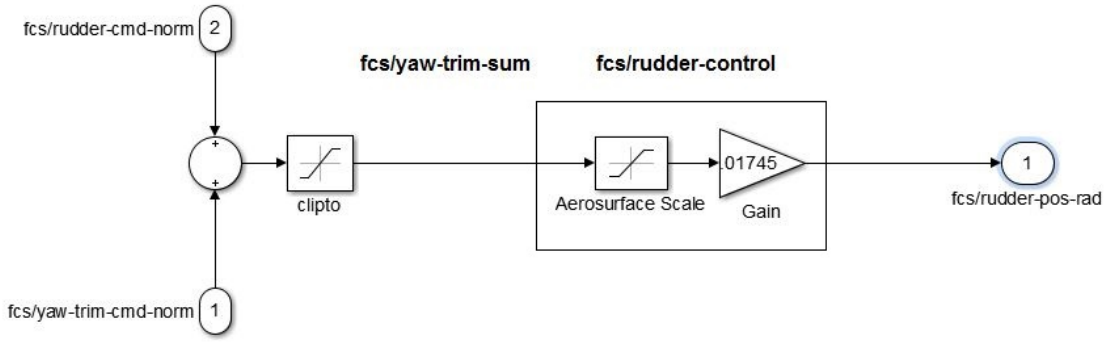

Figure 25. T-41 Yaw Channel Flight Control System

The effect of nonlinearities such as surface deflection limits and rate limiting was added into the actuator dynamics to create a more realistic flight simulation. The incorporated surface deflections corresponded to the T-41 position limits previously shown in Table 6. For simplicity, hysteresis and bias effects were neglected. For manned aircraft, nonlinearities such as rate limiting, hysteresis, and abrupt control system gain changes were likely causes for pilot-induced oscillations (PIO) and should be taken into consideration. If an aircraft is PIO-prone, it should be be predicted to obtain poor flying qualities ratings.

There must be a limit to the capabilities of the system to generate acceleration, rates, and positions despite how hard the system is pushed. Due to the disruption

between the demands of the control system and the capability of the actuator, rate limiting will occur. The effect of rate limiting on the elevator actuator can be seen in Figure 26. The model was validated by running the simulation with various rate limits in order to confirm that rate limiting was having the anticipated effect. The beginning of the familiar triangle wave pattern becomes more readily apparent in the 5 deg/s rate limit. In addition to the decreased rate limit, the amplitude of the control input and oscillation frequency both decrease. From the simulation result, the effects of rate limiting are confirmed.

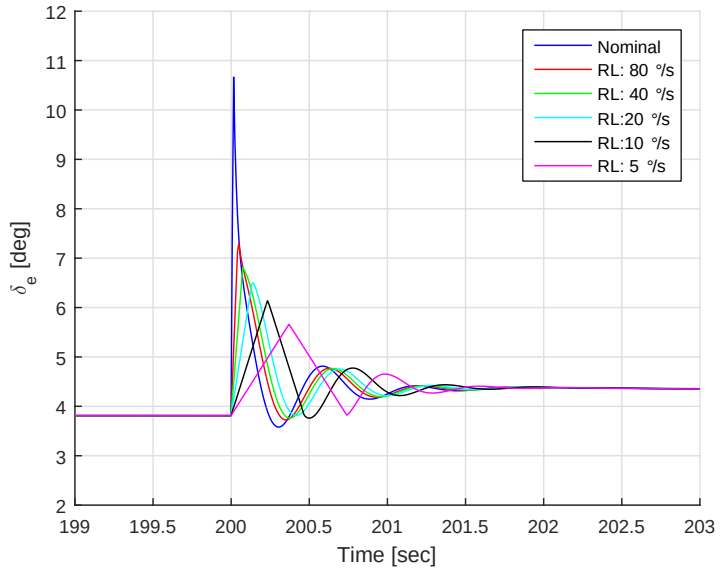

Figure 26. T-41 Elevator Actuator Rate Limit Variation

3.4.3 Automation Level and Autopilot Design

The use of automatic control coupled with scripting providing commands to the automatic control system allows the aircraft to perform desired maneuvers repeatedly. For the purposes of this research, the aircraft will be fully automated to model the behavior of a fully autonomous UAV. A fully autonomous system "receives goals from humans and translates them into tasks to be performed without human interaction"

[55]. By engaging autopilots through manipulating the flight control laws, the UAV can be directed to the desired outcome. This autonomous role is what gives UAVs such a distinct advantage over manned aircraft.

This also brings about the question about which loops are closed during UAV automation. Typically, the stability augmentation system (SAS) is closed to improve the performance of the bare airframe which could be unstable [50]. The control is provided to improve the handling qualities of the aircraft over those of the bare airframe by providing suitable damping and natural frequencies. For aircraft without any stability augmentation, the level of static margin which is a measure of the aircraft's inherent stability can be quite high. Typically, trainer aircraft such as the T-41 have a high level of static margin where pilot skill level can be assumed to be low.

The control augmentation system (CAS) is closed to shape the particular response of an aircraft to a command [50]. The normal-acceleration CAS is an example of this type of system in which the pilot's inputs control the acceleration in the vertical plane of the aircraft. The main concern is focused on the aircraft's completion of the task and less so on the aircraft response.

In order to execute the maneuver, several autopilot controllers were implemented into JSBSim. The JSBSim autopilot file was modified to include a series of setpoints, auto-switches, PID controller gains, and normalization elements. Four parameter setpoints were added acting as the desired parameter that the autopilot is trying to achieve by adjusting the controls. The four autopilot switches essentially turn each autopilot on or off. Three PID gains were added for each autopilot channel, resulting in a total of 12 autopilot gains. Figure 27 shows the general structure of the JSBSim autopilot for one channel. The aircraft is flown autonomously by on-board autopilots using the built-in generic PID (proportional, integral, and derivative) controller which

has the ability to hold aircraft velocity, rate of climb, bank angle, and side slip angle.

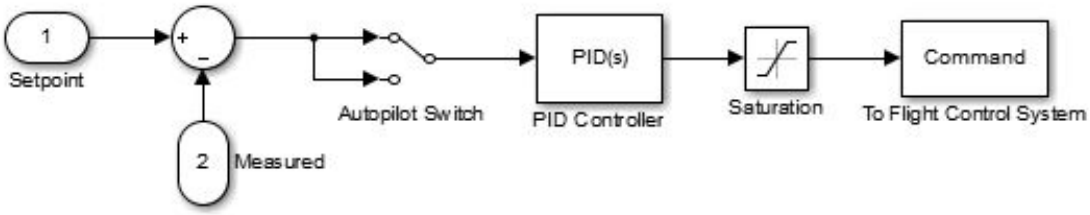

Figure 27. Outer Autopilot Controller Structure

PID stands for "proportional, integral, derivative" which are the three basic elements of the PID controller. These three elements are "driven by a combination of the system command and the feedback signal from the object that is being controlled" typically referred to as the plant [52]. The purpose of the PID controller is to drive the signal error as small as possible. The signal error is the difference between the desired signal and the actual signal. Mathematically, a PID controller can be represented as:

$$K_p e(t) + K_i \int_0^t e(\tau)d\tau + K_d \frac{d}{dt}e(t),\ t > 0 \tag{15}$$

where K_p, K_i, K_d represent the proportional, integral, and derivative gains respectively. τ is the control signal which is being sent through the PID controller. Each element performs a certain function and has a different effect on the system response. The proportional control simply multiplies the error signal by the gain. Increasing the proportional control increases the system response but ends up overshooting resulting in oscillations. If the gain is further increased, the system eventually reaches an unstable point where the system never settles out. Integral control is used to improve the steady-state error to bring the response to the desired set point. The integral element calculates the integral of the error signal and adjusts the control signal value accordingly. As the error signal exists longer, the autopilot will adjust

to reach the desired set point thus eliminating the problem from the proportional element. One problem associated with the integral device is that the aircraft may oscillate as it continues to go past the reference point and needing to adjust back the other way. The derivative device alleviates this problem by calculating the derivative of the error curve, which is the change rate of the error. When the response closes in on the desired set point, the derivative element will adjust the control gain to reach the reference point without oscillations.

Figure 28 shows the step responses of the P, PI, and PID controller for the rate of climb autopilot. The signal sent to the autopilot commands the aircraft to attain a rate of climb of 4 ft/s. With the simplest proportional controller, the step response overshoots and does not settle out at the desired rate of climb. The addition of the integral control improves the long term precision of attaining the desired rate of climb but does so at the cost of overshoot and oscillations. In order to improve the response, derivative control is added in order to reduce the overshoot as it approaches the desired set point resulting in an acceptable response.

Figure 29 is a block diagram of a PID controller with all three elements. Combining the three elements results in a smooth response but it takes some tuning in order to refine the system response. The gains, K_p, K_i, K_d were tuned manually. If the range is known, it is simple to tune them manually by simulating multiple cases and deciding which values will give a satisfactory behavior. According to Olson, the best way to begin constructing the autopilot configuration file is by copying the autopilot configuration file from an existing, similar aircraft, and modifying the parameters in order to adapt it [35]. Olson provides a typical trial and tuning approach for a PID controller for acceptable performance.

1. Eliminate integral and derivative action by setting the derivative time, T_d, to its minimum value (zero) and the integral time, T_i to its maximum value.

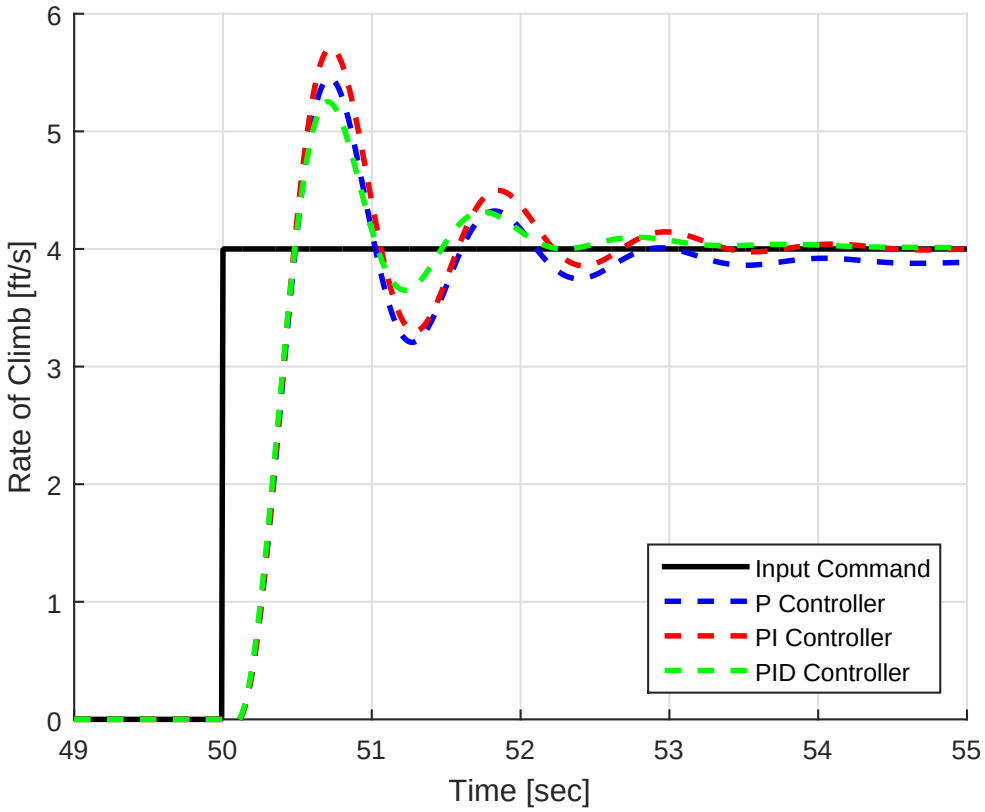

Figure 28. Rate of Climb vs. Time Response for Various Controllers

2. Set the proportional gain, K_P to a low value (0.5) and enable the controller.

3. Increase the proportional gain by small increments until continuous cycling occurs after a small set-point or load change. The term "continuous cycling" refers to a sustained oscillation with constant amplitude. At first it might be useful to increment K_P by an order of magnitude (i.e. multiply or divide by 10) just to get yourself in the right ball park. Then you might consider doubling or dividing by two to get closer.

4. Reduce the gain by a factor of two.

5. Decrease the integral time until continuous cycling occurs again. Set integral time, T_i to three times this value. Note that because of the way the formulas are constructed, a smaller integral time means a larger integral component.

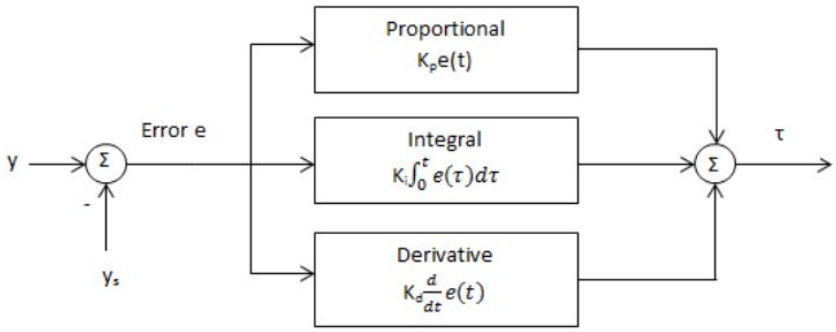

Figure 29. Block Diagram of a PID Controller [29]

6. Increase derivative time, T_d until continuous cycling occurs. Set derivative time to one-third of this value. Note that because of the way the formulas are constructed, a larger derivative time means a larger derivative component (which is opposite from the effect of changing T_i).
[35].

In JSBSim, the PID controller is implemented in the autopilot file defined in a separate XML format configuration file. Extending the autopilot function requires knowledge in control theory in order to successfully implement it. JSBSim includes a generic autopilot to keep wing leveler hold, heading hold, and altitude hold. An example of a PID controller in an autopilot XML file is shown in Figure 30.

When the signal error converges to zero without higher overshoot and oscillations within a reasonable amount of time, the controller is considered stable. The outcome was an accurate model of the maneuver with an effective autopilot. The PID controller is linear and is applied to a nonlinear system but it works nonetheless. Table 8 shows the PID gains for the four autopilots used in JSBSim to perform the climbing spiral.

Table 8. PID Gains for Autopilots

Tracking Parameter	Control	K_p	K_i	K_d
Rate of Climb ($\dot{h}$)	Elevator (δ_e)	.030	.030	.009
Airspeed (V_t)	Throttle (δ_t)	.040	.0008	.009
Bank Angle (ϕ)	Ailerons (δ_a)	.015	.001	.01
Sideslip Angle (β)	Rudder (δ_r)	.013	.02	.05

```
<autopilot name="C172X Autopilot">

  <!-- Wing leveler -->

  <channel name="Roll wing leveler">

    <pid name="fcs/roll-ap-error-pid">
      <input>attitude/phi-rad</input>
      <kp> 1.0 </kp>
      <ki> 0.01</ki>
      <kd> 0.1 </kd>
    </pid>

    <switch name="fcs/roll-ap-autoswitch">
      <default value="0.0"/>
      <test value="fcs/roll-ap-error-pid">
        ap/attitude_hold == 1
      </test>
    </switch>

    <pure_gain name="fcs/roll-ap-aileron-command-normalizer">
       <input>fcs/roll-ap-autoswitch</input>
       <gain>-1</gain>
    </pure_gain>

  </channel>

  <channel name="Pitch attitude hold">
    … components …
  </channel>

  … additional channels …

</autopilot>
```

Figure 30. Autopilot Example in JSBSim [5]

The closed-loop performance of the autopilot and aircraft is simulated in a climbing spiral maneuver. The climbing spiral is the non-precision non-aggressive maneuver used to evaluate the aircraft's longitudinal and lateral abilities. This maneuver will also examine potential coupling between the longitudinal and lateral motion. The baseline performance maneuver was initiated at 4,000 feet which is in the middle of the T-41's flight envelope. The aircraft is initialized at position [0,0] in latitude, longitude convention. The aircraft flew for 20 seconds after it was initially trimmed to ensure that the aircraft was in steady and level flight. The climbing spiral maneuver was initiated 20 seconds into the simulation. Upon initiation of the maneuver, the aircraft climbed and banked at the specified rate of climb and bank angle. The dura-

tion of maneuver was set long enough in order to complete one complete spiral. Upon termination of the maneuver, the aircraft returned back to steady and level flight.

The autopilot tracking time history for the four states is shown in Figure 31. As can be seen from Figure 31a, the flight control system follows the desired rate of climb path with a small overshoot. This small overshoot is considered small enough to not cause problems. Figure 31b shows the velocity controlled by PID control. One of the constraints during the maneuver was to maintain airspeed by adjusting the throttle. From Figures 31c and 31d, it can be seen that the flight control system follows the desired bank angle and sideslip angle effectively. The climbing spiral maneuver is executed successively in tracking all four parameters without any significant problems.

Figure 32 shows the complete maneuver with key points such as the maneuver initiation and termination denoted by various symbols. The climbing spiral maneuver was initiated after 20 seconds of trimmed flight. Through this simulation, it was concluded that the PID controllers could adequately control the pitch, velocity, roll, and heading of the aircraft. It should be noted that no disturbances were incorporated into the simulation. "However, in turbulence, for instance, the response may be different than what is expected, perhaps even unstable"[5]. The incorporation of disturbance into this simulation is a topic reserved for later research.

Once the climbing spiral was successively implemented, the maneuver was broken down into its longitudinal and lateral-directional components. The longitudinal component of the climbing spiral maneuver consists of a straight climb and the lateral-directional component consists of a constant altitude turn. Through this decomposition, it allows the analysis of the longitudinal and lateral motion separately which are also examined separately in the determination of an aircraft's flying qualities.

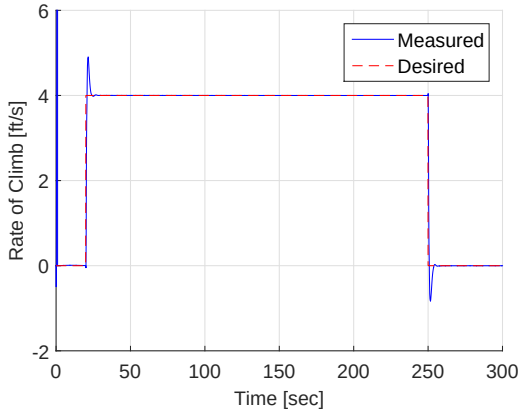

(a) Response in Rate of Climb ($\dot{h}$)

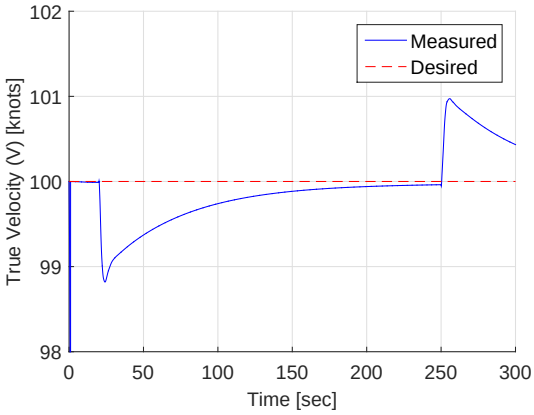

(b) Response in Velocity (V_t)

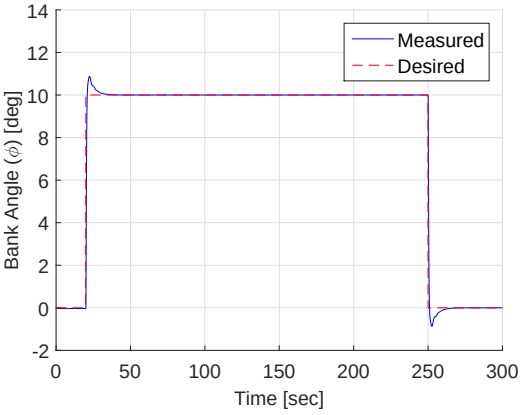

(c) Response in Bank Angle (ϕ)

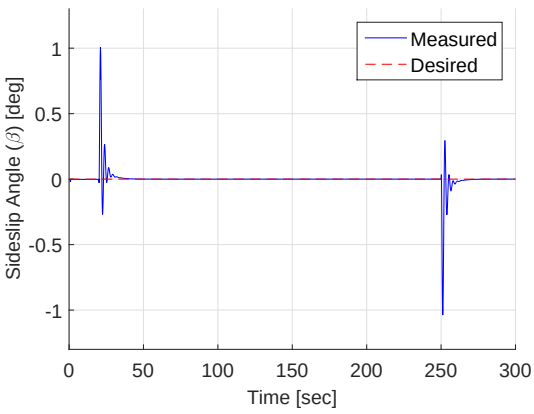

(d) Response in Sideslip Angle (β)

Figure 31. Climbing Spiral Closed-Loop Tracking Responses

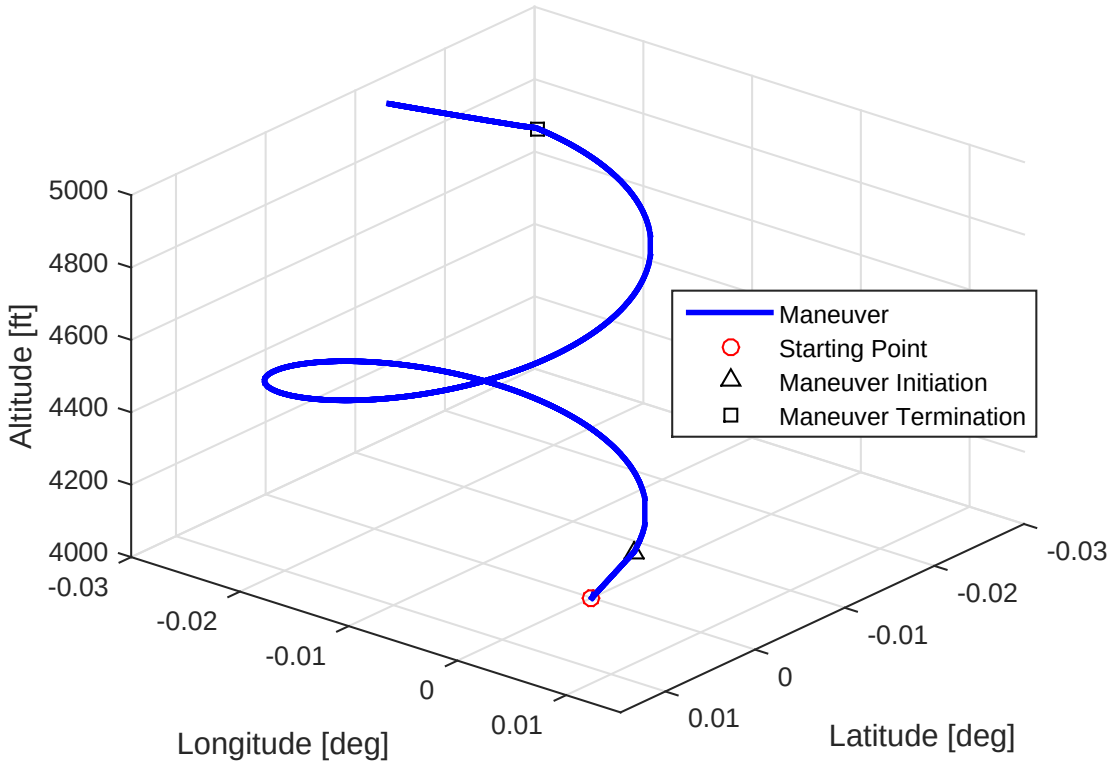

Figure 32. 3-Dimensional View of Performance Maneuver

3.4.4 Variation of Stability and Control Derivatives

The longitudinal and lateral motion will be analyzed separately by varying the stability and control derivatives. The flying qualities will be characterized for the longitudinal and lateral-directional response modes and compared to the evaluation of a dedicated set of flight maneuvers. The maneuvers to be performed are the straight climb, constant altitude turn, and climbing spiral. Such a sequence of maneuvers will allow the observation of the longitudinal only, lateral-directional only, and cross coupling of the longitudinal and lateral-directional modes. Figures 33 and 34 show the forces acting on the aircraft as the T-41 executes the climb and turn respectively. The control system during the longitudinal maneuver will be mainly concerned with the elevator and throttle. Likewise, the control system during the lateral-directional

maneuver will be mainly concerned with the ailerons and rudder.

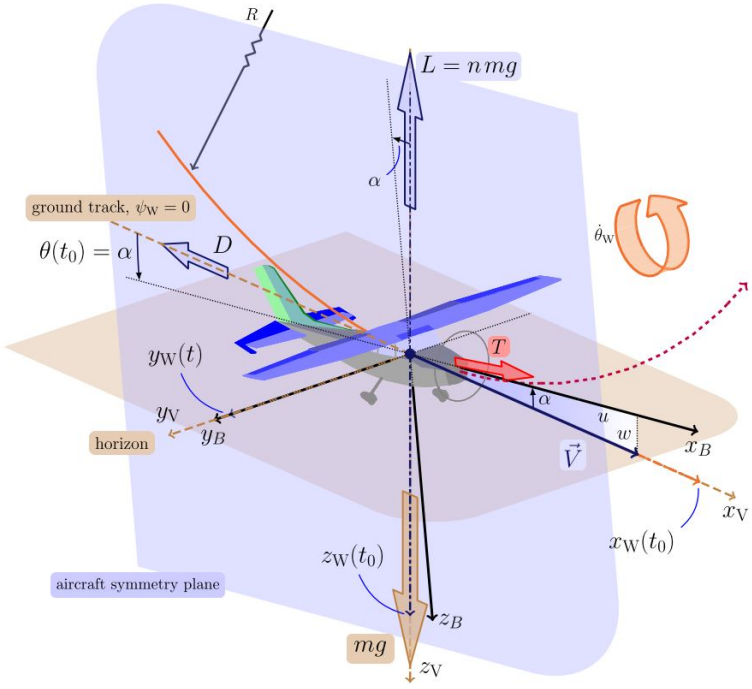

Figure 33. Longitudinal Component of Climbing Spiral Maneuver [15]

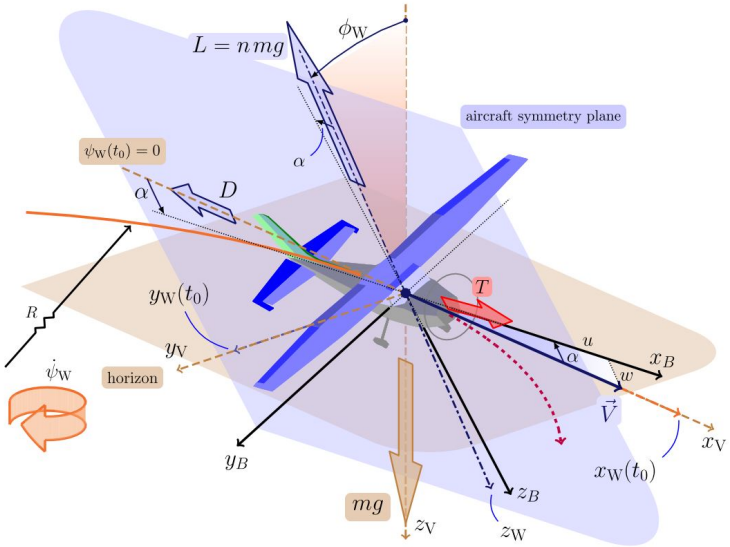

Figure 34. Lateral-Directional Component of Climbing Spiral Maneuver [15]

A large number of cases will be computed to express the connection between vehicle configuration, represented by stability derivatives, and the response character-

istics. McRuer stated that such an appreciation is important in "assessing the effects of configuration changes on aircraft response and on airframe/autopilot/pilot system characteristics and showing the detailed effects of particular stability derivatives (and their estimated accuracies) on the poles and zeros, and hence on aircraft and airframe/autopilot/pilot characteristics" [17]. The understanding of the above process will give implications to the direct influence of the dominant stability derivatives on the major response modes.

The data obtained was for an airspeed of 100 knots (168.78 ft/s) at 4,000 ft altitude by varying each stability derivative individually and then determining the flight characteristics such as the damping ratios and natural frequencies. It should be noted that in general changing one stability derivative usually changes other stability derivatives. In identifying the key stability derivatives and knowing what quantity is most affected, the design of the aircraft problem is better understood. The main purpose is to show the trend because the amount varied will differ for each aircraft. Since the stability derivatives of an airplane change with aircraft configuration and flight conditions, some derivatives were in the form of look-up tables. Adjustment and modification of these stability derivatives allows the modeling of an aircraft in an altered state.

A number of papers and books have been published on the adjustment and modification of stability derivatives and their associated effects. Stability derivatives are often applied to trimmed-flight conditions at a given altitude and Mach number. The trimmed coefficients are measured by applying the control surfaces to make small perturbations from the aircraft's trimmed state. "Furthermore, the stability derivatives do not provide an adequate model of aircraft behavior for large amplitude maneuvers and very nonlinear regimes such as stall" [50]. As a result, the non-precision non-aggressive mission task will provide the closest link to the stability derivatives since

it will avoid large amplitude maneuvers associated with aggressive tasks. Stevens and Lewis identified the importance of certain longitudinal and lateral-directional stability derivatives as shown in Table 9 and 10 respectively, starting with the most important.

Table 9. Importance of Longitudinal Stability Derivatives [50]

$C_{L\alpha}$	Lift-curve Slope	Determines Ride Quality
$C_{m\alpha}$	Pitch Stiffness	<0 for Static Stability
C_{mq}	Pitch Damping	<0 for Short-period Damping
C_{mv}	Tuck Derivative	<0 gives unstable tuck
$C_{m\dot{\alpha}}$	Alpha-dot Derivative	Less important than C_{mq}

Table 10. Importance of Lateral Stability Derivatives [50]

$C_{l\beta}$	Dihedral Derivative	<0 for positive stiffness
$C_{n\beta}$	Yaw Stiffness	>0 for positive stiffness
C_{lp}	Roll Damping	<0 for roll damping
C_{nr}	yaw Damping	<0 for yaw damping

Blakelock concluded that certain stability derivatives have the most effect on the damping ratios and natural frequencies. The data was obtained by varying each stability derivative individually and then determining the damping ratios and natural frequencies. It should be noted that "this is an artificial situation; in general, any one of the stability derivatives cannot be changed without changing at least some of the other stability derivatives. However, in performing a dynamic simulation of an aircraft in connection with the design of an autopilot, the engineer must know which stability derivatives should be known most accurately for his particular design problem" [6]. Tables 11 and 12 list the stability derivatives with the most effect on the longitudinal and lateral-directional modes of oscillation. The trends shown in these tables will be verified with the results from the simulation for each stability derivative change.

Flying qualities levels are often characterized by their damping ratios and natural

Table 11. Stability Derivatives with Largest Effects on Longitudinal Damping Ratios and Natural frequencies [6]

Stability Derivative	Quantity Most Affected	How Affected
C_{mq}	ζ_{sp}	Increase C_{mq} to increase damping
$C_{m\alpha}$	ω_{sp}	Increase $C_{m\alpha}$ to increase frequency
C_{xu}	ζ_p	Increase $C_{xu}$to increase damping
C_{zu}	ω_p	Increase C_{zu} to increase frequency

Table 12. Stability Derivatives with Largest Effects on Lateral Damping Ratios and Natural frequencies [6]

Stability Derivative	Quantity Most Affected	How Affected
C_{nr}	ζ_d	Increase C_{nr} to increase damping
$C_{n\beta}$	ω_d	Increase $C_{n\beta}$ to increase frequency
C_{lp}	T_r	Increase C_{lp} to increase $\frac{1}{T_r}$
$C_{l\beta}$	T_s	Increase $C_{l\beta}$ for spiral stability

frequencies; thus, it is imperative to identify these parameters. Of the two longitudinal characteristic modes, the short-period mode is the more important; therefore, the pitch stiffness derivative, C_{m_α}, and the pitch damping derivative, C_{m_q} were varied. The elevator control power also known as the elevator effectiveness, $C_{m_{\delta_e}}$ was also varied. From the lateral-directional derivatives, the roll damping derivative, C_{l_p} was chosen to be varied. The roll mode is the main method to control the lateral attitude of the aircraft, thus the roll damping derivative was selected. The roll damping derivative "provides a moment that damps rolling motion, plays the major role in the response of the aircraft to aileron inputs, and determines the associated handling qualities" [50]. With the roll performance as one of the primary considerations in setting the lateral control power, the aileron effectiveness is a key consideration. Since the predetermined maneuvers require more roll control than yaw control, the roll control derivative, $C_{l_{\delta_a}}$, was varied. McRuer stated that "the value of C_{l_p} does directly affect the design of the ailerons, however, since C_{l_p} in conjunction with $C_{l_{\delta_a}}$ establishes the airframe's maximum available rolling velocity; this is an important criterion of flying qualities" [17]. For this reason, the roll control derivative was also

chosen as a variable parameter.

The effect of the variation of the stability and control derivatives on flying qualities was determined by using the lower-order equivalent system (LOES). LOES is in essence a simplified system of the higher-order system which is valid for a specifiable condition. "Their most important application in flight control is for aircraft transfer functions, for which the approximate factors are expressions which relate the poles and zeros with the stability derivatives and inertial properties of the vehicle" [17]. In the LOES concept, the coefficients are matched for a lower-order transfer function matching the actual frequency response over a specified frequency range. The Bode plot gain and phase are matched by minimizing a cost function from MIL-STD-1797A shown previously in Equation 1. The cost function was minimized using a multivariable optimization search routine using MATLAB's *fmincon* function. The algorithm chosen for this function was sequential quadratic programming (SQP). Because of SQP's ability to handle nonlinearities, relatively quick convergence, and robustness, SQP was the ideal algorithm. Once the cost passed below a certain threshold, the mismatch between the actual transfer function and lower-order transfer function is not considered significant, thus producing a good fit.

$$J = \frac{20}{n}\sum_{\omega_1}^{\omega_n}[(G_{HOS} - G_{LOES})^2 + .02(\phi_{HOS} - \phi_{LOES})^2] \qquad \text{(1 revisited)}$$

From the lower-order equivalent system, the natural frequencies and damping ratios for the short period, phugoid, Dutch roll modes as well as the roll mode and spiral mode time constants were calculated. The military requirements document specifies dynamic responses mainly through pole-zero requirements. The military specification dictates the range for different levels of flying qualities linked to the Cooper-Harper ratings scale. In doing so, it allows an analytic performance criterion for the dynamic behavior of the aircraft used for handling qualities studies.

3.5 Evaluation of UAV Maneuvers

In flying qualities, one of the key factors in an aircraft's rating is its mission effectiveness. For both unmanned and manned systems, one of the key criteria in evaluating an aircraft is how well the task or maneuver was performed. The pilot or autopilot commands the aircraft to perform a specific maneuver. This deviation from the "perfect" maneuver is a quantitative measure on the evaluation on the aircraft's performance. By analyzing the deviation of the aircraft's actual state from its desired state, the flying qualities of UAVs can be better understood.

For manned aircraft, one of the most important pieces of data in evaluating the aircraft are the pilot comments. Although the mission effectiveness of the aircraft is important, the workload of the pilot can not be too excessive. The combination of the system task accomplishment and pilot workload are crucial in evaluating the overall effectiveness of an aircraft. Due to the absence of the pilot in unmanned systems, other criteria will be utilized to substitute for the absence of pilot workload evaluation. For an unmanned system, particular attention will be paid to the workload of the flight control system. Specifically, the control deflection will provide an estimate on the flight control system's workload. The aircraft's deviation from the "perfect" maneuver may be within a desired margin but if the control system is being overloaded, the maneuver may not be feasible. Saturation of position limits may point towards excessive flight control system workload and loss of control effectiveness, which is undesirable.

Similarly to control deflection, the control deflection rates will provide insight into the workload of the flight control system. If the flight control system is consistently rate limiting, the workload on the flight control system may overload the system and lead to a degradation in flying qualities ratings. Rate limiting is also a primary concern as a nonlinear cause of pilot-induced oscillation (PIO) tendencies [31]. PIO

may result from both "nonlinear events such as saturation of control rate or position limits at too low a command" [32]. Although PIOs are not associated to UAVs, system induced oscillations (SIOs) must be considered. By analyzing the maneuvers, parameters and their associated values can be correlated to various levels of flying qualities.

A major part of flight control design is how to quantify the workload of the flight control system. The workload can be defined as the relationship between resource supply and task demand [47]. For smaller UAVs that may be battery powered with a shorter flight time, the resource supply aspect cannot be neglected in the workload analysis. For manned aircraft human–system integration evaluations, the workload is evaluated on task type, duration, difficulty, and resource type and demand. Physiological concerns such as cognitive and emotional stress have to be taken into account as well; however, with UAVs, the measurement is more quantitative. "Engineers, oblivious to the philosophical fact that measuring a quality transforms it into a quantity, define metrics for handling qualities" [40]. Workload is something much more difficult to quantify. For manned aircraft, the measure of the workload is quantified by asking how easy or difficult the task was for the pilot. The goodness of the aircraft is generally referenced to the pilot's comments in flight of the simulator. For remotely piloted vehicles flown by an operator from a ground station, the workload can correspond to the operator's workload. For an unmanned system with a higher level of automation, the workload can be more difficult to quantify. Although the term "workload" is a multifaceted concept for UAVs, the primary focus here is on the most critical performance based index on task workload — loss of performance from its task level imposed by the distribution of resources to multiple tasks.

In order to provide a comparison baseline among the various maneuvers, Theil's Inequality Coefficient (TIC) provides a measure of analyzing the time history of flight

data between simulations and flight tests. TIC was originally used in the field of economics as a statistical forecasting evaluator [51]. Modified for use in the aerospace industry, TIC has been used to measure the similarity between two time histories of data. Dorobantu, Seiler, and Balas have extended this analysis to "nonlinear systems, culminating in the validation of an aircraft simulation model using flight test data" [16]. TIC is defined by the following relationship shown in Equation 16:

$$TIC = \frac{\sqrt{\frac{1}{n}\sum_{i=1}^{n}(x_i - \tilde{x}_i)^2}}{\sqrt{\frac{1}{n}\sum_{i=1}^{n}x_i^2} + \sqrt{\frac{1}{n}\sum_{i=1}^{n}\tilde{x}_i^2}} \tag{16}$$

where x is the simulation time history, $\tilde{x}$ is the flight test time history, and n is the number of data samples. For the purpose of this thesis, the simulation time history will be compared to the desired tracking time history in substitute of the flight test time history. TIC values less than .25 correspond to sufficiently accurate models. The closer the value is to 0, the better the time histories match. A TIC value of 1 represents the worst case deviation indicating that the time histories are no better than a naive guess. "The normalized scale associated with the TIC is a significant advantage over the standard error metrics such as the direct $\mathcal{L}_2$ norm of the error $e = x - \tilde{x}$. By scaling the TIC based on the $\mathcal{L}_2$ norm of the two time histories being compared, the analysis is decoupled from signal units and amplitudes" [16]. The approach of using TIC as a standard will be effective in comparing the autopilot tracking performance of the various states. TIC will be used as a performance measure with the controllers set to drive the aircraft model to track desired states with nonlinearities present. Another crucial aspect of flying qualities is the workload associated with the task. Since no comparison between two control surface histories are being compared in the same maneuver, another measure type of norm must be utilized to measure how hard the flight control system was working.

The workload of the flight control system during the maneuver was measured as the deviation of the control away from its trimmed configuration. TIC was not a viable method to quantify the workload since the desired control deflection was constant. The reason for desiring a constant control deflection is because it minimizes the deviation away from the trimmed deflection, resulting in a low workload. The TIC value approached a value of one, signifying strong dissimilarity when one of the time histories was constant. Dorobantu, Seiler, and Balas stated, "Values near 1 represent the worst-case deviation, where one of the time histories is constant and zero" [16]. The fact that the desired time history was constant threw off the TIC metric even if the two time histories showed a strong similarity; therefore, another method of quantifying the workload must be applied. The most popular norm used in almost every field of engineering and science as a whole is the $\mathcal{L}_2$ norm. The $\mathcal{L}_2$ error norm is shown in Equation 17:

$$\mathcal{L}_2 = \sqrt{\frac{1}{n}\sum_{i=1}(x_1(i) - x_2(i))^2} \tag{17}$$

where x_1 is the control history and x_2 is the constant trimmed configuration. The $\mathcal{L}_2$ error norm represents a measure of average error. The higher the error norm is, the harder that the flight control system is working, accounting for large control inputs and oscillations. While the TIC was normalized, the $\mathcal{L}_2$ norm is not. In order to compare the various control surface workload, the control deflections were normalized about their minimum and maximum deflection using the aerosurface scaling component in JSBSim. The aerosurface scaling component takes control inputs from a known domain range and maps them to a specified range. By adjusting the deflection values on different scales to a notionally common scale, a more accurate assessment of the flight control system workload is accomplished, equivalent to TIC. The method of utilizing both TIC and $\mathcal{L}_2$ error norm as a measure of aircraft performance and

workload will provide a useful comparison method for the various simulation cases in this research.

3.6 Summary

By first classifying UAVs by mission task elements, the complex problem of developing flying qualities requirements can be broken down and made more manageable. The state and control vectors were defined along with a discussion of the T-41 model in JSBSim. A discussion of the flight control design was included in order to show how the model was modified to reflect the actual aircraft. The implementation of the autopilot design in order to simulate the desired closed-loop maneuver was discussed. The chapter concluded with a discussion on how the performance and workload would be assessed in the simulated maneuver. The hope is that a trend will emerge in the flying qualities with a proposal to push towards flying qualities requirements. The following chapter will present and discuss the results of the simulations.

IV Results

The baseline Cessna 172 JSBSim model was modified to reflect the characteristics of the T-41 Mescalero aircraft, reflected in the updated flight envelope. A trim analysis was completed for the aircraft at various altitudes along with an initial evaluation of the flying qualities using requirements for fixed-wing aircraft. Following the trim analysis, the simulation cases were investigated for the various cases of the performance maneuver. For each case investigated, the simulation and flying qualities were compared and analyzed.

4.1 T-41 Flight Envelope

JSBSim comes with a library of aircraft, one of which is the Cessna 172. The T-41 is the military variant of the Cessna 172 manufactured by Cessna Aircraft Company. Modifications were made to the existing Cessna 172 xml file to reflect those changes; however, the two aircraft are overall quite similar. The Cessna 172 in the JSBSim aircraft library is powered by the four-cylinder Lycoming Model O-320 engine rated at 160 hp. The T-41 is powered by a six-cylinder Continental Model I0-360-D engine, rated at 210 hp at 2,800 RPM [48]. The overall dimensions of the T-41 are very similar to the Cessna 172 but some slight adjustments such as the wing span and propeller diameter were made. The flight envelopes for the original Cessna 172 and adjusted T-41 are graphed on Figure 35. With the T-41's more powerful engine, the flight envelope is extended but retains its general trend and shape.

The goal of this research was not to validate JSBSim's capability to model a T-41 aircraft to a high degree of fidelity. Instead, an aircraft model with reasonable characteristics to what is being modeled is desired. Comparing the flight envelope to the T-41 performance specifications in the flight manual, the flight envelope portrays

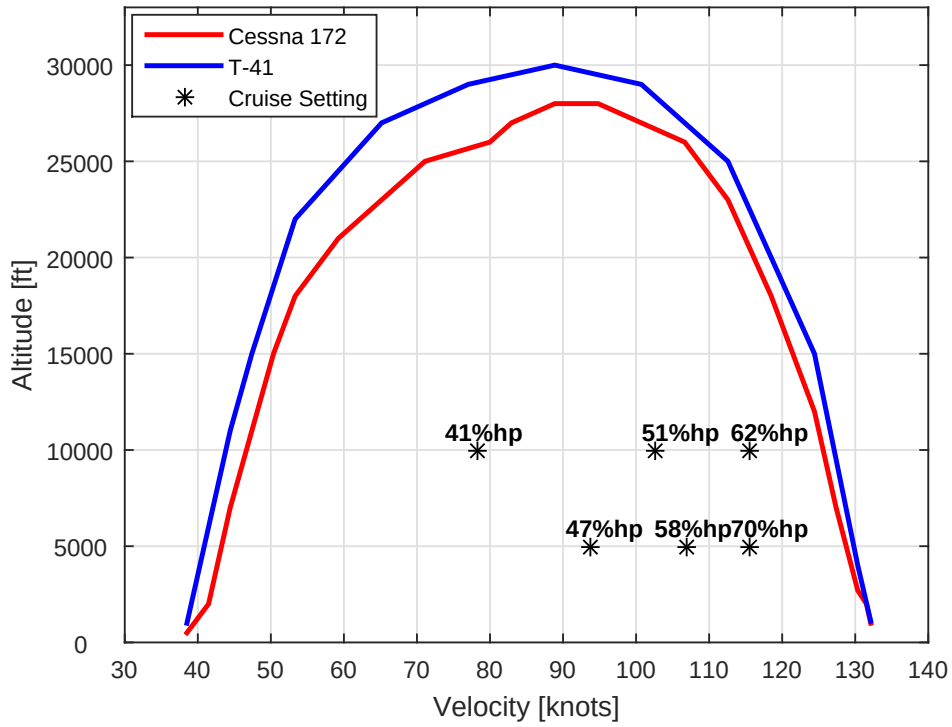

Figure 35. Flight Envelope

the T-41 to a acceptable degree of accuracy. For these performance parameters, it was assumed that the aircraft's weight was 2,500 lbs, standard atmospheric conditions with zero wind, and 45 gallons of fuel. Figure 35 has specific cruise conditions from the flight manual plotted at 5,000 and 10,000 ft on the flight envelope. Typically, the cruise conditions are intended to maximize the aircraft's range without overexerting the aircraft's capability. The cruise conditions should not be near the edge of the flight envelope. All the cruise conditions points are within the flight envelope comfortably. At the 41% hp and 47% hp conditions, these points lie comfortably in the middle of the flight envelope. As the power is increased over 50% hp at the same altitude, the cruise performance points approach the edge of the flight envelope in a nonlinear fashion.

Other key performance parameters shown in Table 13 that were verified were

the normal operating airspeed range, maximum structural speed, and stall speed. From the T-41C Flight Manual, the normal operating range is between 55 and 126 knots. The flight envelope in Figure 35 extends from 41 to 131 knots. The maximum structural speed is 128 knots which lies close to the right edge of the flight envelope. The stall speed is 46 knots lying close to the left edge of the flight envelope. Often times, the manufacturer includes a buffer zone to mitigate the risk of approaching the edge of the operating envelope which should be taken into consideration as well. The stated service ceiling of 14,000 ft is due to the fact that the cockpit is not pressurized. The Federal Aviation Regulations state that "no person may operate a civil aircraft of U.S. registry at cabin pressure altitudes above 14,000 feet unless the required flight crew is provided with and uses supplemental oxygen during the entire flight time at those altitudes" [18]. Otherwise, the aircraft itself has the capability to achieve higher altitudes.

Table 13. Flight Envelope Limits [48]

Stall Speed (V_{stall}), KCAS	40
Maximum Structural Speed (V_{no}), KCAS	126
Normal Operating Range, KCAS	55-126
Service Ceiling, ft	14000

In the flight envelope, the aircraft is bounded by stall limits at low speeds and available thrust at high speeds. Figures 36 and 37 depict the angle of attack and throttle setting for the velocity range at the edge of the flight envelope, thus verifying the stall and thrust limits. The altitude setting on the flight envelope's edge is also noted on Figures 36 and 37. At low speeds near the stall velocity, the aircraft is pitched at a high angle of attack. As the aircraft increases in speed, the angle of attack decreases and the throttle setting increases and plateaus at 100%, which becomes a limiting factor.

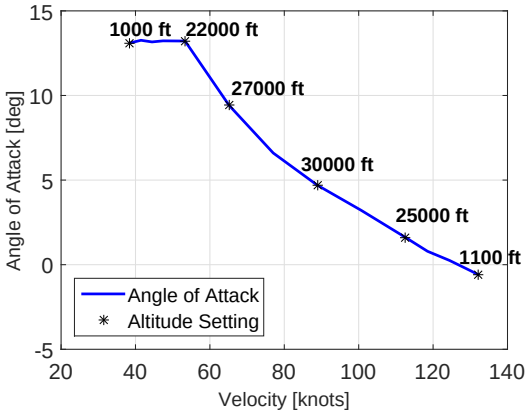

Figure 36. Angle of Attack at Trim for T-41

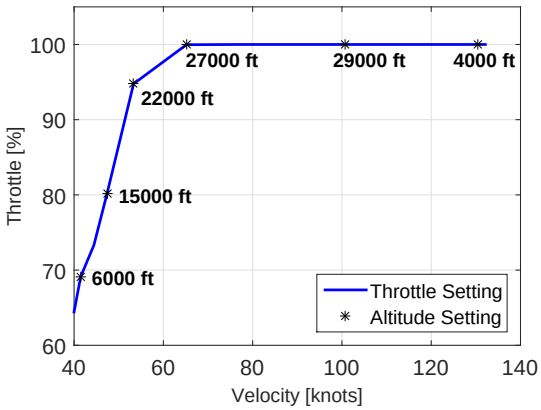

Figure 37. Throttle at Trim for T-41

4.2 Flying Qualities in Trimmed Configuration

An initial flying qualities assessment was performed with the T-41 model in its trimmed configuration. Within the flight envelope displayed in Figure 35, flight conditions were analyzed on five different flight levels: 4000 ft, 8000 ft, 12000 ft, 16000 ft, and 20000 ft. The velocity was kept constant at 100 knots or approximately 169 ft/s. These five flight conditions are located towards the center of the flight envelope, thus it should produce good flying qualities. The aircraft model was linearized in a particular trimmed flight condition. Table 14 shows the trimmed conditions for the five flight conditions. Figure 38 is a graphical depiction of the control deflection trends with increasing altitude in order to keep the aircraft trimmed.

Table 14. Trim Results for Five Flight Conditions

FC	Altitude, ft	TAS, kt	α_{trim}, °	δ_t, %	δ_e, °	δ_a,°	δ_r, °
1	4000	100	.51	75.67	4.32	-.161	-.024
2	8000	100	.79	77.12	3.84	-.163	-.017
3	12000	100	1.13	78.91	3.27	-.167	-.0094
4	16000	100	1.52	81.21	2.59	-.173	.00040
5	20000	100	1.98	83.98	1.78	-.179	.013

It is important to note the flight control system's workload at the trim condition

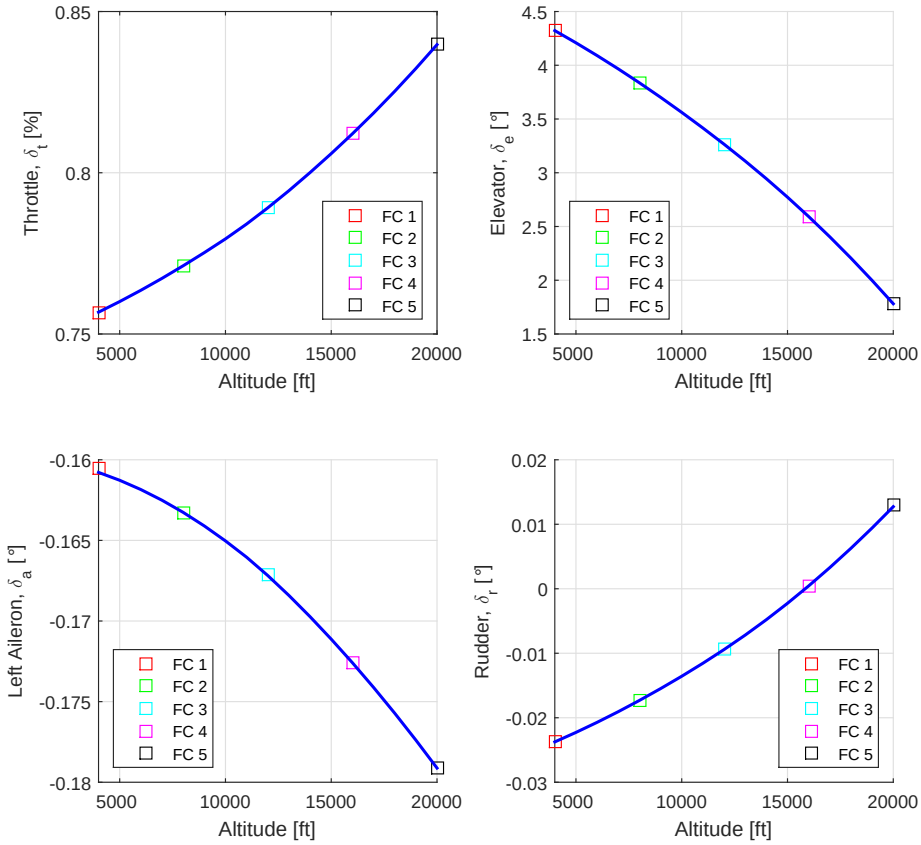

Figure 38. Control Surface Deflection and Throttle Variation with Altitude

because if the control system is "requiring 90% of pitch effectors to keep the aircraft trimmed and stable, a high rate pitch task may not be possible, and the aircraft handling qualities would be affected by purely by lack of control authority or possibly actuator rate limiting, and not just the dynamic controller response" [12]. There is ample control for trim in level flight at the five flight conditions. The control surfaces are interlinked with the flying qualities, specifically the area size and angle of deflection for the control surfaces. From Figure 38, the control surfaces operate in a small regime of angle deflection, especially the ailerons and rudders. This can be a cause of concern in the use of the control surfaces "by making the UAV more sensitive to disturbances in control surface deflection. Moreover, deflection with this precision

is difficult to achieve even though operated by power servos" [46]. In this analysis, the basic stable airframe of the T-41 is used; therefore, a stability augmentation system was not necessary. It is important to note the application of this to other basic airframes in UAVs which may not be as stable. As the basic airframe becomes more unstable, the flight control system must work harder to compensate for the unstable platform. Some key considerations for the automatic control system is the likelihood of hitting position or rate limits which often degrade the aircraft performance. The level of instability of the basic airframe must be kept below a certain value in order to mitigate the effects on the aircraft's flying qualities.

Suppose the longitudinal and lateral dynamics are decoupled, only considering one axis at a time. In addition, linear dynamic behavior will be assumed. From the actual transfer function over a limited frequency range, a lower-order equivalent system (LOES) transfer function can be matched by minimizing a cost function, previously shown in Equation 1. If the cost of 10.0 or less is achieved, a good fit to the LOES is obtained [1]. The longitudinal flying qualities will be analyzed first, followed by an analysis of the lateral directional motion.

4.2.1 Longitudinal Motion Flying Qualities

The elevator-to-pitch-angle transfer function plays a critical role in the assessment of the longitudinal-axis flying qualities. The assumed LOES form for the pitch axis is

$$\frac{\theta}{\delta_e} = \frac{K_\theta(s + 1/T_{\theta_1})(s + 1/T_{\theta_2})e^{-\tau_e s}}{(s^2 + 2\zeta_p\omega_p s + \omega_p^2)(s^2 + 2\zeta_{sp}\omega_{sp}s + \omega_{sp}^2)} \tag{18}$$

where the subscripts p and sp represent the phugoid and short-period modes respectively. Transfer functions like this and others for the lateral motion are obtained from the linearized Laplace-transformed airframe equations as ratios between the output

and input quantities. According to military regulations, the maximum allowable value for the equivalent time delay should be 10.0 ms [50]. The LOES for $\frac{\theta}{\delta e}$ is closely matched with the HOS as shown in Figure 39 which lie almost on top of each other. The mismatch between the HOS and LOES is shown in blue in Figure 40 which falls between the envelope lines; hence, the mismatch between the HOS and LOES is not significant. The Bode plots comparing the HOS and LOES as well as the envelope plots for the other four flight conditions are shown in Appendix B. The error envelope reflects that the lower-order model matches the actual model. This analysis was performed for all five flight conditions with the results tabulated in Table 15.

Table 15. LOES for Longitudinal Motion

Altitude	K_θ	T_{θ_1}	T_{θ_2}	τ_e	ω_p	ω_{sp}	ζ_p	ζ_{sp}
4000 ft	10.6850	14.679	0.2292	0.01	0.2098	7.5620	0.1297	0.7257
8000 ft	9.3092	15.589	0.2558	0.01	0.2160	7.0339	0.1115	0.6857
12000 ft	8.0923	17.377	0.2871	0.01	0.2213	6.5046	0.0938	0.6493
16000 ft	7.0184	17.935	0.3242	0.01	0.2268	6.0543	0.0813	0.6089
20000 ft	6.0711	18.203	0.3686	0.01	0.2319	5.6391	0.07052	0.5684

The phugoid mode is a low-frequency mode where the forward speed and altitude are interchanged. According to MIL-STD-1797A, the long-term response, characteristically the phugoid mode, has the flying qualities requirements shown in Table 16. Level 1 flying qualities requires the phugoid damping ratio to be greater than .04. No distinction is made between classes of aircraft. The five flight conditions shown in Table 15 all have ζ_p greater than .04, thus having Level 1 flying qualities. It should be noted that as the altitude is increased, the phugoid damping ratio approaches close to the border of having Level 2 flying qualities. As the aircraft moves further away from the center of its flight envelope, the trend shown here is that the flying qualities start to degrade.

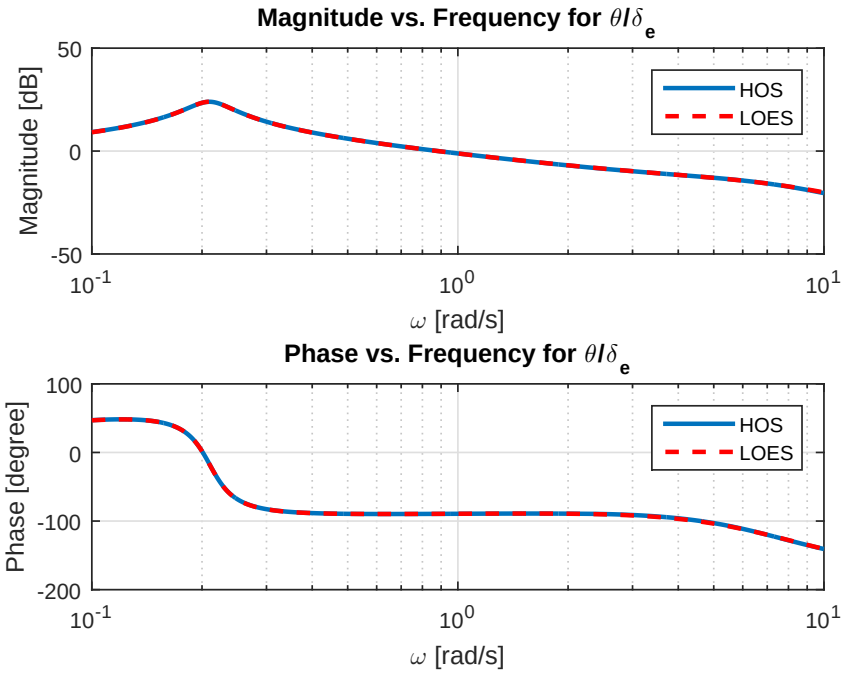

Figure 39. Bode Plot for θ/δ_e

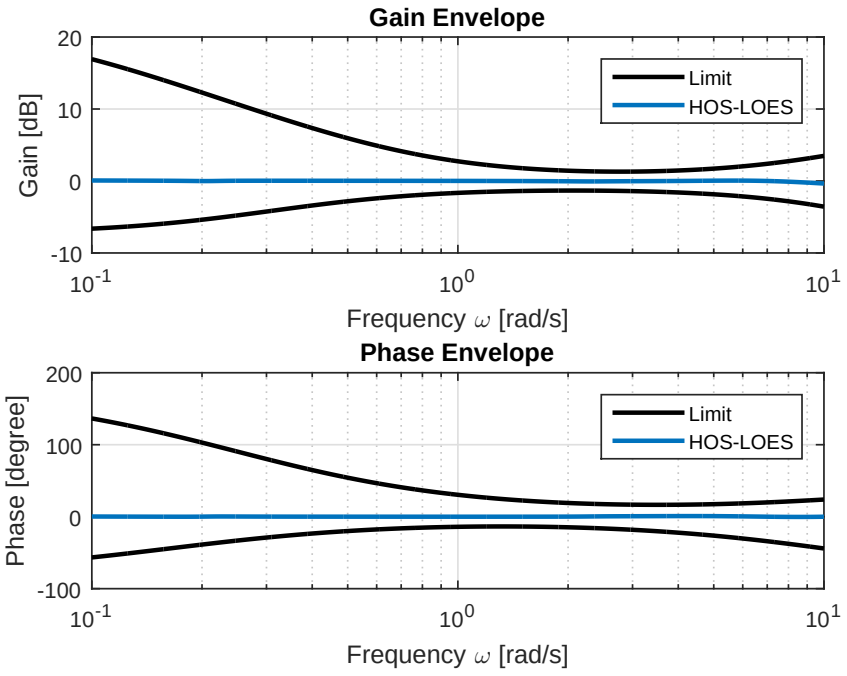

Figure 40. Error Envelope for θ/δ_e

Table 16. Phugoid Flying Qualities Requirements [1]

Level 1	equivalent $\zeta_p > .04$
Level 2	equivalent $\zeta_p > 0.0$
Level 3	$T_2 > 55$ seconds

Requirements on the equivalent pitch time delay, τ_θ apply to the $\frac{\theta}{\delta e}$ transfer function for a deflection control system. Table 17 outlines the levels for the time delay requirements. All five flight conditions contain Level 1 flying qualities with τ_θ below the defined requirement of .10 second.

Table 17. Equivalent Pitch Time Delay Requirements [1]

Level 1	$\tau_\theta < .10$ sec
Level 2	$\tau_\theta < .20$ sec
Level 3	$\tau_\theta < .25$ sec

The short period is a rapid mode governing the transient changes in angle of attack, pitch, flight path and normal load factor that occur following rapid control or gust inputs [27]. The short-term response known as the short-period mode has requirements specified in terms of $\omega_{sp}, T_{\theta_2}$, and ζ_{sp} of the LOES shown in Figure 41. The term $\omega_{sp}T_{\theta_2}$ is similar to the literal factor CAP; therefore, is used as a measure to determine the level of flying qualities. Also shown are the results from the five flight conditions.

As expected, the T-41 has good flying qualities achieving borderline Level 1 and 2 for Category A Flight Phase. Category A Flight Phase involves high-precision and high-workload tasks, making it the most difficult of the flight phases to achieve the best flying qualities. For Category B Flight Phase, the T-41 attains all Level 1 flying qualities. For Category C Flight Phase, it also attains Level 1 flying qualities. As the altitude increases, the aircraft approaches the left borderline for Level 2 flying qualities. Overall, the short-term pitch response is quite satisfactory for all three flight phases.

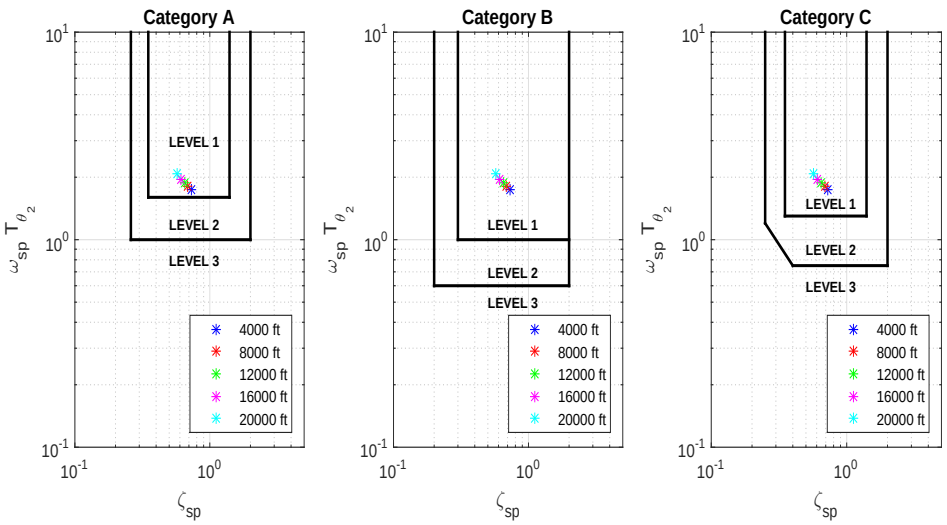

Figure 41. Results for Short-term Pitch Response to Pitch Controller [1]

"A measure of the handling qualities of an aircraft is its stability margin when operated in a closed-loop compensatory tracking task" [1]. The maximum frequency at which the closed-loop tracking can occur without approaching instability is called bandwidth (ω_{BW}). The assumption is that the pilot or control system can sufficiently follow input commands with frequencies up to the bandwidth. The Bode plot was used to estimate the flying qualities bandwidth using the robust definition of 6 dB of gain margin and 45 degrees of phase margin with the results presented in Table 18.

Table 18. Bandwidth Results

Altitude	Bandwidth
4000 ft	$\omega_{BW} = 9.036$ rad/s
8000 ft	$\omega_{BW} = 8.471$ rad/s
12000 ft	$\omega_{BW} = 7.869$ rad/s
16000 ft	$\omega_{BW} = 7.343$ rad/s
20000 ft	$\omega_{BW} = 6.884$ rad/s

From the bandwidth results, an estimate of the flying qualities can be predicted for Category A Flight Phase by plotting the time delay τ_p vs. ω_{BW} as illustrated in Figure 42. All five flight conditions are contained inside the perimeter of the Level 1 flying qualities. As the altitude increases from 4,000 to 20,000 feet, the T-41

approaches the edge of the Level 2 flying qualities as expected. The trend seen here is that as the altitude increases, there is a degradation in flying qualities confirming the previous trends seen in other literal factors. As the aircraft deviates from the center of its flight envelope towards the edge of the envelope, the flying qualities of the aircraft suffer as well.

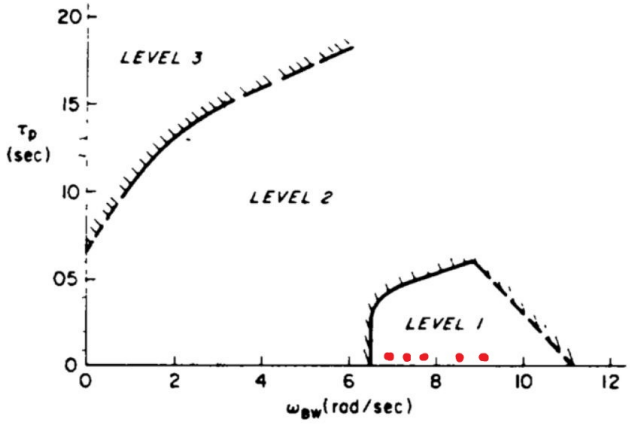

Figure 42. Bandwidth and Time Delay Requirements [1]

4.2.2 Lateral Motion Flying Qualities

Similar to the analysis of the longitudinal-axis flying qualities, a LOES was assumed for the lateral-axis transfer function. MIL-STD-1797A recommends using the aileron-to-roll-angle transfer function in the assessment of the lateral-axis flying qualities [1]. The assumed LOES for the lateral axis is

$$\frac{\phi}{\delta_a} = \frac{K_\phi(s^2 + 2\zeta_\phi\omega_\phi s + \omega_\phi^2)e^{-\tau_{e\phi}s}}{(s + 1/T_S)(s + 1/T_R)(s^2 + 2\zeta_d\omega_d s + \omega_d^2)} \tag{19}$$

where the subscripts ϕ and d represent the roll and Dutch roll modes respectively. Mathematically, when the complex roots cancel($\omega_\phi = \omega_d$ and $\zeta_\phi = \zeta_d$), the Dutch roll is not excited at all from the bank angle response [1]. An equivalent system fit to the higher-order system over the frequency range from .1 rad/s to 10.0 rad/s was

utilized. The comparison of the HOS and LOES is shown in Figure 43 with the T-41 configured at 4000 ft. The low cost confirms that the LOES approximates the HOS dynamics quite well. The mismatch between the HOS and LOES shown in Figure 44 also validates that the mismatch between the HOS and LOES is not significant. The LOES fit was performed for all five flight conditions with the results tabulated in Table 19. The mismatch plots and error envelopes for the other four flight conditions are shown in Appendix B.

Table 19. LOES for Lateral Motion

Altitude	K_ϕ	ζ_ϕ	ω_ϕ	τ_ϕ	T_S	T_R	ζ_d	ω_d
4000 ft	0.5770	2.0649	1.6555	0.1398	54.682	0.2524	0.1722	2.3501
8000 ft	0.4589	2.3188	1.7523	0.1225	63.675	0.2500	0.16043	2.2173
12000 ft	0.3630	2.5678	1.8124	0.1016	78.675	0.2596	0.1490	2.0894
16000 ft	0.2976	2.7649	1.8048	0.07898	109.43	0.2797	0.1380	1.9669
20000 ft	0.2669	2.8337	1.6920	0.05794	205.03	0.3095	0.1277	1.8501

The requirement on the roll mode is directed at precision of the aircraft's roll control. The equivalent roll mode time constant, T_R, describes the aircraft roll damping. When the aircraft rolls about its x-axis, "the roll inertia produces a resisting moment proportional to the product of the roll inertia and the roll acceleration" [27]. The roll rate causes one wing to move upward and the other wing to move downward, thus producing a resisting damping moment. The requirement on the roll-mode time constant, T_R, for the various flight phase categories is shown in Table 20. For Category A Flight Phase, the T-41 is considered a Class I aircraft with a maximum roll-mode time constant of 1.0 in order to have Level 1 flying qualities. From the five flight conditions in Table 19, all five roll-mode time constants were below 1.0 second resulting in Level 1 flying qualities for Category A Flight Phase. With Category A Flight Phase containing the strictest requirements, the T-41 automatically passes the Level 1 flying qualities criteria for Category B and C Flight Phases. It should be noted that as the altitude increased, the roll mode time constant increased as well, degrading

the flying qualities.

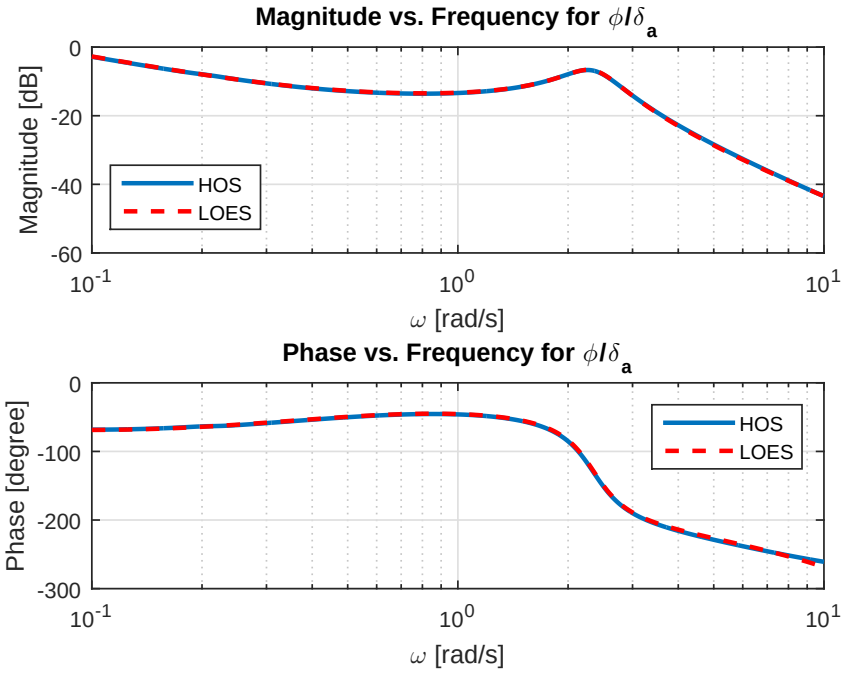

Figure 43. Bode Plot for ϕ/δ_a

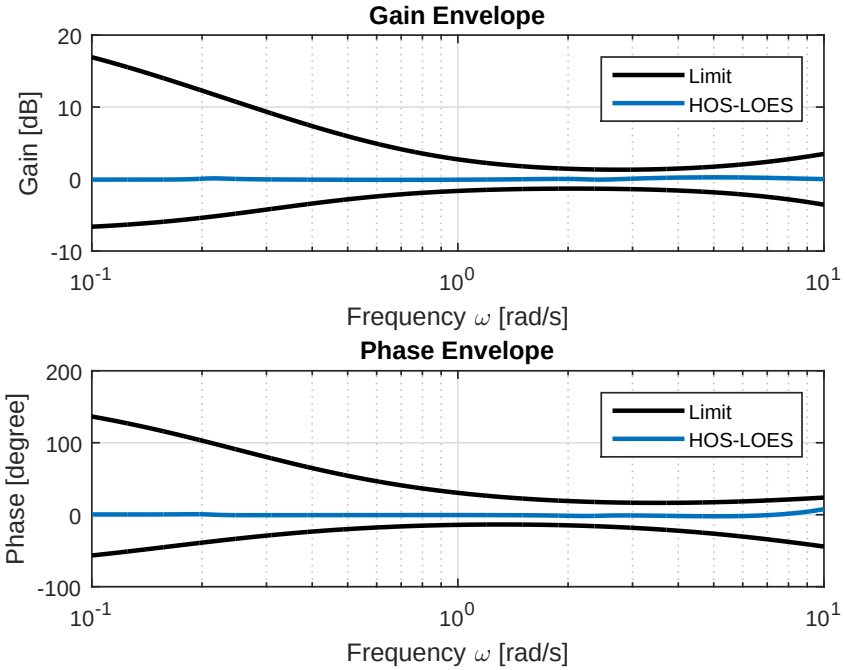

Figure 44. Error Envelope for ϕ/δ_a

Table 20. Recommended Maximum Roll-Mode Time Constant [1]

Flight Phase Category	Class	Level		
		1	2	3
A	I, IV	1.0	1.4	10
	II, III	1.4	3.0	
B	All	1.4	3.0	
C	I, II-C, IV	1.0	1.4	
	II-L, III	1.4	3.0	

The spiral mode is characterized by slow rolling and yawing motion to a roll disturbance. The spiral mode is allowed to be unstable, but military specifications contain a requirement to prevent too-rapid divergence. The limits are placed on the minimum time to double amplitude for unstable poles, as shown in Table 21. "These requirements must be met following a roll-angle disturbance of up to 20 degrees from trimmed for zero-yaw-rate wings-level flight, with the cockpit controls free" [50]. From the LOES in Equation 19, the pole corresponding to the spiral mode is $\lambda = -1/T_S$. The spiral-mode time constant, T_S, for all five conditions is positive resulting in stable poles. As a result, the T-41 model possesses Level 1 flying qualities for the spiral mode. With increasing altitude, the time constant of the spiral mode increased as well, indicating that the spiral mode was coming closer to instability. The closer the spiral mode was to becoming unstable, the worse the flying qualities became. The flying qualities became more undesirable as the altitude increased for both the roll mode and spiral mode. The degradation in flying qualities with increasing altitude was seen previously in the longitudinal modes as well.

Table 21. Recommended Minimum Time to Double Amplitude

Flight Phase Category	Level 1	Level 2	Level 3
A and C	12 sec	8 sec	4 sec
B	20 sec	8 sec	4 sec

The Dutch roll mode is the lateral-axis short period oscillatory mode, typically occurring in the frequency range from 1-5 rad/s [27]. The rudder primarily excites the

Dutch roll mode. The Dutch roll caused by aileron deflection is caused by the yawing moment from the control deflection. The Dutch roll response must be sufficiently damped in order to produce good flying characteristics. The flying qualities criteria Dutch roll have been specified by the Dutch roll undamped natural frequency, ω_d, and the damping ratio ζ_d. These criteria are specified in Table 22.

Table 22. Recommended Minimum Dutch Roll Frequency and Damping [1]

Level	Flight Phase Category	Class	Min ζ_d	Min $\zeta_d\omega_d$	Min ω_d
1	A	I, IV	.19	.35	1.0
		II, III	.19	.35	.4
	B	All	.08	.15	.4
	C	I, II-C, IV	.08	.15	1.0
		II-L, III	.08	.10	.4
2	All	All	.02	.05	.4
3	All	All	0	-	.4

The quantity $\zeta_d\omega_d$ is the s-plane real-axis coordinate, and ω_d is the distance from the origin for complex roots. Together, these two parameters outline the area on the s-plane in which the Dutch roll roots must lie. The results for the Dutch roll mode for the five flight conditions are specified in Table 23. For Category A Flight Phase, the T-41 contains Level 2 flying qualities, but it should be noted that at low altitudes, it is quite close to reaching Level 1 flying qualities. For Category B and C Flight Phases, the T-41 contains Level 1 flying qualities. Flying qualities associated with good Dutch roll mode characteristics were seen at the lower altitudes. The roll, spiral, and Dutch roll mode flying qualities were all consistently rated best at the lower altitude, which coincides with the results from the longitudinal flying qualities analysis.

By increasing the flight altitude, the natural mode characteristics started to deteriorate. Figures 45 and 46 provide an overall picture of the natural frequency and damping ratio for both the longitudinal and lateral modes of motion. Both the natural frequency and damping ratios decreased with increasing altitude, deviating further

Table 23. Dutch Roll Mode Specification Results

Altitude	ζ_d	$\zeta_d\omega_d$	ω_d
4000 ft	0.1722	.4046	2.3501
8000 ft	0.1604	.3557	2.2173
12000 ft	0.1490	.3113	2.0894
16000 ft	0.1380	.2715	1.9669
20000 ft	0.1277	.2362	1.8501

away from Level 1 flying qualities. The short period mode exhibited the greatest reduction in its damping ratio by approximately 20% climbing from 4,000 ft to 20,000 ft. All the poles for all five flight conditions were however stable lying on the left-half plane of the root locus.

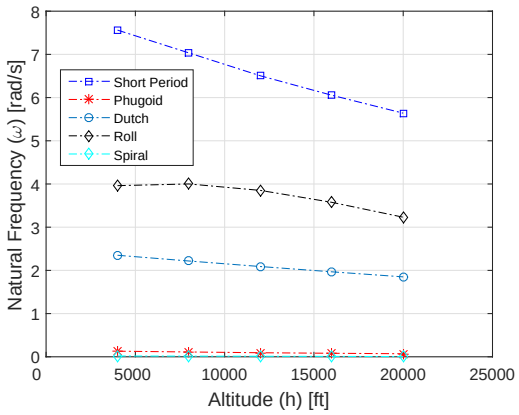

Figure 45. Natural Frequency as Function of Flight Altitude

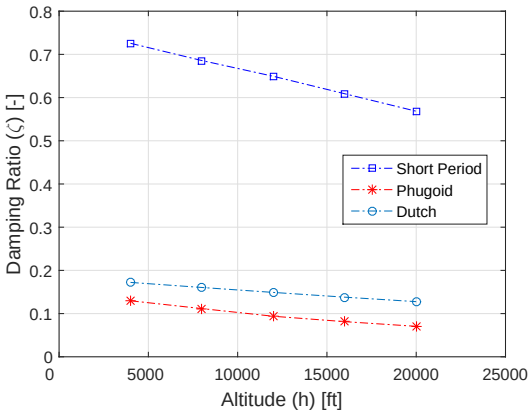

Figure 46. Damping Ratio as Function of Flight Altitude

4.3 Nominal Non-Precision Non-Aggressive Maneuver

Mission Task Elements (MTEs) provide a link to top level mission requirements. "MTEs set expectations for precise control of an aircraft, define levels of aggressiveness required to adequately stress the system, and can provide provisions for environmental conditions" [28]. As the maneuvers increase in aggressiveness and precision, the aircraft deficiencies are illuminated. The maneuver analyzed in this investigation

is a non-precision, non-aggressive maneuver.

A set of simulations have been performed to verify the the handling qualities of the T-41 based on the requirements from MIL-STD-1797A. All the simulations started at 0° latitude, 0° longitude and initiated the maneuver after 20 seconds of trimmed flight. 250 seconds into the simulation, the maneuver was terminated and the aircraft returned to straight level flight. The implemented autopilot is a series of PID controllers as explained in Chapter III. During the autonomous flight, the vehicle will perform three climbing spirals at various rates of climb and bank angles. The purpose of this simulation is to verify whether the mission task can be accomplished with a sufficient amount of control authority. The control system should not be pushed to its limit for the non-precision, non-aggressive maneuver. Before analyzing the coupled maneuvers, the climbing spiral will be decoupled into its two parts, one in the longitudinal plane, and one in the lateral-directional plane. Once the simulations in the longitudinal and lateral-directional plane are completed, the simulation of the coupled maneuver will be presented.

4.3.1 Longitudinal Decomposition

The climbing spiral's longitudinal component is composed of a straight wing level climb at a constant rate of climb. Small, moderate, and large control inputs were defined in the form of the rate of climb autopilot. Three separate simulations were carried out at the desired rates of climb as shown in Table 24. This portion of the climbing spiral was used to examine the rate of climb and velocity hold requirement using the elevator and throttle controls. The lateral-directional requirements for bank angle and sideslip angle were ignored for this maneuver.

The aircraft was successful in performing all three maneuvers with no noticeable difficulty. Figure 47 shows the longitudinal component for all three maneuvers at the

Table 24. Longitudinal Maneuvers

Maneuver	Rate of Climb ($\dot{h}$)
1	4 ft/s
2	6 ft/s
3	8 ft/s

specified rates of climb at 4, 6, and 8 ft/s. All three maneuvers initially trimmed for 20 seconds to ensure that the aircraft was kept at level, unaccelerated flight. After the trimmed flight, the aircraft commenced the climb and leveled out 250 seconds into the simulation. Figure 48 shows how well the autopilot functioned in achieving its desired rate of climb and velocity. The aircraft's altitude and pitch angle are also shown in Figure 48. The aircraft was successful in adjusting the controls to climb at the specified rate and maintaining its velocity. Figure 49 shows the control initiation and termination plots for the maneuver. As the aircraft continued its climb, the throttle slightly increased in order to compensate for the thinner air. The elevator deflected at the initiation and termination of the maneuver. Between the maneuver's initiation and termination, the elevator returned very closely back to its trimmed configuration.

Table 25 shows the quantitative assessment of the maneuver using TIC and $\mathcal{L}_2$ norm. All the TIC values are below .25; hence, the autopilot did a sufficient job at attaining and maintaining the desired values. It is important to note that the small magnitude for the TIC values stems from the fact that besides the initiation and termination of the maneuver, the aircraft is in steady flight. In other words, the autopilot does an adequate job of maintaining the desired states throughout the maneuver except during the transient initiation and termination periods; therefore, small values of TIC were expected. As the maneuver's rate of climb increased, the TIC values and $\mathcal{L}_2$ norm values increased as well. The increasing TIC values signify that the time histories between the desired and actual states are deviating away

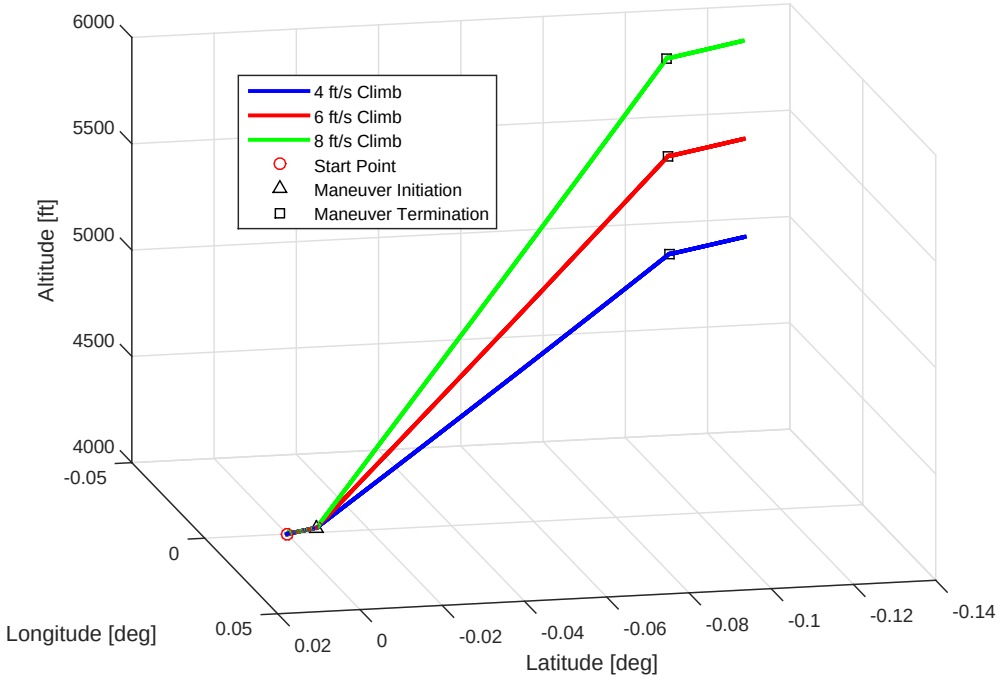

Figure 47. Climbing Performance Plots

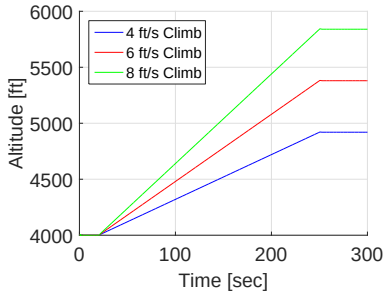

(a) Altitude, h

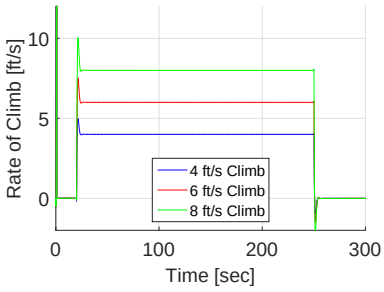

(b) Rate of Climb, $\dot{h}$

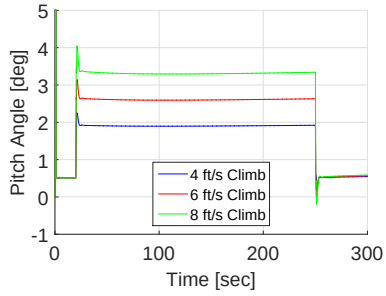

(c) Pitch Angle, θ

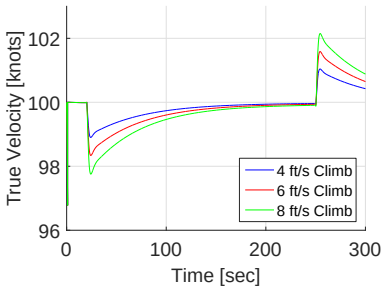

(d) Velocity, v_t

Figure 48. Climb Performance Plots

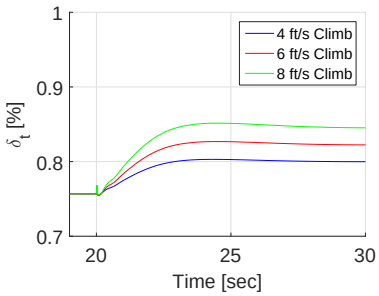

(a) Throttle Initiation

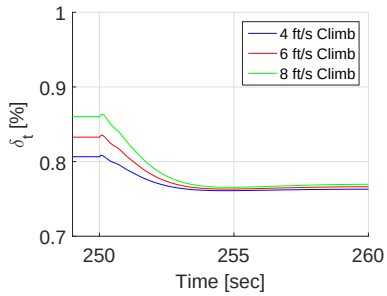

(b) Throttle Termination

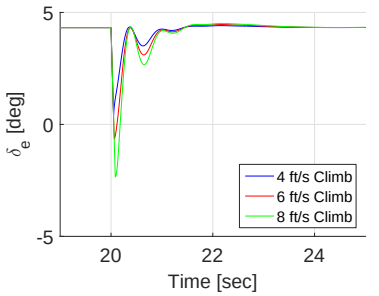

(c) Elevator Initiation

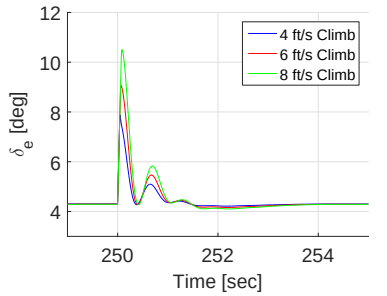

(d) Elevator Termination

Figure 49. Climb Control Plots

from each other. The increasing $\mathcal{L}_2$ norm values represent the control's increased workload as the maneuver's rate of climb increased. As expected, the autopilot was not able to track the desired states as closely and the control workload increased as the maneuver's aggressiveness increased. Performance degradation and workload escalation were associated with the more aggressive maneuvers.

Table 25. Evaluation of Nominal Climbing Maneuver

Climb	TIC ($\dot{h}$)	TIC (v_t)	$\mathcal{L}_2$ (δ_t)	$\mathcal{L}_2$ (δ_e)
4 ft/s	0.02745	0.002167	0.0427	0.0047
6 ft/s	0.02808	0.003293	0.0649	0.0070
8 ft/s	0.02851	0.004456	0.0877	0.0092

4.3.2 Lateral-Directional Decomposition

The climbing spiral's lateral-directional component is composed of a banked turn at a constant altitude. Like in the longitudinal decomposition, three separate simula-

tions were carried out at the desired bank angles as shown in Table 26. This element of the climbing spiral was used to examine the bank angle and sideslip requirements using the aileron and rudder controls. The longitudinal requirements were ignored for this maneuver.

Table 26. Lateral-Directional Maneuvers

Maneuver	Bank Angle (ϕ)
1	10°
2	20°
3	30°

The maneuver was successfully implemented by the autopilot without much difficulty. Figure 50 shows the lateral-directional performance maneuver at the specified bank angles of 10°, 20°, and 30°. As the maneuver's bank angle increased, the turning radius decreased. Like in the previous maneuver, the aircraft was trimmed for 20 seconds to ensure that the aircraft was in level, unaccelerated flight. After trimming, the aircraft banked while maintaining its altitude. Like in the longitudinal maneuver, the maneuver ended at 250 seconds with the aircraft returning to straight and level flight. Figure 51 shows the performance plots associated with the lateral mode of motion. With increasing bank angle, the overshoot and settling time started to increase in the bank angle's response. In addition, the sideslip's oscillation amplitude increased as the maneuver's bank angle increased. The control history used to obtain these responses is shown in Figure 52. The ailerons deflected at the initiation and termination of the maneuver and returned back to its trimmed configuration in-between these two points. As the maneuver's bank angle increased, the rudder deflection increased simultaneously. The rudder remained continuously deflected during the turn in order to keep the sideslip angle constant throughout the entire turn.

Table 27 shows the quantitative assessment of the lateral maneuver. Since there was no climb involved with the maneuver, the TIC values for velocity were much lower

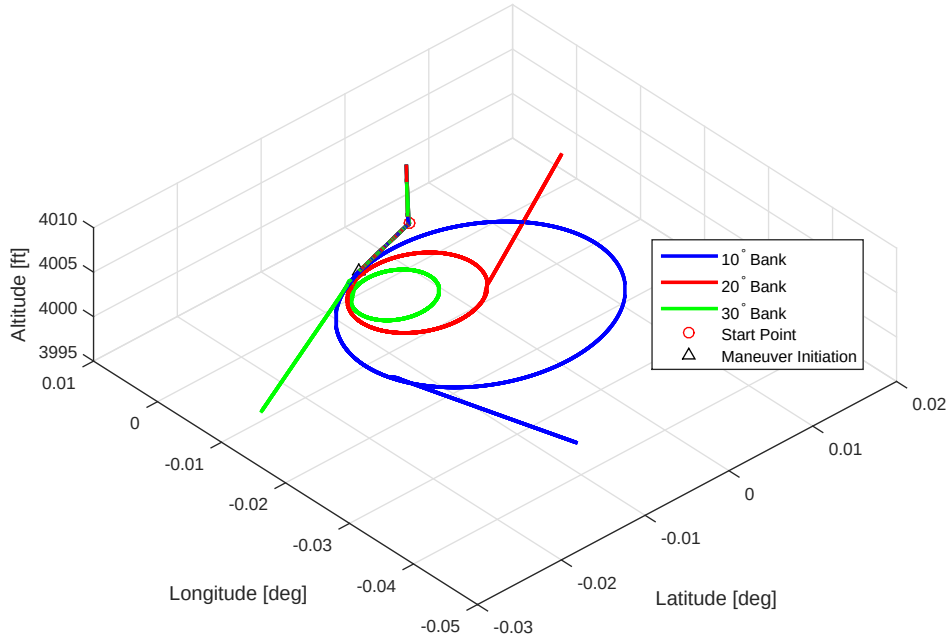

Figure 50. Banking Performance Plots

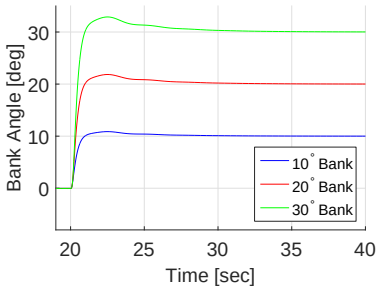

(a) Bank Angle Initiation

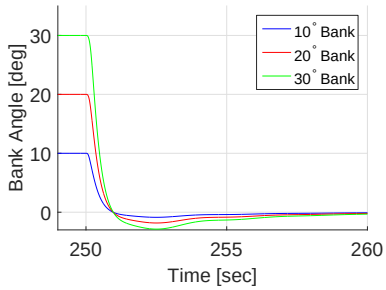

(b) Bank Angle Termination

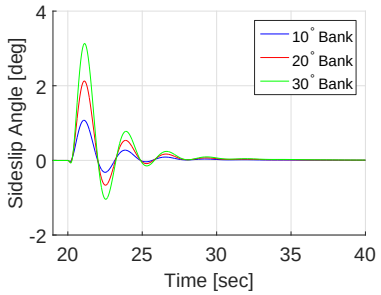

(c) Sideslip Angle Initiation

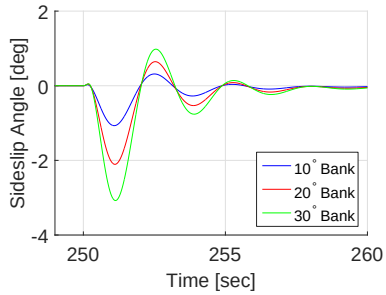

(d) Sideslip Angle Termination

Figure 51. Bank Turn Performance Plots

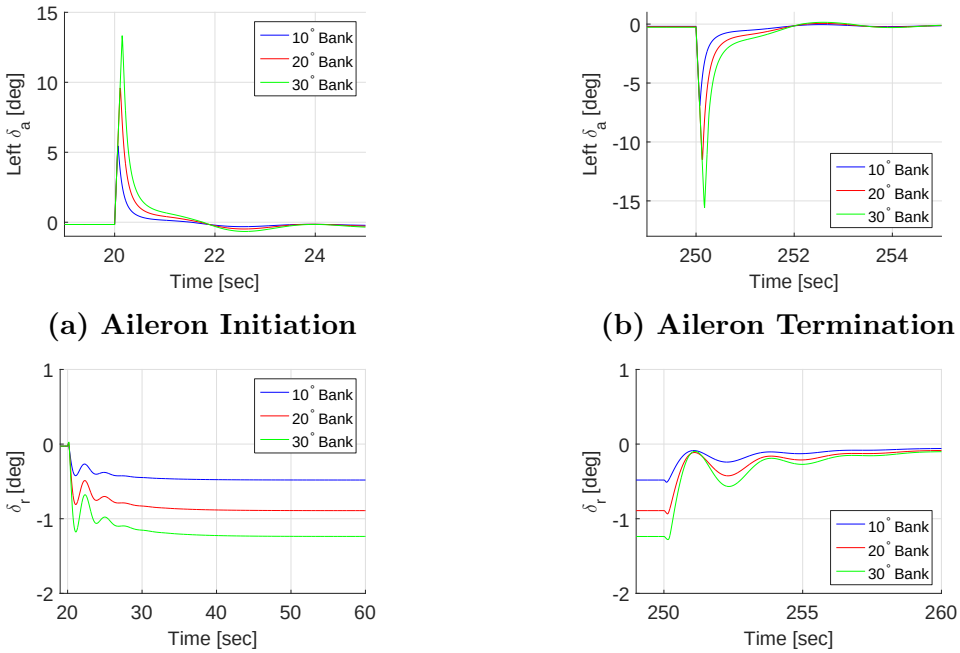

(a) Aileron Initiation **(b) Aileron Termination**

(c) Rudder Initiation **(d) Rudder Termination**

Figure 52. Bank Turn Control Plots

than in the longitudinal maneuver indicating that the velocity was tracked better for the lateral maneuver. The $\mathcal{L}_2$ norm value for the rudder is larger than the ailerons because the rudder has to stay continuously deflected during the turn. The ailerons obtained a large deflection angle for a short amount of time as shown in Figures 52a and 52b explaining the lower $\mathcal{L}_2$ norm value. With such large aileron deflections, consideration has to be taken for position limiting. Upon initiation of the 30° banked maneuver, the ailerons deflected 13.3°, which is 89% of the ailerons' deflection limit of 15°. On the other hand, the rudder had only reached a peak deflection of 1.2°, which is 8% of the rudder's deflection limit of 16°. It is insufficient to conclude that the $\mathcal{L}_2$ norm values capture the control workload entirely. The deflection limits of the various controls have to be investigated as well as the $\mathcal{L}_2$ norm values. In the lateral maneuver, the aircraft had a sufficient amount of control authority to complete the maneuver in a satisfactory manner; however, there is some concern about potentially

saturating the position limits of the ailerons.

Table 27. Evaluation of Nominal Banking Maneuver

Bank	TIC (v_t)	TIC (ϕ)	$\mathcal{L}_2$ (δ_a)	$\mathcal{L}_2$ (δ_r)
10°	0.0001102	0.02403	0.0093	0.0255
20°	0.0002187	0.02530	0.0179	0.0486
30°	0.0003387	0.02632	0.0262	0.0680

4.3.3 Climbing Spiral

Combining the longitudinal and lateral-directional maneuvers into a single coupled maneuver, the resulting maneuver is a climbing spiral requiring the aircraft to climb and bank simultaneously. Three separate simulations were done at the desired rates of climb and bank angles as shown in Table 28. The coupled maneuver examined the rate of climb, velocity, bank angle, and sideslip requirements using all available controls.

Table 28. Coupled Maneuvers

Maneuver	Rate of Climb ($\dot{h}$)	Bank Angle (ϕ)
1	4 ft/s	10°
2	6 ft/s	20°
3	8 ft/s	30°

The aircraft was able to successfully complete all three coupled maneuvers without any significant difficulty. The three-dimensional view for all three climbing spirals is shown in Figure 53. It is clearly evident that the more aggressive maneuvers had a tighter turning radius as well as a higher final altitude than the less aggressive maneuvers. The simulation was timed long enough in order to allow at least one complete cycle of the climbing spiral for the least aggressive maneuver.

The aircraft was able to successfully implement the autopilot in reaching the four desired setpoints as shown in Figure 54. The aircraft was able to reach and maintain its commanded rate of climb, bank angle, velocity, and sideslip angle. As

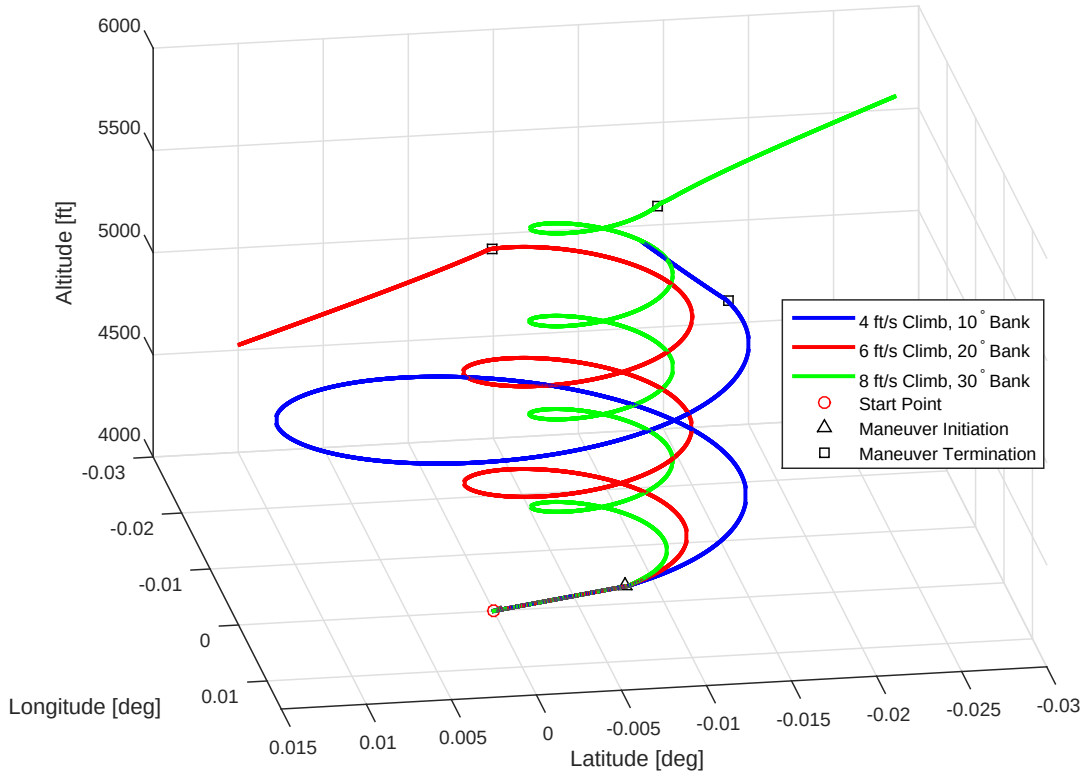

Figure 53. Climbing Spiral Performance Plots

the maneuver increased in bank angle and rate of climb amplitude, the control surfaces were deflecting further away from their trimmed values. The corresponding control deflections for all three maneuvers are shown in Figure 55. While the results from the longitudinal and lateral-directional maneuvers largely match the coupled maneuver, there were some subtle differences. The throttle's control overshoot had more than doubled in the coupled maneuver due to the loss in velocity associated with a banked maneuver as shown in Figure 55a. In the longitudinal maneuver, the throttle had an overshoot of .75%, but in the coupled maneuver the throttle had an overshoot of 1.65%. Further inspection of the graph, specifically the elevator deflection in Figures 55c and 55d, reveals that the elevator does not return to its trimmed deflection configuration throughout the maneuver like in the longitudinal maneuver. In the most

aggressive maneuver, the elevator maintains a constant deflection of 3.1° without returning back to its trimmed deflection of 4.3°. Since there was banking involved in the coupled maneuver, the elevator had to compensate for the loss in climb rate stemming from the lateral component of the maneuver. In the coupled maneuver, the controls have to account for the drop in airspeed and altitude with a banked turn.

Table 29 shows all the TIC and $\mathcal{L}_2$ norm values for the tracked autopilot values and controls. The TIC values are all below 0.25; hence, the autopilot did a sufficient job at attaining and maintaining the desired values. All the controls were not pushed to the limit, noted by their low $\mathcal{L}_2$ norm values. In comparing the control effort, the throttle had the largest $\mathcal{L}_2$ norm signifying that the throttle may be the limiting factor for more advanced maneuvers. It can be seen from Figures 55a and 55b that the throttle is positioned around 85% of its maximum limit for the climb at 8 ft/s and bank at 30°. Overall, there is ample control authority to perform more aggressive maneuvers as expected. Since this is considered a non-precision, non-aggressive maneuver, the controls should not be overexerted. It is important to note that the aircraft response is also dependent on the autopilot controller design.

Comparing the TIC and $\mathcal{L}_2$ norm values to the longitudinal maneuver, one may expect that the TIC values for the climb would be lower than the climbing spiral; however, this was not the case. Looking at the pitch angle, θ, in Figure 48c, the overshoot and oscillation is noticeably less than the response for the coupled maneuver in Figure 54c. It is speculated that the coupled maneuver's rate of climb did not overshoot as much due to the loss in altitude and velocity associated with the coupled maneuver. The throttle and elevator controls had a higher workload in the coupled maneuver than in the longitudinal maneuver. Upon comparison with the lateral maneuver, the TIC values for bank angle were higher than the values for the lateral maneuver, revealing that it was harder to track the bank angle in the coupled

maneuver. Examining the $\mathcal{L}_2$ norm values for the lateral controls, the aileron control surfaces accomplished the climbing spiral with a higher workload; however, the rudder had a lower workload at the higher bank angle maneuvers. In this maneuver, more effort is to be made on focusing on the ailerons than the rudder. Taking that into account, this has verified that a coupled maneuver should involve more control effort than a lateral-directional maneuver. The flight control system was not pushed to its limit, thus allowing ample control authority for more aggressive and precise maneuvers.

Table 29. Evaluation of Nominal Climb Spiral Maneuver

Climb	Bank	TIC ($\dot{h}$)	TIC (v_t)	TIC (ϕ)	$\mathcal{L}_2$ (δ_t)	$\mathcal{L}_2$ (δ_e)	$\mathcal{L}_2$ (δ_a)	$\mathcal{L}_2$ (δ_r)
4 ft/s	10°	.02692	.002173	.02409	.0430	.0064	.0097	.0256
6 ft/s	20°	.02699	.003335	.02538	.0659	.0196	.0187	.0483
8 ft/s	30°	.02702	.004575	.02641	.0905	.0445	.0276	.0668

From these simulations, the best results were obtained for the minimum rate of climb and bank angle. As the maneuver increases in its aggressiveness, the flight control system is working harder to minimize the tracking error. One consideration worth noting is that excessive control compensation may induce an oscillatory response. If it becomes severe enough, it may cause the aircraft to enter a limit cycle oscillation. The flying qualities are analyzed separately through the longitudinal and lateral modes of motions. The decomposition of this maneuver included a climb in the longitudinal plane and a banked turn in the lateral-directional plane. The coupled maneuver combined the two maneuvers into a climbing spiral. These three maneuvers formed the nominal baseline for later use in comparison purposes. The following sections will start an investigation in varying the stability and control derivatives and comparing it to these nominal cases.

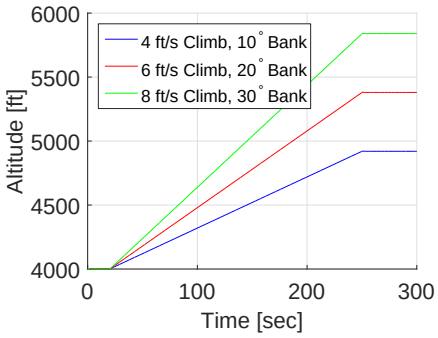

(a) Altitude, h

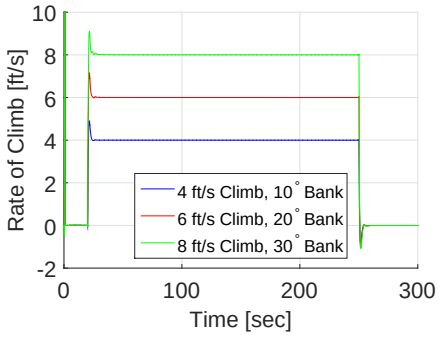

(b) Rate of Climb, $\dot{h}$

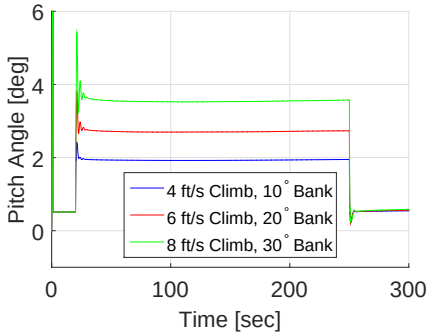

(c) Pitch Angle, θ

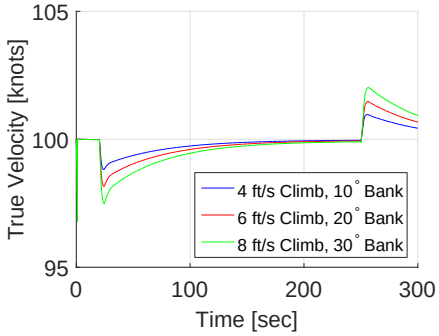

(d) Velocity, v_t

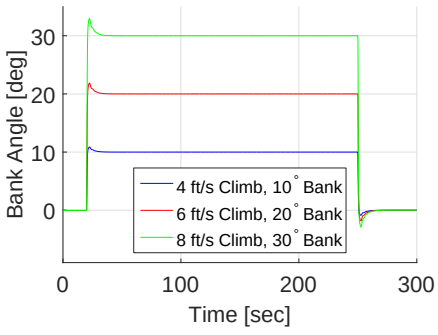

(e) Bank Angle, ϕ

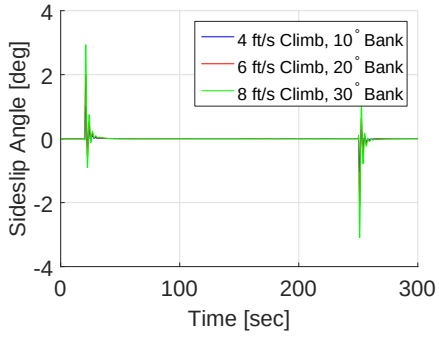

(f) Sideslip Angle, β

Figure 54. Climbing Spiral Performance Plots

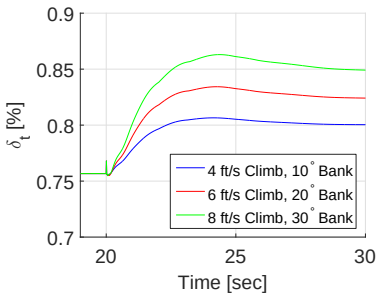

(a) Throttle Initiation

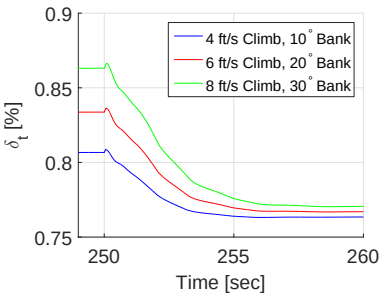

(b) Throttle Termination

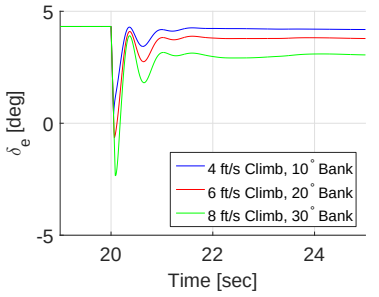

(c) Elevator Initiation

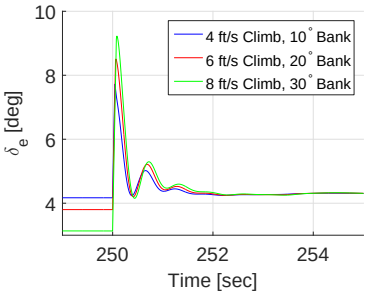

(d) Elevator Termination

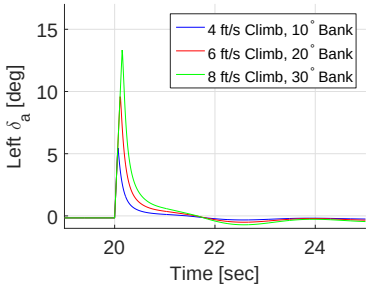

(e) Aileron Initiation

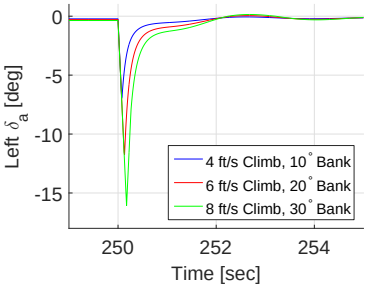

(f) Aileron Termination

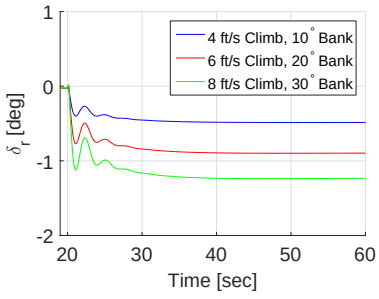

(g) Rudder Initiation

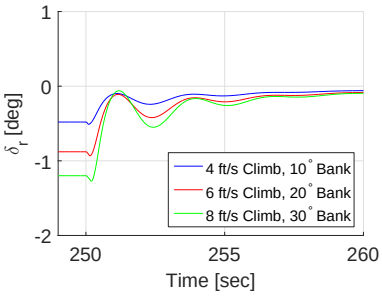

(h) Rudder Termination

Figure 55. Climbing Spiral Control Plots

4.4 Effect of Variation of Longitudinal Stability and Control Derivatives

Following the nominal longitudinal, lateral-directional, and coupled simulations, cases with variation in stability derivatives in their respective modes of motion were simulated in JSBSim. In this section, the longitudinal plane will be analyzed by varying key parameters that affect the longitudinal plane. The performance maneuver for these cases involved trimming the aircraft and then climbing with wings level, thus investigating the longitudinal plane only. The flying qualities analysis was compared to the various simulation cases. The flying qualities level of the aircraft was determined according to requirements for manned aircraft in MIL-STD-1797A. For the longitudinal cases in this section, particular attention was focused on requirements on the phugoid and short-period modes of motion, which are divided into three levels of flying qualities.

4.4.1 Pitch Damping Case

The first change made was to the pitch damping by varying the stability derivative, C_{m_q}. This change prompted a change in the pitch response as shown in Figure 56. With less pitch damping, the responses for the rate of climb and pitch angle become oscillatory as expected. When this case is applied, the response is much quicker due to the low damping; however, the aircraft's performance is not as smooth as before. The controls shown in Figure 57 reflect the same trend with the elevator oscillating back and forth in order to compensate for the quick response. Due to the oscillatory response, the flight control system may be in danger of rate limiting. Figures 57c and 57d show that the flight control system started to exhibit rate limiting nonlinearities with large elevator control inputs.

Figures 58 and 59 show the performance and control plots for the same maneuver with the pitch damping increased by an order of magnitude. It is clearly evident

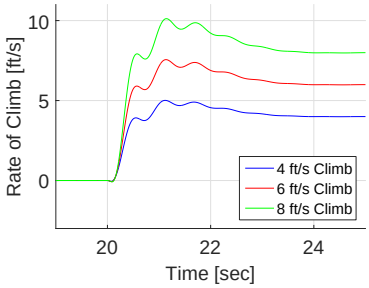

(a) Rate of Climb Initiation

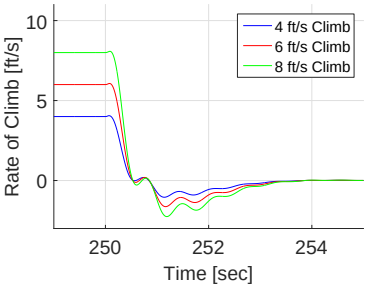

(b) Rate of Climb Termination

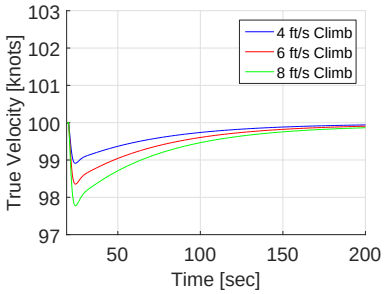

(c) Velocity Initiation

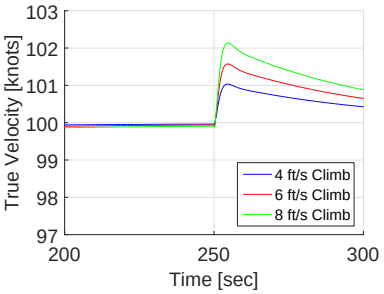

(d) Velocity Termination

Figure 56. Longitudinal Maneuver: C_{m_q} x $\frac{1}{10}$ Performance Plots

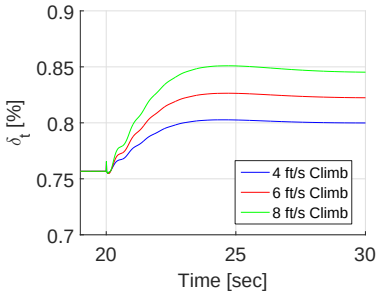

(a) Throttle Initiation

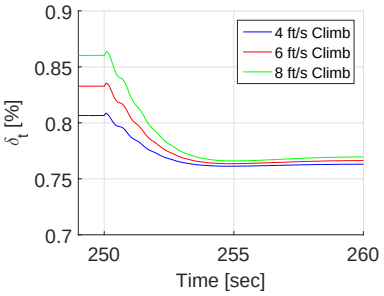

(b) Throttle Termination

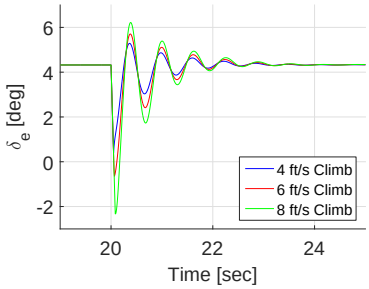

(c) Elevator Initiation

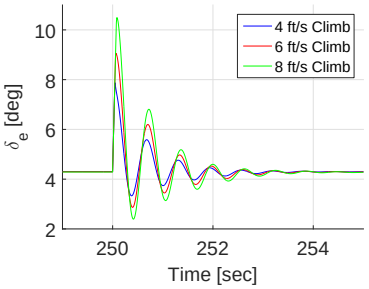

(d) Elevator Termination

Figure 57. Longitudinal Maneuver: C_{m_q} x $\frac{1}{10}$ Control Plots

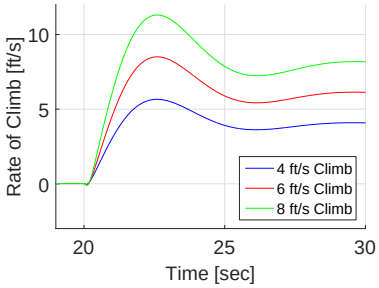

(a) Rate of Climb Initiation

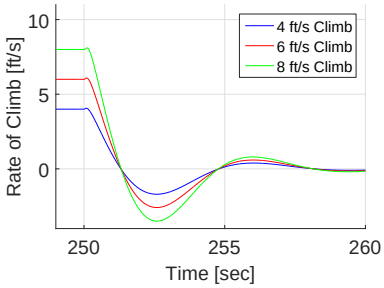

(b) Rate of Climb Termination

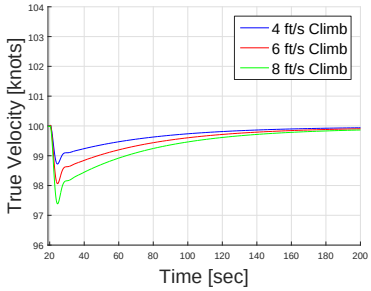

(c) Velocity Initiation

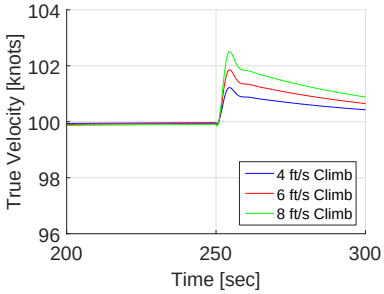

(d) Velocity Termination

Figure 58. Longitudinal Maneuver: C_{m_q} x 10 Performance Plots

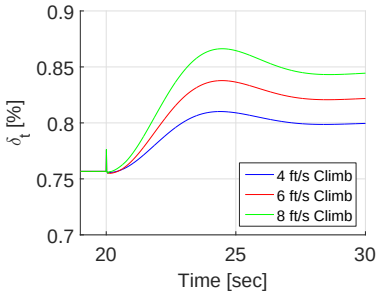

(a) Throttle Initiation

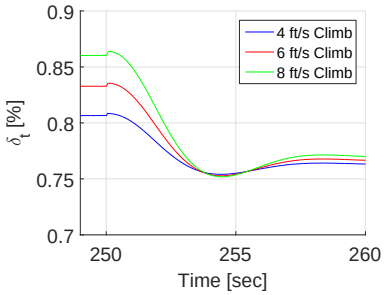

(b) Throttle Termination

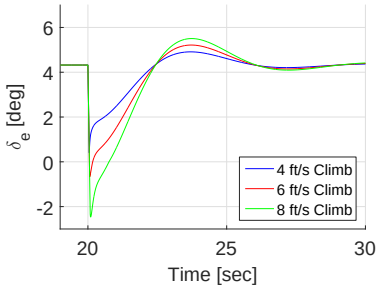

(c) Elevator Initiation

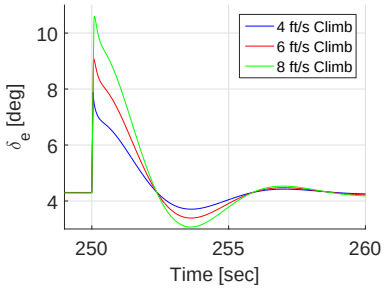

(d) Elevator Termination

Figure 59. Longitudinal Maneuver: C_{m_q} x 10 Control Plots

from these figures that the response is much slower with increased pitch damping. The rate of climb response shown in Figure 58a reached its steady-state value after approximately eight seconds, nearly doubling the case with decreased pitch damping, which reached its steady-state value within four seconds as shown in Figure 56a. With increased damping, it takes much longer for the responses to reach their steady-state values.

The quantitative evaluation of both maneuvers was compared to the nominal maneuver using TIC and $\mathcal{L}_2$ norm as shown in Figure 60. Tables showing the TIC and $\mathcal{L}_2$ norm values are located in Appendix C. It was observed that with less pitch damping, the response became quicker at the cost of oscillations. That quickness resulted in lower TIC values than in the nominal case, verifying that the aircraft achieved better tracking performance with lower pitch damping; however, the elevator had to work slightly harder than in the nominal longitudinal case. The throttle control effort is very similar to the nominal case, revealing that the elevator is most affected by the pitch damping. The trend observed in Figure 60 is that as the pitch damping increased, the TIC values for the rate of climb and the $\mathcal{L}_2$ norm values for the elevator increased as well. Heavier pitch damping resulted in loss of aircraft tracking performance for the rate of climb. The TIC values for the rate of climb has almost doubled for the case of increased pitch damping due to the sluggish response. The elevator control effort has more than doubled as well since the elevator works for a longer period of time stemming from the sluggish response as well. The TIC for velocity, however, remains quite similar. The throttle workload, although slightly higher, remains very similar for the maneuver. In both cases for the variation in pitch damping, the effect was primarily on the rate of climb tracking and elevator workload.

The effect of stability derivatives on aircraft performance for the longitudinal motion are presented in Table 30, specifically the effect on the damping ratios and

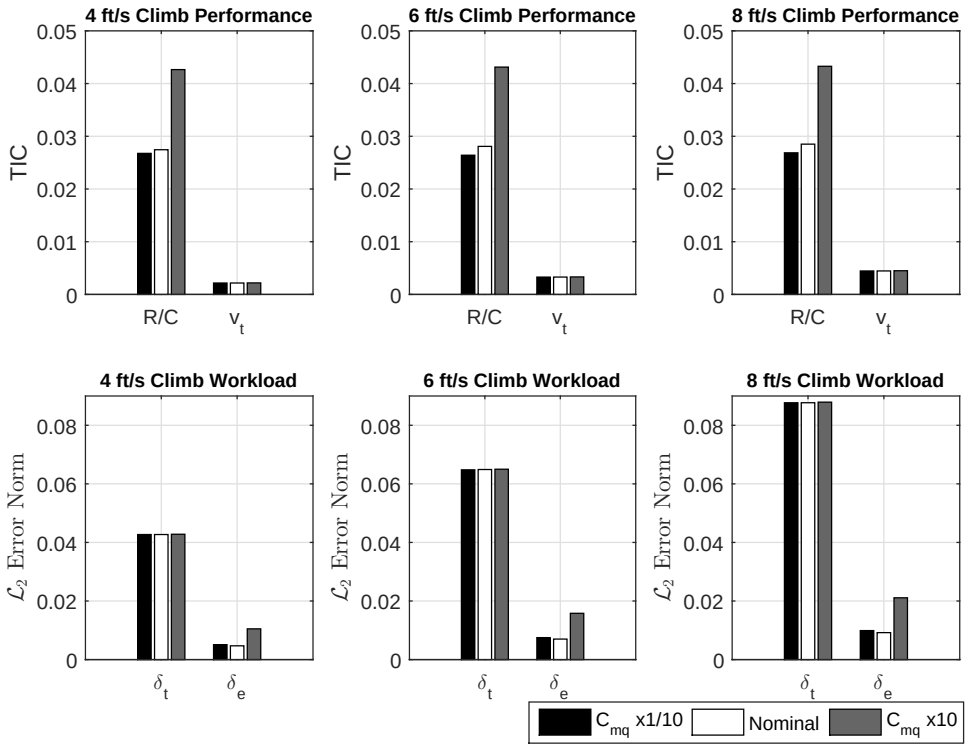

Figure 60. Longitudinal Maneuver: Performance and Workload Comparison of Nominal and C_{m_q} Variation

natural frequencies. The maximum amount that the stability derivatives are increased or decreased is by one order of magnitude; however, if a value shows extreme trends for the damping ratios or natural frequencies, the stability derivative was not changed by that order. The effect of variation of longitudinal stability derivatives matches the trend described by Blakelock previously shown in Table 11. As C_{m_q} was increased, the damping was increased as well, affecting the damping of the short period the most.

Comparing the short-period damping ratio to requirements in MIL-STD-1797A in Table 31, the case with decreased pitch damping obtained Level 1 flying qualities; however, the case with pitch damping increased by an order of magnitude obtained Level 3 handling qualities. The sluggish behavior caused by heavy damping is undesirable by manned piloted aircraft. The comparisons between the simulation and flying

Table 30. Effect of Variation of C_{m_q} on Longitudinal Motion

Stability Derivative	Change	ζ_{sp}	ω_{sp}	ζ_p	ω_p
C_{m_q}	x10	4.38	10	.29	.11
	x4	1.29	10	.19	.15
	x2	.86	8.82	.15	.18
	x$\frac{1}{2}$	.65	6.89	.12	.23
	x$\frac{1}{4}$	.61	6.55	.11	.24
	x$\frac{1}{10}$	.58	6.33	.10	.25

qualities evaluation both point towards obtaining lower pitch damping for enhanced aircraft performance. With lower damping came quicker responses which eventually resulted in better tracking. With higher damping ratios, the flying qualities evaluation labeled it as obtaining Level 3 handling qualities. The aircraft was able to successfully execute the maneuver, albeit much slower. The control workload was also lower for the smaller pitch damping case. The problem that the lower pitch damping presents is the oscillations associated with it. The MIL-STD-1797A requirements are however based on pilot control feel such as the force and deflection characteristics of the control stick which do not pertain to UAVs. As long as the oscillations do not interfere with the task to a significant degree, it is more desirable for the UAV to have lower values of pitch damping, which was confirmed by the lower TIC values and flying qualities level specified by MIL-STD-1797A. How hard the flight control system is working does not matter as much but what does become a concern is how fast the control surfaces are moving. As the rate of climb increases with each maneuver, the elevator shows the beginning signs of rate limiting as shown in Figures 57c and 57d.

Table 31. Short Period Damping Ratio Limits [1]

Level	Cat. A,C Flight Phase		Cat. B Flight Phase	
	Min	Max	Min	Max
1	.35	1.30	.30	2.0
2	.25	2.0	.20	2.0
3	.15	no limit	.15	no limit

4.4.2 Static Pitch Stability Case

After completing the pitch damping cases, the cases for the static pitch stability, C_{m_α}, were run. The pitch stability is an important aspect in the longitudinal stability of an aircraft, ultimately affecting the flight control system. Some modern fighters such as the F-16 are intentionally designed to be unstable in order to improve maneuverability. The computerized flight control system deflects the elevator control surface to provide the artificial stability. "The Cessna 172 has a static stability of about 19%" which is an immense benefit in pilot training [43]. Aircraft that are too stable, however, take considerable time and effort to change their course, taking away from their maneuverability. A fine balance between stability and maneuverability needs to be struck without compromising away from one area too much.

The performance and control plots for the decreased static pitch stability case are shown in Figures 61 and 62 respectively. It is evident from Figures 61a and 61b that decreasing the static pitch stability resulted in some minor oscillations but not as severe as in the case of decreased pitch damping. The corresponding elevator control history in Figures 62c and 62d show the fluctuation as well. The reduction in static pitch stability led to quicker response times but induced an oscillatory response. On the contrary, the increase in static pitch stability saw longer deflection times followed by slower response times as seen in the performance and control plots in Figures 63 and 64. The rate of climb settling time more than doubled to eight seconds as seen in Figure 61a compared to the previous adjustment with a settling time of three seconds. These observations are in line with the previous increased pitch damping case that more stable platforms and heavier damping results in slower dynamic responses.

The quantitative evaluation of the results are shown in Figure 65 comparing the static pitch stability cases with the nominal case. The TIC and $\mathcal{L}_2$ norm values are tabulated in Appendix C. From Figure 65, it is evident that as the stability coefficient,

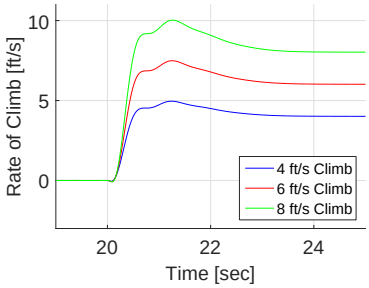

(a) Rate of Climb Initiation

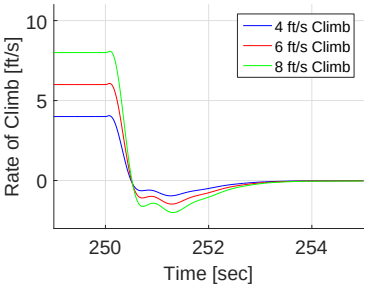

(b) Rate of Climb Termination

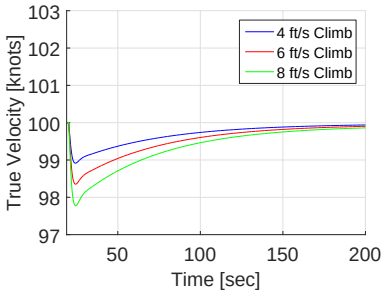

(c) Velocity Initiation

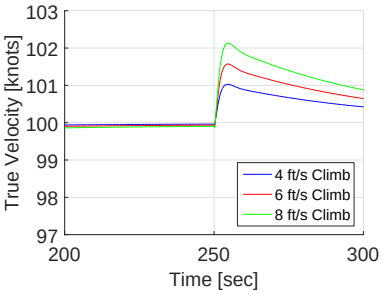

(d) Velocity Termination

Figure 61. Longitudinal Maneuver: C_{m_α} x $\frac{1}{10}$ Performance Plots

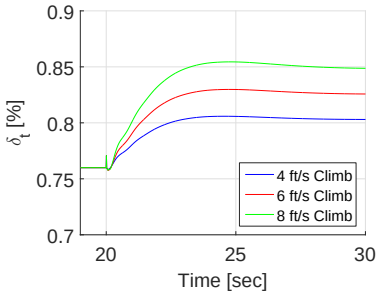

(a) Throttle Initiation

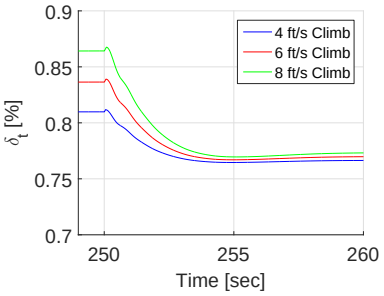

(b) Throttle Termination

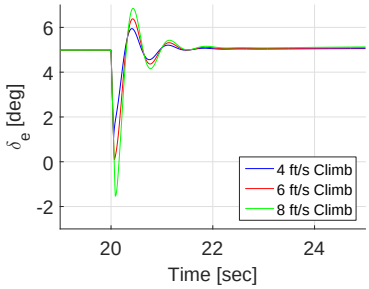

(c) Elevator Initiation

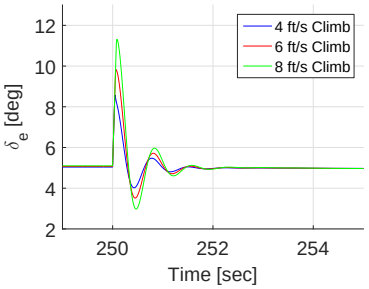

(d) Elevator Termination

Figure 62. Longitudinal Maneuver: C_{m_α} x $\frac{1}{10}$ Control Plots

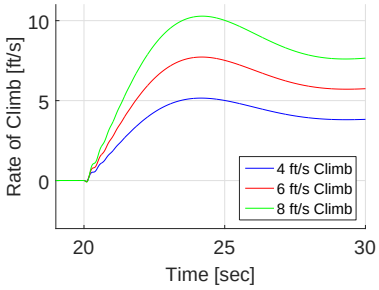

(a) Rate of Climb Initiation

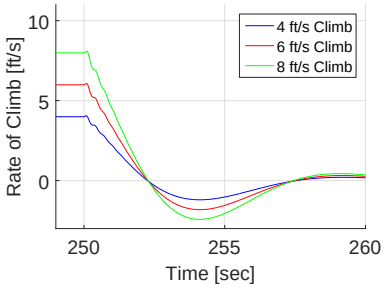

(b) Rate of Climb Termination

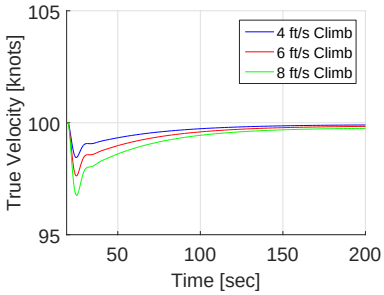

(c) Velocity Initiation

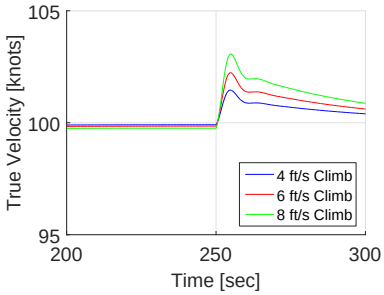

(d) Velocity Termination

Figure 63. Longitudinal Maneuver: C_{m_α} x 10 Performance Plots

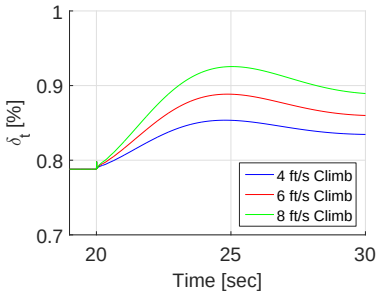

(a) Throttle Initiation

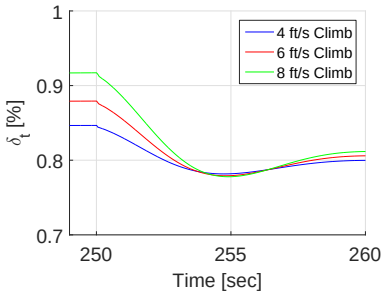

(b) Throttle Termination

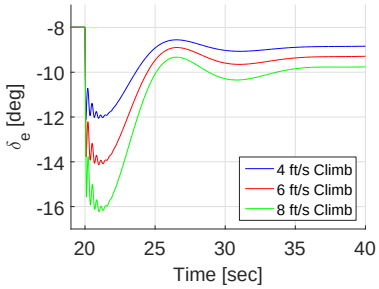

(c) Elevator Initiation

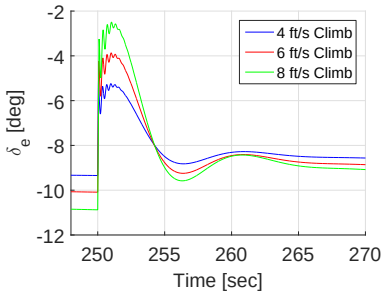

(d) Elevator Termination

Figure 64. Longitudinal Maneuver: C_{m_α} x 10 Control Plots

C_{m_α}, decreased, the aircraft became more unstable allowing quicker responses in the aircraft; however, the elevator has to compensate for that, which may lead to rate limiting. This was verified by the lower TIC values for this case against the nominal climbing maneuver. Comparing this case with the pitch damping case, the case with the lowered pitch damping had a lower TIC value for rate of climb as well as a lower elevator workload. It is therefore more beneficial to decrease pitch damping rather than static pitch stability from a performance and workload standpoint.

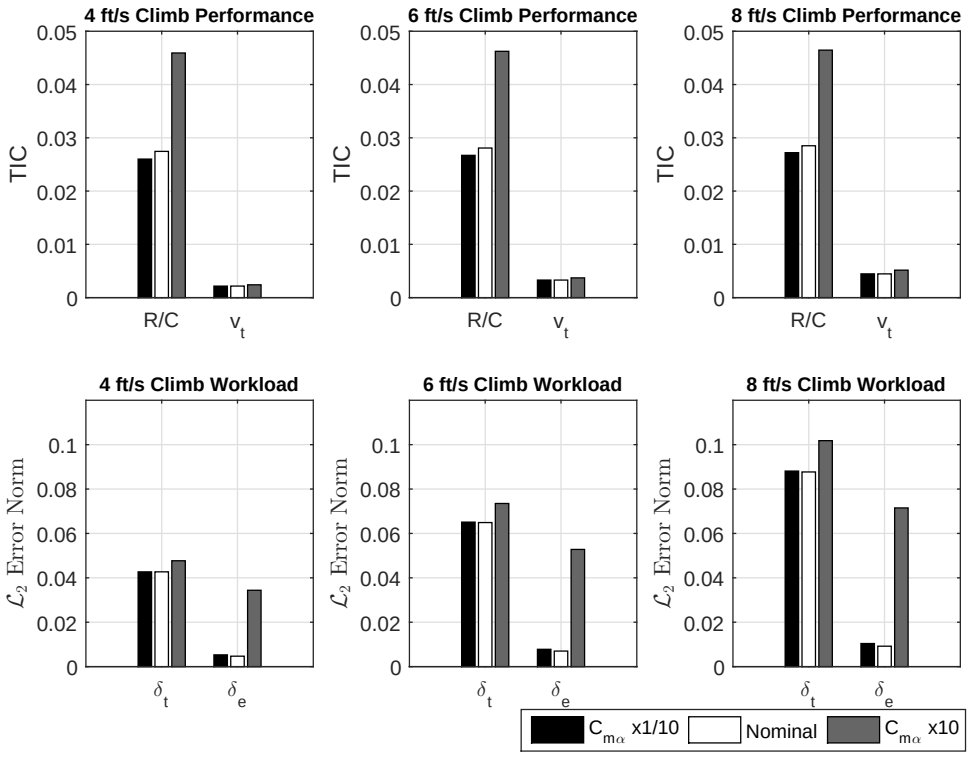

Figure 65. Longitudinal Maneuver: Performance and Workload Comparison of Nominal and C_{m_α} Variation

Another interesting point to notice is that when the static pitch stability was increased by an order of magnitude, there was a noticeable increase in the workload for the elevator and throttle, with the elevator's workload over seven times more than that of the nominal case. Upon examination of the elevator control history, the elevator was initially trimmed at -8° and going as far as -16° for the most aggressive

maneuver. This unusually high deflection angle associated with a very stable platform may lead to position limiting. Overall, the case of the increased static pitch stability resulted in the worst tracking performance and highest workload for the flight control system. Increasing C_{m_α} resulted in the worst-case scenario that can become a concern when performing coupled or more aggressive maneuvers.

Blakelock stated that the quantity most affected by the stability derivative, C_{m_α}, was the short-period natural frequency. Increasing C_{m_α} would increase the short-period natural frequency as described in Chapter III. That trend is verified in Table 32. The range for the short-period natural frequency varies from 3.15 rad/s to 10 rad/s. Comparing this range to the case for the variation in pitch damping in Table 30, the natural frequency ranges from 6.33 rad/s to 10 rad/s, which verifies Blakelock's statement, thus the most influential parameter on the short-period mode natural frequency is the static pitch stability.

Table 32. Effect of Variation of C_{m_α} on Longitudinal Motion

Stability Derivative	Change	ζ_{sp}	ω_{sp}	ζ_p	ω_p
C_{m_α}	x10	.17	10	.12	.26
	x4	.32	10	.11	.25
	x2	.56	9.75	.12	.24
	x$\frac{1}{2}$	.87	6.01	.15	.17
	x$\frac{1}{4}$	.98	4.88	.19	.14
	x$\frac{1}{10}$	1.18	3.15	.25	.10

Comparing the short-period damping ratio to requirements in MIL-STD-1797A in Table 31, the case with C_{m_α} decreased by an order of magnitude obtained Level 1 flying qualities; however, the case with C_{m_α} increased by an order of magnitude obtained Level 3 handling qualities. Since the phugoid damping ratios were all greater than .04, Level 1 flying qualities was attained for the phugoid mode for all variations. The simulation reinforced the assumption that the more agile aircraft was able to track the rate of climb better although it obtained Level 2 flying qualities pointed out

from MIL-STD-1797A. The case with C_{m_α} increased by an order of magnitude was able to successfully perform the maneuver without any significant problems, although at a much slower response noted by the higher TIC values. From a performance standpoint, the requirements of static stability can be relaxed without degrading the aircraft's flying qualities.

4.4.3 Elevator Control Power Case

$C_{m_{\delta_e}}$ is the primary control derivative for the longitudinal axis. Also known as the elevator effectiveness, $C_{m_{\delta_e}}$ relates the elevator deflection to its influence on pitching moment. "If the absolute value of the derivative is higher, then for a given deflection, more moment is generated. This can be regarded as higher control sensitivity for a given moment of inertia" [42]. During the design of the aircraft, $C_{m_{\delta_e}}$ is a key design parameter for specifying the longitudinal axis control power. In typical convention, the more negative the parameter is, the more control effectiveness there is. It relates to the control authority to do a mission task such as the ability to generate sufficient forces and moments on the vehicle dictated by the sizing of the control surface. More elevator control power means more effective control in generating the pitch moment for the aircraft. It is important to note that unstable platforms will require more control power than stable platforms.

The aircraft must have sufficient elevator effectiveness to trim in flight and some additional elevator authority must be available for control. As the elevator control effectiveness was increased, then for a given deflection, more pitching moment is generated. The oscillations associated with higher control sensitivity are shown in Figures 66 and 67 in the rate of climb response and elevator history. Due to the higher control sensitivity, the elevator oscillates as it reaches its steady-state value. It is important to note that due to the increased effectiveness, the elevator trimmed

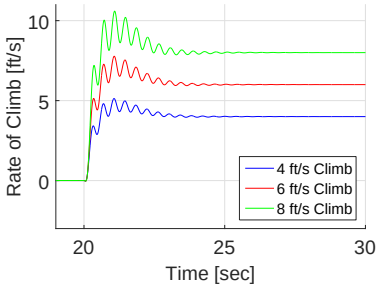

(a) Rate of Climb Initiation

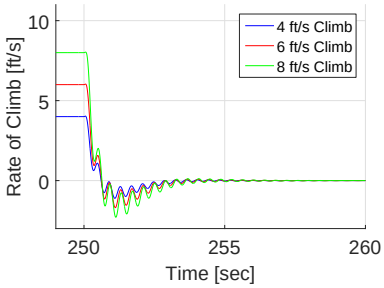

(b) Rate of Climb Termination

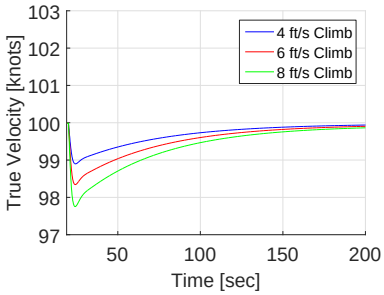

(c) Velocity Initiation

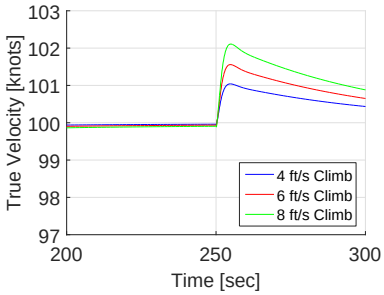

(d) Velocity Termination

Figure 66. Longitudinal Maneuver: $C_{m_{\delta_e}}$ x 3 Performance Plots

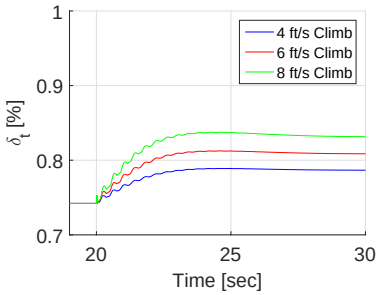

(a) Throttle Initiation

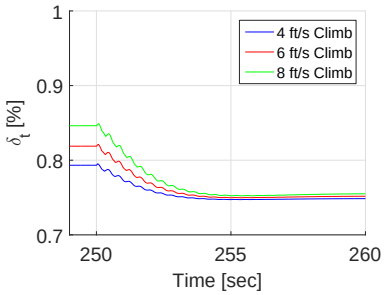

(b) Throttle Termination

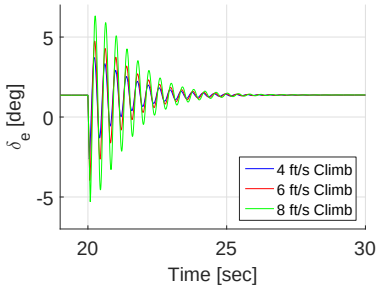

(c) Elevator Initiation

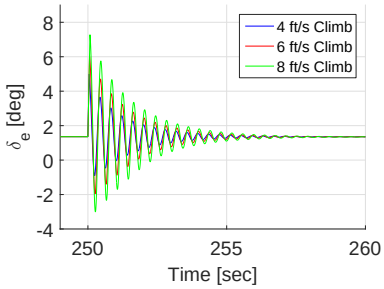

(d) Elevator Termination

Figure 67. Longitudinal Maneuver: $C_{m_{\delta_e}}$ x 3 Control Plots

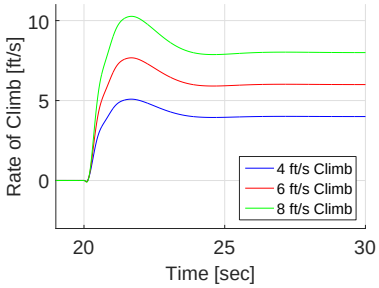

(a) Rate of Climb Initiation

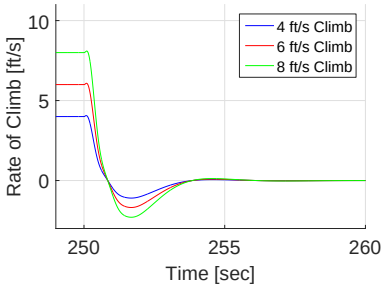

(b) Rate of Climb Termination

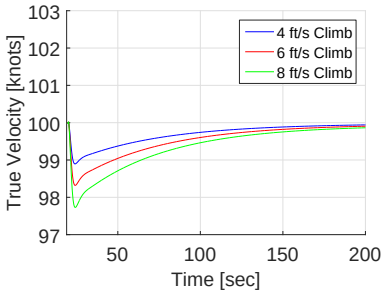

(c) Velocity Initiation

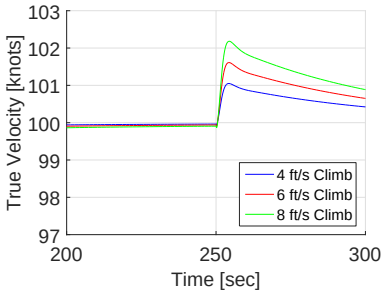

(d) Velocity Termination

Figure 68. Longitudinal Maneuver: $C_{m_{\delta_e}}$ x $\frac{3}{4}$ Performance Plots

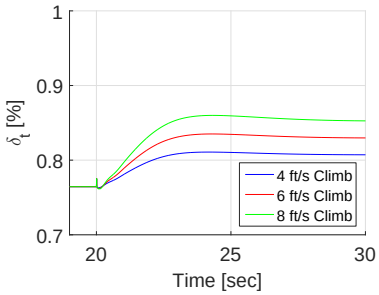

(a) Throttle Initiation

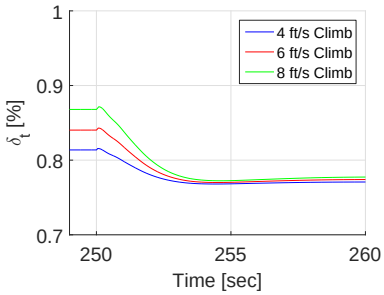

(b) Throttle Termination

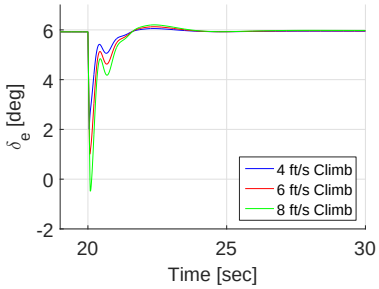

(c) Elevator Initiation

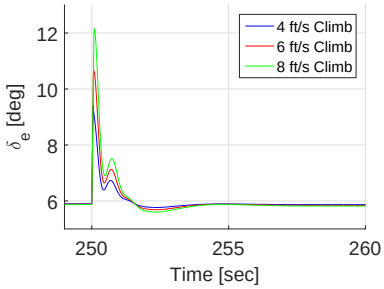

(d) Elevator Termination

Figure 69. Longitudinal Maneuver: $C_{m_{\delta_e}}$ x $\frac{3}{4}$ Control Plots

out closer to its neutral position at 1.4° compared to the elevator deflection in the nominal case at 4.3°. For a given deflection, there is a larger influence on the pitching, thus the elevator does not have to deflect as much as the nominal case.

The increased elevator effectiveness modification responses are shown in the performance and control plots in Figures 68 and 69. In comparison to the case with the decreased elevator effectiveness trimmed at 1.4°, the elevator was trimmed further away from its neutral position at 5.9° as shown in Figure 69a. As the control effectiveness gets continually decreased, the elevator may not generate enough pitching moment which may drive the elevator to hit its position limit, thereby degrading aircraft performance. An apparent loss of control effectiveness deceives the control system into making larger command inputs. Also with less control effectiveness, there is not as much available power to perform more aggressive maneuvers.

The performance and control workload for the variation in elevator effectiveness were compared to the nominal case. Figure 70 compares the TIC and $\mathcal{L}_2$ norm values for each simulation to the nominal case. As the elevator effectiveness increased, the TIC for rate of climb decreased. These results confirmed the observation that as the control effectiveness is increased, the aircraft's performance is enhanced; however, a negative consequence associated with increased elevator effectiveness is increased workload due to the oscillations. The elevator has to work harder to compensate for the increased effectiveness shown by the $\mathcal{L}_2$ norm values. The throttle control also experiences an increased workload trend when the elevator effectiveness is increased.

The longitudinal response characteristics are related to its stability derivatives. For an aircraft performing gentle maneuvering tasks, it may be realistic to define lower effectiveness requirements; however, this does not account for more aggressive maneuvering, disturbances, or failure modes. While the control power is coupled with the capability of an aircraft to perform a maneuver, it does not have a great

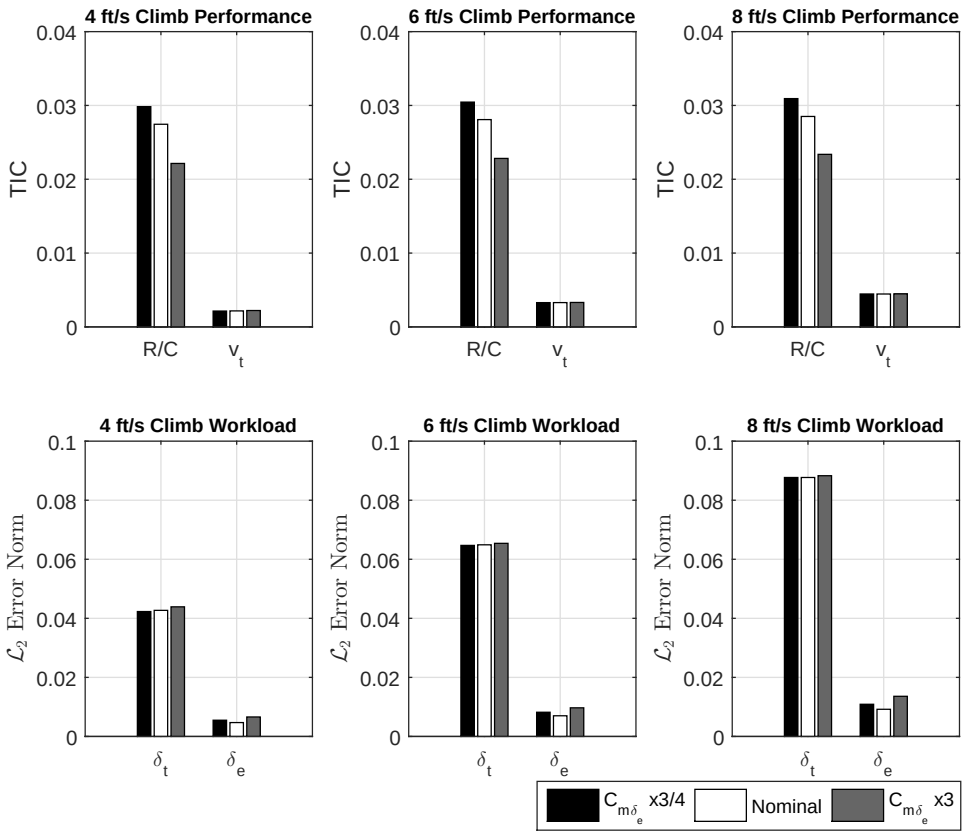

Figure 70. Longitudinal Maneuver: Performance and Workload Comparison of Nominal and $C_{m_{\delta_e}}$ Variation

bearing on the short-period and phugoid modes as shown in Table 33. The elevator effectiveness does not have as great an effect as the pitch damping and static pitch stability on the longitudinal modes of motion which are used to evaluate the flying qualities. Based on the phugoid and short-period damping ratio requirements, all the case variations of the elevator effectiveness presented in Table 33 have Level 1 flying qualities. From the longitudinal cases, the change in the elevator effectiveness obtained the closest tracking to the desired rate of climb without affecting the short-period and phugoid modes of motion. In exchange for the lowest TIC value for rate of climb, the elevator workload was the highest with oscillations worse than the pitch damping case. Although increasing the elevator effectiveness resulted in the lowest TIC values while maintaining Level 1 flying qualities, an unexpected result that

came about is that the flight control system became the limiting factor. Excessive control compensation induced an oscillatory response while the opposite case became a concern for hitting position saturation limits.

Table 33. Effect of Variation of $C_{m_{\delta_e}}$ on Longitudinal Motion

Stability Derivative	Change	ζ_{sp}	ω_{sp}	ζ_p	ω_p
$C_{m_{\delta_e}}$	x3	.7254	7.5494	.1230	.2108
	x2	.7255	7.5526	.1246	.2106
	x$\frac{3}{4}$	.7258	7.5680	.1333	.2093
	x$\frac{1}{2}$	.7261	7.5793	.1412	.2081

4.5 Effect of Variation of Lateral-Directional Stability and Control Derivatives

In this section, the lateral-directional plane will be analyzed varying key parameters that affect the lateral mode of motion. The lateral maneuver performed in the simulation is the banked turn at three specified bank angles of 10°, 20°, and 30° while maintaining its altitude. Major stability derivatives in the lateral-directional plane were varied to see their effects on the simulation and flying qualities. The criteria for the level of flying qualities was based on the requirements for manned aircraft in MIL-STD-1797A for the various lateral modes.

4.5.1 Roll Damping Case

Recall that for the pitch damping case, there was a relationship between the pitch damping derivative, C_{m_q}, and the short-period damping, ζ_{sp}. Similarly, the rolling damping derivative, C_{l_p}, plays a major part in the roll response of the aircraft. Figure 71 reveals the effect of lowered pitch damping on the three performance responses. Due to the lowered damping, oscillations appear in the step response; however, it was able to reach its steady-state value quickly. The aileron and rudder controls for the

simulation are shown in Figure 72. The aileron control attains the triangular pattern associated with rate limiting for the 30° bank angle maneuver in Figures 72a and 72b. It becomes readily apparent that as the maneuver's bank angle increases, the effects of rate limiting became more noticeable.

In the case of increased roll damping by an order of magnitude, similar trends were found as in the increased pitch damping case. As the responses show in Figure 73, it takes much longer for the aircraft to reach its steady-state bank angle due to the increased damping. The responses are much slower, which can also be verified by the control history shown in Figure 74. It can be seen that the roll control does need to work as hard especially when simulating the maneuver with the largest bank angle. The ailerons have reached the maximum deflection limits, shown by the flat line trend at the start and end of the maneuver shown in Figures 74a and 74b. The increased damping has caused a slower response in the aircraft's performance causing the controls to work for a longer period of time. It appears that small values of C_{l_p} are more desirable than large ones because the aircraft will respond more quickly to a given aileron input.

In the evaluation of the simulations shown in Figure 75, there was a definite trend relating performance and workload. As the roll damping increased, the aircraft's performance degraded and the control workload increased. Considering the bank angle's TIC values almost doubled for the increased roll damping case, the increased roll damping had a significant effect in degrading the aircraft's performance. The aileron control experienced the greatest increase in workload when the roll damping was increased by an order of magnitude as shown by the $\mathcal{L}_2$ norm values. The aileron workload was almost four times that of the nominal case. Correspondingly, the bank angle's TIC value was nearly doubled. Meanwhile, the rudder control experienced a slight increase, but not comparable to the increase experienced by the ailerons. The

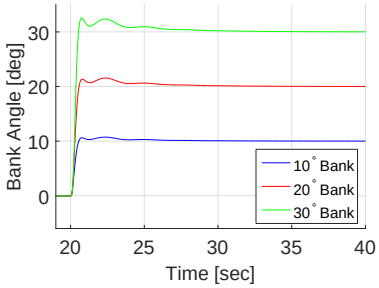

(a) Bank Angle Initiation

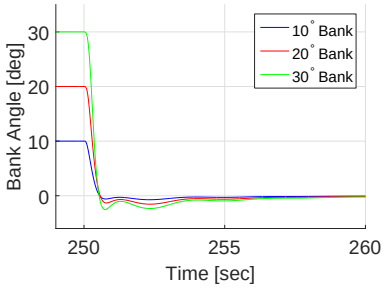

(b) Bank Angle Termination

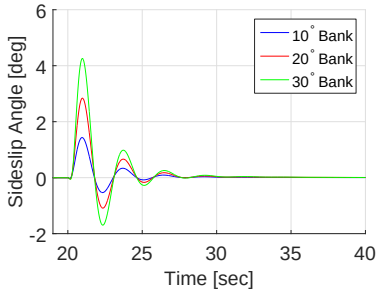

(c) Sideslip Angle Initiation

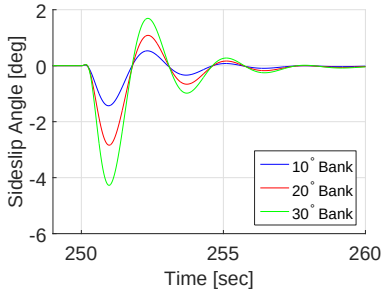

(d) Sideslip Termination

Figure 71. Lateral Maneuver: C_{l_p} x $\frac{1}{10}$ Performance Plots

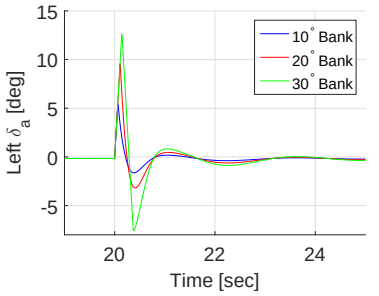

(a) Aileron Initiation

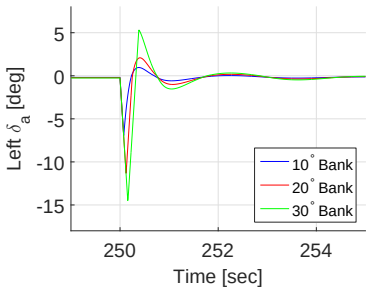

(b) Aileron Termination

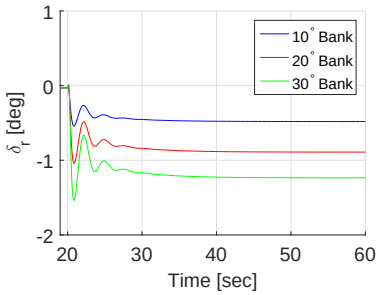

(c) Rudder Initiation

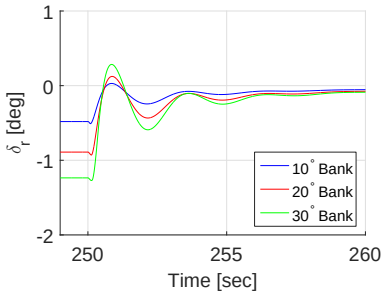

(d) Rudder Termination

Figure 72. Lateral Maneuver: C_{l_p} x $\frac{1}{10}$ Control Plots

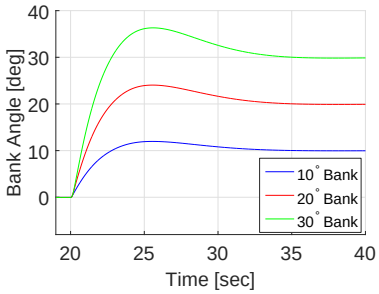

(a) Bank Angle Initiation

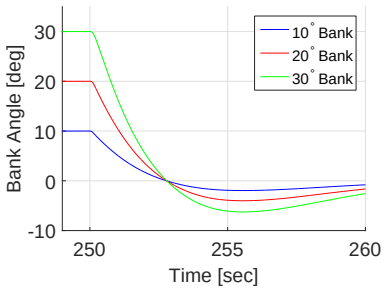

(b) Bank Angle Termination

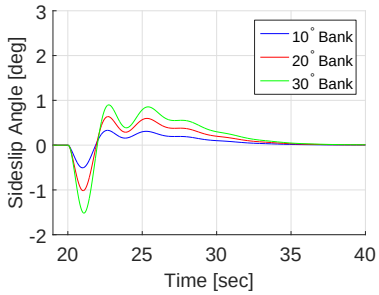

(c) Sideslip Angle Initiation

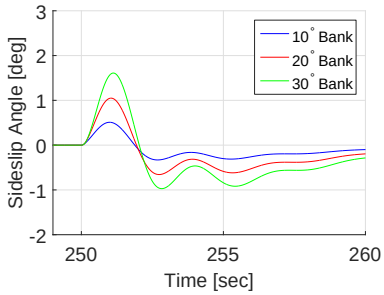

(d) Sideslip Termination

Figure 73. Lateral Maneuver: C_{l_p} x 10 Performance Plots

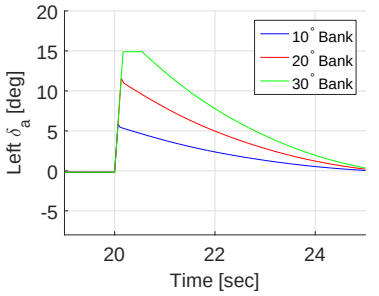

(a) Aileron Initiation

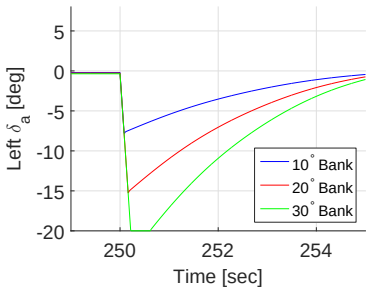

(b) Aileron Termination

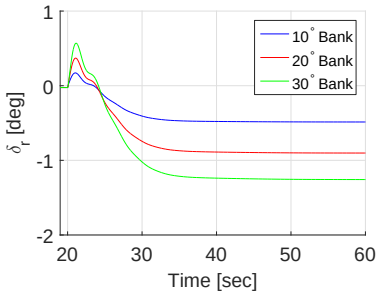

(c) Rudder Initiation

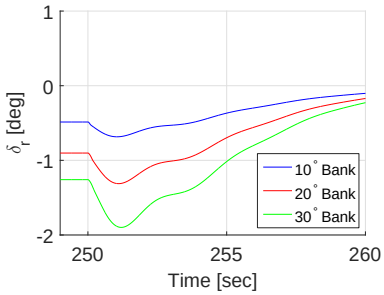

(d) Rudder Termination

Figure 74. Lateral Maneuver: C_{l_p} x 10 Control Plots

velocity TIC values were quite insignificant for this maneuver because the aircraft was maintaining its altitude in steady flight. The change in roll damping mainly affected the roll performance and aileron workload as expected. The trends seen for the roll damping case were similar to its counterpart in the pitch damping case.

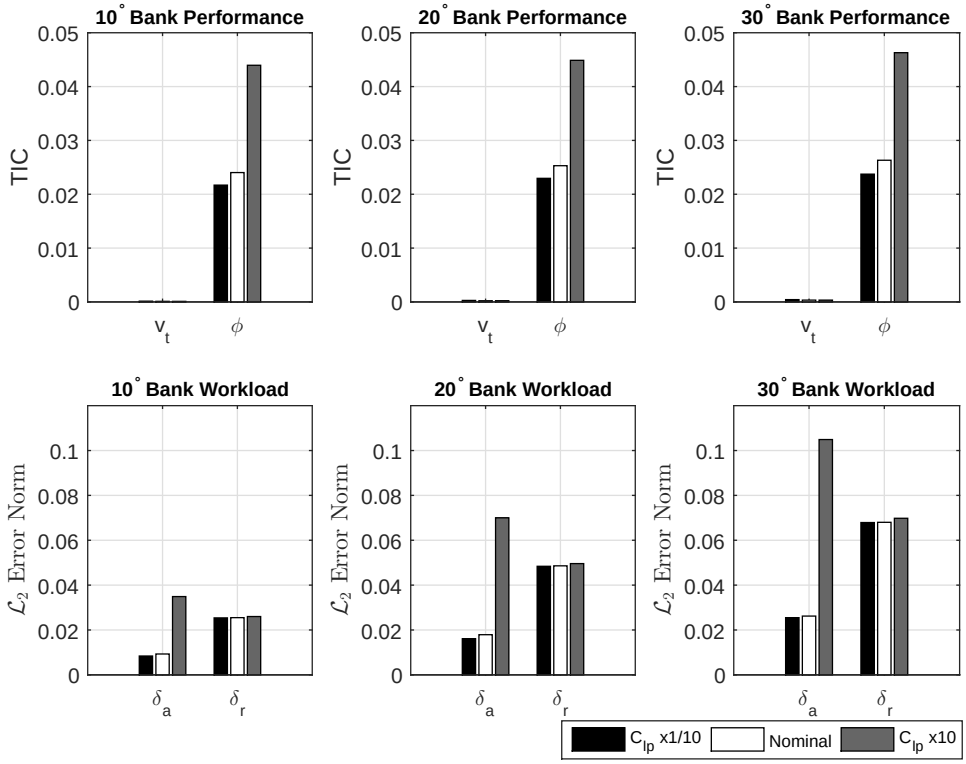

Figure 75. Lateral Maneuver: Performance and Workload Comparison of Nominal and C_{l_p} Variation

Recall that Blakelock stated that the quantity most affected by the stability derivative, C_{l_p}, was the roll mode time constant, T_r. As the roll damping was increased, $\frac{1}{T_r}$ would increase as well, verified in Table 34. In order to attain Level 1 flying qualities for the roll axis, the recommended maximum value for T_r is 1.0 s for Flight Phase Category A. From the results, all variations of the rolling damping attained Level 1 flying qualities for the roll mode. A LOES was not successfully fit to the data for the cases where the roll damping was increased by an order of magnitude; however, the trends give insight that it would still be below 1.0 second. The roll subsidence

mode is caused by the high roll damping effect of the wing. The roll time constant mostly affects roll subsidence; therefore, governing the entry to, and exit from, rolling motion. Although the case of low roll damping resulted in better tracking of the bank angle, the roll mode time constant increased, pushing it closer to Level 2 flying qualities. When considering the roll mode, the mission tasks can tell far more about the genuine capabilities of the aircraft rather than the published requirements. A flight computer in a UAV can be designed to tolerate longer roll mode time constants, T_R, than those rated acceptable by a pilot. While the human operator needs to feel the physical feedback from the input commands, the flight computer does not.

Although the roll mode time constant was most affected by the roll damping, an examination of the Dutch roll mode and spiral mode provides another aspect of the flying qualities examination. When the roll damping was multiplied by two, the Dutch roll mode obtained properties of Level 1 flying qualities by meeting the minimum requirements for ζ_d, $\zeta_d\omega_d$, and ω_d, which are shown in Table 22. As the roll damping decreased, the Dutch roll mode flying qualities started to degrade. In the case of decreasing the roll damping by an order of magnitude, the Dutch roll mode flying qualities are now considered borderline Level 3 flying qualities. The quantitative assessment of the simulation and flying qualities specifications did not match for the roll damping case. As the maneuver was tracked more closely, the flying qualities veered towards Level 2 and 3 flying qualities in terms of the roll mode and Dutch roll mode respectively.

Table 34. Effect of Variation of Stability Derivatives on Lateral Motion

Stability Derivative	Change	ζ_d	ω_d	T_r	T_s
C_{lp}	x2	.20	2.26	.0068	114.5
	x$\frac{1}{2}$	.12	2.40	.35	28.98
	x$\frac{1}{4}$	.062	2.37	.52	17.52
	x$\frac{1}{10}$	.018	2.31	.76	10.79

4.5.2 Aileron Control Power Case

$C_{l_{\delta_a}}$ is the change in rolling moment coefficient with change in aileron deflection, which is commonly referred to as the aileron effectiveness. "As far as lateral dynamics are concerned, the derivative $C_{l_{\delta_a}}$ is most important of the control surface derivatives. The aileron effectiveness in conjunction with the damping in roll (C_{l_p}) establishes the maximum available rate of roll of an airframe" [17]. The effectiveness of the ailerons is especially important in the terminal phases of the aircraft during takeoff and landing where adequate lateral control is essential in the face of gust disturbances which roll the aircraft. Special attention must be paid to the aileron effectiveness for analysis as well as their context in flying qualities.

The same trends occured for the lateral and directional control derivatives as in the longitudinal control derivatives. "If the absolute value of these derivatives is higher, then for a given deflection, more rolling and yawing moments are generated. This is regarded as higher control sensitivity for a given moment of inertia" [42]. As stated in Chapter III, only the aileron control effectiveness, $C_{l_{\delta_a}}$, was varied and was analyzed for this case. With modifications in the aileron effectiveness, the focus will be primarily on the bank angle tracking performance and aileron workload. The performance and control plots for both increased and decreased aileron effectiveness are presented in Figures 76 to 79. In the maneuver bank at 30°, the increased aileron effectiveness reduced the overshoot in the bank angle response to 6% compared to the overshoot of 11% in the decreased aileron effectiveness case. A similar trend for the increased aileron effectiveness case to that seen in the increased elevator effectiveness case was that the aileron controls were more prone to rate limiting as shown in Figures 77a and 77b. The sharp saw-tooth pattern is clearly evident in the aileron response in the effort to reach the desired states quickly.

For the decreased aileron effectiveness case, limiting on position limits became a

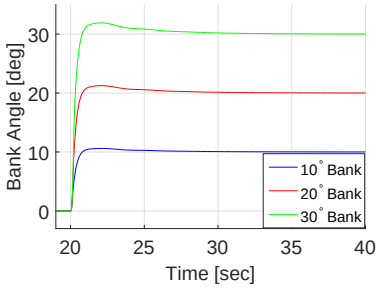

(a) Bank Angle Initiation

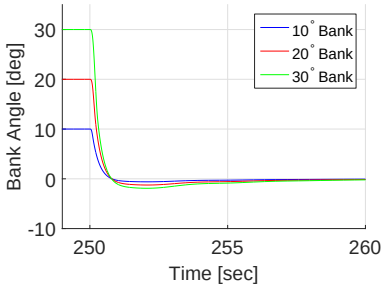

(b) Bank Angle Termination

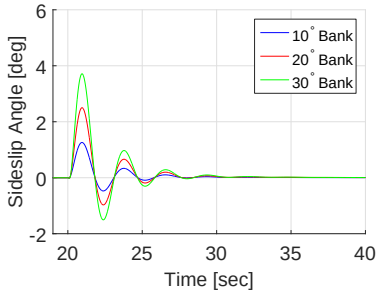

(c) Sideslip Angle Initiation

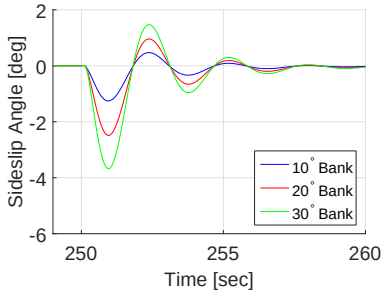

(d) Sideslip Termination

Figure 76. Lateral Maneuver: $C_{l_{\delta_a}}$ x 3 Performance Plots

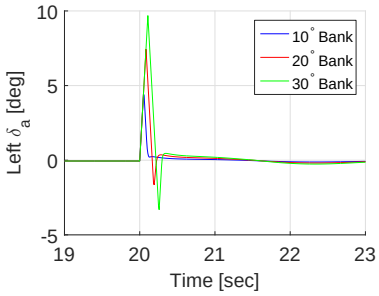

(a) Aileron Initiation

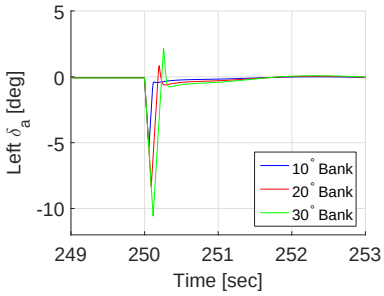

(b) Aileron Termination

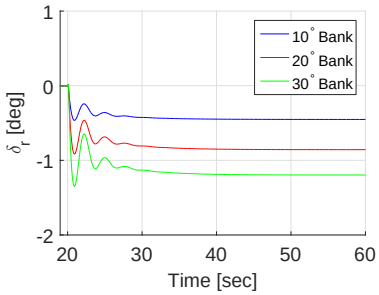

(c) Rudder Initiation

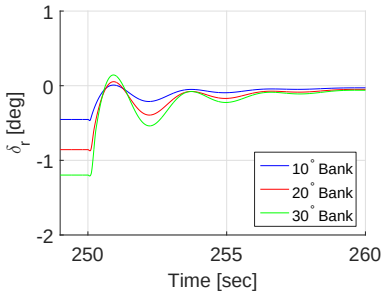

(d) Rudder Termination

Figure 77. Lateral Maneuver: $C_{l_{\delta_a}}$ x 3 Control Plots

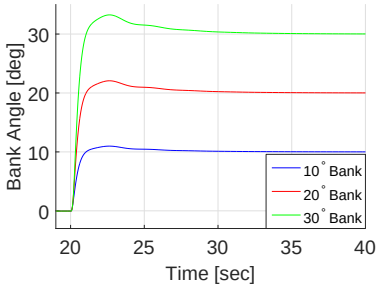

(a) Bank Angle Initiation

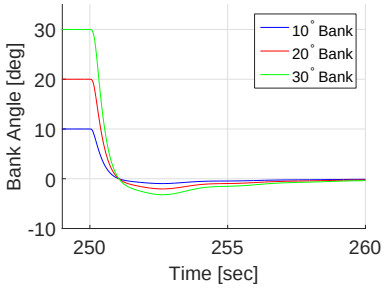

(b) Bank Angle Termination

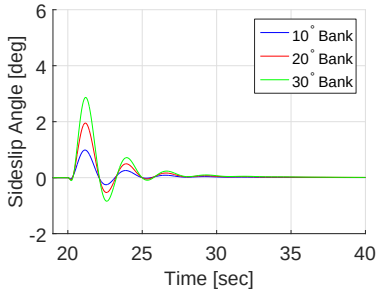

(c) Sideslip Angle Initiation

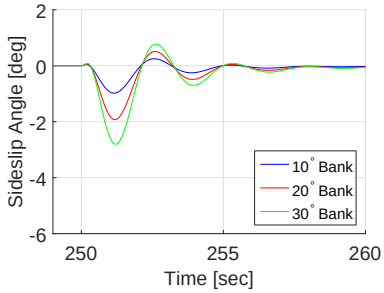

(d) Sideslip Termination

Figure 78. Lateral Maneuver: $C_{l_{\delta_a}}$ x $\frac{3}{4}$ Performance Plots

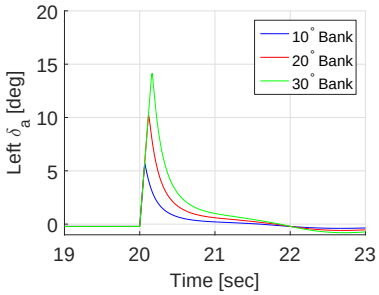

(a) Aileron Initiation

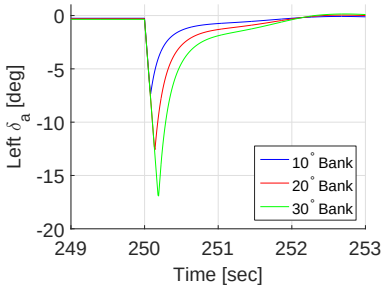

(b) Aileron Termination

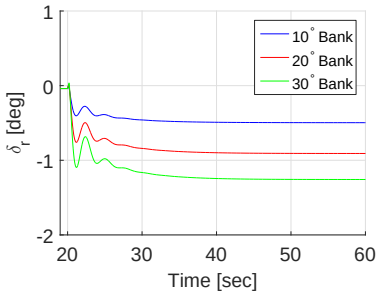

(c) Rudder Initiation

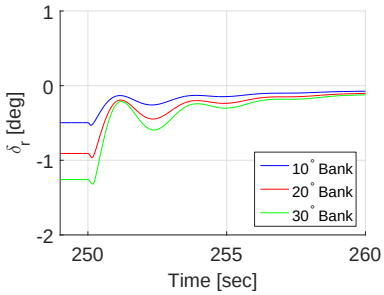

(d) Rudder Termination

Figure 79. Lateral Maneuver: $C_{l_{\delta_a}}$ x $\frac{3}{4}$ Control Plots

parameter of interest. For the maneuver banked at 30°, the ailerons were deflected at 14.15°, close to their position limit of 15° as shown in Figures 79a and 79b. Both the decreased elevator and aileron effectiveness cases displayed high deflection angles, either hitting or coming close to their control surface's position limit.

As with the other variations, the performance and workload for the three lateral maneuvers were quantified. Figure 80 shows the comparison between the aileron effectiveness cases and the nominal case. Tables showing the TIC and $\mathcal{L}_2$ norm values are collected in Appendix D. Once again, the bank angle's TIC values decreased as the aileron effectiveness increased like in the elevator effectiveness case. The aircraft was able to track the bank angle more closely than in the nominal case when the aileron effectiveness increased, noted by the lower TIC values; however, the lateral controls had a lower workload than in the nominal case. In contrast, as the aileron effectiveness decreased, the TIC value was larger than in the nominal case, which is a signal that the bank angle was not tracked as closely throughout the maneuver. For this case, the workload trend departed from that of the elevator effectiveness case. A new trend can be identified for the lateral case, where the lateral controls workload decreased with increasing control effectiveness. The opposite was true for the elevator effectiveness case in the longitudinal plane. Due to the difference in workload trend for the control effectiveness cases, the agreement of the workload trends in the longitudinal and lateral plane is in question. What remains consistent between the elevator and aileron effectiveness cases are the trends for TIC in evaluating the aircraft's performance.

The control effectiveness of the ailerons had the greatest effect on the roll mode time constant as shown in Table 35. The Dutch roll damping ratio and natural frequency did not vary as much as in the previous cases. As the the aileron effectiveness was decreased, the roll mode time constant approached Level 2 flying qualities. In other words, as the ailerons became less effective in generating the aircraft's roll re-

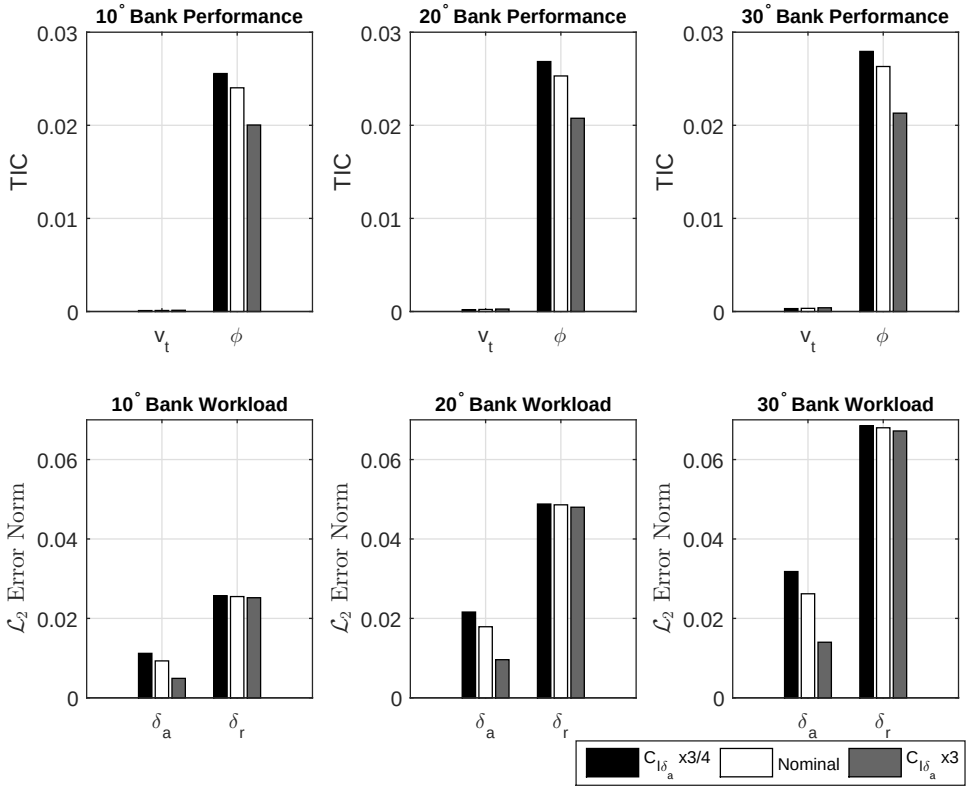

Figure 80. Lateral Maneuver: Performance and Workload Comparison of Nominal and $C_{l_{\delta_a}}$ Variation

sponse, the predicted flying qualities became worse as well. Another trend confirmed by this case is that as the aileron effectiveness decreased, the spiral mode became more unstable as well. Table 35 reveals another trend about the flying qualities for the Dutch roll mode. Once again, as the aileron effectiveness decreased, the Dutch roll damping ratio decreased resulting in less desirable characteristics. There was a recognizable trend in the control effectiveness that as the ailerons became less effective, the lateral flying qualities suffered as well. Overall, the lateral flying qualities were kept relatively constant matching the behavior exhibited by the longitudinal control power case. For UAVs engaged in missions not requiring aggressive maneuvers, the roll effectiveness requirements would be minimal. In the task that the UAV does require aggressive maneuvering, the requirements on the roll effectiveness would

be a driving force in the requirements.

Table 35. Effect of Variation of $C_{l_{\delta_a}}$ on Lateral Motion

Stability Derivative	Change	ζ_d	ω_d	T_r	T_s
$C_{l_{\delta_a}}$	x3	.1749	2.3442	.1818	50.06
	x2	.1746	2.3455	.1903	50.65
	x$\frac{3}{4}$	.1693	2.3490	.3464	60.18
	x$\frac{6}{10}$	.1672	2.3401	.5556	70.31

4.6 Effect of Variation of Single Stability or Control Derivative on Coupled Maneuver

Following the longitudinal and lateral analysis, the next set of simulations was to examine the effect of varying only one stability derivative during the simulation of the coupled maneuver, the climbing spiral. These results were compared to the previous results in the longitudinal and lateral maneuver. The variation of the longitudinal stability derivatives will be presented first followed by the variation in the lateral stability derivative. This section will conclude with the individual variation of the control derivatives in the coupled maneuver. The criteria for the level of flying qualities was based on the requirements for manned aircraft in MIL-STD-1797A for both the longitudinal and lateral-directional modes. While these cases varied a single derivative in the coupled maneuver, similar results and patterns to the previous cases were found. The performance and control plots for these prescribed cases are presented in Appendix E. The tables containing the quantitative assessment of the maneuvers using TIC and $\mathcal{L}_2$ norm values are collected in Appendix E as well.

4.6.1 Pitch Damping Case

Recall that in the pitch damping case for the longitudinal plane maneuver, a decrease in the pitch damping resulted in better performance but at the cost of os-

cillations with an increased elevator workload. The throttle control effort remained largely unaffected by the pitch damping. Figure 81 presents the quantitative assessment of the coupled maneuver for the cases of both decreased and increased pitch damping. Both longitudinal and lateral performance and workload assessments are now included.

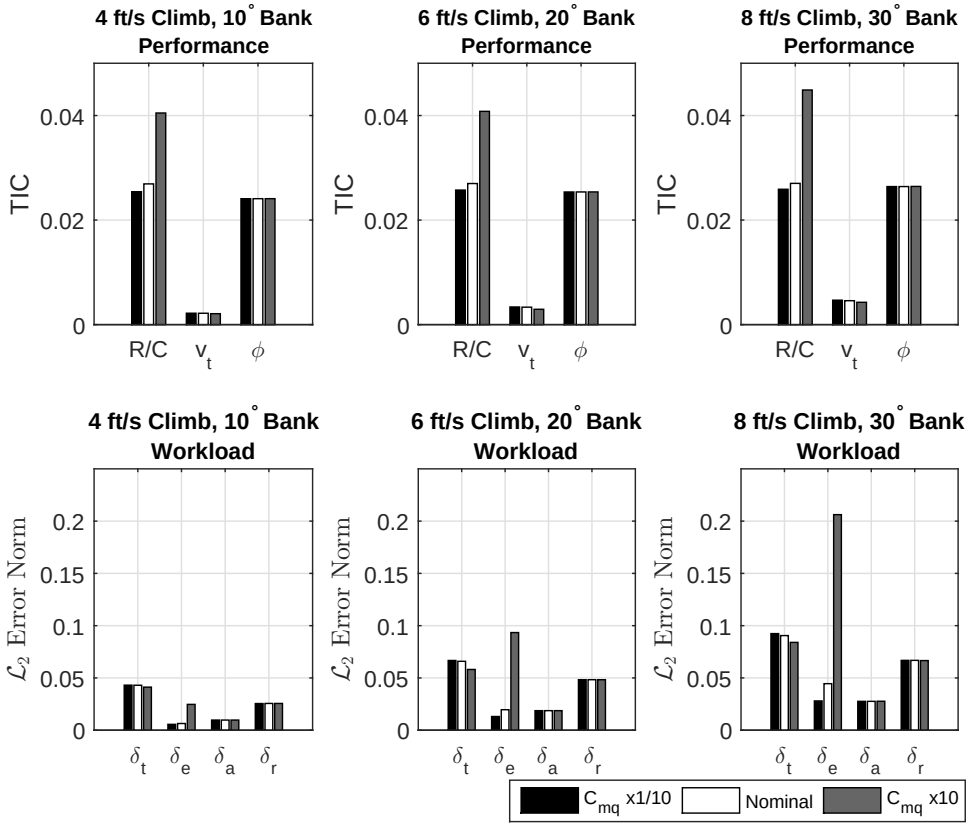

Figure 81. Coupled Maneuver: Performance and Workload Comparison of Nominal and C_{m_q} Variation

Continuing the trend as seen in the pitch damping case in the longitudinal maneuver, the aircraft's performance in tracking rate of climb worsened and elevator workload increased as the pitch damping increased. As expected, the aircraft was able to track the rate of climb closer throughout the maneuver than in the nominal case with decreased pitch damping, noted by the lower TIC values. The TIC values for the bank angle were slightly lower than in the nominal case but were largely unaf-

fected. The elevator workload was also lower; however, as the maneuver became more aggressive, the elevator saw the beginning signs of rate limiting. Due to the faster response, the control surfaces worked for a shorter period of time. The aileron workload and rudder workload remained almost identical as in the nominal case because there was no variation in the lateral-directional stability derivatives. An important observation made in this case is that the longitudinal stability derivative did not largely affect the lateral control of the ailerons and rudder.

The same comparisons were then made for the case of increased pitch damping. Recall that an increase in the pitch damping created a much more sluggish response and a control effort that almost doubled. This observation held true for over all three maneuvers in the coupled case. It is apparent from Figure 81 that the TIC value for rate of climb nearly doubled capturing the trend that as the damping increased, the aircraft was unable to track the rate of climb as closely as in the nominal case. An interesting observation was the dramatic increase in elevator workload as the maneuver became more aggressive. In the most aggressive maneuver, the elevator's workload was nearly four times the amount as in the nominal case. Comparing this to the longitudinal maneuver with increased pitch damping, the elevator workload is almost an order of magnitude higher, signifying a dramatic increase in elevator workload for coupled maneuvers. As in the case of decreased pitch damping, the workload for the ailerons and rudder remain largely unaffected since only the longitudinal stability derivative was changed.

The effect of the variation of pitch damping on only the longitudinal flying qualities have already been presented. In that simulation, the variation of the pitch damping largely affected the longitudinal tracking and elevator workload with minimal impact on the lateral plane. This trend is verified in Table 36 where the lateral parameters stayed relatively constant. According to MIL-STD-1797A, the roll mode time con-

stant and spiral mode classify the aircraft as having Level 1 flying qualities and the Dutch roll mode damping ratio classify the aircraft as having Level 2 flying qualities. It is however quite close to reaching the requirements for Level 1 Dutch roll mode flying qualities. The key observation made here is that the lateral flying qualities stay constant as the longitudinal stability derivative varies. The parameter most affected was a longitudinal parameter, the short-period damping ratio as predicted by Blakelock.

Table 36. Effect of Variation of C_{m_q} on Coupled Motion

Stability Derivative	Change	ζ_{sp}	ω_{sp}	ζ_p	ω_p	ζ_d	ω_d	T_r	T_s
C_{m_q}	x10	4.38	10	.29	.11	.17	2.35	.250	59.90
	x4	1.29	10	.19	.15	.17	2.35	.249	56.08
	x2	.86	8.82	.15	.18	.17	2.35	.250	54.96
	x$\frac{1}{2}$	.65	6.89	.12	.23	.17	2.35	.254	54.67
	x$\frac{1}{4}$	.61	6.55	.11	.24	.17	2.35	.256	54.71
	x$\frac{1}{10}$	.58	6.33	.10	.25	.17	2.35	.256	54.76

4.6.2 Static Pitch Stability Case

The second case of simulations run in this series was the variation in static pitch stability. Remembering the trend from the case of static pitch stability in the longitudinal plane, C_{m_α} affected the TIC value for rate of climb and the elevator workload. The calculated TIC and $\mathcal{L}_2$ values for the simulations are collected and compared in Figure 82. As anticipated, the decreased static pitch stability resulted in a lower TIC value for rate of climb, which improved the aircraft's tracking performance. The elevator workload has also decreased naturally because the elevator works for a shorter amount of time stemming from the aircraft's improved maneuverability. Like in the previous case, the control surfaces in the lateral-directional plane remained minimally impacted by the change in the static pitch stability.

Naturally, the increase in stability took away from the aircraft's maneuverability

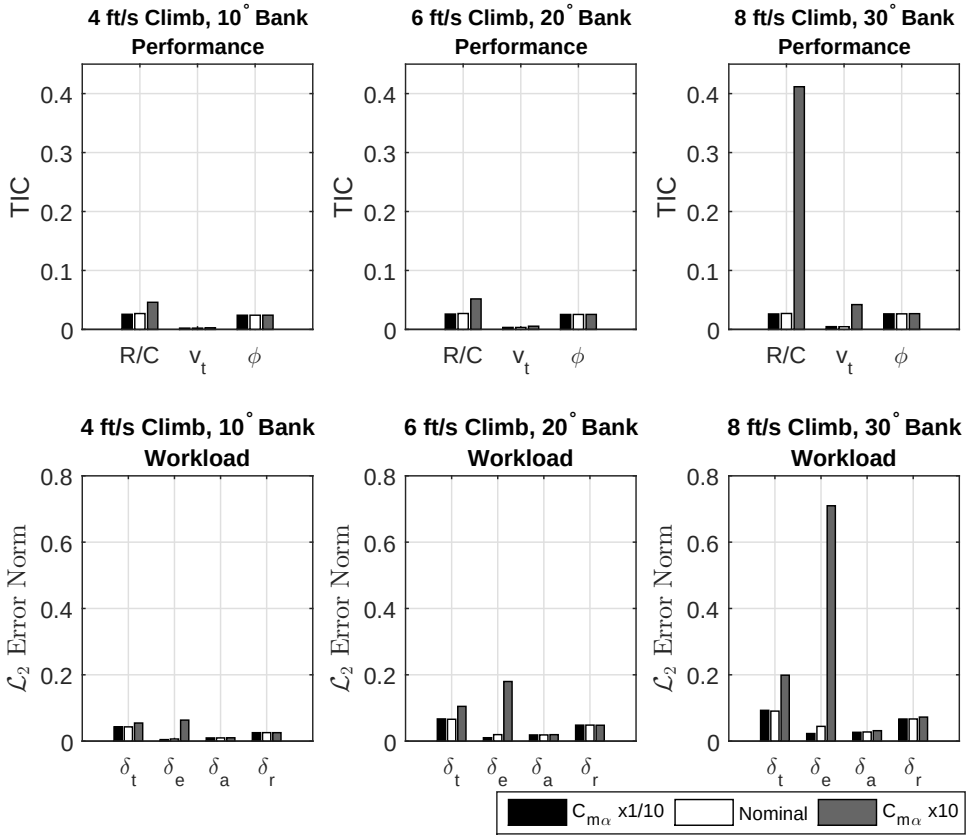

Figure 82. Coupled Maneuver: Performance and Workload Comparison of Nominal and C_{m_α} Variation

resulting in higher TIC values and larger control efforts. For the maneuver with a rate of climb of 8 ft/s and bank angle of 30°, the aircraft was unsuccessful in completing the maneuver. The rate of climb TIC value of 0.41 reveals that the control system was unsuccessful at obtaining the desired rate of climb. In order to confirm an accurate performance of the maneuver, the TIC value must be less than 0.25. In addition, the $\mathcal{L}_2$ norm value for the elevator of 0.71 reveals a high control effort throughout the maneuver. This confirms that the increased static pitch stability was the cause of the aircraft's unsuccessful coupled maneuver. By having the aircraft too stable, the flight control system was burdened with overcoming the large margin of static stability for the coupled maneuver.

Examining the flying qualities in Table 37, the lateral flying qualities remained largely constant as in the previous case with pitch damping. The simulation also confirmed that the lateral controls remained quite identical to the nominal case. The spiral mode was the most affected lateral parameter but its flying qualities still classified it as having Level 1 characteristics. The longitudinal parameters were affected by the static pitch stability, especially the short period frequency ranging from 3.15 to 10 rad/s. Overall, the longitudinal flying qualities and maneuver performance improved with decreasing static pitch stability and the lateral plane remained unperturbed.

Table 37. Effect of Variation of C_{m_α} on Coupled Maneuver

Stability Derivative	Change	ζ_{sp}	ω_{sp}	ζ_p	ω_p	ζ_d	ω_d	T_r	T_s
$C_{m\alpha}$	x10	.17	10	.12	.26	.18	2.36	.23	76.00
	x4	.32	10	.11	.25	.17	2.35	.25	62.34
	x2	.56	9.75	.12	.24	.17	2.35	.25	58.47
	x$\frac{1}{2}$	.87	6.01	.15	.17	.17	2.35	.25	50.08
	x$\frac{1}{4}$	.98	4.88	.19	.14	.17	2.35	.24	46.99
	x$\frac{1}{10}$	1.18	3.15	.25	.10	.17	2.35	.24	57.70

4.6.3 Roll Damping Case

Similar to the pitch damping case analysis, the roll damping case in the coupled maneuver was examined and compared to the flying qualities from the linearized model. The calculated TIC and $\mathcal{L}_2$ values for the roll damping cases are presented in Figure 83. Like in the lateral plane maneuver, the TIC value for the bank angle is lower than its nominal case with decreased roll damping, while the TIC for the rate of climb was relatively identical to its value in the nominal case. Recall that in the decreased pitch damping case, the workload for the longitudinal control was lower than in the nominal case and the workload for the lateral control remained largely unaffected. In the case for decreased roll damping, the lateral control workload remained lower than in the nominal case and the longitudinal controls were duplicated

from the nominal case.

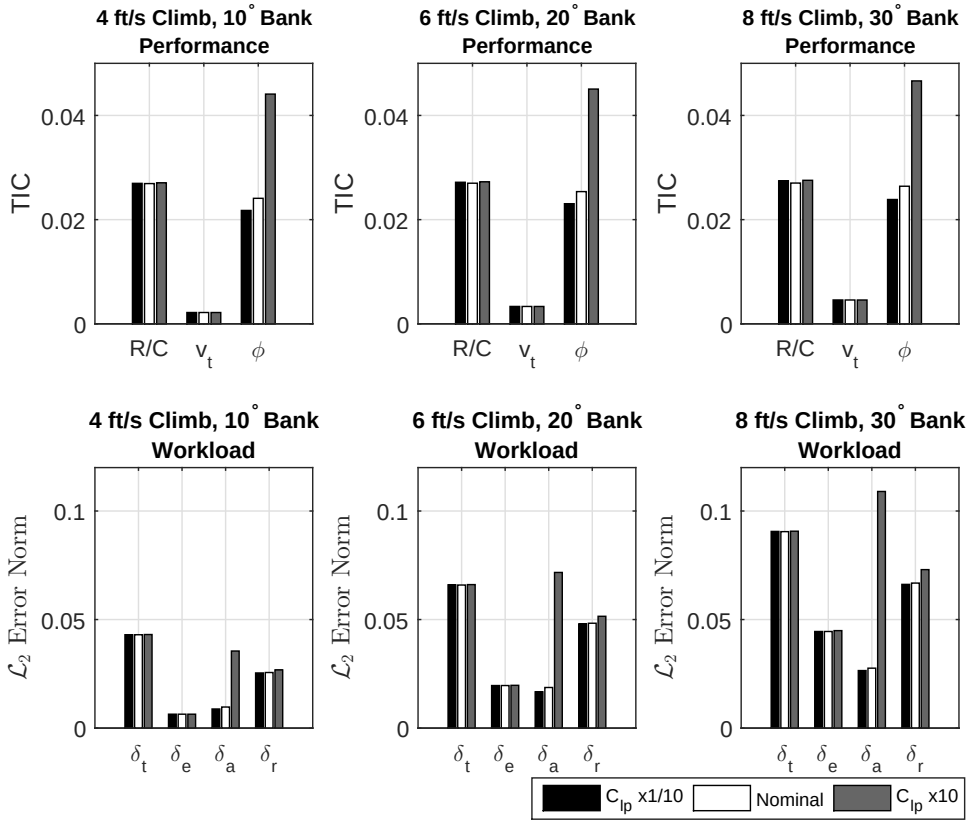

Figure 83. Coupled Maneuver: Performance and Workload Comparison of Nominal and C_{l_p} Variation

Decreased damping resulted in a faster response, making the response more susceptible to fluctuations which may be subject to rate limiting. Conversely, increased damping slowed the response. It is important to set the damping no higher than required, or the response may become too slow to be considered at a satisfactory level. In the case of increased roll damping, the TIC values for the bank angle were higher than in the nominal case and the ailerons' workload was over three times the amount than that in the nominal case. Some general conclusions can be made at this point from the various cases. A change in either the longitudinal or lateral plane mostly affects the response and flight controls in that plane, even in a coupled maneuver.

It is apparent from Table 38 that the trends reflected in the simulation cases were

also present in the linearized model. The short-period and phugoid mode were nearly identical in all four cases, verifying that the longitudinal flying qualities were largely unaffected by the change in the lateral stability derivative. Based on the short period damping ratio and phugoid damping ratio, the aircraft has Level 1 flying qualities in the longitudinal plane. The Dutch roll mode, roll mode time constant, and time to double for the spiral mode were all affected by the variation of the roll damping like in the previous roll damping cases. The parameter most affected by the roll damping was the roll mode time constant as predicted by Blakelock.

Table 38. Effect of Variation of Stability Derivatives on Coupled Maneuver

Stability Derivative	Change	ζ_{sp}	ω_{sp}	ζ_p	ω_p	ζ_d	ω_d	T_r	T_s
C_{lp}	x2	.73	7.56	.13	.21	.20	2.26	.0068	114.5
	x$\frac{1}{2}$	.73	7.57	.13	.21	.12	2.40	.35	28.98
	x$\frac{1}{4}$	.73	7.57	.13	.21	.062	2.37	.52	17.52
	x$\frac{1}{10}$	.73	7.56	.13	.21	.018	2.31	.76	10.79

4.6.4 Elevator Control Power Case

In the previous sections involving the elevator effectiveness, $C_{m_{\delta_e}}$, it was shown that the elevator effectiveness affected the simulation response but not the longitudinal flying qualities enough in order to degrade it to the next level. As the effectiveness increased, the aircraft's performance improved, but it came at the danger of potentially rate limiting. On the other hand, as the effectiveness decreased, the control surfaces were unable to generate enough moment with a given deflection and were potentially in danger of hitting position limits. Figure 84 compares the cases with variation in elevator effectiveness to the nominal case.

From the simulation results for the increased elevator effectiveness, the aircraft's performance in tracking the rate of climb was improved. With the exception of the least aggressive climbing spiral which was slightly higher than in the nominal case, the elevator workload was generally much smaller than in the nominal case. The

lateral control workload was very similar to that of the nominal case. In the opposite case for decreased elevator effectiveness, the trend seen was just the opposite with worse tracking performance and higher elevator workload.

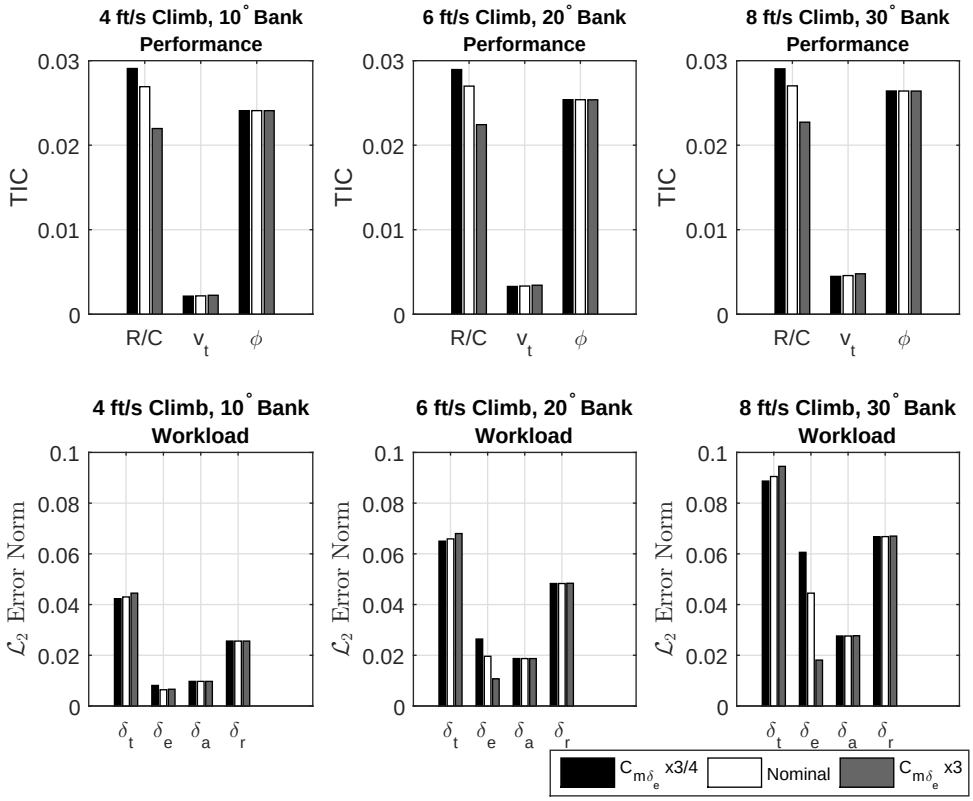

Figure 84. Coupled Maneuver: Performance and Workload Comparison of Nominal and $C_{m_{\delta_e}}$ Variation

In terms of flying qualities, it was seen in the previous cases that the elevator effectiveness did not have a strong effect on the longitudinal modes of motion. Table 39 confirms this trend. The longitudinal flying qualities are still classified as Level 1 flying qualities without much variation in either the short period or phugoid modes. The lateral flying qualities are not affected by the change in longitudinal stability derivative, meeting the requirements for Level 1 lateral flying qualities with the exception of the Dutch roll mode damping ratio. The resulting Dutch roll mode damping ratio of .17 was slightly lower than the minimum requirement of .19 in order

to be considered Level 1 flying qualities. Ultimately the important evaluation is that the lateral flying qualities stayed consistent throughout the variation in the elevator effectiveness.

Table 39. Effect of Variation of $C_{m_{\delta_e}}$ on Coupled Maneuver

Stability Derivative	Change	ζ_{sp}	ω_{sp}	ζ_p	ω_p	ζ_d	ω_d	T_r	T_s
$C_{m_{\delta_e}}$	x3	.7254	7.5494	.1230	.2108	.17	2.35	.25	57.87
	x2	.7255	7.5526	.1246	.2106	.17	2.35	.25	57.01
	x$\frac{3}{4}$	.7258	7.5680	.1333	.2093	.17	2.35	.26	53.11
	x$\frac{1}{2}$	.7261	7.5793	.1412	.2081	.17	2.35	.27	50.03

4.6.5 Aileron Control Power Case

The last case involved the variation of the aileron effectiveness, $C_{l_{\delta_a}}$, in the climbing spiral maneuver. As with the previous maneuvers, in order to fully understand the simulation results, one must examine the TIC and $\mathcal{L}_2$ values in Figure 85. Similar to the elevator control power case, the trends exhibited in this case favored increasing the aileron effectiveness. Increasing the aileron effectiveness resulted in better tracking performance of the bank angle along with lower workload for the lateral control surfaces. The longitudinal controls remained largely unaffected by the change in aileron effectiveness. It is important to remember that the increased aileron effectiveness came at the cost of rate limiting for the ailerons, which can lead to system induced oscillations if proper control margins are not met.

While the elevator effectiveness had minimal effect on the longitudinal modes of motion, the aileron effectiveness did affect the roll mode time constant as observed in previous cases. Table 40 presents the results for the aircraft's various longitudinal and lateral modes. The simulation showed that the longitudinal modes were largely unaffected. The short-period and phugoid modes remained constant in all cases. The lateral flying qualities started to degrade as the aileron effectiveness decreased. In addition, the Dutch roll mode damping ratio started to deviate further away from its

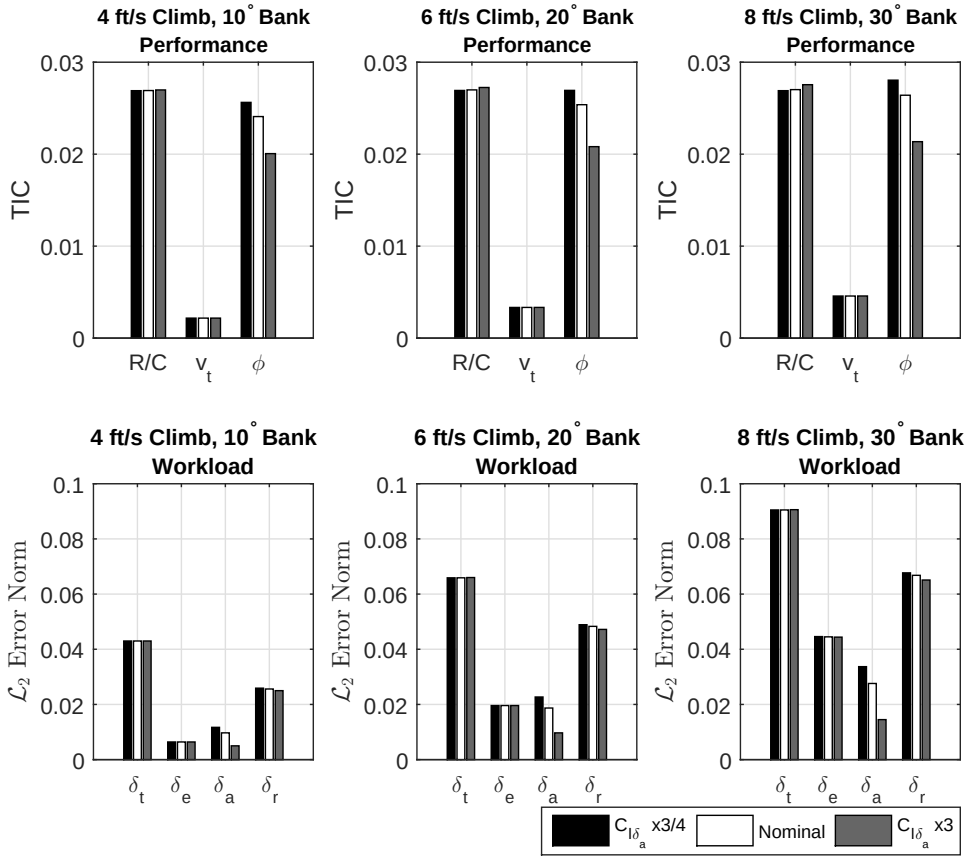

Figure 85. Coupled Maneuver: Performance and Workload Comparison of Nominal and $C_{l_{\delta_a}}$ Variation

Level 1 specification of .19 as the aileron effectiveness decreased. The roll mode time constant started to increase towards the boundary between Level 1 and 2 flying qualities specification of 1.0 second. The simulation and flying qualities assessment both point towards increasing the aileron effectiveness to improve the handling qualities resulting in better tracking performance and lower workload for the control system.

Table 40. Effect of Variation of $C_{l_{\delta_a}}$ on Coupled

Stability Derivative	Change	ζ_{sp}	ω_{sp}	ζ_p	ω_p	ζ_d	ω_d	T_r	T_s
$C_{l_{\delta_a}}$	x3	.73	7.56	.13	.21	.1749	2.3442	.1819	50.06
	x2	.73	7.56	.13	.21	.1746	2.3455	.1903	50.65
	x$\frac{3}{4}$	.73	7.56	.13	.21	.1693	2.3490	.3464	60.18
	x$\frac{6}{10}$	.73	7.56	.13	.21	.1673	2.3401	.5556	70.31

4.7 Effect of Variation of Coupled Stability and Control Derivatives

The final set of simulations examined the effect of variation of both longitudinal and lateral derivatives in the coupled maneuver, the climbing spiral. Whether the trends from the previous cases were carried over into the coupled maneuver were investigated in this section as well. The flying qualities were compared to the simulation results to see if they were in agreement with each other.

4.7.1 Pitch Damping and Roll Damping Case

The climbing spiral maneuver was conducted with pitch and roll damping adjustments. For this case, the pitch and roll damping were both varied by an order of magnitude and compared to results from the nominal climbing spiral in Table 29. With less roll and pitch damping, the results of the longitudinal and lateral cases were reflected in the coupled maneuver. The performance and control plots for the decreased roll and pitch damping simulation are presented in Figures 86 and 87. As expected, the responses in the rate of climb and bank angle are much quicker in reaching their steady state value but have the tendency to oscillate. The control surfaces exhibited the similar trends shown separately in the longitudinal and lateral cases. The elevator and aileron surfaces both obtained the sawtooth pattern as the maneuver increased in rate of climb and bank angle. In all cases where the pitch or roll damping were decreased, the control surfaces became more prone to rate limiting.

Figure 88 shows the assessment of the maneuvers and the corresponding workload of the control system. It was observed that in the case that the pitch and roll damping were both decreased, the rate of climb and bank angles were tracked better than in the nominal case, confirming the trends seen in the longitudinal and lateral cases. The decreased damping provides the most important contribution to the damping of the dynamic behavior, resulting in quicker responses and the corresponding lower

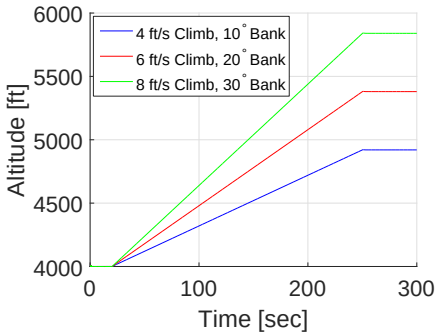

(a) Altitude, h

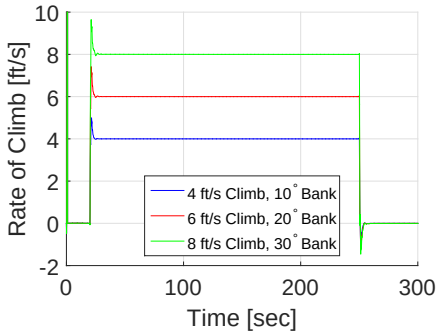

(b) Rate of Climb, $\dot{h}$

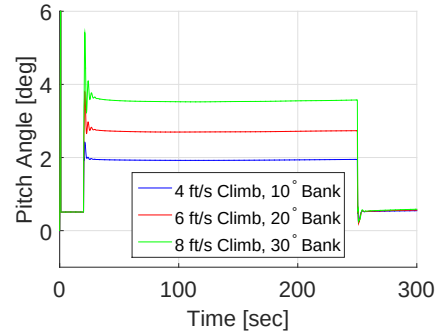

(c) Pitch Angle, θ

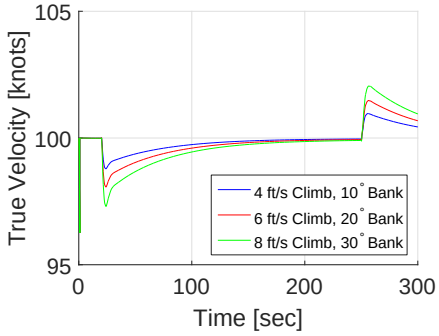

(d) Velocity, v_t

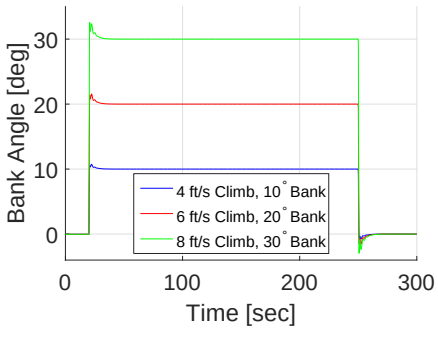

(e) Bank Angle, ϕ

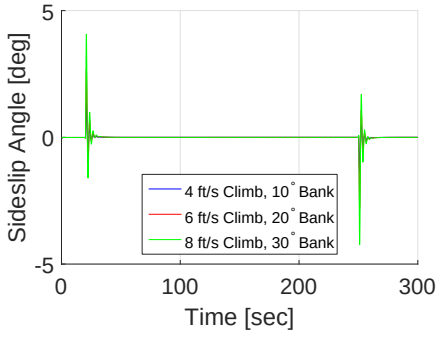

(f) Sideslip Angle, β

Figure 86. Coupled Maneuver: C_{m_q} and C_{l_p} x $\frac{1}{10}$ Performance Plots

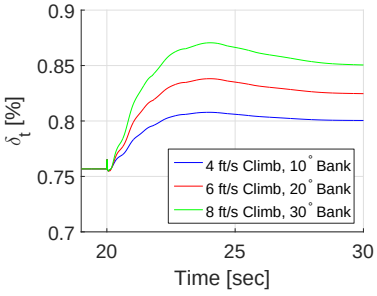

(a) Throttle Initiation

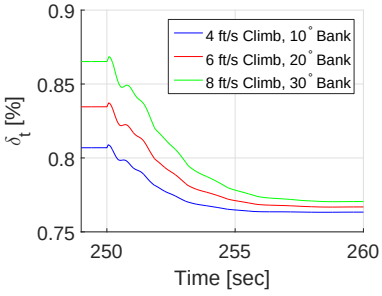

(b) Throttle Termination

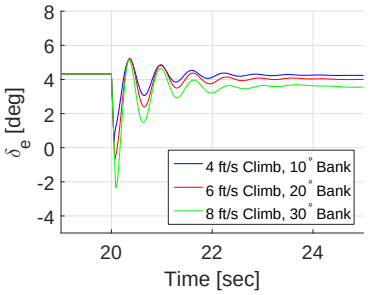

(c) Elevator Initiation

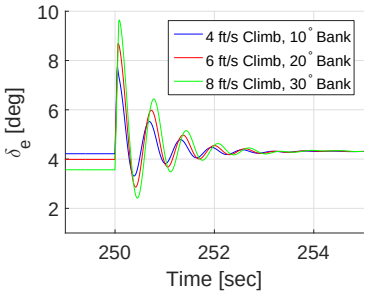

(d) Elevator Termination

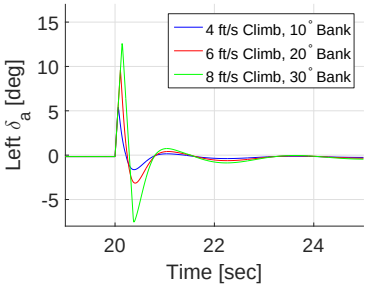

(e) Aileron Initiation

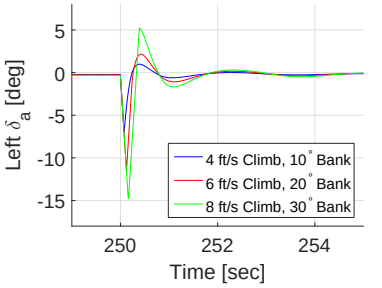

(f) Aileron Termination

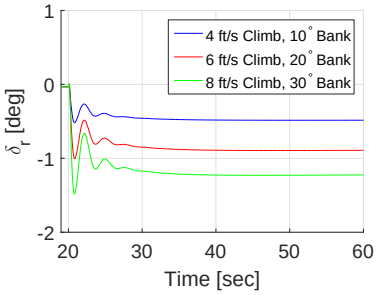

(g) Rudder Initiation

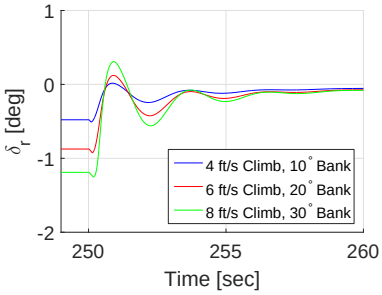

(h) Rudder Termination

Figure 87. Coupled Maneuver: C_{m_q} and C_{l_p} x $\frac{1}{10}$ Control Plots

TIC values. In the coupled maneuver, all the control surfaces for decreased damping had lower $\mathcal{L}_2$ norm values than in the nominal case. This is in contrast to the workload trend for the simulation in the longitudinal plane in which the elevator had a higher workload than in the nominal case. The explanation for this disconnect is not trivial because all the inputs are now coupled. The oscillatory response and rate limiting tendency are however both carried over from the longitudinal and lateral plane simulations.

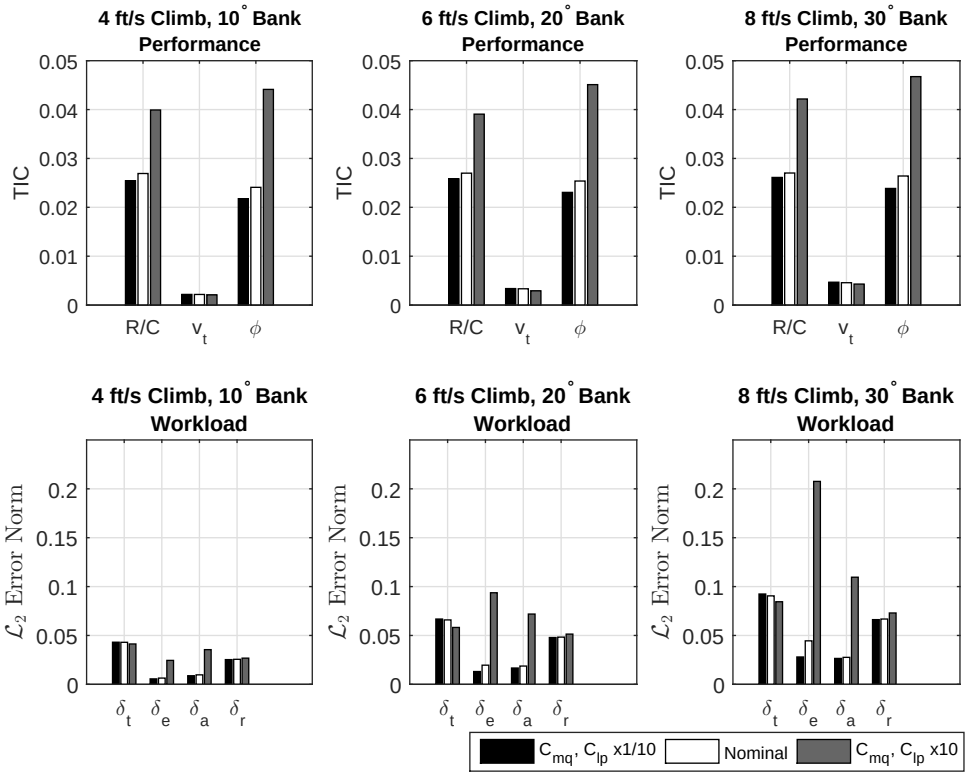

Figure 88. Coupled Maneuver: Performance and Workload Comparison of Nominal and C_{m_q}, C_{l_p} Variation

The quantitative assessment of the case with increased pitch and roll damping is also shown in Figure 88. The simulation performance and control plots for this prescribed case are shown in Appendix F. The longitudinal response in the coupled maneuver appears to be worse than the longitudinal maneuver. In the longitudinal maneuver, the elevator deflection returned back to its trimmed deflection during

the maneuver. In the coupled maneuver, the elevator deflection stays continuously deflected away from its trimmed deflection configuration. In addition, the oscillations in the rate of climb and pitch response have larger amplitudes due to the velocity drop. For the most aggressive maneuver, the ailerons were hitting their position limits just like in the lateral plane simulation. In the case of the increased pitch and roll damping, the rate of climb and bank angle were not tracked as well as in the nominal case. The TIC values for rate of climb and bank angle are almost double those of the nominal case. This was the case of the separate pitch damping and roll damping cases, which are now both reflected in this coupled maneuver. In the case with the pitch and roll damping increased, all the control surfaces were working harder than in the nominal case. In particular, the elevator and ailerons were both working over three times harder than in the nominal case.

Combining all the previous cases at this point, some general observations can be made. The elevator workload comparison between the longitudinal and coupled maneuver have not been consistent; however, when the overall results are combined, it is sufficient to say that that the workload typically decreases with decreased damping and the workload increases with increased damping. A consistent phenomenon seen across all cases was the tendency to rate limit as damping decreased and the tendency to position limit as damping increased. Ultimately, these two tendencies will dictate the limits of the control system affecting the flying qualities rating.

The linearized values for the various modes of the aircraft are listed in Table 41. Comparing the longitudinal parameters to the linearized values from varying just the pitch damping, C_{m_q} in Table 30, the values are almost identical. Investigating the lateral parameters to the linearized model from varying just the roll damping, C_{l_p}, in Table 34, the values are almost identical as well. While there were slightly different values, the coupled case maintains continuity with the individual longitudinal and

lateral cases. Since the trends in the individual cases are reflected in the coupled case, this gives an initial indication that trends seen in the separate longitudinal and lateral modes should translate into the coupled maneuver.

Table 41. Effect of Variation of C_{m_q} and C_{l_p} on Aircraft Dynamics

Change	ζ_{sp}	ω_{sp}	ζ_p	ω_p	ζ_d	ω_d	T_r	T_s
x10	4.3793	10.0	.2892	.1103	-	-	-	-
x5	1.6267	10.0	.2112	.1411	-	-	-	-
x2	.8615	8.8190	.1549	.1835	.1953	2.2552	.0100	100.0
x$\frac{3}{4}$	.6890	7.2335	.1226	.2184	.1529	2.3772	.2758	41.22
x$\frac{1}{2}$	.6508	6.8975	.1150	.2281	.1186	2.3973	.3517	29.02
x$\frac{1}{10}$	.5858	6.3382	.1007	.2469	.01866	2.3107	.7704	10.92

Examining the longitudinal flying qualities characteristics, the phugoid damping ratio for all cases are above .04 in order to qualify for Level 1 flying qualities. In addition, the short period damping ratio requirement for Level 1 is between .35 an 1.30. All the variations in C_{m_q} and C_{l_p} qualify for Level 1 flying qualities based on the short period damping ratio except the two heavily damped cases. The case where the stability derivatives were multiplied by five is considered a Level 2 flying qualities while the heaviest damping case is considered Level 3 flying qualities. The trends from the longitudinal cases were represented in the coupled maneuver as well.

Following the examination of the longitudinal flying qualities, the lateral component was examined based on the requirements for the roll mode, spiral mode, and Dutch roll mode. All the roll mode time constants, T_R, were below one second, labeling the cases as Level 1 flying qualities. All spiral modes were stable as well labeling them Level 1 flying qualities as well. Based on the Dutch roll damping ratio, the aircraft attains Level 1 flying qualities since it meets the minimum value of .19; however, based on $\zeta_d\omega_d$, the aircraft is no longer considered Level 1 after multiplying the pitch and roll damping by .50 and .10, reaching Level 2 and Level 3 flying qualities respectively. Like the longitudinal trends, the lateral flying qualities trends from the

lateral plane simulation were reflected in the coupled maneuver.

Comparing the simulation with the linearized results, the case of multiplying the stability derivatives by .10 resulted in worse roll mode characteristics. The lower TIC and $\mathcal{L}_2$ values resulting in better performance and workload point towards having lower damping properties; however, the requirements in MIL-STD-1797A reveal that the aircraft attains Level 3 lateral flying qualities and Level 1 longitudinal flying qualities. The case with high pitch and roll damping had worse performance and a higher workload. In addition, it had Level 3 longitudinal flying qualities based on the short-period damping ratio and Level 1 lateral flying qualities based on the Dutch roll mode and roll mode specifications. While a LOES was not successfully obtained for the x1/10 damping case, the trend is that the spiral mode became more unstable as the damping was increased. There is clearly a disconnect between the simulation evaluation and the manned MIL-STD-1797A flying qualities requirements.

4.7.2 Static Pitch Stability and Roll Damping Case

In this case, the static pitch stability and roll damping were both varied in the coupled maneuver. Appendix F contains the performance and control plots for the case in which the static pitch stability and roll damping were decreased. The effects of rate limiting were seen again when the roll damping was decreased like in the previous cases. It was also noticed that the elevator's response did not oscillate as much as in the pitch damping case which was seen previously as well.

Some interesting observations were made in the case where the static pitch stability and roll damping were increased by an order of magnitude. In this case, the maneuverability of the aircraft is essentially reduced. The aircraft unable to successfully reach the desired rate of climb and maintain its velocity as shown in the performance plots in Figure 89. The bank angle and sideslip angle were maintained

in all three maneuvers so only the longitudinal axis was compensated. The control plots in Figure 90 reveal that the elevator was deflecting at its maximum deflection and the throttle was also hitting its upper limit. At the large bank angles, the aircraft was unable to recover from the large drop in velocity and maintain a steady rate of climb of 8 ft/s.

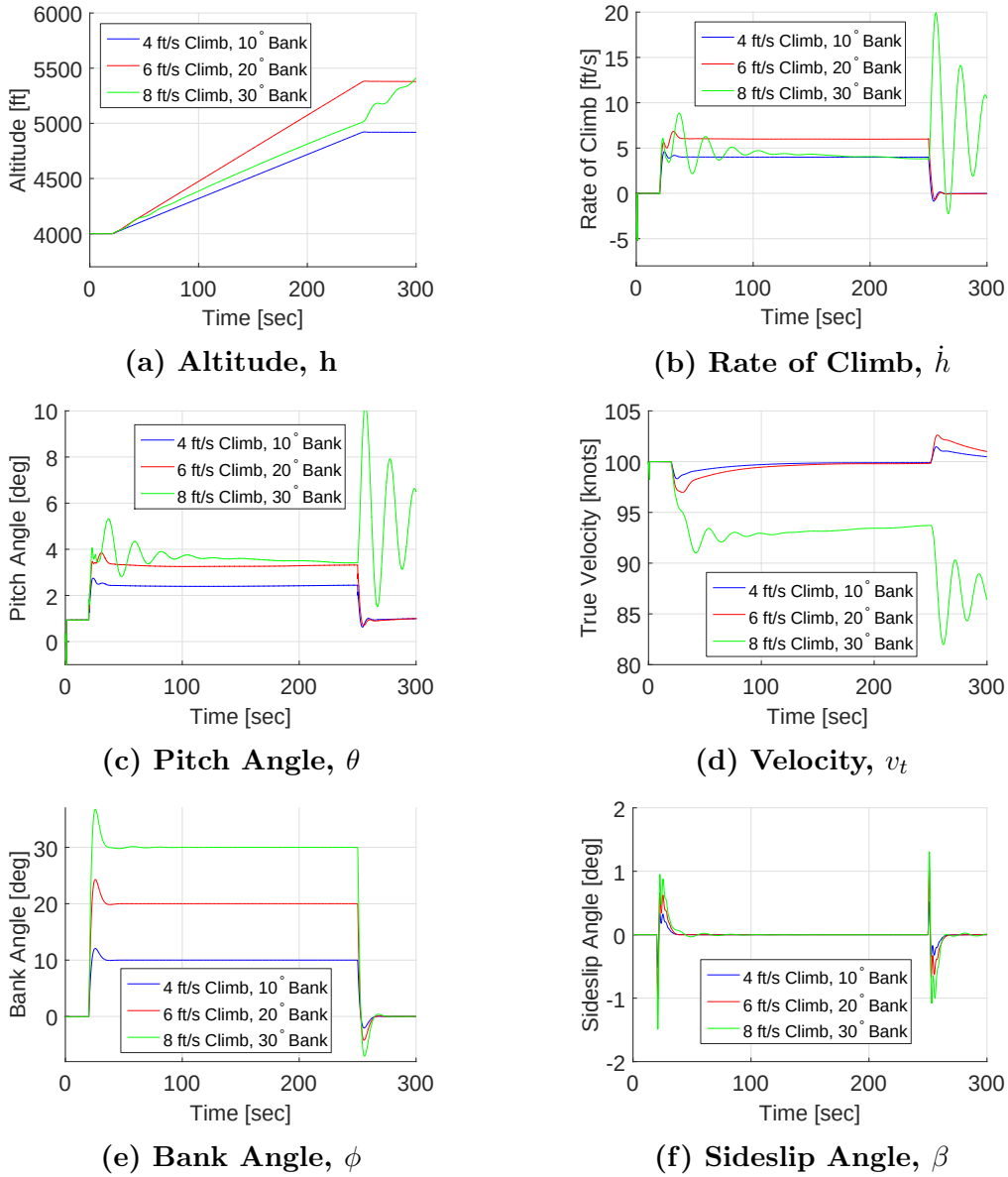

(a) Altitude, h **(b) Rate of Climb, $\dot{h}$**

(c) Pitch Angle, θ **(d) Velocity, v_t**

(e) Bank Angle, ϕ **(f) Sideslip Angle, β**

Figure 89. Coupled Maneuver: C_{m_α} and C_{l_p} x 10 Performance Plots

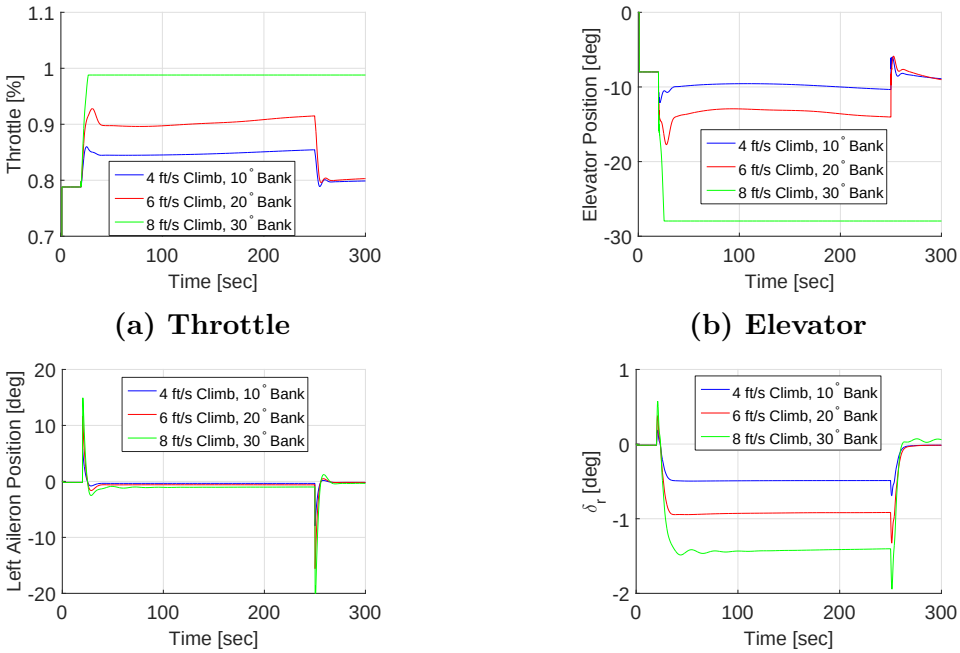

(a) Throttle **(b) Elevator**

(c) Left Aileron **(d) Rudder**

Figure 90. Coupled Maneuver: C_{m_α} and C_{l_p} x 10 Control Plots

Figure 91 presents the TIC and $\mathcal{L}_2$ norm values for the variation in static pitch stability and roll damping. In the case that both static pitch stability and roll damping were decreased by an order of magnitude, the aircraft was able to perform the maneuver more effectively than the nominal case, verified by the lower TIC values. All the control surfaces had a lower workload than the nominal case as well, verified by the lower $\mathcal{L}_2$ norm values. The combination of increased maneuverability and decreased damping made it possible to enhance the aircraft's performance without increasing the flight control system's workload.

The increased static pitch stability and roll damping case was identical to the coupled case varying only the static pitch stability. Recall that in the coupled case in varying just the static pitch damping, the aircraft was unable to perform the maneuver climbing at 8 ft/s and banking at 30°. The quantitative assessment of the aircraft's maneuver in Figure 91 reflect that the TIC value for the rate of climb, $\dot{h}$, was over

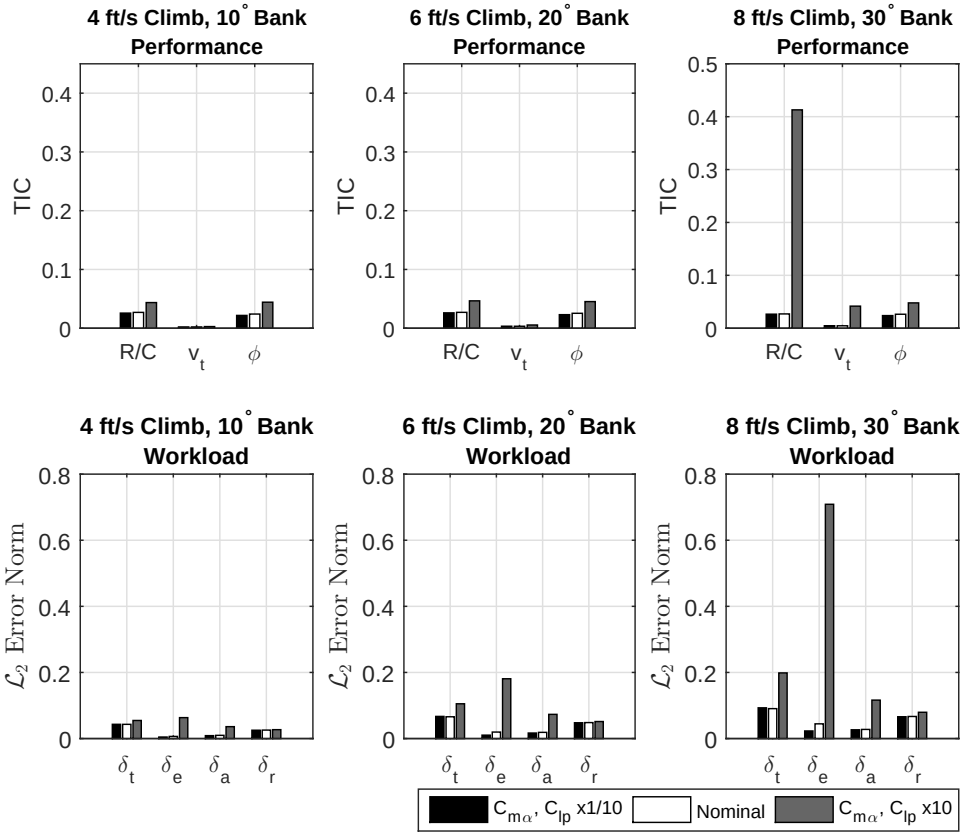

Figure 91. Coupled Maneuver: Performance and Workload Comparison of Nominal and C_{m_α}, C_{l_p} Variation

.25, indicating that the deviation from the desired rate of climb was quite significant as well. Based on Figure 89d, the velocity was unable to be tracked successfully, but its TIC value is still below .25, thus TIC may not be a viable option for comparing the time history of velocity. Dorobantu, Seiler, and Balas stated that if "one of the time histories is constant and zero," it represented worst-case deviation [16]. The fact that the desired velocity time history is a constant may explain why TIC was unable to capture the unsuccessful tracking. The $\mathcal{L}_2$ norm value for the elevator was much higher than the nominal case reflecting that the elevator was positioned at high angles of deflection throughout the maneuver. The combination of sluggish response from the high roll damping and loss of maneuverability from high static stability resulted in unsatisfactory mission performance.

Based on the linearized analysis shown in Table 42, the x4 and x10 cases were unable to converge on a LOES solution for the linearized model, but the trends indicate to the range of values that the x10 case might be. Examining the x1/10 case first, the short-period damping ratio is considered Level 2 flying qualities and the phugoid damping ratio is considered Level 1 flying qualities. In order to be conservative, the aircraft is considered a Level 2 flying qualities in the longitudinal plane. In the lateral plane, the aircraft is considered Level 3 flying qualities due to the low Dutch roll damping ratio; however, it is important to note that the roll mode time constant is considered Level 1 flying qualities.

Table 42. Effect of Variation of C_{m_α} and C_{l_p} on Aircraft Dynamics

Change	ζ_{sp}	ω_{sp}	ζ_p	ω_p	ζ_d	ω_d	T_r	T_s
x2	.5636	9.7475	.1172	.2355	.1955	2.2551	.01	100.0
x$\frac{1}{2}$	.8680	6.0639	.1512	.1772	.1182	2.3961	.3447	26.67
x$\frac{1}{4}$	.9830	4.8761	.1772	.1429	.06186	2.3729	.4950	14.97
x$\frac{1}{10}$	1.6039	2.0	.1942	.1063	.01870	2.3098	.7060	10.82

Examining the x10 case where the aircraft had its static pitch stability and roll damping increased, a prediction of the flying qualities can be made by looking at the x2 case and the trends associated for each parameter. With the short-period requirements, it is speculated that the short-period damping ratio would be below .35, putting it into the Level 2 or Level 3 flying qualities category. With the lateral requirements, the trend seen is that the Dutch roll mode damping ratio, ζ_d, and the parameter $\zeta_d\omega_d$ continue to increase above .19 and .35 respectively, thus attaining Level 1 flying qualities in the lateral plane. A key observation noted is that there is a trade-off between the longitudinal and lateral flying qualities as the stability derivatives were varied. In the x1/10 case, the aircraft had better longitudinal characteristics, whereas the x10 case had better lateral characteristics. The lack of satisfactory longitudinal flying qualities in the x10 case may explain the failure to perform the longitudinal aspect of the climbing spiral maneuver.

Overall, the comparison between the simulation and flying qualities requirements is not necessarily in agreement with each other. In the x1/10 case, the aircraft had achieved better mission performance and lower workload than the nominal case, yet the flying qualities labeled it as having Level 2 and Level 3 flying qualities in the longitudinal and lateral planes respectively. In the x10 case, the aircraft was unable to perform one of the climbing spirals, yet the aircraft attained a Level 2/3 rating and Level 1 flying qualities rating for the longitudinal and lateral planes respectively. For this reason, the simulation results and flying qualities analysis are not necessarily in agreement with each other.

4.7.3 Elevator and Aileron Control Power Case

The final coupled adjustment investigated in this section was the variation of the elevator and aileron effectiveness. As the control effectiveness was increased, it was expected that the aircraft task evaluation would improve. The previous two cases had the stability derivatives increased or decreased by one order of magnitude; however, the control effectiveness derivatives showed extreme trends. As a result, the derivatives were only multiplied by 3 and .75. These simulations showed that the differences in the control effectiveness were confined to a narrow band. The performance and control plots for the case in which the control effectiveness were multiplied by three are shown in Figures 92 and 93. As mentioned before, the increased effectiveness case produces more influence on the moment for a given control deflection. In other words, the sensitivity increases as the effectiveness increases. Figure 93 shows that excessive control compensation induced an oscillatory response and the control surfaces were more prone to rate limiting. The classical saw-tooth wave was apparent for the elevator and ailerons in Figures 93c - 93f as the maneuver required larger control inputs.

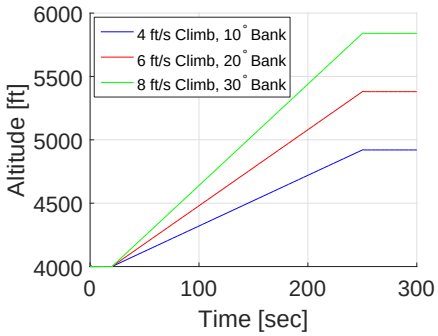

(a) Altitude, h

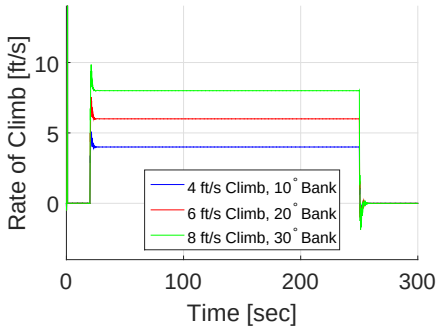

(b) Rate of Climb, $\dot{h}$

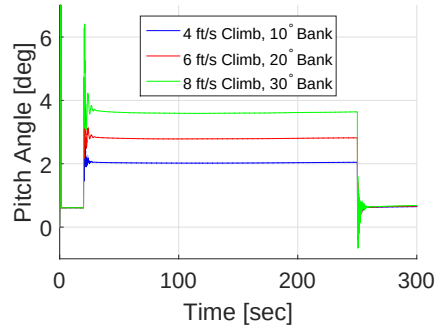

(c) Pitch Angle, θ

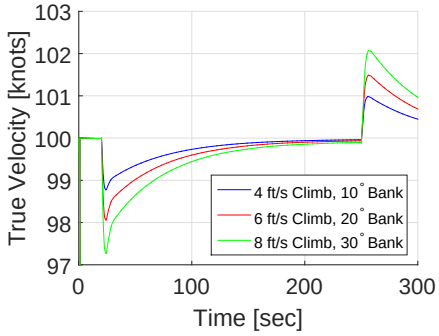

(d) Velocity, v_t

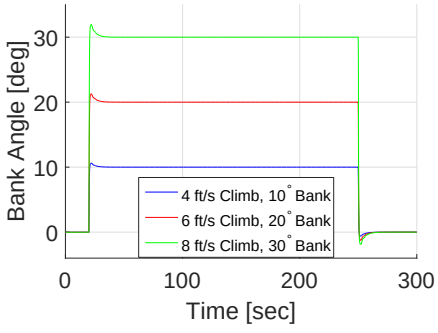

(e) Bank Angle, ϕ

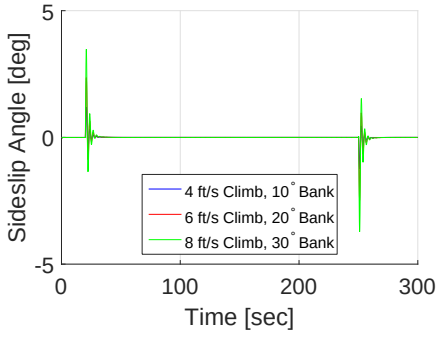

(f) Sideslip Angle, β

Figure 92. Coupled Maneuver: $C_{m_{\delta_e}}$ and $C_{l_{\delta_a}}$ x 3 Performance Plots

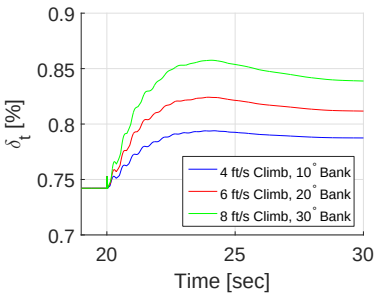

(a) Throttle Initiation

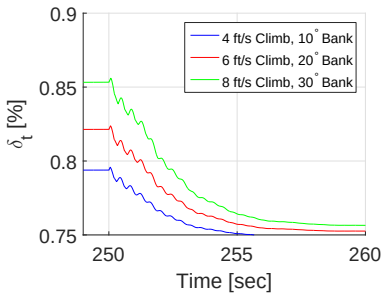

(b) Throttle Termination

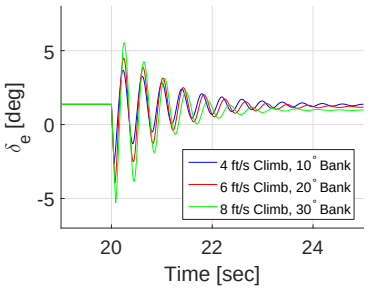

(c) Elevator Initiation

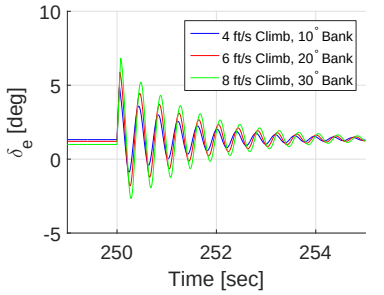

(d) Elevator Termination

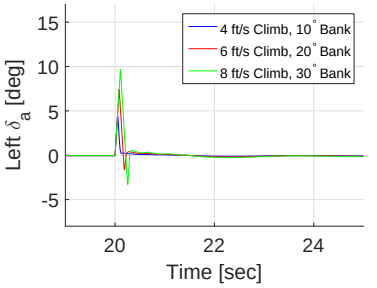

(e) Aileron Initiation

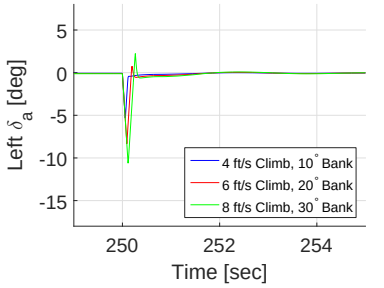

(f) Aileron Termination

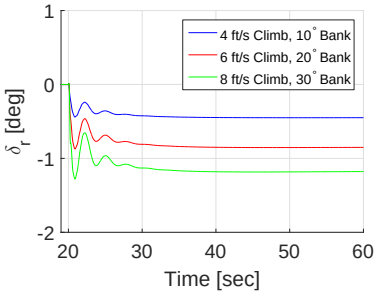

(g) Rudder Initiation

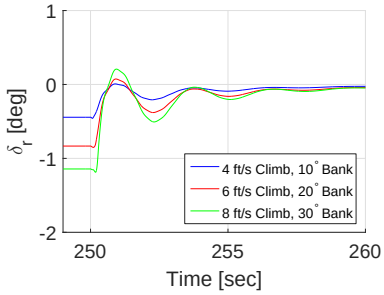

(h) Rudder Termination

Figure 93. Coupled Maneuver: $C_{m_{\delta_e}}$ and $C_{l_{\delta_a}}$ x 3 Control Plots

Recall that in the previous cases for the individual elevator and aileron power cases that as the effectiveness increased, the TIC values were smaller than the nominal cases; however, the controls were oscillating. That definitive trend for lower TIC values with increased control effectiveness was translated into the coupled maneuver as well as shown in Figure 94. As the control effectiveness increased, the aircraft's performance improved, as seen in the lower TIC values. The trends for the workload did not all translate over from the previous simulations. In the increased elevator effectiveness case, the elevator had a higher workload than in the nominal case. In contrast, the increased aileron effectiveness case saw a decreased workload than in the nominal case. In the coupled case, most of the control surfaces' workload was lower than in the nominal case as shown in Figure 94. In general, the control surfaces had a lower workload than in the nominal case when the control effectiveness was increased.

Some general conclusions can be made from Figure 94 about the decreased control effectiveness case. The decreased elevator and aileron effectiveness represented a configuration diminishing control authority available to the control system. The TIC values were higher than in the nominal case representative of sluggish response modes. All the control surfaces had a higher workload than in the nominal case and the throttle had a lower workload in all three maneuvers. From a simulation perspective, increasing the the control effectiveness was most beneficial producing smaller TIC and $\mathcal{L}_2$ norm values. Appendix F contains the performance and control plots for the case with the elevator and aileron effectiveness decreased.

Another important aspect of the simulation is the consideration for hitting position limits and rate limits. As the control effectiveness increased, the control surface deflections were closer to their neutral position but were close to rate limiting. In the other case where the control effectiveness decreased, the control surfaces were deflected further away from their neutral position but close to hitting their position

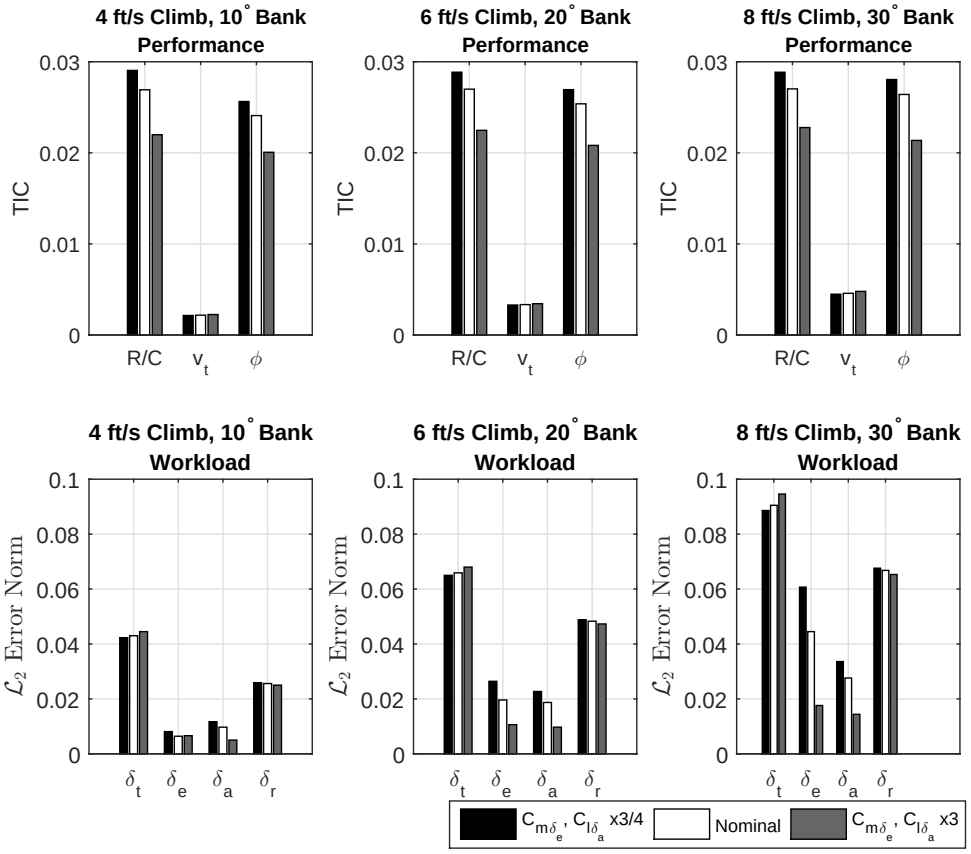

Figure 94. Coupled Maneuver: Performance and Workload Comparison of Nominal and $C_{m_{\delta_e}}$, $C_{l_{\delta_a}}$ Variation

limits. A logical distinction among aggressive tasks is the requirements for control power, and the likelihood of reaching aircraft physical limits while performing large-amplitude tasks. Control power has been typically achieved with increased control surface sizing. "This is, however, in direct conflict with the primary performance objectives that led to active control design in the first place. The result is smaller surfaces that must move very rapidly. This stresses the actuators, resulting in lags and rate limiting as an inherent problem in the design" [33]. With the least aggressive maneuver, the elevator's deflection comes out in a sinusoidal shape, but as the maneuver increases its aggressiveness, the shape becomes more triangular into a sawtooth pattern.

Recall that in the individual elevator effectiveness case, $C_{m_{\delta_e}}$ did not have a strong effect on the short-period or phugoid modes. In the individual aileron effectiveness case, $C_{l_{\delta_a}}$ had the strongest effect on the roll mode time constant, T_R. Those trends are reflected in the coupled case presented in Table 43. The aircraft maintains its Level 1 longitudinal flying qualities in the x3 and x3/4 case. According to the roll mode time constant, T_R, the aircraft is considered to have Level 1 lateral flying qualities. Note that as the control effectiveness decreases, the roll mode time constant increases, pushing it closer to being considered as Level 2 flying qualities. Based on the Dutch roll mode specifications, the aircraft is considered borderline Level 2 flying qualities, barely missing the minimum Dutch roll mode damping ratio of .19 in order to be considered Level 1 flying qualities.

Table 43. Effect of Variation of $C_{m_{\delta_e}}$ and $C_{l_{\delta_a}}$ on Aircraft Dynamics

Change	ζ_{sp}	ω_{sp}	ζ_p	ω_p	ζ_d	ω_d	T_r	T_s
x3	.7253	7.5500	.1223	.2108	.1757	2.3449	.1812	53.14
x2	.7254	7.5531	.1241	.2106	.1752	2.3460	.1890	52.95
x$\frac{17}{20}$	.7258	7.5650	.1318	.2095	.1704	2.3500	.2973	56.35
x$\frac{3}{4}$	.7259	7.5676	.1338	.2093	.1687	2.3482	.3543	58.46
x$\frac{7}{10}$	.7259	7.5692	.1350	.2091	.1678	2.3461	.4007	60.12

The simulation and flying qualities evaluation are both in parallel in desiring increased control effectiveness. With increased control effectiveness, the aircraft attained a better performance metric from the TIC values along with a lower workload for the control system. From a flying qualities aspect, the aircraft received Level 1 longitudinal flying qualities and was closer to obtaining Level 1 lateral flying qualities.

4.8 Chapter Summary

The results for the flight envelope were presented and compared to the performance specifications in the T-41 flight manual. The method for trimming the aircraft has been shown to result in reasonable results. An initial flying qualities assessment was presented as the altitude was varied producing Level 1 flying qualities as expected. With an initial flying qualities assessment complete, an initial simulation of the performance maneuver was completed including the decomposition into its longitudinal and lateral components. Lastly, the variation of the stability and control derivatives cases was simulated in JSBSim, capturing some trends exhibited by certain derivatives. The specific connections between vehicle configuration represented by stability derivatives and response characteristics represented by the transfer function poles and zeros ultimately impacting the flying qualities have been laid out. The simulation reinforced the idea that a control effectiveness requirement will be highly correlated to the mission task, and a classification system is essential to bring about an applicable UAV standard. The variation in stability derivatives does not necessarily correspond accurately to its manned flying qualities. What constituted as "good" flying qualities in manned aircraft was based on the pilot's preference on the aircraft's dynamic modes. With UAVs, that is no longer a concern and more attention needs to be focused on the limitations of the flight control system and task accomplishment.

V Conclusions and Recommendations

5.1 Conclusions

The overall objective for this research was to provide data on the flying quality assessments on a UAV in the hope of propelling the development of a UAV flying qualities standard. Successful identification of flying qualities trends would allow researchers to use JSBSim to model and characterize the aircraft response. In summary, the objectives of this research were as follows:

1. Evaluate the flying qualities of unmanned aircraft using JSBSim's capability to simulate maneuvers.
2. Determine how best to analyze the flying qualities for the various maneuvers. Current flying qualities requirements for manned aircraft were a major source for the methods for this analysis.
3. Validate the data and post-processed results by comparing it to known databases for the T-41.

The goal of evaluating the flying qualities of an unmanned aircraft was met using JSBSim's capability to accurately model and simulate an aircraft, validated by referencing known flight manuals and textbooks. It was determined that JSBSim has the capability to model performance maneuvers and accurately output linearized models with stability derivative adjustments. The trends seen in the stability derivative adjustments were verified by published works in that field. An initial analysis with regards to the aircraft's deviation from the perfect maneuver and control system workload aided in the comparison between maneuvers. The application of methods of flying qualities analysis was met but not with the expected results. The simulation

results did not consistently correspond to its manned flying qualities requirements. Although the simulation results and flying qualities assessments are specific to the T-41 for this research, the disconnect findings between manned requirements and unmanned aircraft performance can be extended to other unmanned systems. The flight control system was designed to perform certain maneuvers with enough control authority and power. In varying the stability derivatives, the basic airframe was essentially altered affecting the speed and rate at which the controls were moved. If the controls have a high likelihood of hitting position or rate limits due to the rate at which they are moving, it could degrade performance or even lose control of the aircraft. An important aspect of flying qualities that pertain to UAVs is the automatic control system. How much the control system is working is not so much a main concern but what is important is the speed and rate at which control surfaces are moving. The likelihood of hitting position and rate limits can severely degrade an aircraft's performance. This research was concerned about the non-precision, non-aggressive maneuver. As the maneuver increases in precision and aggressiveness, the effects of position and rate limiting became more apparent. The evaluation in terms of task performance showed a consistent trend using TIC as a metric. TIC is not however accurate in capturing the comparison between time histories if one of the time histories is constant. The use of TIC should not be used indiscriminately for all mission task evaluations if a constant time history is included in the comparison.

The trend in the amount of workload was not consistent among the cases since it was dependent on the design of the autopilot controller; however, the inclination towards hitting position and rate limits was consistent. In the longitudinal maneuver with decreased pitch damping, the elevator workload was slightly higher than the nominal case when it was expected that it would be lower. The excessive oscillation of the elevator control surface stemming from the controller design caused this uneven

trend; however, in the lateral cases, all the workload trends were consistent. An investigation into an optimal autopilot controller for JSBSim should be conducted to gain a more consistent workload trend. The $\mathcal{L}_2$ norm was accurate in capturing the workload such as in the coupled case with increased static pitch stability and roll damping. In that case, the aircraft was unsuccessful in executing the most aggressive maneuver with an elevator workload dwarfing the other control surfaces' workload. This research formed an initial investigation to measure the workload but another metric based directly on the control signal or measuring the distance from the limits may provide another useful comparison metric. Overall, the small inconsistencies in the workload trend revealed that the autopilot controller played an integral role in the UAV's performance and should be a key criteria in the flying qualities requirements for unmanned systems.

The requirements should be focused on the aircraft's control surface ability to generate the necessary forces and moments to perform the task and the likelihood of hitting position or rate limits. In nearly all cases investigated, a decrease in the pitch or roll damping resulted in improved maneuver performance but came at the cost of the tendency to rate limit. In the coupled maneuver with an increase in static pitch stability, it was seen that the aircraft was unable to successfully perform the most aggressive maneuver. The forces and moments generated by the elevator and throttle were insufficient in overcoming the pitch stability boundaries even with the controls hitting their maximum limit. The pertinent flying qualities requirements should be on the control authority and less on pilot preference. UAVs have the advantage that the aircraft does not need the classical response shape employed in MIL-STD-1797. The natural frequency and damping ratios were designed to meet the expectations of human pilots which are no longer applicable to UAVs. Instead, the requirements should be geared towards task accomplishment and restrictions on the flight control

system. For example, the simulation results in the roll damping case failed to match the trend in the flying qualities analysis. For the decreased roll damping case, the roll performance in the maneuver had improved but the flying qualities analysis characterized it as veering away from Level 1 flying qualities. Sufficient control power and authority should be available without the detrimental effects of saturating rate limits or position limits. The mission task carried out by the UAV will most likely define the elevator and roll control effectiveness. The increased elevator and aileron effectiveness cases were the most effective in accomplishing the flight task while simultaneously decreasing the workload. In addition, the level of flying qualities for the dynamics modes remained relatively constant at a rating of Level 1 flying qualities. It is also reasonable to assume that UAVs do not require the same level of effectiveness as recommended by MIL-STD-1797. This brings about the notion that the flying qualities should be focused on the task and not the aircraft's dynamic modes.

5.2 Future Research Recommendation

In any academic endeavor, the more that was uncovered in the research, the more areas of potential investigation were discovered. The true potential of JSBSim as a flight dynamics model had just been beginning to be understood at a deeper level. While some of the basic aspects of UAVs and its flying qualities have been explored, there is still much yet to be learned.

First, bandwidth was a useful criterion when applied to a classical manned aircraft using the methods of MIL-STD-1797; however, this does not incorporate the automatic control system. Cotting recommended using the bandwidth criterion as the basis for the UAV flying qualities criterion. One problem with bandwidth is that it is not used in the evaluation of the lateral flying qualities in MIL-STD-1797. A method to apply the bandwidth criterion to UAVs as a measure of the system's robustness

could be investigated further. The gain and phase margin associated with bandwidth could be useful as another criteria for flying qualities. Assuming that the flight control laws are sound, ensuring control margins should prevent things like system induced oscillation. The bandwidth is based on the Bode plot of the open-loop system since the pilot's gains were unknown. With an automatic flight control system in a UAV, the controller gains are known. As a result, in place of bandwidth, the gain and phase margin of the closed-loop system can be monitored. Preliminary results have shown a compromise between aircraft performance and control margin. Application of this criteria seems promising to UAVs as a method to evaluate the flying qualities.

Further research could be done in investigating the effects of turbulence and nonlinear dynamics in the simulation. The ability to check an autonomous UAV in an operating environment is crucial in the flying qualities examination of any aircraft. JSBSim has the ability to model wind gusts into the simulation allowing further controller testing. The discrete gust model discussed in MIL-STD-1797A is a built-in feature of JSBSim that can contribute to the analysis of atmospheric disturbances. Additional nonlinear effects such as hysteresis known to contribute to limit cycle oscillations can be investigated as well. JSBSim's capability to model these effects proves JSBSim to be a valuable tool in the assessment of the aircraft's flying qualities. For satisfactory performance of a UAV in real-life situations, the aircraft needs to effectively handle turbulence.

Another concept pertinent to flying qualities requirements is the allowable degradation with failures in the aircraft flight control system. A result of those trends can drive requirements for performance robustness across a variety of degraded states. As stated by Holmberg, "failure states, flight envelopes, gusts, aircraft and ship wakes, stall, departure recovery, and stability and control margins are all in need of research to understand the differences between piloted and unpiloted aircraft safety" [28]. Fail-

ure analysis becomes an integral part to ensure airworthiness allowing safe operation of the aircraft.

While this study investigated only one non-precision, non-aggressive maneuver, real-world UAVs must perform flight tasks requiring higher levels of aggression and/or precision. Some key ingredients to flying qualities testing are aggressive and precision flying. In doing so, the deficiencies are illuminated in either the capability of the aircraft system to accomplish a task or the workload necessary to carry out that task. With a more demanding task or even in the face of turbulence, the flight control system would likely need to input large amplitudes and corrections, illuminating the aircraft's flying qualities. The results presented in this research were for the non-precision, non-aggressive task. The flying qualities requirements are ultimately tied to the task being performed and in order to further understand the flying qualities, simulations of aggressive and precision flying need to be carried out.

5.3 Summary

In conclusion, it has been shown that applying manned flying qualities requirements to autonomous UAVs is not an optimum solution. Previous manned requirements focused on optimizing the aircraft's response to the pilot's inputs. The bulk of MIL-STD-1797A is composed of open-loop requirements due to the problems associated with pilot variability. With UAVs, the use of closed-loop requirements poses less risk. The flying qualities requirements should remain focused on the aircraft performance but also on the control system as well. In parallel, the tolerance of the task should be taken into account. This research has shown that JSBSim is capable of modeling maneuvers and evaluating the flying qualities; however, there remain many improvements that can be applied to increase the level of fidelity in the JSBSim model for UAVs and extend the flying qualities assessment. UAVs have unique

characteristics different from their manned counterparts that should be reflected in the flying qualities standards in order to realize their full potential. The rise of UAVs has begun to reorient the traditional approach to the assessment of flying qualities requiring a paradigm change in evaluation methods applicable to the autonomous control scheme. Future research should be continued in this field to explore applicable methods of flying qualities assessments to UAVs and ultimately create a flying qualities criteria for unmanned systems.

Appendix A Cessna 172 and T-41 Aircraft Data

This appendix contains data from flight manuals and textbooks relevant to model the Cessna 172 and T-41 aircraft. This data was compared to the information in the *XML* file used in JSBSim to model the aircraft.

Table 44. Cessna 172 Geometric Parameters [45]

Variable	Units	Value
Wing Area	ft^2	174
Wingspan	ft	36
Mean Chord	ft	4.9
Weight	lbs	2645
I_{xx}	$slug\ ft^2$	948
I_{yy}	$slug\ ft^2$	1346
I_{zz}	$slug\ ft^2$	1967
I_{xz}	$slug\ ft^2$	0

Table 45. T-41 Performance Specifications [48]

Variable	Unit	Value
Maximum Airspeed (glide, dive, or smooth air)	knots	158
Caution Range	knots	126-158
Normal Operating Range	knots	55-126
Maneuvering Speed	knots	110

Table 46. Cessna 172P Performance Specifications [10]

Variable	Unit	Value
Maximum Speed at Sea Level	knots	123
Maximum Structural Speed	knots	128
Stall Speed (flaps up, power off)	knots	51
Stall Speed (flaps down, power off)	knots	46
Service Ceiling	ft	13,000
Lycoming Engine O-320-D2J	bhp	160
Fuel Capacity (standard tanks)	gal	43

The stability derivatives were pulled from Dr. Jan Roskam's book *Airplane Design, Part VI: Preliminary Calculation of Aerodynamic, Thrust, and Power Characteristics.*

Table 47. Cessna 172 Steady State Coefficients [45]

Variable	Unit	Value
C_{L_1}	-	.31
C_{D_1}	-	.031
$C_{T_{X_1}}$	-	.031
C_{m_1}	-	0
$C_{m_{T_1}}$	-	0

Table 48. Cessna 172 Derivative Data [45]

Longitudinal Derivatives		Lateral Directional Derivatives	
C_{m_u}	0	C_{l_β}	-.089
C_{m_α}	-.89	C_{l_p}	-.47
$C_{m_{\dot{\alpha}}}$	-5.2	C_{l_r}	.096
C_{m_q}	-12.4	$C_{l_{\delta_a}}$	.178
$C_{m_{T_u}}$	0	$C_{l_{\delta_r}}$	.0147
$C_{m_{T_\alpha}}$	0	C_{m_β}	.065
C_{L_u}	0	C_{n_p}	-.03
C_{L_α}	4.6	C_{n_r}	-.099
$C_{L_{\dot{\alpha}}}$	1.7	$C_{n_{\delta_a}}$	-.053
C_{L_q}	3.9	$C_{n_{\delta_r}}$	-.0657
C_{D_α}	.13	C_{y_β}	-.31
C_{D_u}	0	C_{y_p}	-.037
$C_{T_{X_u}}$	-.093	C_{y_r}	.21
$C_{l_{\delta_e}}$	.43	$C_{y_{\delta_a}}$	0
$C_{D_{\delta_e}}$	.06	$C_{y_{\delta_r}}$	.187
$C_{m_{\delta_e}}$	-1.28		

ALT.	RPM	% BHP	TAS MPH	GAL/ HOUR	ENDR. HOURS	RANGE MILES
2500	2600	67	128	10.3	4.5	575
	2500	61	123	9.3	4.9	610
	2400	55	118	8.5	5.4	640
	2300	60	111	7.7	6.0	670
	2200	44	103	6.9	6.6	680
5000	2700	70	133	10.6	4.5	575
	2600	64	128	9.7	4.7	610
	2500	58	123	8.8	5.2	640
	2400	52	116	8.0	5.7	665
	2300	47	108	7.3	6.9	685
	2200	41	96	6.6	7.0	675
7500	2800	72	138	11.0	4.2	580
	2700	66	133	10.0	4.6	610
	2600	60	128	9.2	5.0	640
	2500	54	121	8.4	5.5	670
	2400	49	113	7.6	6.1	685
	2300	44	102	5.9	6.7	680
10000	2800	68	138	10.4	4.4	615
	2700	62	133	9.5	4.8	640
	2600	57	126	8.7	5.3	670
	2500	51	118	7.8	6.3	690
	2400	46	107	7.2	6.4	690
	2300	41	90	6.5	7.1	635

Figure 95. T-41C Cruise and Range Performance [48]

Appendix B T-41 Linearization Trim Analysis

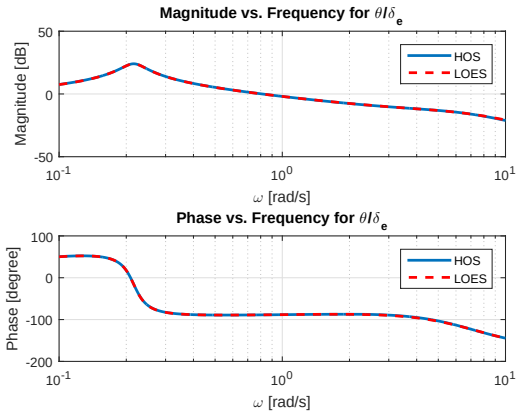

Figure 96. Bode Plot for θ/δ_e at 8000 ft

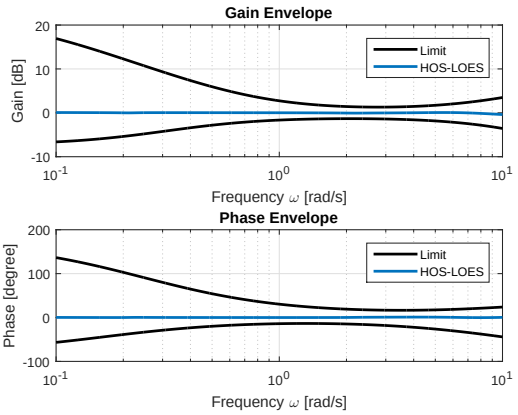

Figure 97. Envelope θ/δ_e at 8000 ft

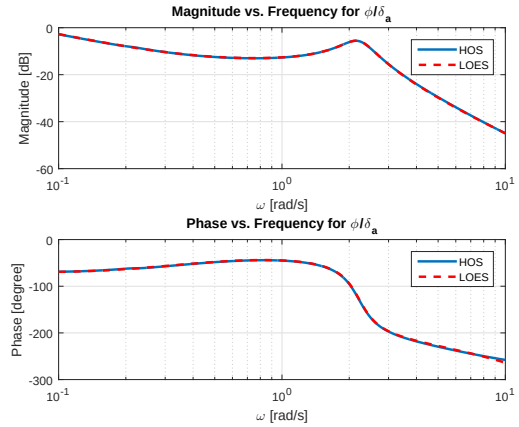

Figure 98. Bode Plot for ϕ/δ_a at 8000 ft

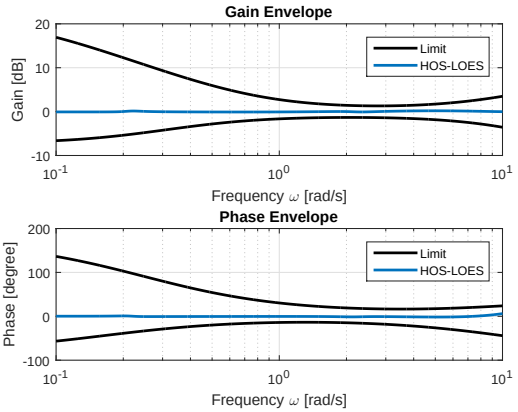

Figure 99. Envelope ϕ/δ_a at 8000 ft

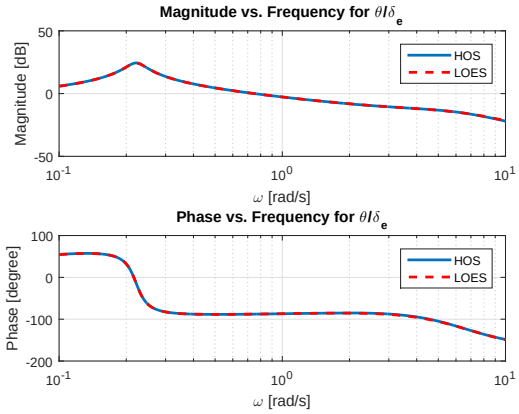

Figure 100. Bode Plot for θ/δ_e at 12000 ft

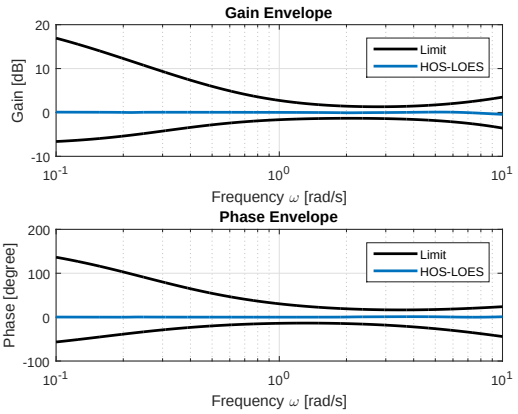

Figure 101. Envelope θ/δ_e at 12000 ft

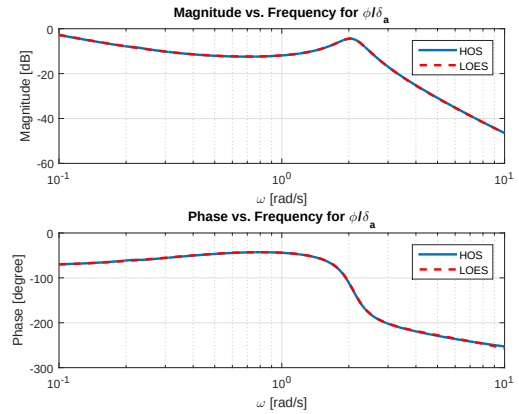

Figure 102. Bode Plot for ϕ/δ_a at 12000 ft

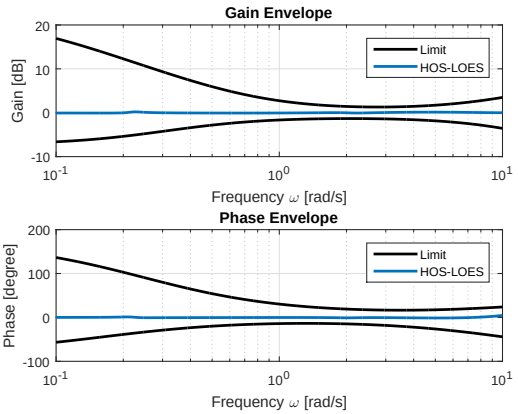

Figure 103. Envelope ϕ/δ_a at 12000 ft

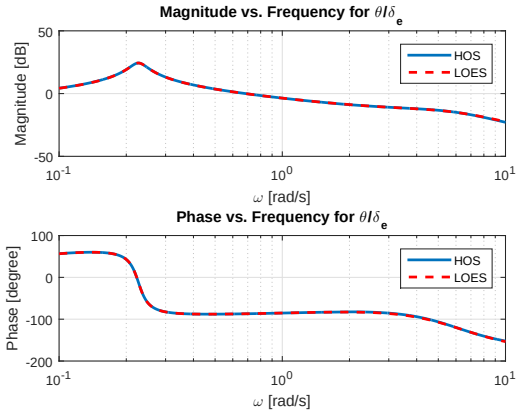

Figure 104. Bode Plot for θ/δ_e at 16000 ft

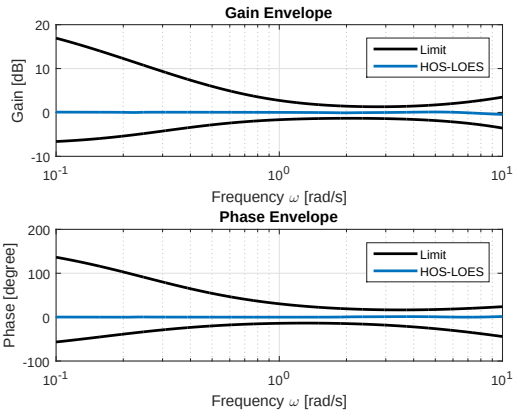

Figure 105. Envelope θ/δ_e at 16000 ft

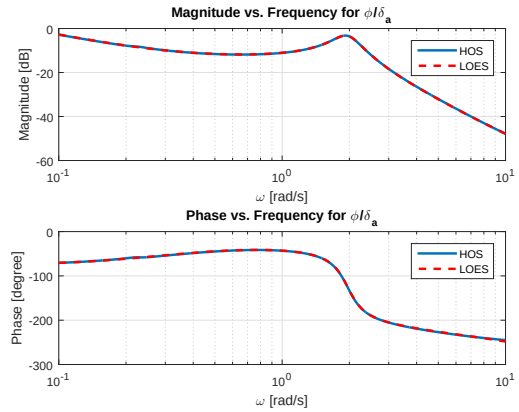

Figure 106. Bode Plot for ϕ/δ_a at 16000 ft

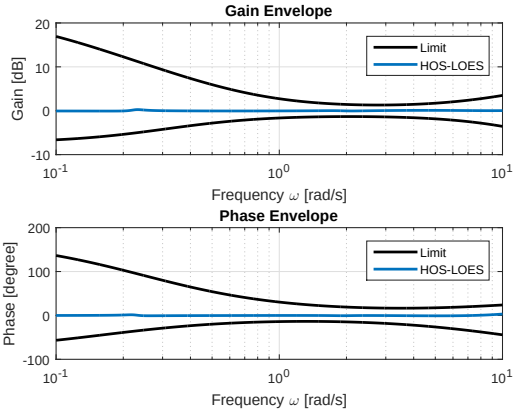

Figure 107. Envelope ϕ/δ_a at 16000 ft

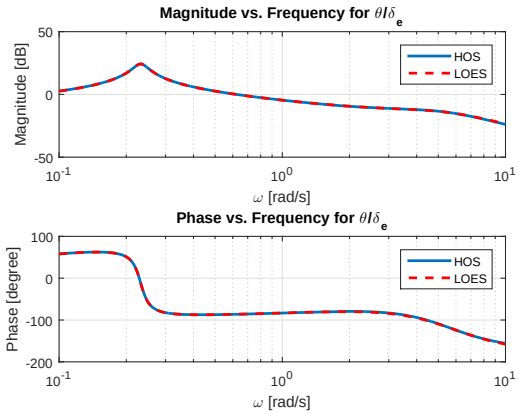

Figure 108. Bode Plot for θ/δ_e at 20000 ft

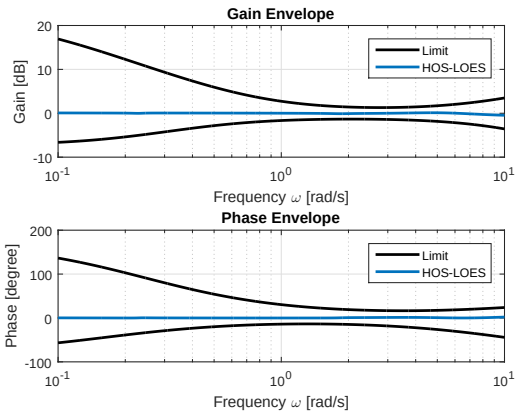

Figure 109. Envelope θ/δ_e at 20000 ft

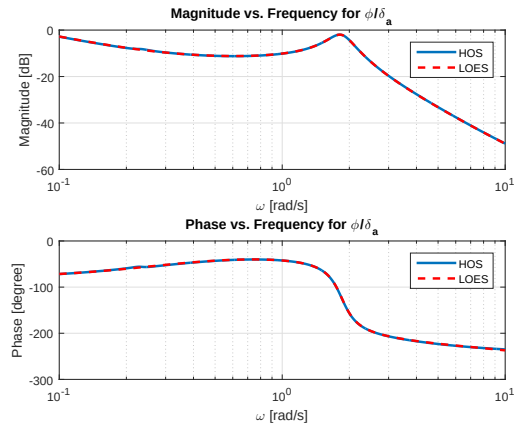

Figure 110. Bode Plot for ϕ/δ_a at 20000 ft

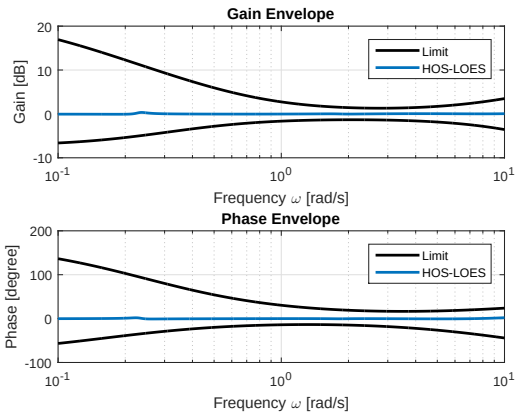

Figure 111. Envelope ϕ/δ_a at 20000 ft

Appendix C Variation of Longitudinal Derivative in Longitudinal Maneuver Data

Table 49. Longitudinal Change: C_{m_q} x $\frac{1}{10}$

Climb	TIC ($\dot{h}$)	TIC (v_t)	$\mathcal{L}_2$ (δ_t)	$\mathcal{L}_2$ (δ_e)
4 ft/s	0.025759	0.0021654	0.0427	0.0051
6 ft/s	0.026411	0.0032898	0.0648	0.0075
8 ft/s	0.026867	0.0044525	0.0877	0.0099

Table 50. Longitudinal Change: C_{m_q} x 10

Climb	TIC ($\dot{h}$)	TIC (v_t)	$\mathcal{L}_2$ (δ_t)	$\mathcal{L}_2$ (δ_e)
4 ft/s	0.042651	0.0021875	0.0428	0.0105
6 ft/s	0.043126	0.0033236	0.0650	0.0158
8 ft/s	0.043279	0.0044972	0.0879	0.0211

Table 51. Longitudinal Change: C_{m_α} x $\frac{1}{10}$

Climb	TIC ($\dot{h}$)	TIC (v_t)	$\mathcal{L}_2$ (δ_t)	$\mathcal{L}_2$ (δ_e)
4 ft/s	0.026006	0.0021597	0.0427	0.0053
6 ft/s	0.026708	0.0032955	0.0651	0.0078
8 ft/s	0.027211	0.0044636	0.0881	0.0104

Table 52. Longitudinal Change: C_{m_α} x 10

Climb	TIC ($\dot{h}$)	TIC (v_t)	$\mathcal{L}_2$ (δ_t)	$\mathcal{L}_2$ (δ_e)
4 ft/s	0.045924	0.002409	0.0477	0.0344
6 ft/s	0.046237	0.0037089	0.0735	0.0528
8 ft/s	0.046458	0.005156	0.1018	0.0715

Table 53. Longitudinal Change: $C_{m_{\delta_e}}$ x 3

Climb	TIC ($\dot{h}$)	TIC (v_t)	$\mathcal{L}_2$ (δ_t)	$\mathcal{L}_2$ (δ_e)
4 ft/s	0.022144	0.0022198	0.0439	0.0066
6 ft/s	0.022824	0.0033123	0.0654	0.0097
8 ft/s	0.023375	0.0044737	0.0883	0.0136

Table 54. Longitudinal Change: $C_{m_{\delta_e}}$ x $\frac{3}{4}$

Climb	TIC ($\dot{h}$)	TIC (v_t)	$\mathcal{L}_2$ (δ_t)	$\mathcal{L}_2$ (δ_e)
4 ft/s	0.029834	0.0021473	0.0423	0.0055
6 ft/s	0.030452	0.0032897	0.0647	0.0082
8 ft/s	0.030928	0.00446	0.0877	0.0109

Appendix D Variation of Lateral Derivative in Lateral Maneuver Data

Table 55. Lateral-Directional Change: C_{l_p} x $\frac{1}{10}$

Bank	TIC (v_t)	TIC (ϕ)	$\mathcal{L}_2$ (δ_a)	$\mathcal{L}_2$ (δ_r)
10°	0.00014092	0.021697	0.0084	0.0254
20°	0.00027977	0.022958	0.0161	0.0484
30°	0.000431	0.023736	0.0255	0.0679

Table 56. Lateral-Directional Change: C_{l_p} x 10

Bank	TIC (v_t)	TIC (ϕ)	$\mathcal{L}_2$ (δ_a)	$\mathcal{L}_2$ (δ_r)
10°	0.0001059	0.043959	0.0349	0.0260
20°	0.0002115	0.044875	0.0700	0.0496
30°	0.00033712	0.046292	0.1049	0.0698

Table 57. Lateral-Directional Change: $C_{l_{\delta_a}}$ x 3

Bank	TIC (v_t)	TIC (ϕ)	$\mathcal{L}_2$ (δ_a)	$\mathcal{L}_2$ (δ_r)
10°	0.00013295	0.020033	0.0049	0.0252
20°	0.0002635	0.020757	0.0096	0.0480
30°	0.00040328	0.021307	0.0140	0.0672

Table 58. Lateral-Directional Change: $C_{l_{\delta_a}}$ x $\frac{3}{4}$

Bank	TIC (v_t)	TIC (ϕ)	$\mathcal{L}_2$ (δ_a)	$\mathcal{L}_2$ (δ_r)
10°	0.00010076	0.025561	0.0112	0.0257
20°	0.00020015	0.026849	0.0216	0.0488
30°	0.00031273	0.027937	0.0318	0.0685

Appendix E Variation of Single Derivative in Coupled Maneuver Plots

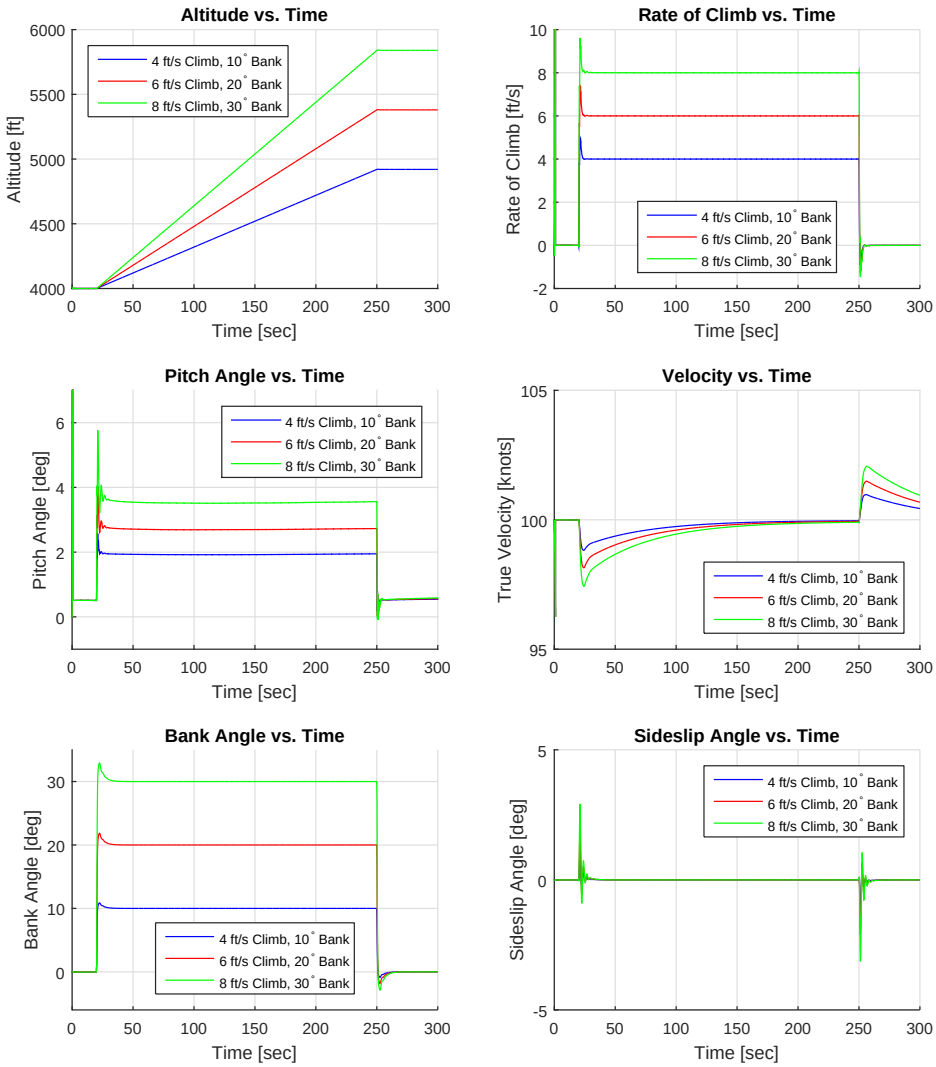

Figure 112. Coupled Maneuver: C_{m_q} x $\frac{1}{10}$ Performance Plots

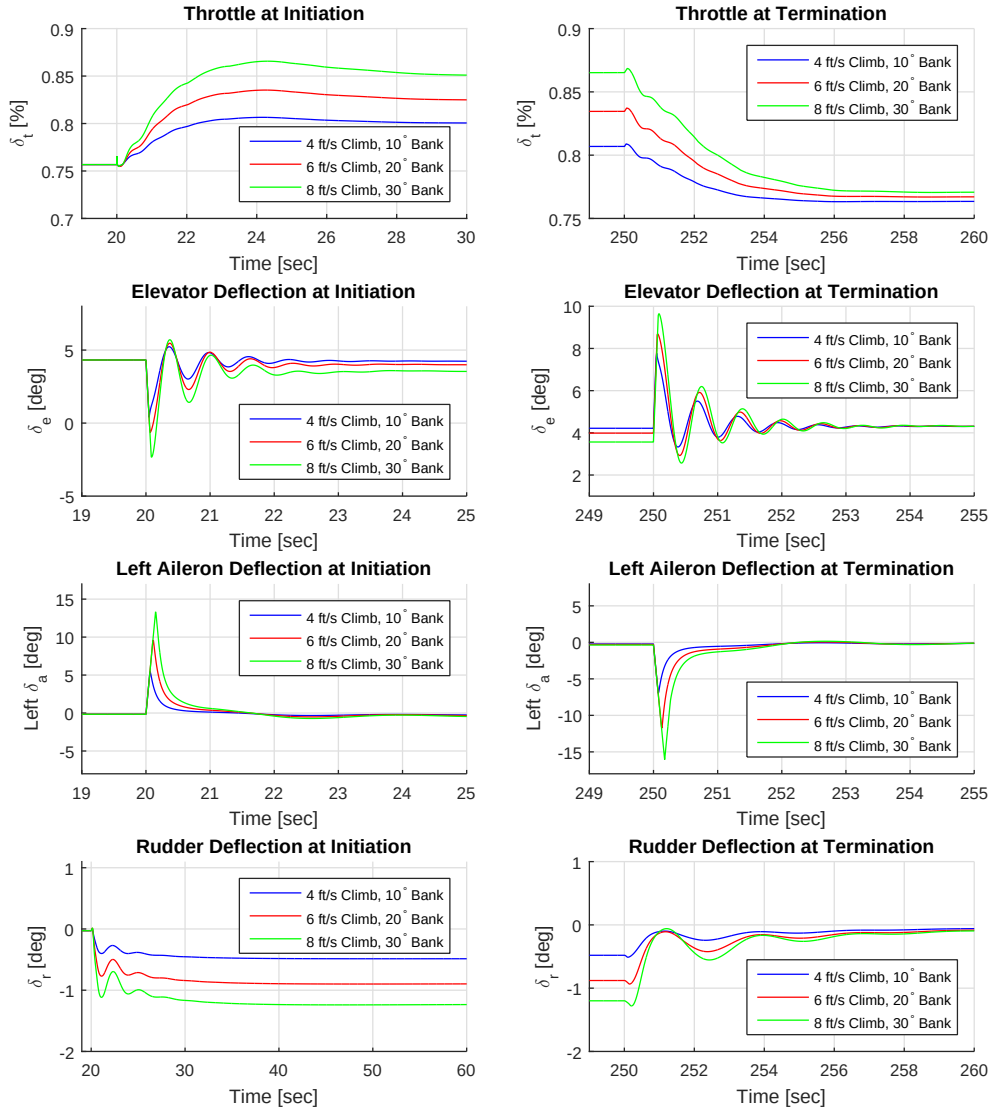

Figure 113. Coupled Maneuver: C_{m_q} x $\frac{1}{10}$ Control Plots

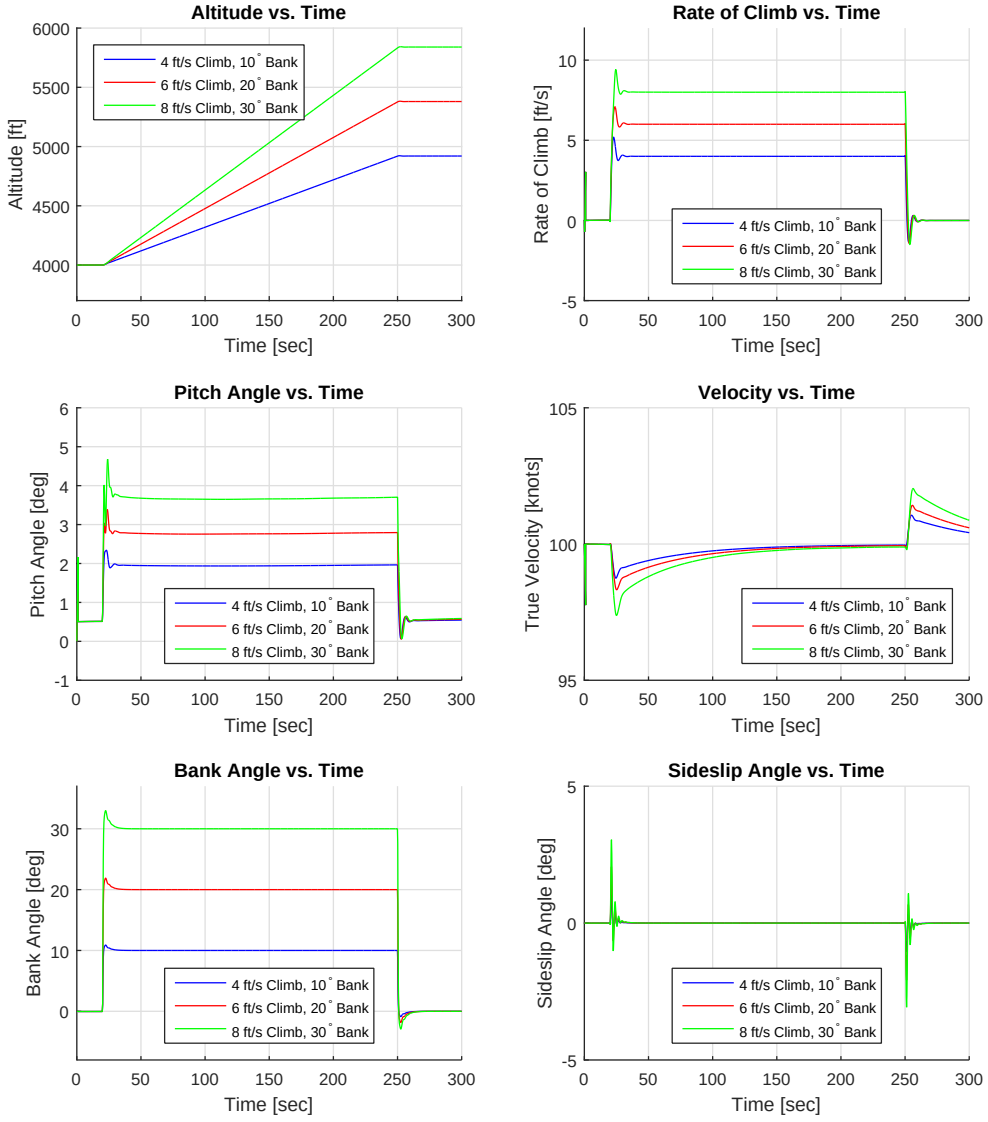

Figure 114. Coupled Maneuver: C_{m_q} x 10 Performance Plots

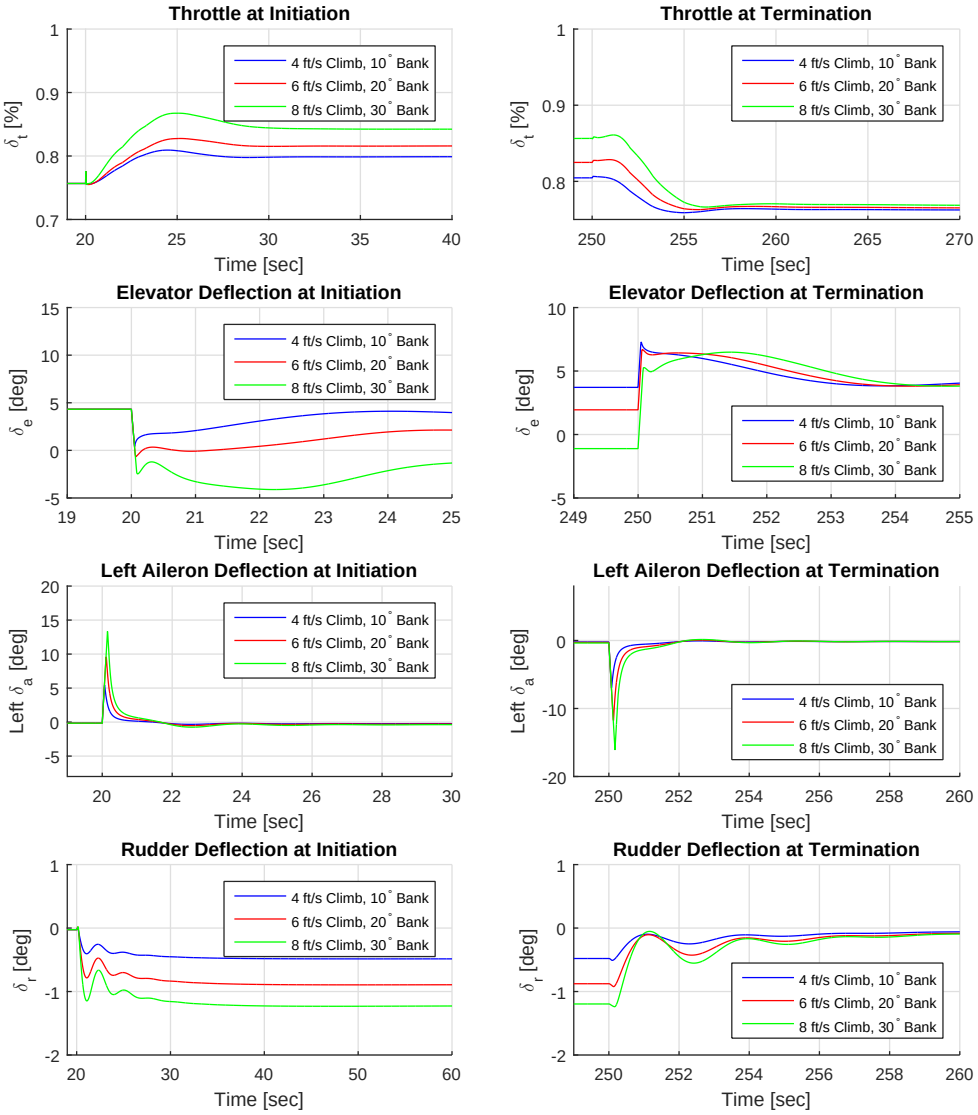

Figure 115. Coupled Maneuver: C_{m_q} x 10 Control Plots

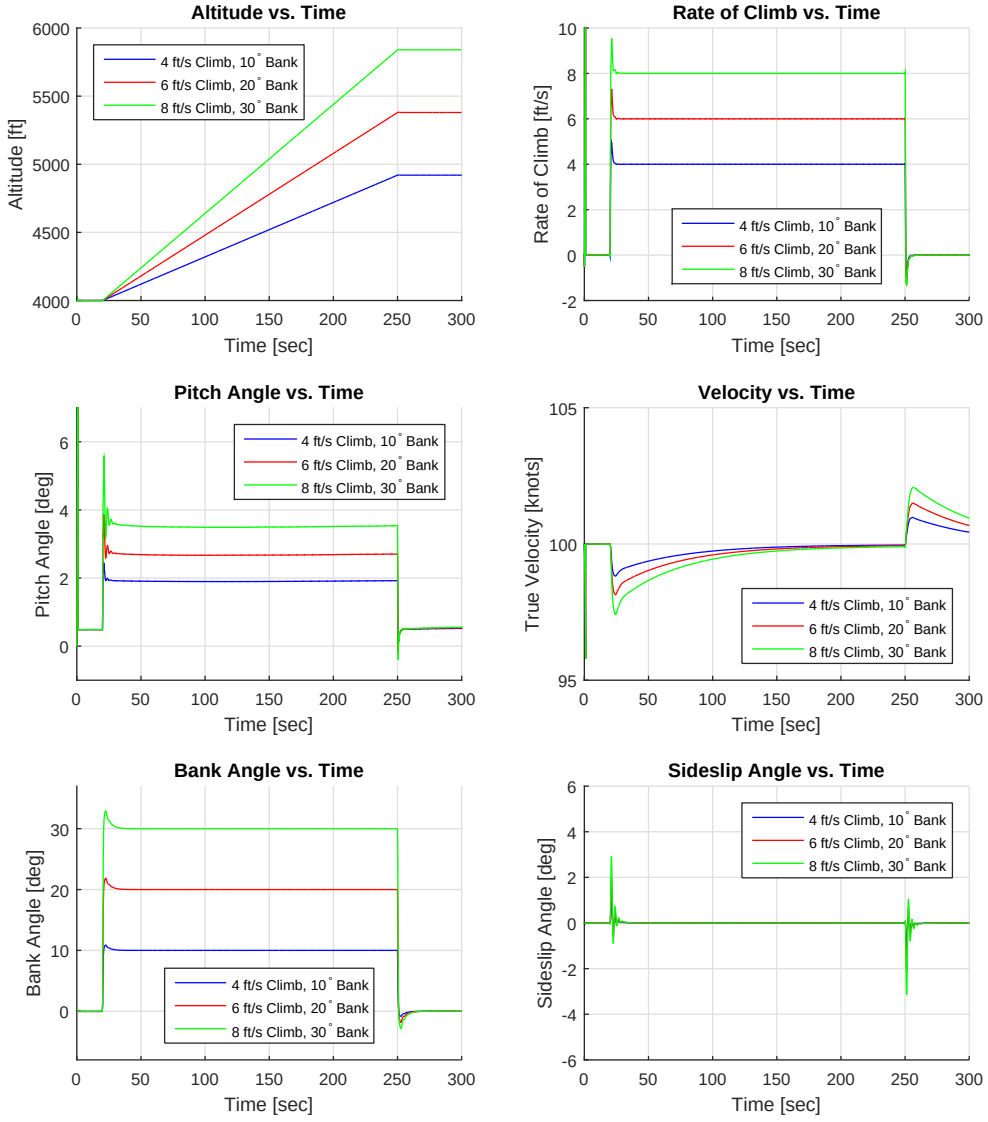

Figure 116. Coupled Maneuver: C_{m_α} x $\frac{1}{10}$ Performance Plots

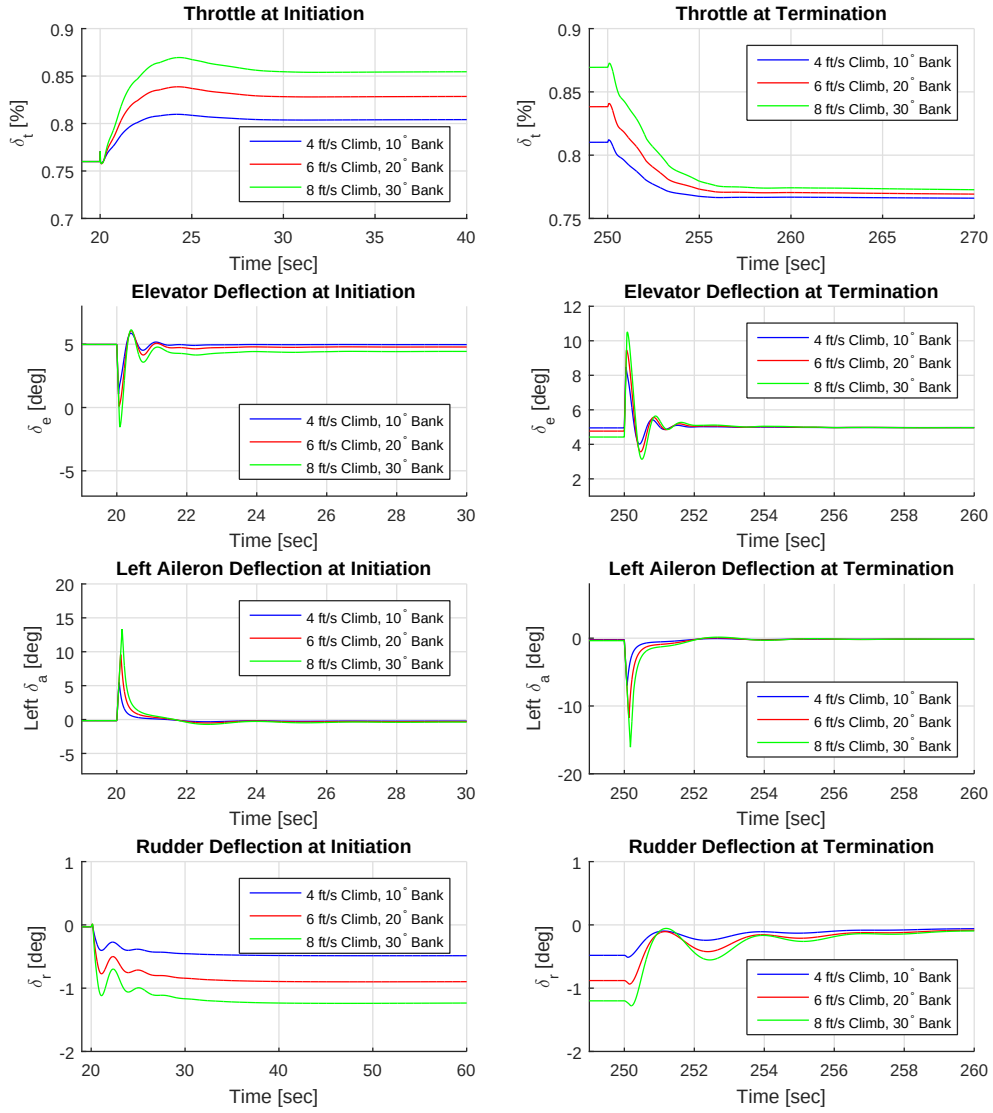

Figure 117. Coupled Maneuver: C_{m_α} x $\frac{1}{10}$ Control Plots

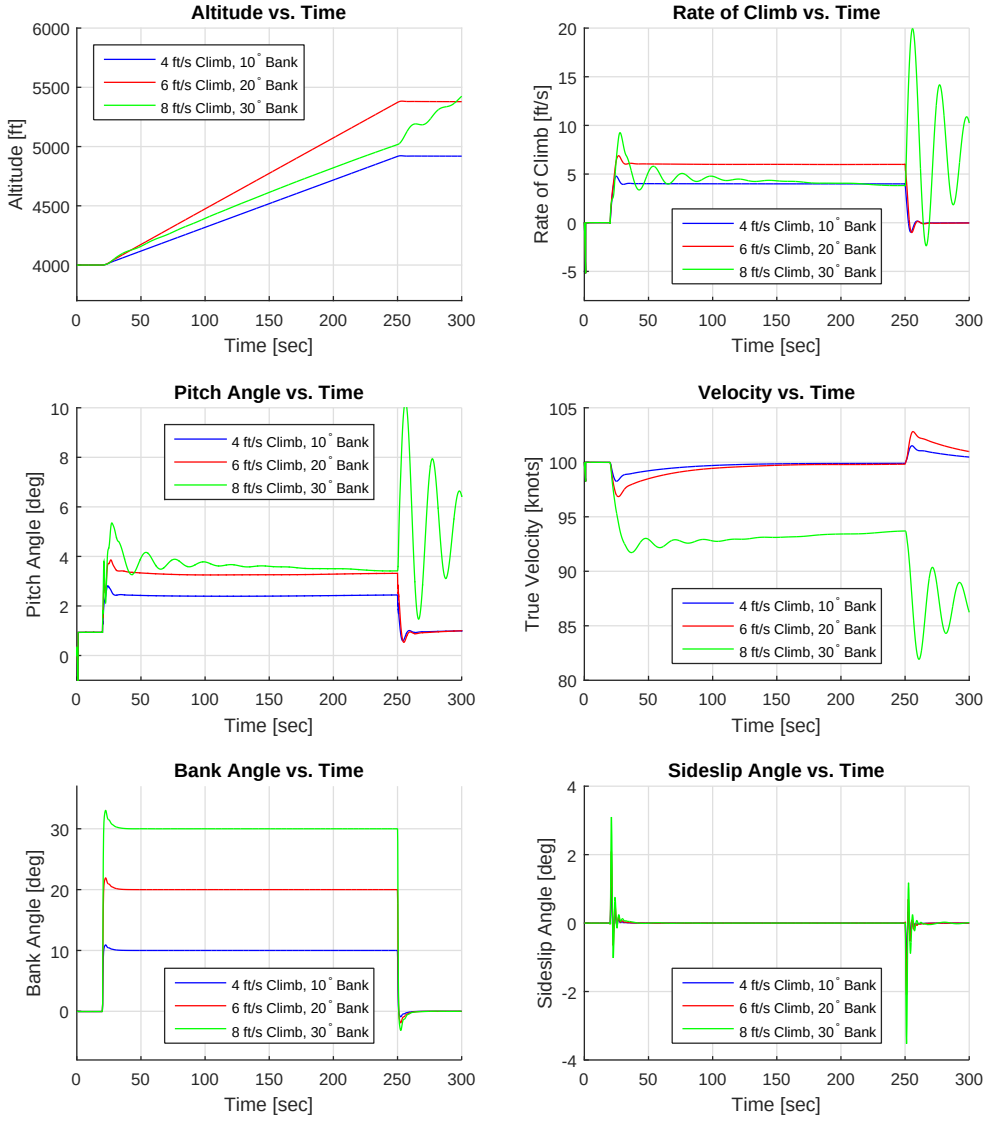

Figure 118. Coupled Maneuver: C_{m_α} x 10 Performance Plots

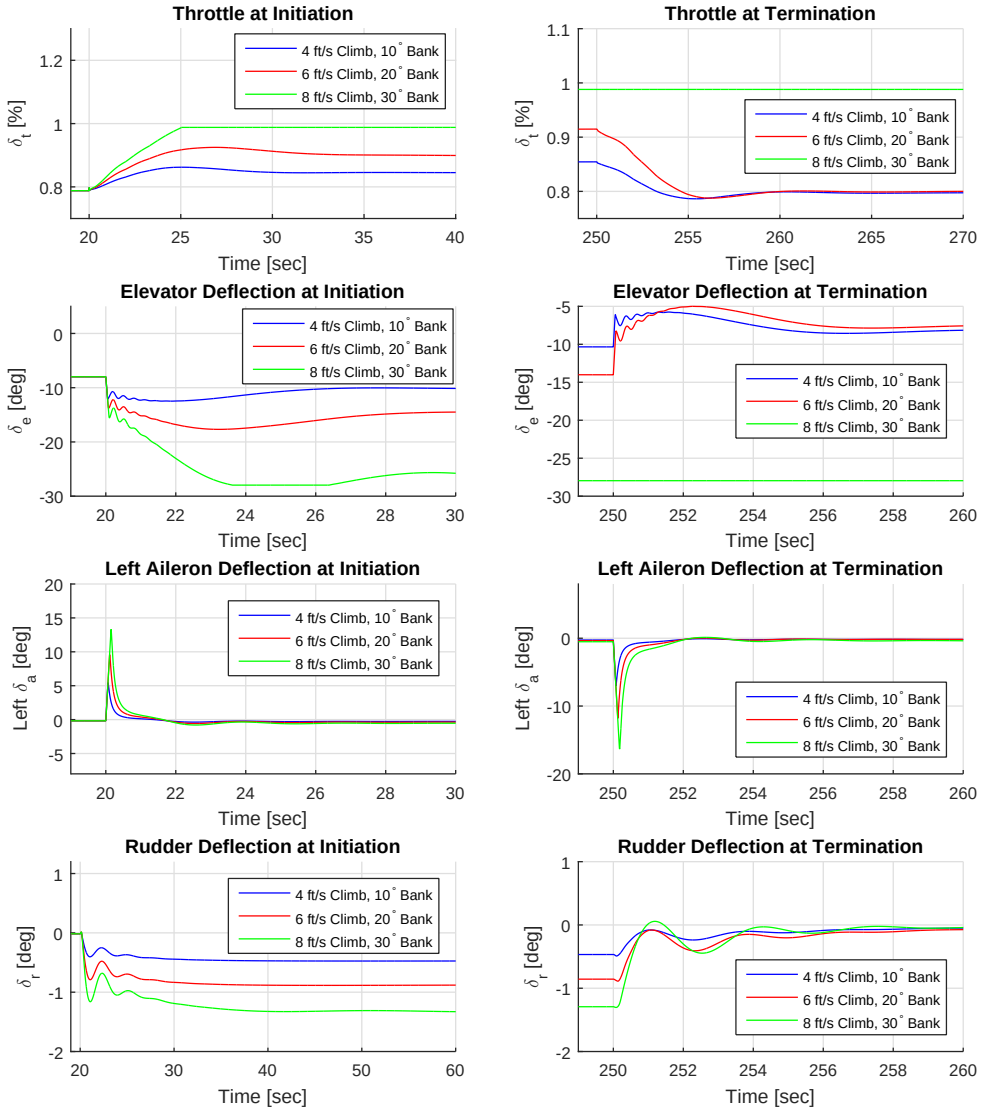

Figure 119. Coupled Maneuver: C_{m_α} x 10 Control Plots

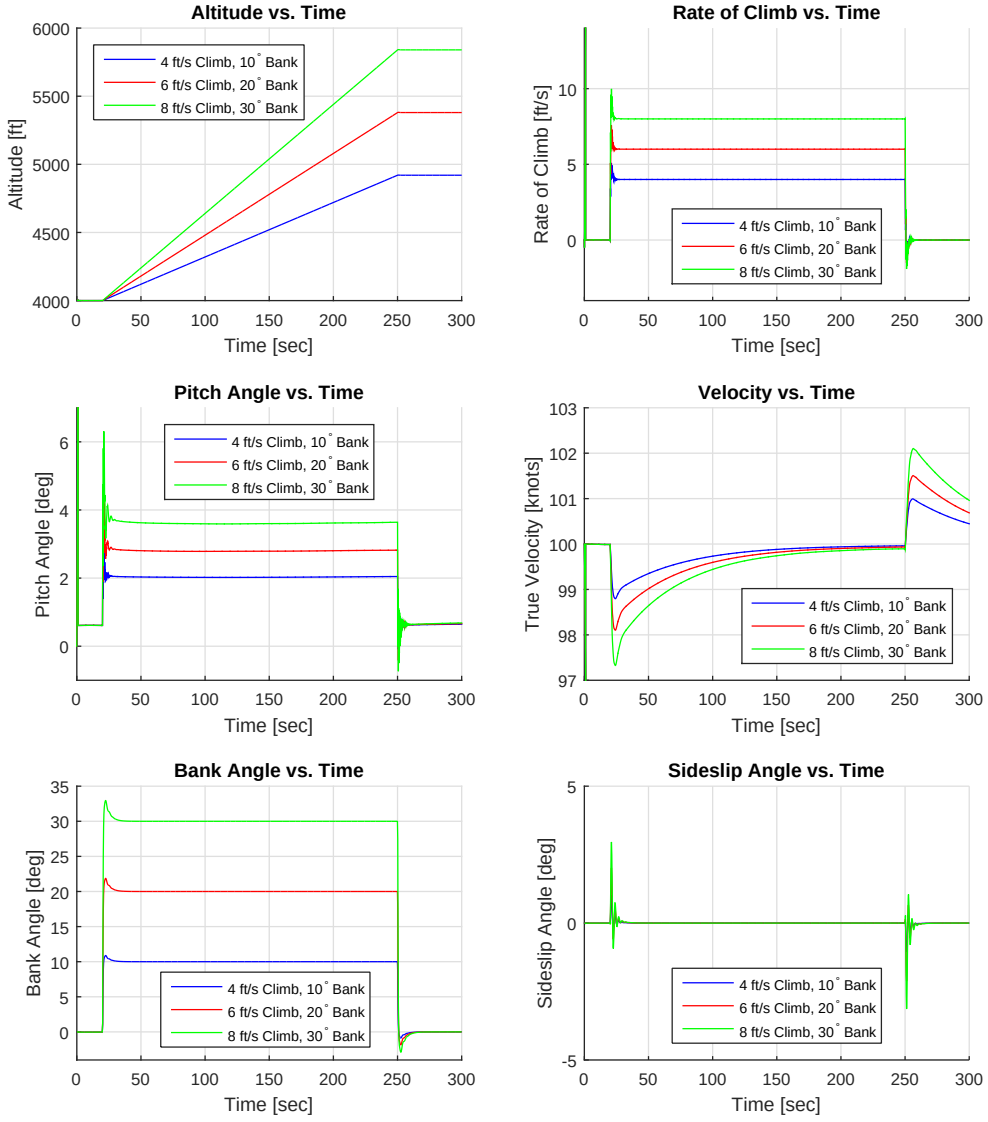

Figure 120. Coupled Maneuver: $C_{m_{\delta_e}}$ x 3 Performance Plots

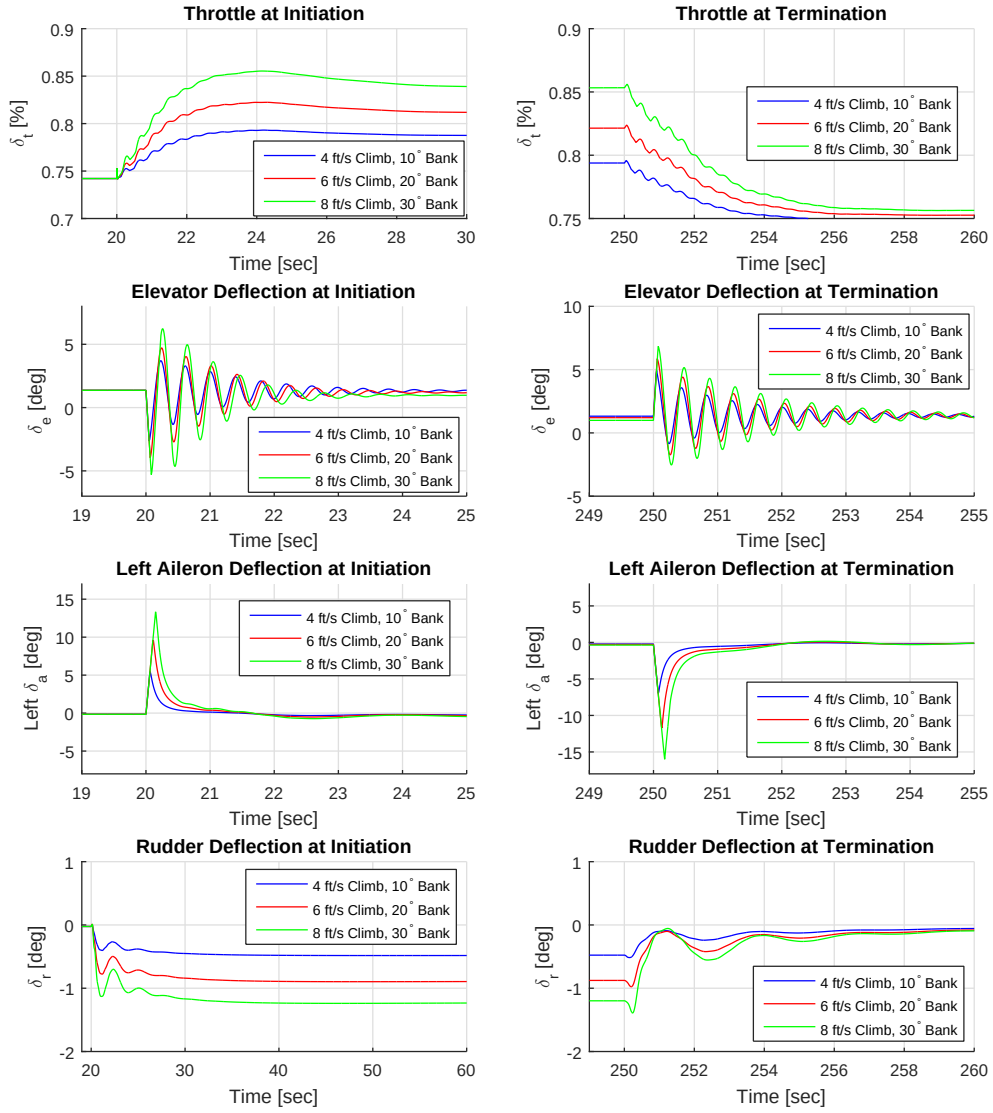

Figure 121. Coupled Maneuver: $C_{m_{\delta_e}}$ x 3 Control Plots

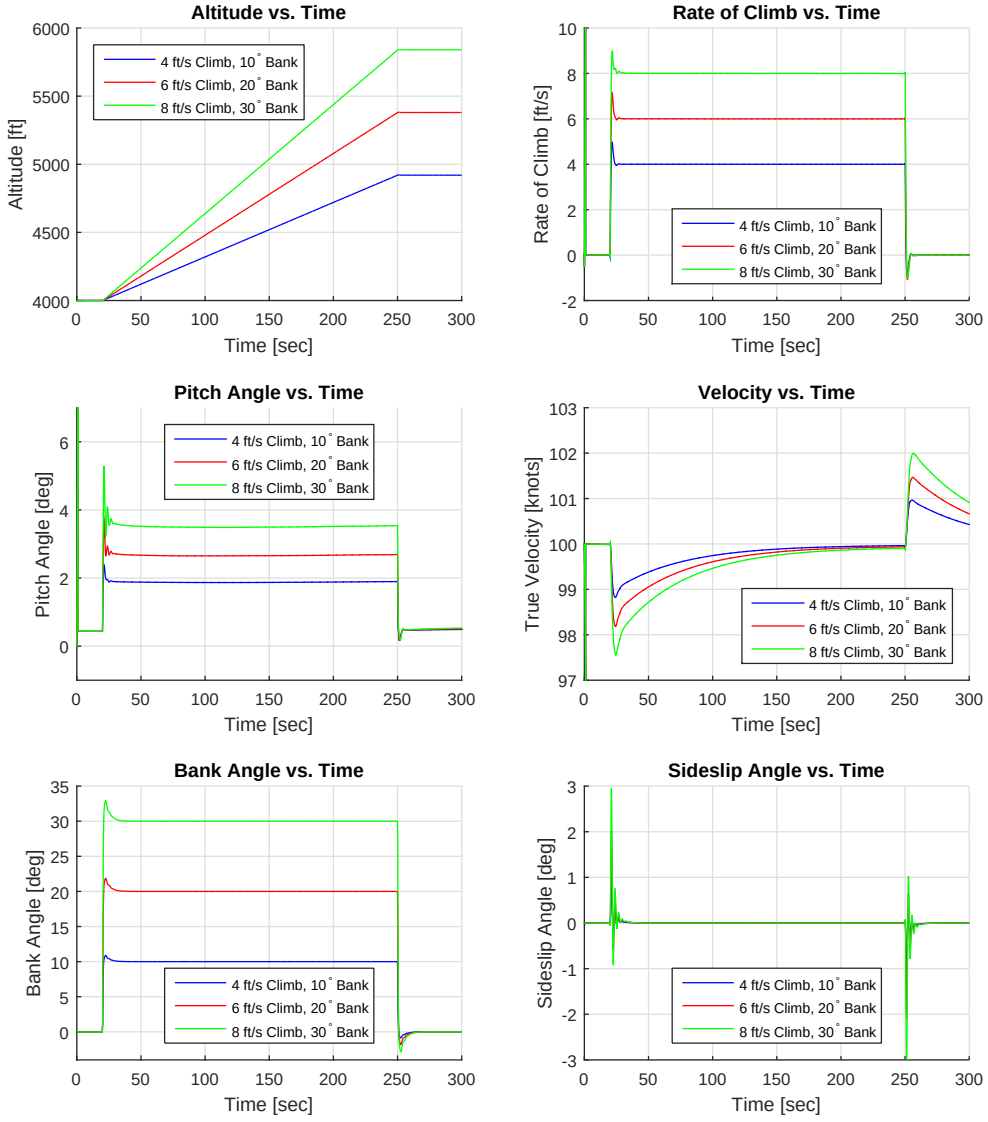

Figure 122. Coupled Maneuver: $C_{m_{\delta_e}}$ x $\frac{3}{4}$ Performance Plots

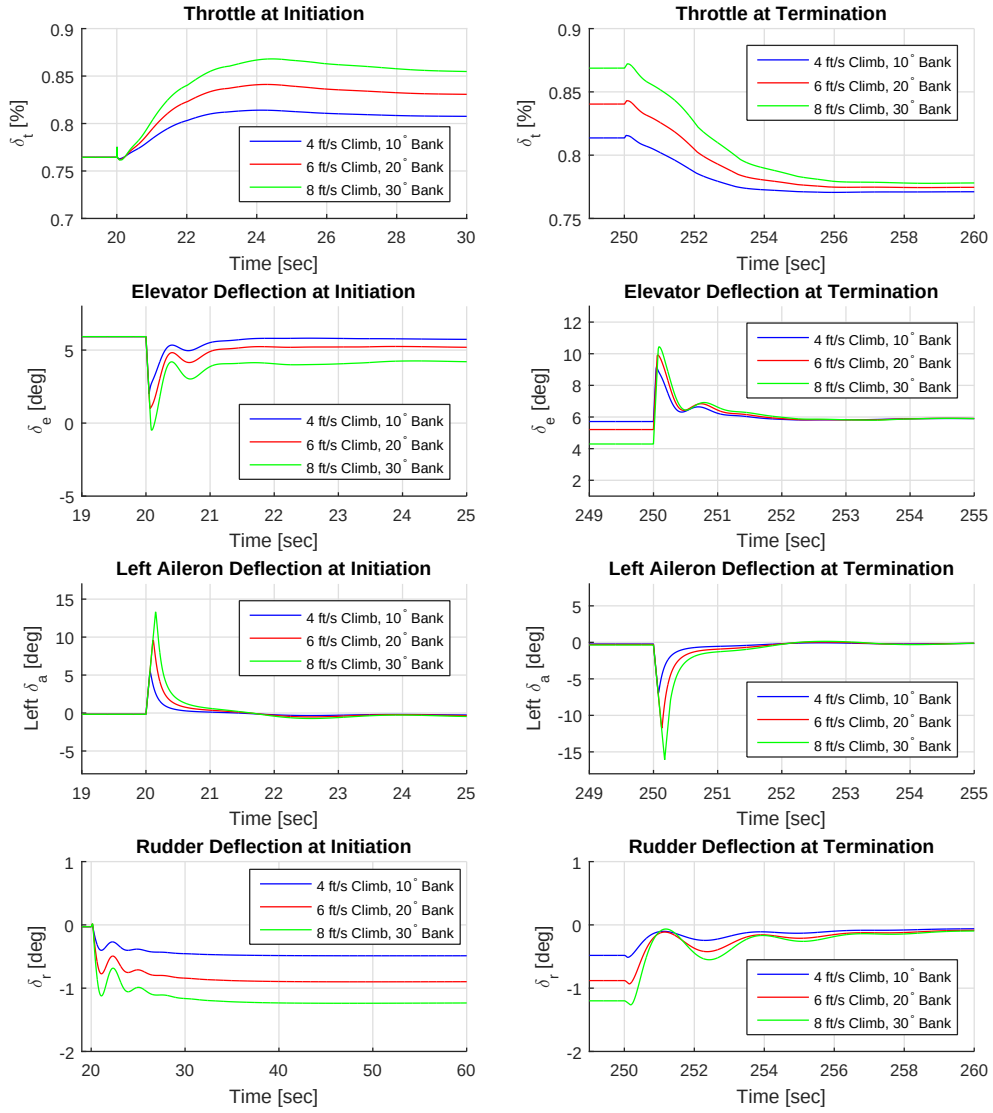

Figure 123. Coupled Maneuver: $C_{m_{\delta_e}}$ x $\frac{3}{4}$ Control Plots

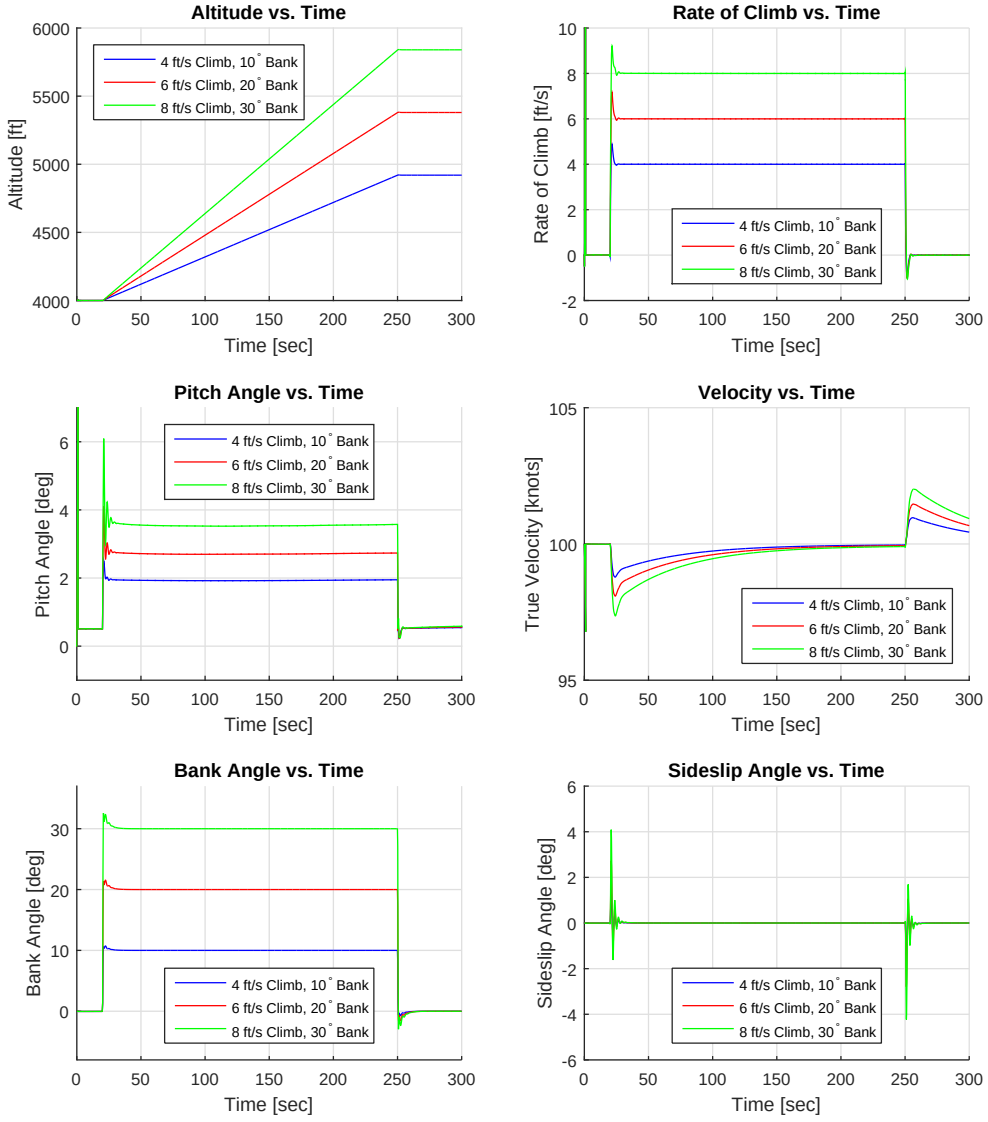

Figure 124. Coupled Maneuver: C_{l_p} x $\frac{1}{10}$ Performance Plots

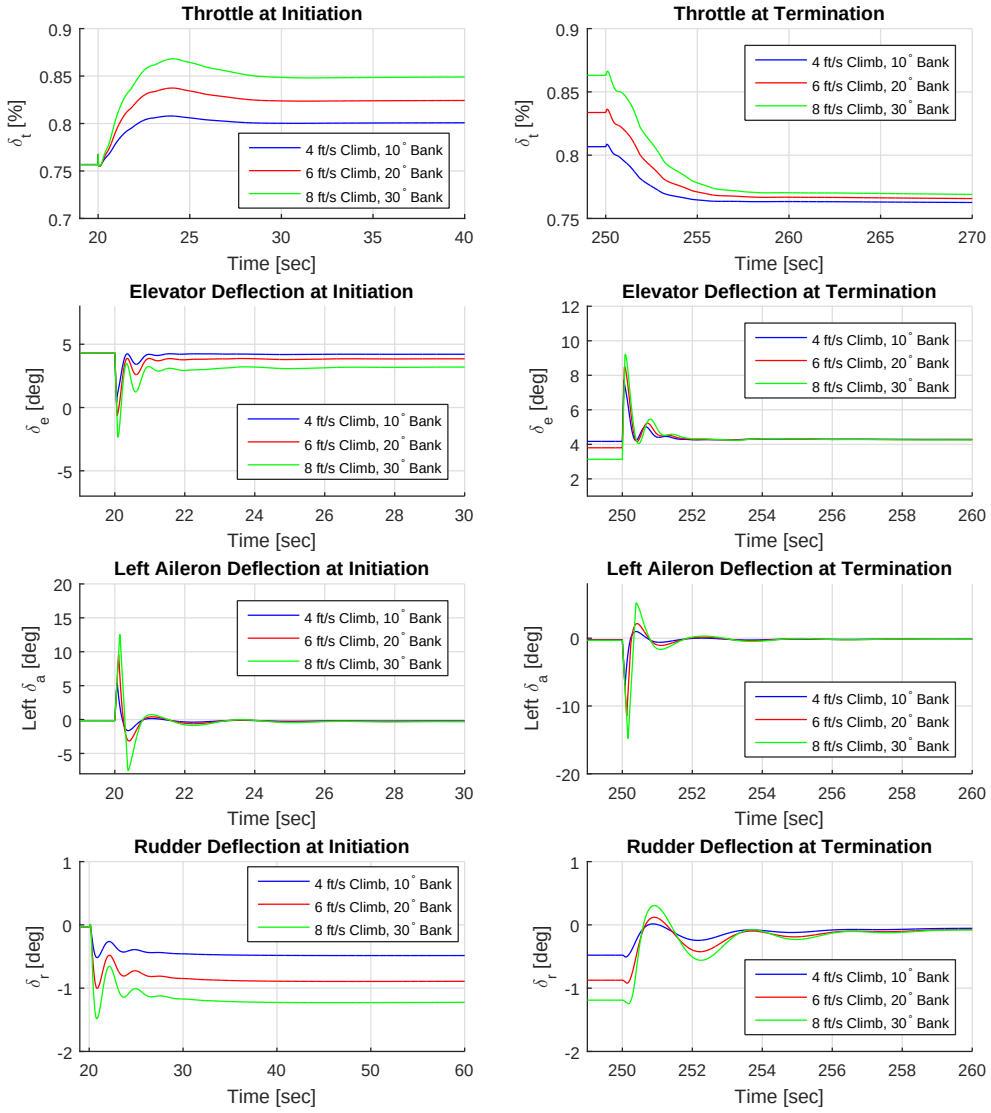

Figure 125. Coupled Maneuver: C_{l_p} x $\frac{1}{10}$ Control Plots

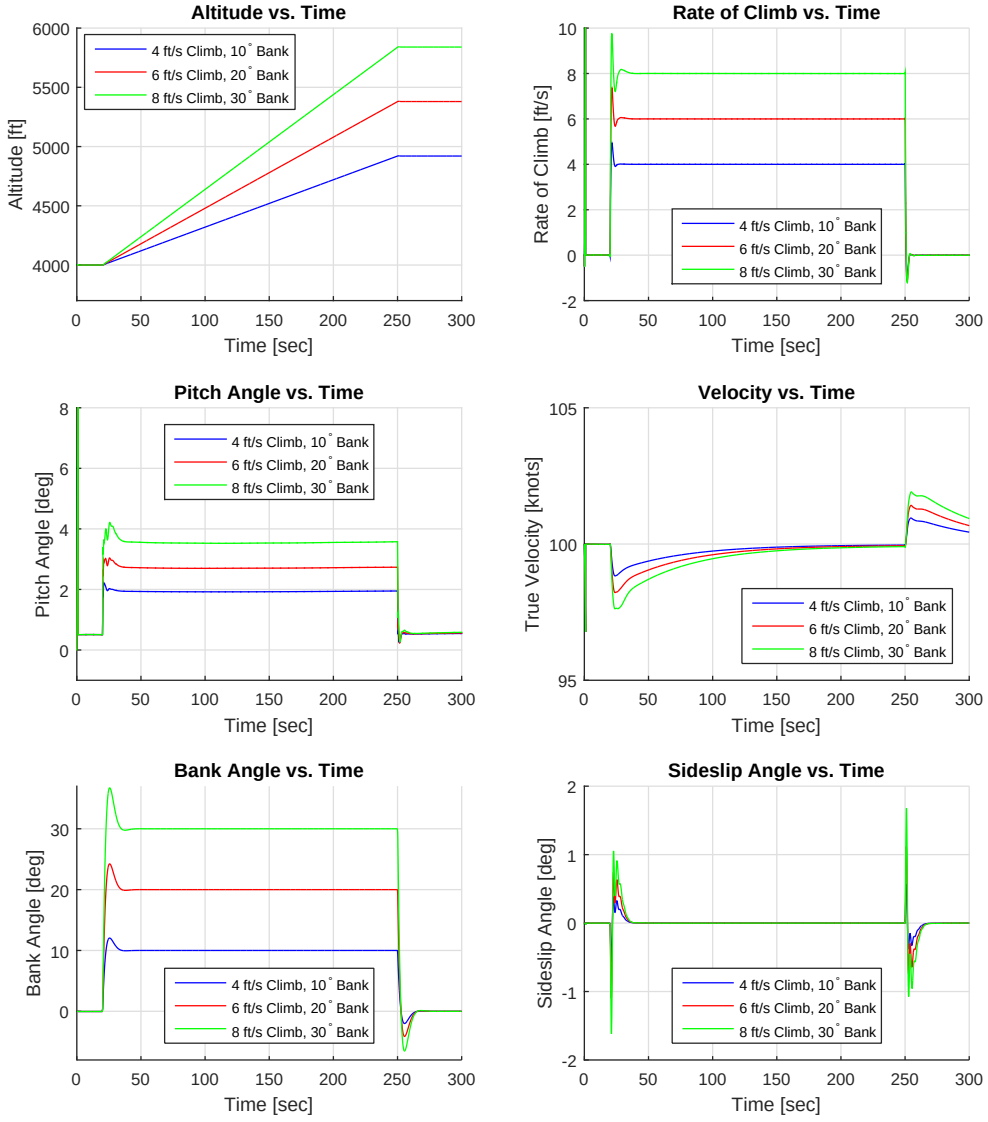

Figure 126. Coupled Maneuver: C_{l_p} x 10 Performance Plots

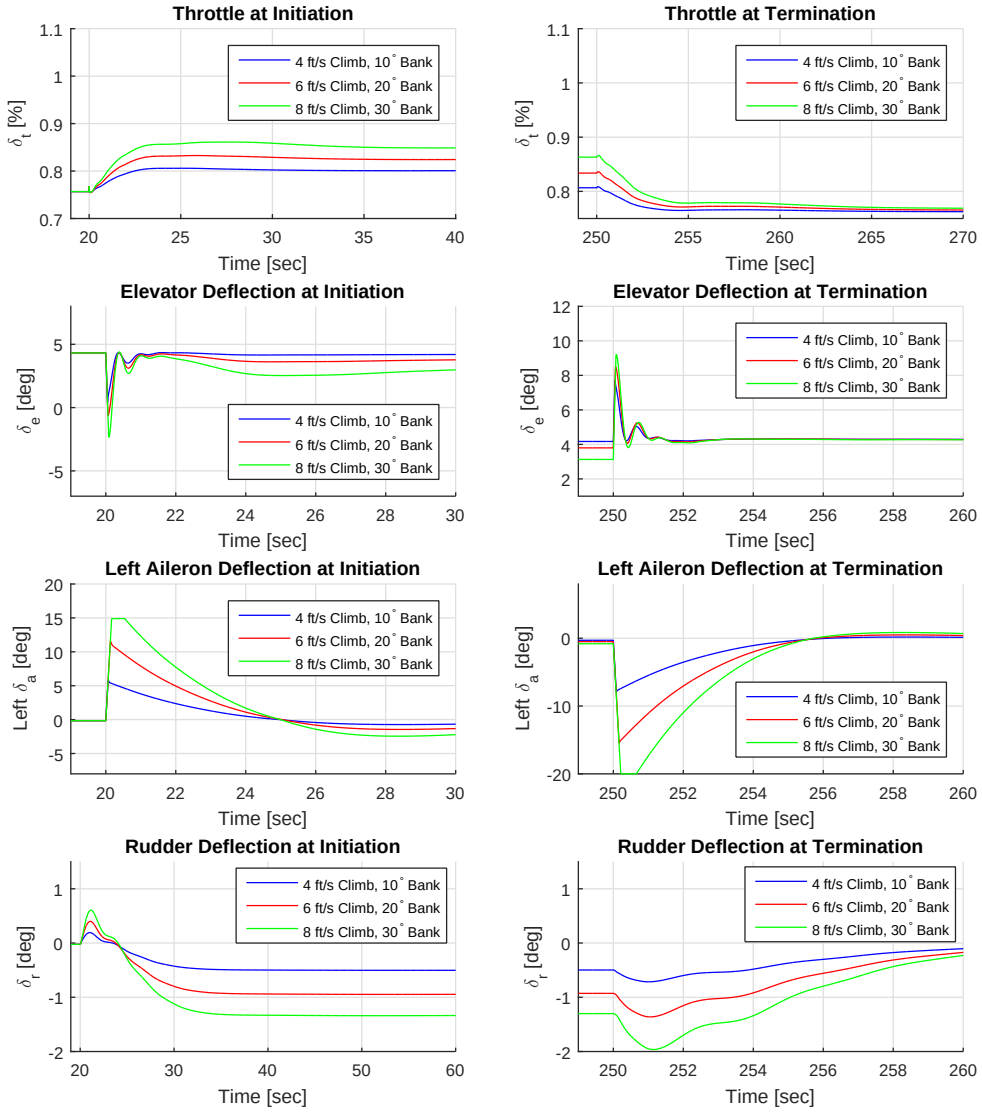

Figure 127. Coupled Maneuver: C_{l_p} x 10 Control Plots

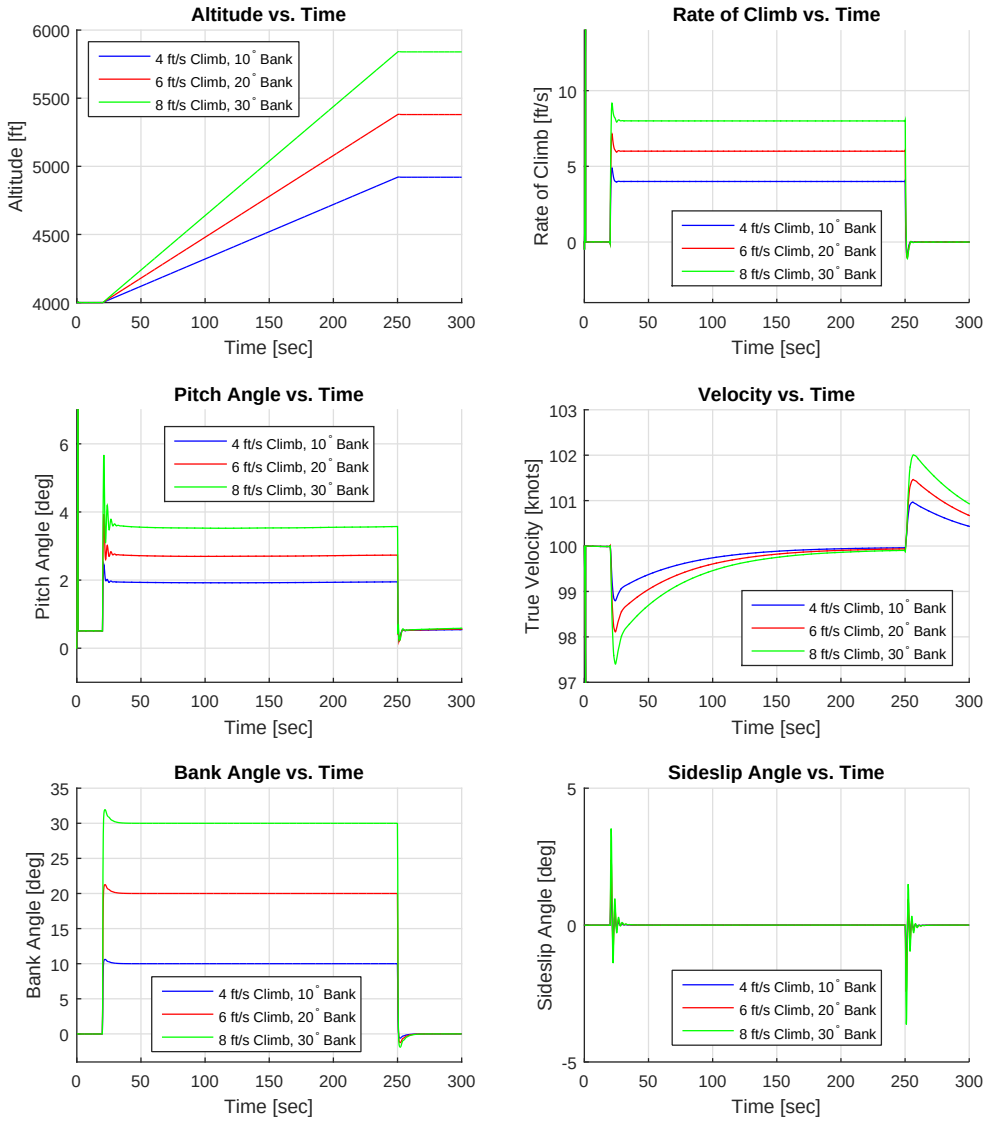

Figure 128. Coupled Maneuver: $C_{l_{\delta_a}}$ x 3 Performance Plots

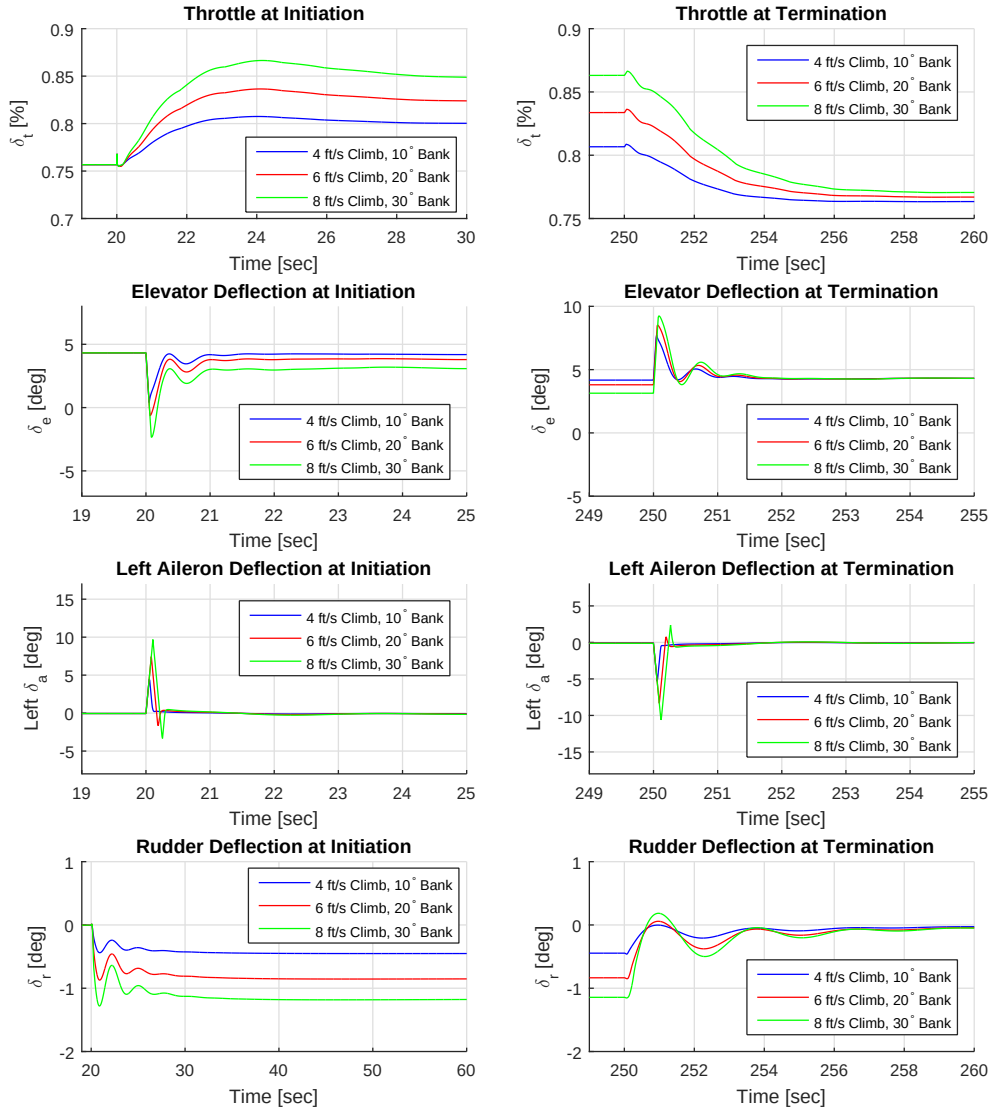

Figure 129. Coupled Maneuver: $C_{l_{\delta_a}}$ x 3 Control Plots

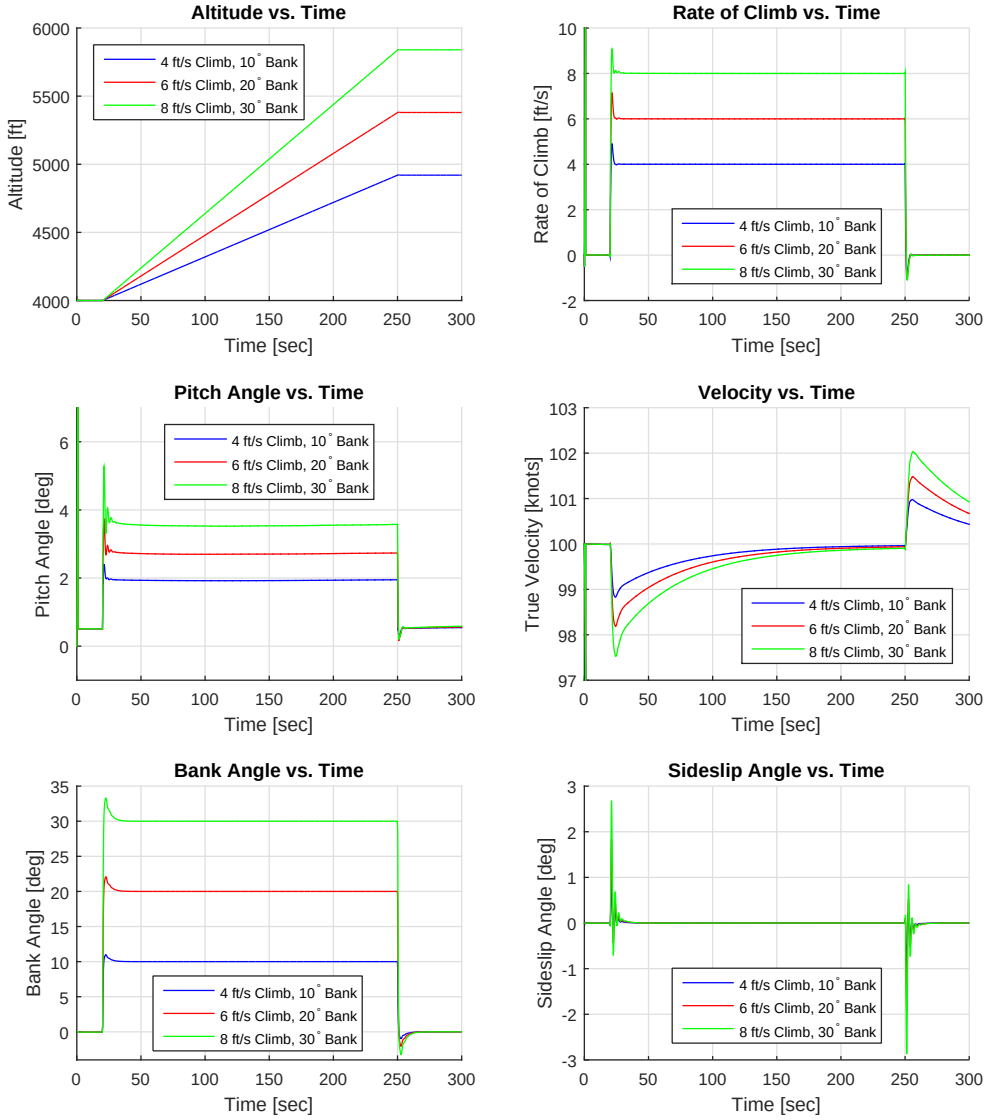

Figure 130. Coupled Maneuver: $C_{l_{\delta_a}}$ x $\frac{3}{4}$ Performance Plots

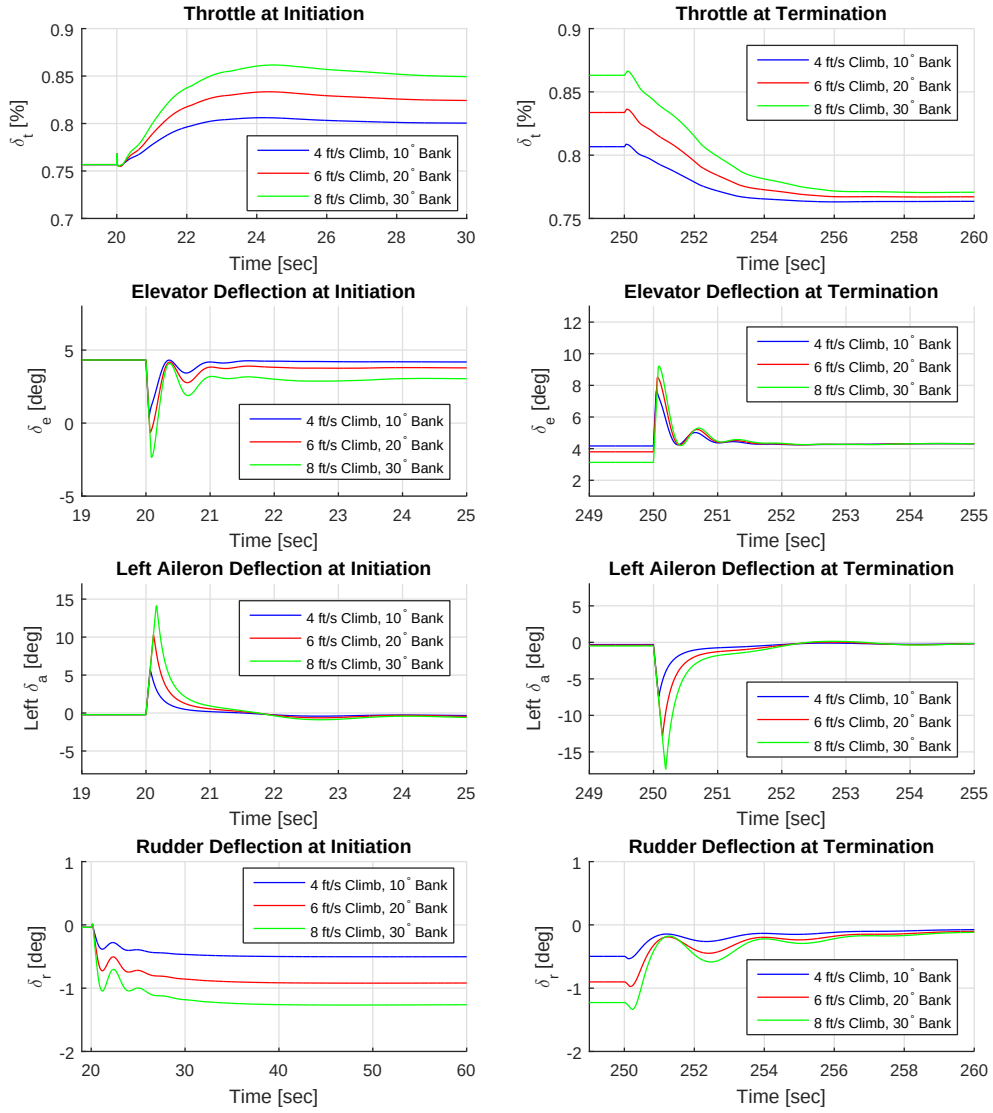

Figure 131. Coupled Maneuver: $C_{l_{\delta_a}}$ x $\frac{3}{4}$ Control Plots

Table 59. Coupled Maneuver: C_{m_q} x $\frac{1}{10}$

Climb	Bank	TIC ($\dot{h}$)	TIC (v_t)	TIC (ϕ)	$\mathcal{L}_2$ (δ_t)	$\mathcal{L}_2$ (δ_e)	$\mathcal{L}_2$ (δ_a)	$\mathcal{L}_2$ (δ_r)
4 ft/s	10°	.025426	.0021808	.024085	.0431	.0056	.0097	.0255
6 ft/s	20°	.02574	.0033751	.025374	.0667	.0131	.0187	.0483
8 ft/s	30°	.025893	.004673	.026409	.0924	.0280	.0276	.0668

Table 60. Coupled Maneuver: C_{m_q} x 10

Climb	Bank	TIC ($\dot{h}$)	TIC (v_t)	TIC (ϕ)	$\mathcal{L}_2$ (δ_t)	$\mathcal{L}_2$ (δ_e)	$\mathcal{L}_2$ (δ_a)	$\mathcal{L}_2$ (δ_r)
4 ft/s	10°	.040484	.0020905	.024095	.0412	.0247	.0097	.0256
6 ft/s	20°	.040801	.0029315	.025386	.0581	.0934	.0187	.0483
8 ft/s	30°	.044883	.0042682	.026436	.0840	.2062	.0277	.0666

Table 61. Coupled Maneuver: C_{m_α} x $\frac{1}{10}$

Climb	Bank	TIC ($\dot{h}$)	TIC (v_t)	TIC (ϕ)	$\mathcal{L}_2$ (δ_t)	$\mathcal{L}_2$ (δ_e)	$\mathcal{L}_2$ (δ_a)	$\mathcal{L}_2$ (δ_r)
4 ft/s	10°	.025686	.0021755	.024085	.0431	.0046	.0097	.0255
6 ft/s	20°	.02604	.0033826	.025373	.0670	.0103	.0187	.0482
8 ft/s	30°	.026244	.0046935	.026408	.0929	.0229	.0276	.0667

Table 62. Coupled Maneuver: C_{m_α} x 10

Climb	Bank	TIC ($\dot{h}$)	TIC (v_t)	TIC (ϕ)	$\mathcal{L}_2$ (δ_t)	$\mathcal{L}_2$ (δ_e)	$\mathcal{L}_2$ (δ_a)	$\mathcal{L}_2$ (δ_r)
4 ft/s	10°	.046012	.00278	.024159	.0546	.0634	.0100	.0255
6 ft/s	20°	.051736	.0054388	.025452	.1048	.1798	.0195	.0479
8 ft/s	30°	.41167	.042101	.026731	.1988	.7097	.0315	.0725

Table 63. Coupled Maneuver: C_{l_p} x $\frac{1}{10}$

Climb	Bank	TIC ($\dot{h}$)	TIC (v_t)	TIC (ϕ)	$\mathcal{L}_2$ (δ_t)	$\mathcal{L}_2$ (δ_e)	$\mathcal{L}_2$ (δ_a)	$\mathcal{L}_2$ (δ_r)
4 ft/s	10°	.026964	.0021732	.021765	.0430	.0064	.0088	.0254
6 ft/s	20°	.027173	.0033381	.023057	.0660	.0196	.0167	.0480
8 ft/s	30°	.027459	.0045822	.023864	.0906	.0445	.0265	.0662

Table 64. Coupled Maneuver: C_{l_p} x 10

Climb	Bank	TIC ($\dot{h}$)	TIC (v_t)	TIC (ϕ)	$\mathcal{L}_2$ (δ_t)	$\mathcal{L}_2$ (δ_e)	$\mathcal{L}_2$ (δ_a)	$\mathcal{L}_2$ (δ_r)
4 ft/s	10°	.027065	.0021721	.044098	.0431	.0064	.0355	.0268
6 ft/s	20°	.027257	.0033326	.045062	.0661	.0197	.0717	.0515
8 ft/s	30°	.027549	.0045735	.046627	.0907	.0449	.1090	.0730

Table 65. Coupled Maneuver: $C_{m_{\delta_e}}$ x 3

Climb	Bank	TIC ($\dot{h}$)	TIC (v_t)	TIC (ϕ)	$\mathcal{L}_2$ (δ_t)	$\mathcal{L}_2$ (δ_e)	$\mathcal{L}_2$ (δ_a)	$\mathcal{L}_2$ (δ_r)
4 ft/s	10°	.021972	.0022457	.024085	.0445	.0066	.0097	.0256
6 ft/s	20°	.022431	.0034356	.025373	.0680	.0107	.0187	.0484
8 ft/s	30°	.022723	.0047863	.026404	.0945	.0181	.0277	.0670

Table 66. Coupled Maneuver: $C_{m_{\delta_e}}$ x $\frac{3}{4}$

Climb	Bank	TIC ($\dot{h}$)	TIC (v_t)	TIC (ϕ)	$\mathcal{L}_2$ (δ_t)	$\mathcal{L}_2$ (δ_e)	$\mathcal{L}_2$ (δ_a)	$\mathcal{L}_2$ (δ_r)
4 ft/s	10°	0.029075	0.0021422	0.024087	0.0423	0.0081	0.0097	0.0256
6 ft/s	20°	0.028951	0.0032893	0.025377	0.0650	0.0264	0.0187	0.0483
8 ft/s	30°	0.029038	0.00448	0.026414	0.0887	0.0606	0.0276	0.0667

Table 67. Coupled Maneuver: $C_{l_{\delta_a}}$ x 3

Climb	Bank	TIC ($\dot{h}$)	TIC (v_t)	TIC (ϕ)	$\mathcal{L}_2$ (δ_t)	$\mathcal{L}_2$ (δ_e)	$\mathcal{L}_2$ (δ_a)	$\mathcal{L}_2$ (δ_r)
4 ft/s	10°	.026986	.0021735	.020061	.0430	.0064	.0050	.0250
6 ft/s	20°	.027252	.0033372	.020819	.0660	.0196	.0097	.0473
8 ft/s	30°	.027557	.0045795	.021361	.0906	.0444	.0145	.0651

Table 68. Coupled Maneuver: $C_{l_{\delta_a}}$ x $\frac{3}{4}$

Climb	Bank	TIC ($\dot{h}$)	TIC (v_t)	TIC (ϕ)	$\mathcal{L}_2$ (δ_t)	$\mathcal{L}_2$ (δ_e)	$\mathcal{L}_2$ (δ_a)	$\mathcal{L}_2$ (δ_r)
4 ft/s	10°	.026906	.0021723	.025633	.0430	.0064	.0117	.0259
6 ft/s	20°	.02693	.0033337	.026938	.0659	.0196	.0227	.0489
8 ft/s	30°	.026907	.0045732	.028049	.0905	.0446	.0337	.0677

Appendix F Variation of Coupled Derivatives in Coupled Maneuver Plots

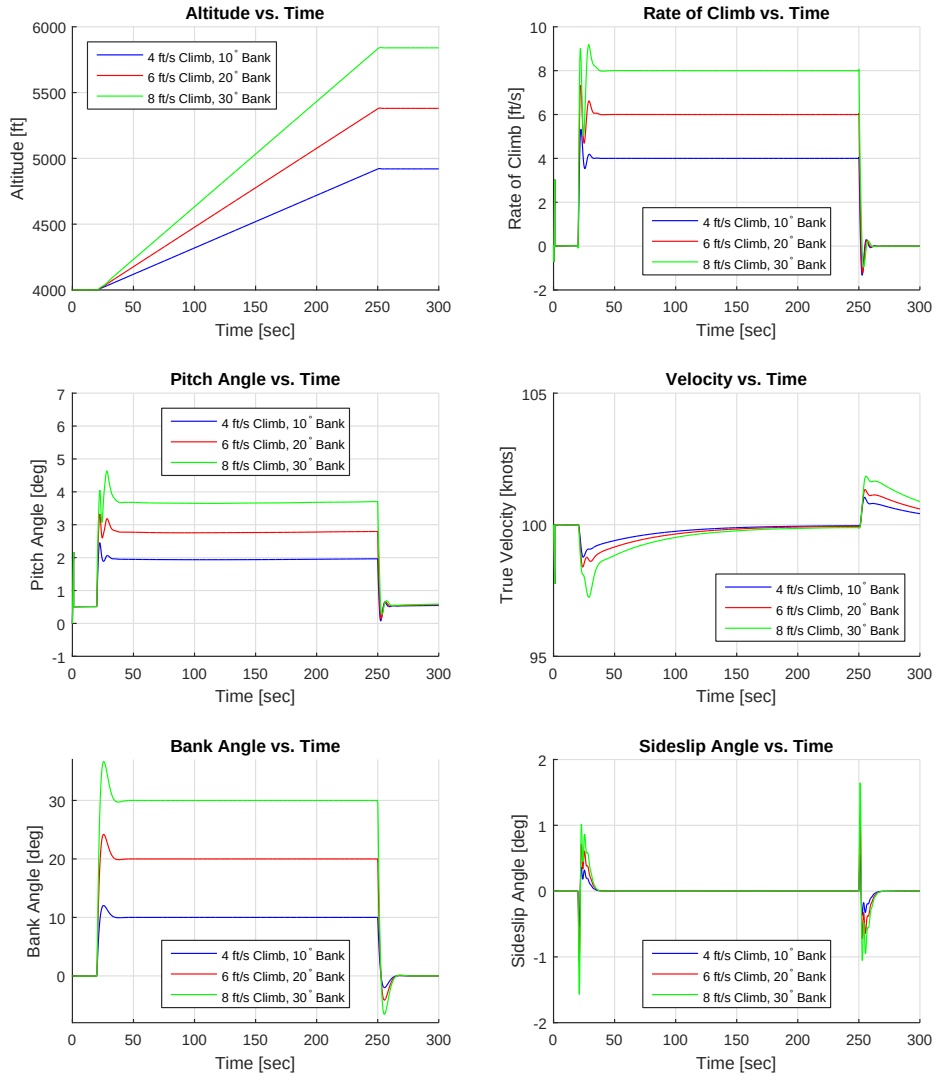

Figure 132. Coupled Maneuver: C_{m_q} and C_{l_p} x 10 Performance Plots

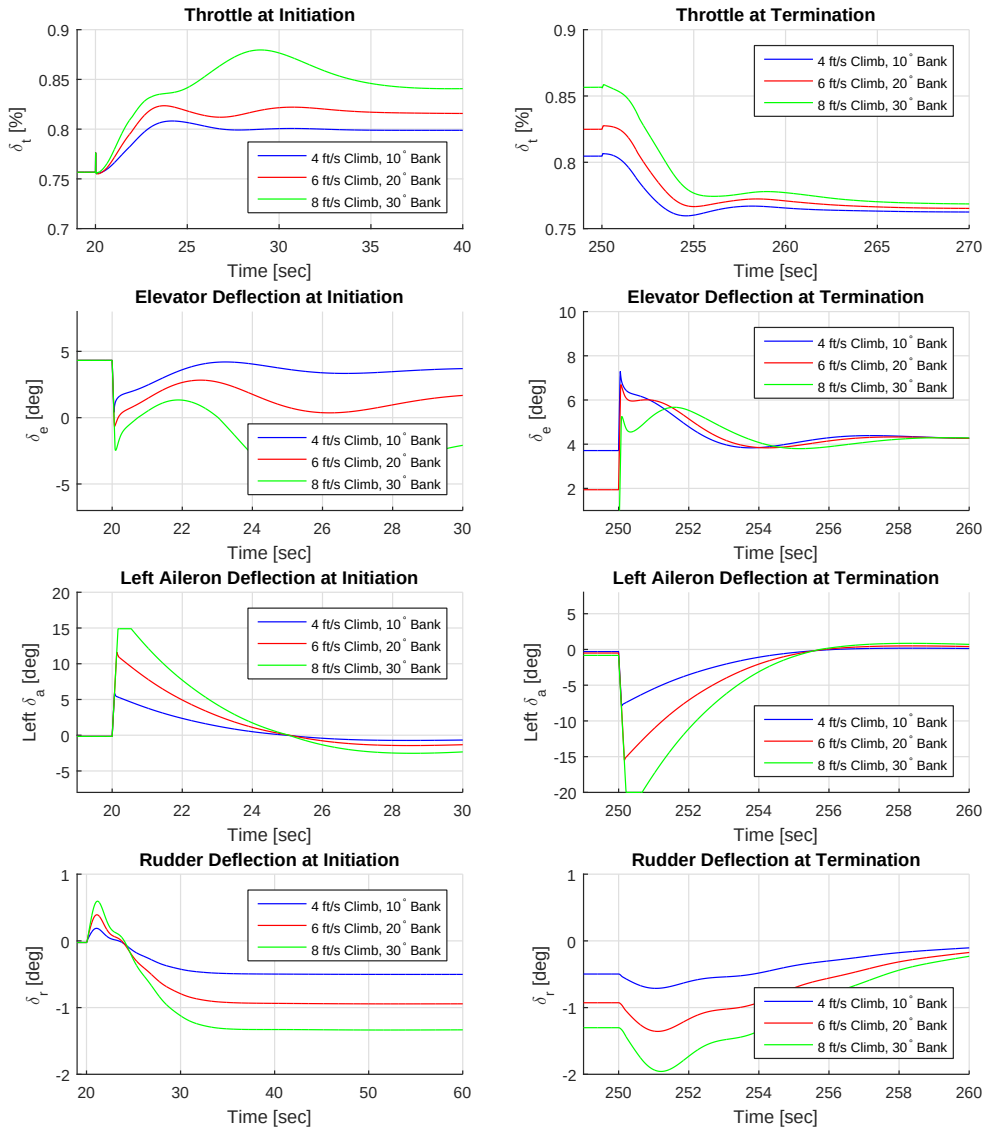

Figure 133. Coupled Maneuver: C_{m_q} and C_{l_p} x 10 Control Plots

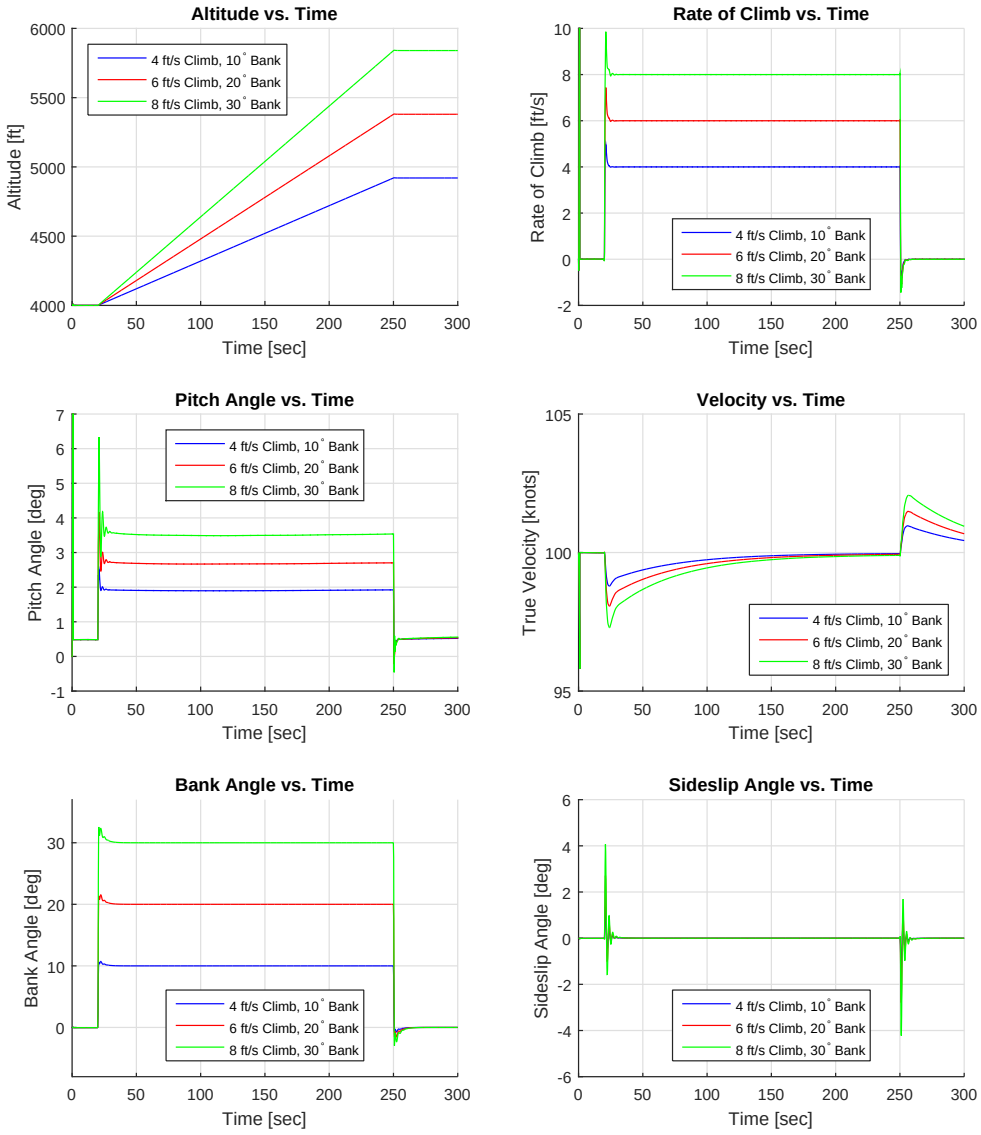

Figure 134. Coupled Maneuver: C_{m_α} and C_{l_p} x $\frac{1}{10}$ Performance Plots

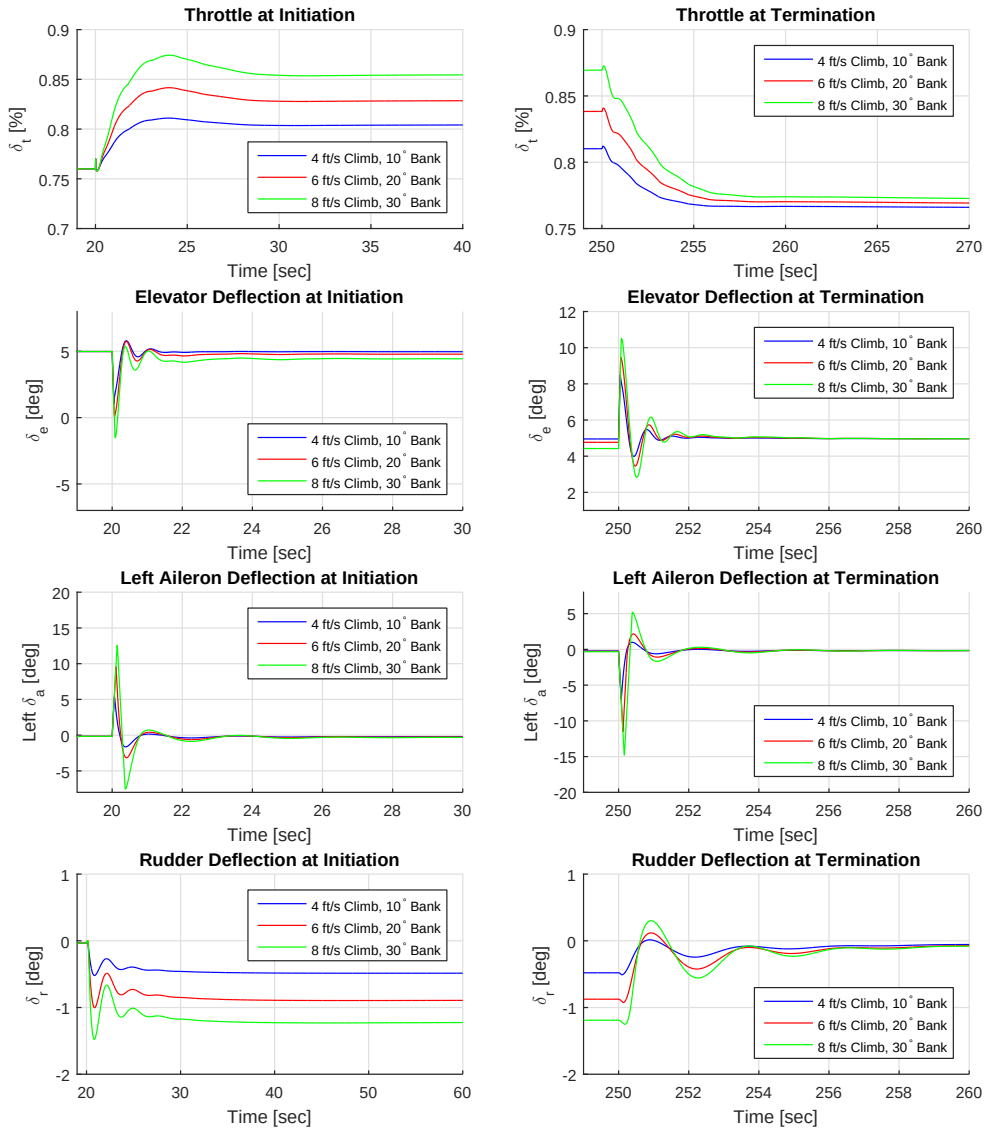

Figure 135. Coupled Maneuver: C_{m_α} and C_{l_p} x $\frac{1}{10}$ Control Plots

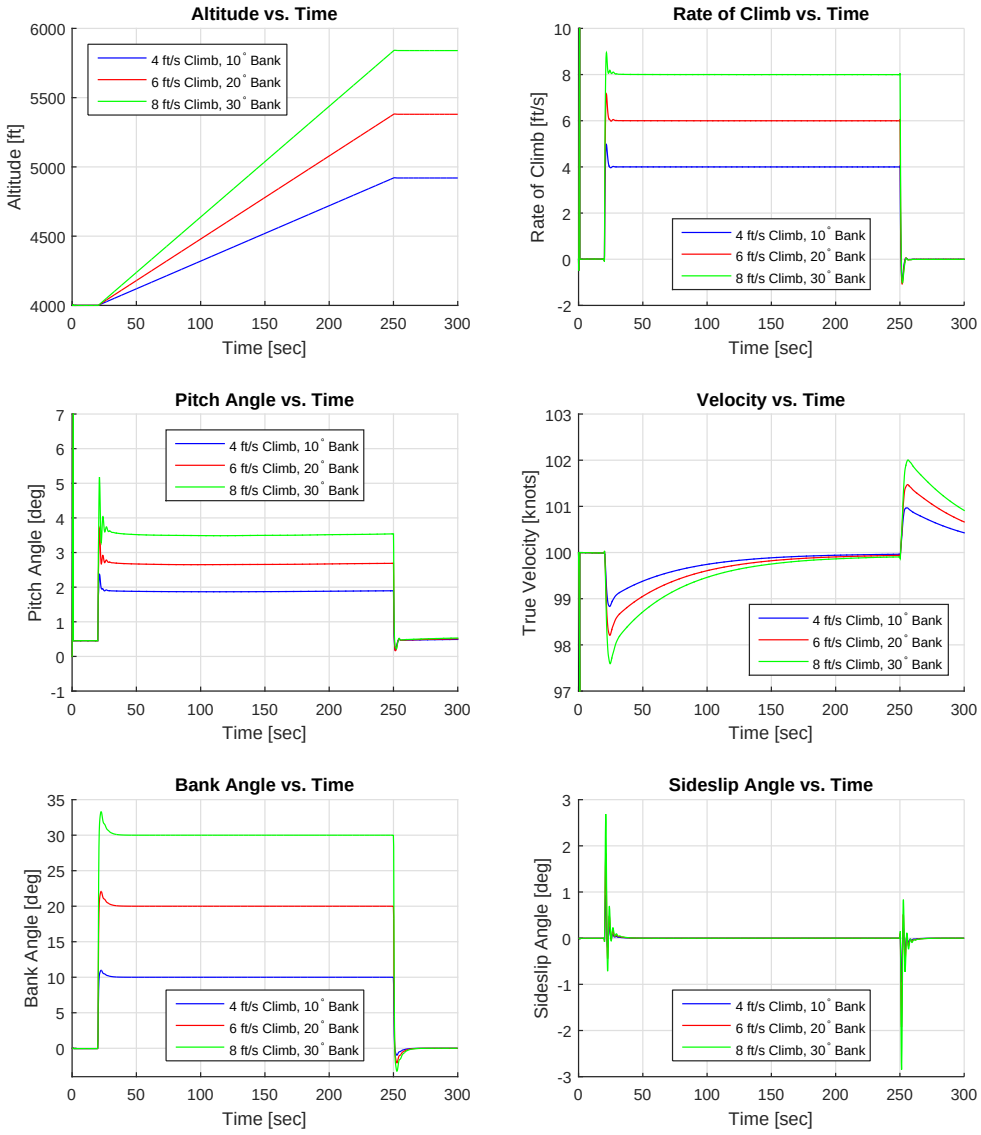

Figure 136. Coupled Maneuver: $C_{m_{\delta_e}}$ and $C_{l_{\delta_a}}$ x $\frac{3}{4}$ Performance Plots

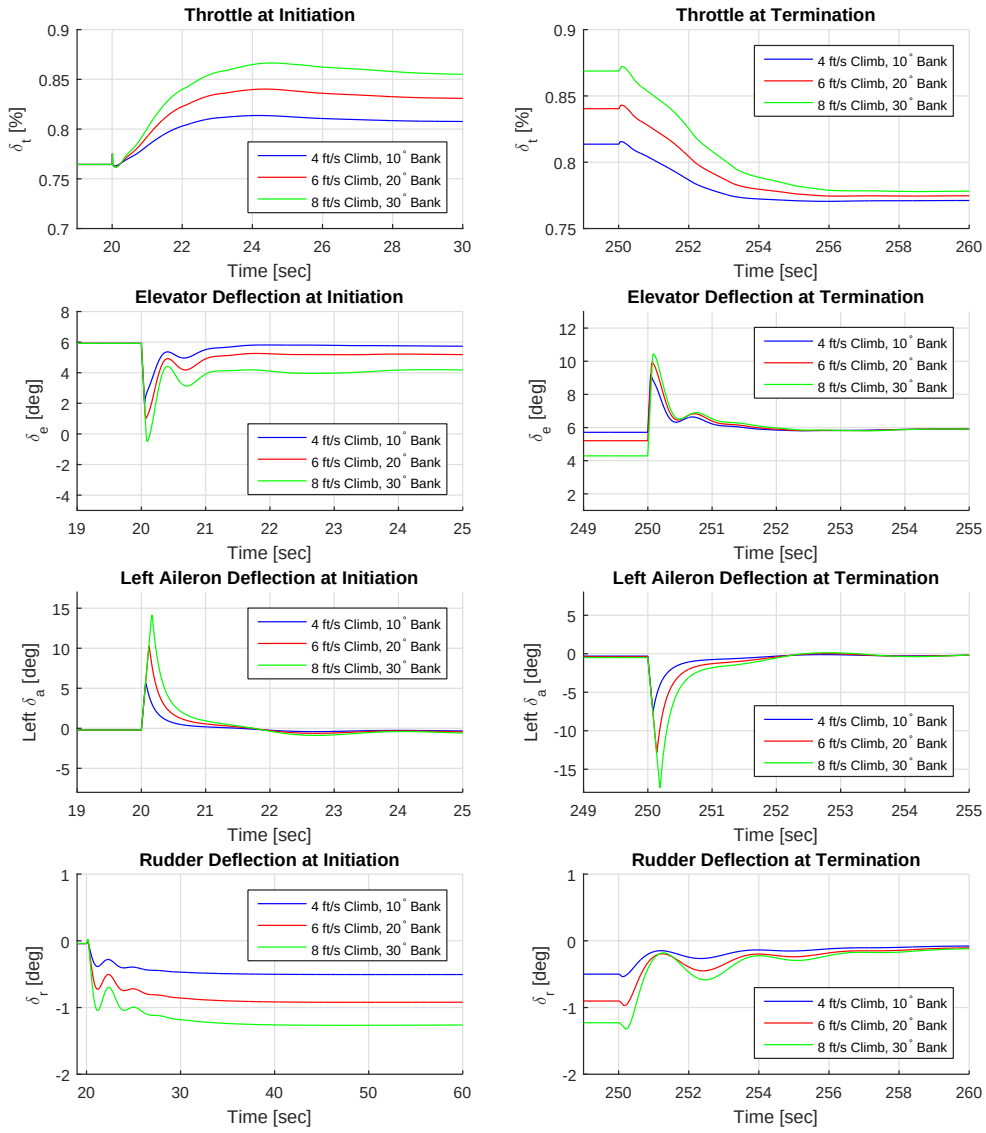

Figure 137. Coupled Maneuver: $C_{m_{\delta_e}}$ and $C_{l_{\delta_a}}$ x $\frac{3}{4}$ Control Plots

Table 69. Coupled Change: C_{m_q}&C_{l_p} **x** $\frac{1}{10}$

Climb	Bank	TIC ($\dot{h}$)	TIC (v_t)	TIC (ϕ)	$\mathcal{L}_2$ (δ_t)	$\mathcal{L}_2$ (δ_e)	$\mathcal{L}_2$ (δ_a)	$\mathcal{L}_2$ (δ_r)
4 ft/s	10°	.025435	.0021811	.021767	.0431	.0056	.0088	.0253
6 ft/s	20°	.025822	.0033781	.023057	.0668	.0131	.0167	.0479
8 ft/s	30°	.026115	.0046796	.023863	.0924	.0280	.0265	.0662

Table 70. Coupled Change: C_{m_q}&C_{l_p} **x** 10

Climb	Bank	TIC ($\dot{h}$)	TIC (v_t)	TIC (ϕ)	$\mathcal{L}_2$ (δ_t)	$\mathcal{L}_2$ (δ_e)	$\mathcal{L}_2$ (δ_a)	$\mathcal{L}_2$ (δ_r)
4 ft/s	10°	.039916	.0020855	.044128	.0413	.0245	.0355	.0268
6 ft/s	20°	.039065	.0029121	.045105	.0582	.0937	.0719	.0514
8 ft/s	30°	.042166	.0043002	.046744	.0845	.2076	.1096	.0730

Table 71. Coupled Change: C_{m_α}&C_{l_p} **x** $\frac{1}{10}$

Climb	Bank	TIC ($\dot{h}$)	TIC (v_t)	TIC (ϕ)	$\mathcal{L}_2$ (δ_t)	$\mathcal{L}_2$ (δ_e)	$\mathcal{L}_2$ (δ_a)	$\mathcal{L}_2$ (δ_r)
4 ft/s	10°	.025713	.0021758	.021767	.0431	.0046	.0088	.0252
6 ft/s	20°	.026161	.0033857	.023057	.0670	.0103	.0167	.0478
8 ft/s	30°	.026547	.0047004	.023863	.0930	.0230	.0265	.0660

Table 72. Coupled Change: C_{m_α}&C_{l_p} **x** 10

Climb	Bank	TIC ($\dot{h}$)	TIC (v_t)	TIC (ϕ)	$\mathcal{L}_2$ (δ_t)	$\mathcal{L}_2$ (δ_e)	$\mathcal{L}_2$ (δ_a)	$\mathcal{L}_2$ (δ_r)
4 ft/s	10°	.043632	.0027766	.044288	.0547	.0633	.0360	.0269
6 ft/s	20°	.046582	.0054539	.045302	.1052	.1809	.0732	.0515
8 ft/s	30°	.41291	.041733	.047885	.1986	.7088	.1163	.0795

Table 73. Coupled Change: $C_{m_{\delta_e}}$&$C_{l_{\delta_a}}$ **x** 3

Climb	Bank	TIC ($\dot{h}$)	TIC (v_t)	TIC (ϕ)	$\mathcal{L}_2$ (δ_t)	$\mathcal{L}_2$ (δ_e)	$\mathcal{L}_2$ (δ_a)	$\mathcal{L}_2$ (δ_r)
4 ft/s	10°	.021986	.0022461	.020061	.0445	.0066	.0050	.0250
6 ft/s	20°	.022471	.0034369	.020817	.0680	.0106	.0097	.0473
8 ft/s	30°	.022776	.0047865	.021364	.0946	.0176	.0144	.0653

Table 74. Coupled Change: $C_{m_{\delta_e}}$&$C_{l_{\delta_a}}$ **x** $\frac{3}{4}$

Climb	Bank	TIC ($\dot{h}$)	TIC (v_t)	TIC (ϕ)	$\mathcal{L}_2$ (δ_t)	$\mathcal{L}_2$ (δ_e)	$\mathcal{L}_2$ (δ_a)	$\mathcal{L}_2$ (δ_r)
4 ft/s	10°	.02905	.0021418	.025634	.0423	.0081	.0117	.0259
6 ft/s	20°	.028854	.0032882	.026938	.0650	.0264	.0227	.0488
8 ft/s	30°	.028852	.0044778	.02805	.0886	.0607	.0336	.0676

Bibliography

1. *Flying Qualities of Piloted Aircraft.* Interface Standard MIL-STD-1797A, NOTICE 1, Department of Defense, June 1995.

2. "Type Certificate Data Sheet NO. 3A12". Department of Transportation, Federal Aviation Administration, December 2012. Certficate Holder: Cessna Aircraft Company.

3. Allen, J. *Advertisement and Specification for a Heavier Than-Air Flying Machine.* Technical report, Signal Corps Specification, No. 486, Washington D.C., January 1908. URL `http://www.ascho.wpafb.af.mil/birthplace/PG14-1.htm`.

4. Berndt, Jon S. "JSBSim: An Open Source Flight Dynamics Model in C++". *AIAA Modeling and Simulation Technologies Conference and Exhibit*, AIAA 2004-4923. Providence, RH, August 2004.

5. Berndt, Jon S. *JSBSim, An Open Source, Platform-Independent, Flight Dynamics Model in C++.* JSBSim, Providence, RH, 2011.

6. Blakelock, John H. *Automatic Control of Aircraft and Missiles.* John Wiley & Sons, Inc., New York, 1965.

7. Breneman, K. and M. Lower. *Flying Qualities of a Remotely Piloted Vehicle.* Technical Report AIAA 92-4083-CP, U.S. Navy, Naval Air Warfare Center, Patuxent River, MD, 1992.

8. Clapper, J. R., J. J. Young, J. E. Grimes, S.C. Payton, S. Stackley, and D. Popps. "FY 2009-2034 Unmanned Systems Integrated Roadmap". *Department of Defense: Office of the Secretary of Defense Unmanned Systems Roadmap*, 92–93, 2009.

9. Clark, Anders. "Cessna 172 Skyhawk". https://disciplesofflight.com/cessna-172-skyhawk/, 2015. [Online; accessed 15-Aug-2015].

10. Company, Cessna Aircraft. *Pilot's Operating Handbook, Cessna Skyhawk 1978 Model 172N*. Wichita, KS, 1977.

11. Cooper, G. E. and R. P. Harper Jr. *The Use of Pilot Rating in the Evaluation of Aircraft Handling Qualities*. Technical Report 567, Advisory Group for Aerospace Research and Development, April 1969.

12. Cotting, M. *Evolution of Flying Qualities Analysis: Problems for a New Generation of Aircraft*. Dissertation, Virginia Polytechnic Institute and State University, Blacksburg, Virginia, March 2010.

13. Cotting, M Christopher. "UAV Performance Rating Scale Based on the Cooper-Harper Piloted Rating Scale". *49th AIAA Aerospace Sciences Meeting including the New Horizons Forum and Aerospace Exposition*, January 2011. URL http://dx.doi.org/10.2514/6.2011-923.

14. Council, National Research. *Review of NASA's Aerospace Technology Enterprise, An Assessment of NASA's Aeronautics Technology Programs*. National Academies Press, Washington D.C., 2004.

15. De Marco, Agnostino, Eugene L. Duke, and Jon S. Berndt. "A General Solution to the Aircraft Trim Problem". *AIAA Modeling and Simulation Technologies Conference and Exhibit*, AIAA 2007-6703. Hilton Head, SC, August 2007.

16. Dorobantu, Andrei, Peter Seiler, and Gary Balas. "Validating Uncertain Aircraft Simulation Models using Flight Test Data". *AIAA Atmospheric Fligth Mechanics Conference*. August 2013.

17. Duane McRuer, Dunstan Graham, Irving Ashkenas. *Aircraft Dynamics and Automatic Control*. Technical Report AD 859330, Naval Air Systems Command, Hawthorne, CA, 1968.

18. Federal Aviation Administration. "Federal Aviation Regulations (FARs) Part 91 Section 211 Supplemental Oxygen", 2005.

19. Friendenthal, Sanford, Alan Moore, and Rick Steiner. *A Practical Guide to SysML*. Morgan Kaufmann Publishers, Amsterdam, 2012.

20. Gareth D. Padfield, John Hodgkinson, Nick Lappos. *The Impact of Flying Qualities on Helicopter Operational Agility*. Technical Report N94-13304, NASA, 1993.

21. Gilruth, R. R. *Requirements for Satisfactory Flying Qualities of Airplanes*. Technical Report NACA Rept. 755, National Advisory Committee for Aeronautics, Langley Field, VA, 1941.

22. Goppert, James and Inseok Hwang. "Constructing BADA Models of Existing UASs from Public Data and Photos using Open Source Tools". *AIAA Modeling and Simulation Technologies (MST) Conference*, AIAA 2013-4904. Boston, MA, August 2013.

23. Goppert, James M., Agnostino De Marco, and Inseok Hwang. "On Some Trim Strategies for Nonlinear Aircraft Flight Dynamics Models with Open Source Software JSBSim". *Proceedings of 3rd CEAS Air and Space Conference*, volume 1 of *Lecture Notes in Computer Science*. Council of European Aerospace Studies (CEAS), Venice, Italy, October 2011.

24. Greene, K., D. Kunz, and M. Cotting. "Toward a Flying Qualities Standard for Unmanned Aircraft". *AIAA Atmospheric Flight Mechanics Conference*, AIAA 2014-2194. Atlanta, GA, June 2014.

25. Hatcher, Robert S. "Intra-office memo", April 1941. USN Bureau of Aeronautics.

26. Hines, Dennis O. *Simulation in Support of Flight Testing*. NATO Research and Technology Organization, September 2000.

27. Hodgkinson, John. *Aircraft Handling Qualities*. Blackwell Science, Oxford, 1999.

28. Holmberg, J. A., D. J. King, J. R. Leonard, and M. C. Cotting. "Flying Qualities Specifications and Design Standards for Unmanned Air Vehicles". *AIAA Atmospheric Flight Mechanics Conference and Exhibit*, AIAA 2008-6555. Honolulu, HI, August 2008.

29. Johansen, I. *Autopilot Design for Unmanned Aerial Vehicles*. Thesis, Norwegian University of Science and Technology, Norway, June 2012.

30. Klyde, D. and D. Mitchell. *Handling Quality Demonstration Maneuvers for Fixed-Wing Aircraft*. Technical Report WL-TR-97-3100, Systems Technology, Inc., October 1997.

31. Leggett, David B. "Lecture notes in Flying Qualities", July 2015.

32. Mitchell, David G., David B. Doman, David L. Key, David H. Klyde, David B. Leggett, David J. Moorhouse, David H. Mason, David L. Raney, and David K. Schmidt. "Evolution, Revolution, and Challenges of Handling Qualities". *Journal of Guidance, Control, and Dynamics*, 27(1):12–28, 2004. ISSN 0731-5090.

33. Mitchell, David G., Roger H. Hoh, Bimal L. Aponso, and David H. Klyde. *Proposed Incorporation of Mission-Oriented Flying Qualities into MIL-STD-A*. Technical Report WL-TR-94-3162, HOH Aeronautics, Inc. and Systems Technology, Inc., 1994.

34. Nelder, J. A. and R. Mead. "Simplex Method for Function Minimization". *Journal of Computing*, 1965.

35. Olson, C.L. "Flight Gear Autopilot: Theory, Configuration, and Tuning". `http://www.flightgear.org/Docs/XMLAutopilot/`, 2004. [Online; accessed 10-Sep-2015].

36. Ou, Qing, XiaoQi Chen, David Park, Aaron Marburg, and James Pinchin. "Integrated Flight Dynamics Modeling for Unmanned Aerial Vehicles". *IEEE*, 1–11, 2008.

37. Padfield, Gareth D. "Rotorcraft Handling Qualities Engineering: Managing the Tension between Safety and Performance". *Journal of the American Helicopter Society*, 58(011001), 2013.

38. Peden, Tony. "Cessna C-172 Skyhawk Model". URL `http://jsbsim.sourceforge.net/JSBSim.xsl`.

39. Phillips, William H. "Flying Qualities from Early Airplanes to the Space Shuttle". *AIAA 26th Aerospace Sciences Meeting*, AIAA 1988-0751. Reno, NV, January 1988.

40. Pratt, Roger. *Flight Control Systems: Practical Issues in Design and Implementation*. The Institution of Electrical Engineers, 2000.

41. Prosser, C.F. and C.D. Wiler. *RPV Flying Qualities Design Criteria*. Technical Report AFFDL-TR-76-125, Rockwell Corporation, 1976.

42. Raol, Jitendra R. and Jatinder Singh. *Flight Mechanics Modeling and Analysis*. CRC Press, Boca Raton, FL, 2008.

43. Raymer, Daniel P. *Aircraft Design: A Conceptual Approach*. AIAA, Reston, Virginia, 2012.

44. Risse, Kristof, Eckhard Anton, and Rlf Henke. "Methodology for Flying Qualities Prediction and Assessment in Preliminary Aircraft Design". *AIAA Aviation Technology, Integration, and Operations (ATIO) Conference*, AIAA 2010-9261. Forth Worth, TX, September 2010.

45. Roskam, Dr. Jan. *Preliminary Calculation of Aerodynamic, Thrust, and Power Characteristics*. Roskam Aviation and Engineering Cooperation, Ottawa, 1987.

46. Samuelsson, Mikael. *Evaluation of Stability and Flying Qualities of a Light Unmanned Aerial Vehicle*. Thesis, KTH, School of Engineering Sciences (SCI), Sweden, 2012.

47. Sarno, K.J. and C.D Wickens. "The role of multiple resources in predicting time-sharing efficiency". *The International Journal of Aviation Psychology*, 107–130, 1995.

48. Secretary of the Air Force. *Flight Manual USAF Series T-41 C/D Aircraft*. Department of Defense, Tinker AFB, OK, 1991.

49. Stengel, Robert. "Lecture Notes on Cruising Flight Performance", 2014.

50. Stevens, B. L. and F. L. Lewis. *Air Control and Simulation*. Wiley, New York, 2003.

51. Theil, H. *Economic Forecasts and Policy*. North-Holland Publishing Company, 1970.

52. Wescott, Tim. "PID Without a PHD". *Embedded Systems Programming*, (October):86–108, 2000.

53. Westbrook, C.B. *The Status and Future of Flying Quality Requirements.* Technical Report AFFDL-FDCC-TM-65-29, Air Force Flight Dynamics Laboratory, Research and Technology Division, Wright-Patterson AFB, OH, June 1955.

54. Williams, W. and M. Harris. "The Challenges of Flight-Testing Unmanned Air Vehicles". *Systems Engineering Test and Evaluation Conference.* Sydney, Australia, October 2002.

55. Winnefeld, JA and Frank Kendall. "Unmanned Systems Integrated Roadmap FY 2011-2036". *Office of the Secretary of Defense. US*, 2011.

56. Winnefeld, JA and Frank Kendall. "Unmanned Systems Integrated Roadmap FY 2013-2038". *Office of the Secretary of Defense. US*, 2013.

57. Zipfel, P. *Modeling and Simulation of Aerospace Vehicle Dynamics.* AIAA, Reston, Virginia, 2007.

Vita

Second Lieutenant Joshua P. Kim graduated from University of California, Los Angeles (UCLA) with a Bachelor of Science in Aerospace Engineering in June 2014. He commissioned into the United States Air Force through the Air Force Reserve Officers' Training Corps (AFROTC) program at UCLA. During his time at UCLA, he assisted a graduate student, David Wirth, on his research on nanotechnology in rocket propulsion under Air Force Research Laboratory, where they were recognized as the first UCLA students to win the major command (MAJCOM) level Air Force Technology & Engineering Award, Cadet Research Category.

After graduation, Lieutenant Kim was selected to attend the Air Force Institute of Technology as his first assignment. In August of 2014, he began his studies towards a Master of Science in Aeronautical Engineering. Upon completion of his studies, he was assigned to Air Force Operational Test and Evaluation Center (AFOTEC) Detachment 6 at Nellis AFB, Nevada to help plan and conduct realistic, objective, and impartial operational testing and evaluation of fighter aircraft.

REPORT DOCUMENTATION PAGE

Form Approved
OMB No. 0704–0188

1. REPORT DATE *(DD–MM–YYYY)*	2. REPORT TYPE	3. DATES COVERED *(From — To)*
24–03–2016	Master's Thesis	Sept 2014 — Mar 2016

4. TITLE AND SUBTITLE

Evaluation of Unmanned Aircraft Flying Qualities Using JSBSim

5a. CONTRACT NUMBER

5b. GRANT NUMBER

5c. PROGRAM ELEMENT NUMBER

6. AUTHOR(S)

Kim, Joshua P., 2d Lt, USAF

5d. PROJECT NUMBER

5e. TASK NUMBER

5f. WORK UNIT NUMBER

7. PERFORMING ORGANIZATION NAME(S) AND ADDRESS(ES)

Air Force Institute of Technology
Graduate School of Engineering and Management (AFIT/EN)
2950 Hobson Way
WPAFB OH 45433-7765

8. PERFORMING ORGANIZATION REPORT NUMBER

AFIT-ENY-MS-16-M-221

9. SPONSORING / MONITORING AGENCY NAME(S) AND ADDRESS(ES)

Department of Aeronautics and Astronautics
2950 Hobson Way
WPAFB OH 45433-7765
DSN 271-0690, COMM 937-255-3636
Email: joshua.kim@afit.edu

10. SPONSOR/MONITOR'S ACRONYM(S)

AFRL/RQQ

11. SPONSOR/MONITOR'S REPORT NUMBER(S)

12. DISTRIBUTION / AVAILABILITY STATEMENT

DISTRIBUTION STATEMENT A:
APPROVED FOR PUBLIC RELEASE; DISTRIBUTION UNLIMITED.

13. SUPPLEMENTARY NOTES

This material is declared a work of the U.S. Government and is not subject to copyright protection in the United States

14. ABSTRACT

Flying qualities data can be used to predict the future performance of aircraft; however, no flying qualities requirements exist for Unmanned Aerial Vehicles (UAVs). The intent of flying qualities requirements is to guarantee the safety and operational effectiveness of the aircraft. Flying qualities requirements have been extensively researched and specified for fixed-wing and rotary-wing manned aircraft based on a substantial database of assessments. The critical issue today in flying qualities is how to extend them to pilotless aircraft. A simulation study using an open-source flight dynamics model (JSBSim) was conducted to perform various performance maneuvers and evaluate how well the aircraft followed the desired maneuver. Criteria from MIL-STD-1797 were used to evaluate the flying quality characteristics and compared to the simulation results. It was found that the application of manned criteria to autonomous UAVs did not provide an accurate depiction of its flying qualities. Instead the requirements should be focused on the closed-loop task evaluation and the limitations of the flight control system.

15. SUBJECT TERMS

Flying Qualities, UAVs, Flight Dynamics Model, Jon S. Berndt Simulation, JSBSim, Mission Task Element, Maneuver Performance, Flight Control System, Workload, Theil's Inequality Coefficient

16. SECURITY CLASSIFICATION OF:			17. LIMITATION OF ABSTRACT	18. NUMBER OF PAGES	19a. NAME OF RESPONSIBLE PERSON
a. REPORT	b. ABSTRACT	c. THIS PAGE			Dr. D. Kunz, AFIT/ENY
U	U	U	UU	241	19b. TELEPHONE NUMBER *(include area code)* (937) 255-3636, x4547; donald.kunz@afit.edu